frontiers | Research Topics

Sustainable nitrogen removal in emerging pollutant contaminated wastewater: Technology, application and risk assessment

Edited by
Zhaoming Zheng, Lijie Zhou, Huike Dong, Yuanyuan Miao, Dingchang Li and Min Long

Published in
Frontiers in Microbiology

ISSN 1664-8714
ISBN 978-2-8325-4364-1
DOI 10.3389/978-2-8325-4364-1

About Frontiers

Frontiers is more than just an open access publisher of scholarly articles: it is a pioneering approach to the world of academia, radically improving the way scholarly research is managed. The grand vision of Frontiers is a world where all people have an equal opportunity to seek, share and generate knowledge. Frontiers provides immediate and permanent online open access to all its publications, but this alone is not enough to realize our grand goals.

Frontiers journal series

The Frontiers journal series is a multi-tier and interdisciplinary set of open-access, online journals, promising a paradigm shift from the current review, selection and dissemination processes in academic publishing. All Frontiers journals are driven by researchers for researchers; therefore, they constitute a service to the scholarly community. At the same time, the *Frontiers journal series* operates on a revolutionary invention, the tiered publishing system, initially addressing specific communities of scholars, and gradually climbing up to broader public understanding, thus serving the interests of the lay society, too.

Dedication to quality

Each Frontiers article is a landmark of the highest quality, thanks to genuinely collaborative interactions between authors and review editors, who include some of the world's best academicians. Research must be certified by peers before entering a stream of knowledge that may eventually reach the public - and shape society; therefore, Frontiers only applies the most rigorous and unbiased reviews. Frontiers revolutionizes research publishing by freely delivering the most outstanding research, evaluated with no bias from both the academic and social point of view. By applying the most advanced information technologies, Frontiers is catapulting scholarly publishing into a new generation.

What are Frontiers Research Topics?

Frontiers Research Topics are very popular trademarks of the *Frontiers journals series*: they are collections of at least ten articles, all centered on a particular subject. With their unique mix of varied contributions from Original Research to Review Articles, Frontiers Research Topics unify the most influential researchers, the latest key findings and historical advances in a hot research area.

Find out more on how to host your own Frontiers Research Topic or contribute to one as an author by contacting the Frontiers editorial office: frontiersin.org/about/contact

Sustainable nitrogen removal in emerging pollutant contaminated wastewater: Technology, application and risk assessment

Topic editors

Zhaoming Zheng — Beijing University of Technology, China
Lijie Zhou — Shenzhen University, China
Huike Dong — Institute of Tibetan Plateau Research, Chinese Academy of Sciences (CAS), China
Yuanyuan Miao — Qingdao University of Technology, China
Dingchang Li — East China Jiaotong University, China
Min Long — Arizona State University, United States

Citation

Zheng, Z., Zhou, L., Dong, H., Miao, Y., Li, D., Long, M., eds. (2024). *Sustainable nitrogen removal in emerging pollutant contaminated wastewater: Technology, application and risk assessment*. Lausanne: Frontiers Media SA.
doi: 10.3389/978-2-8325-4364-1

Table of contents

04 Editorial: Sustainable nitrogen removal in emerging pollutant contaminated wastewater: technology, application and risk assessment
Jun Li, Zhaoming Zheng, Yuanyuan Miao, Dingchang Li, Huike Dong, Lijie Zhou and Min Long

07 Comparative investigation on heterotrophic denitrification driven by different biodegradable polymers for nitrate removal in mariculture wastewater: Organic carbon release, denitrification performance, and microbial community
Yuna Feng, Lu Wang, Zhendong Yin, Zhengguo Cui, Keming Qu, Dawei Wang, Zhanying Wang, Shengmin Zhu and Hongwu Cui

20 Achieving robust and highly efficient nitrogen removal in a mainstream anammox reactor by introducing low concentrations of readily biodegradable organics
Yandong Yang, Yanan Long, Jiarui Xu, Shichong Liu, Lei Liu, Changqing Liu and Yong Tian

31 Preparation and application of Ag plasmon Bi_3O_4Cl photocatalyst for removal of emerging contaminants under visible light
Zeqing Long, Tingting Guo, Chao Chen, Guangming Zhang and Jia Zhu

45 A straightforward approach utilizing an exponential model to compensate for turbidity in chemical oxygen demand measurements using UV-vis spectrometry
Hongliang Wang, Houkui Xiang, Tongqiang Xiong, Jinping Feng, Jianquan Zhang and Xuemei Li

53 Synergistic interactions between anammox and dissimilatory nitrate reducing bacteria sustains reactor performance across variable nitrogen loading ratios
Christian White, Edmund Antell, Sarah L. Schwartz, Jennifer E. Lawrence, Ray Keren, Lijie Zhou, Ke Yu, Weiqin Zhuang and Lisa Alvarez-Cohen

69 Positive effects of lignocellulose on the formation and stability of aerobic granular sludge
Jie Xu, Yuan Gao, Xuejun Bi, Lin Li, Wenjuan Xiang and Shichang Liu

79 Research progress of novel bio-denitrification technology in deep wastewater treatment
Shan Huang, Yuling Fu, Huimin Zhang, Chuqiao Wang, Chenglong Zou and Xiuguo Lu

89 Construction of a mycelium sphere using a *Fusarium* strain isolate and *Chlorella* sp. for polyacrylamide biodegradation and inorganic carbon fixation
Huichao Zhang, Mohan Shangguan, Chang Zhou, Zhaoyang Peng and Zhongyi An

98 *Nitrospira* dominant pin-point flocs with granule-like settleability in stirred tank reactors with oxic/hypoxic/oxic zones
Hussain Aqeel, Bruke Asefa and Steven N. Liss

frontiers | Frontiers in Microbiology

TYPE Editorial
PUBLISHED 12 January 2024
DOI 10.3389/fmicb.2024.1349185

OPEN ACCESS

EDITED AND REVIEWED BY
William James Hickey,
University of Wisconsin-Madison,
United States

*CORRESPONDENCE
Zhaoming Zheng
zhengzhaomingb@sina.com

RECEIVED 04 December 2023
ACCEPTED 02 January 2024
PUBLISHED 12 January 2024

CITATION
Li J, Zheng Z, Miao Y, Li D, Dong H, Zhou L and Long M (2024) Editorial: Sustainable nitrogen removal in emerging pollutant contaminated wastewater: technology, application and risk assessment. *Front. Microbiol.* 15:1349185. doi: 10.3389/fmicb.2024.1349185

Editorial: Sustainable nitrogen removal in emerging pollutant contaminated wastewater: technology, application and risk assessment

Jun Li[1], Zhaoming Zheng[1]*, Yuanyuan Miao[2], Dingchang Li[3], Huike Dong[4], Lijie Zhou[5] and Min Long[6]

[1]National Engineering Laboratory of Urban Sewage Advanced Treatment and Resource Utilization Technology, Beijing University of Technology, Beijing, China, [2]School of Environmental and Municipal Engineering, Qingdao University of Technology, Qingdao, China, [3]School of Civil Architecture, East China Jiaotong University, Nanchang, China, [4]State Key Laboratory of Tibetan Plateau Earth System, Environment and Resources (TPESER), Institute of Tibetan Plateau Research, Chinese Academy of Sciences, Beijing, China, [5]College of Chemistry and Environmental Engineering, Shenzhen University, Shenzhen, China, [6]State Key Laboratory of Pollution Control and Resource Reuse, College of Environmental Science and Engineering, Tongji University, Shanghai, China

KEYWORDS

nitrogen removal process, sludge granulation process, carbon-neutral, emerging contaminants, microbial population analysis, wastewater treatment

Editorial on the Research Topic
Sustainable nitrogen removal in emerging pollutant contaminated wastewater: technology, application and risk assessment

The large-scale release of nitrogen compounds is a major factor for water eutrophication (Li et al., 2023). Traditionally, nitrogen is removed through nitrification and denitrification processes, which leads to external organic carbon addition, high energy consumption, large sludge generation and greenhouse gases emissions (Wu et al., 2023). Many researchers have conducted related research on the autotrophic biological nitrogen removing technology and efficient utilization technology of carbon sources (Al-Hazmi et al., 2023). Anaerobic ammonium oxidation (ANAMMOX) is a crucial autotrophic nitrogen removing process that can reduce the amount of organic matter and energy significantly. Meanwhile, the benefits of aerobic granular sludge (AGS) process are elevated biomass, excellent sludge separation, and small footprint. So far, the comprehensive application of ANAMMOX process and AGS process is facing great challenges (Chen et al., 2022). Besides, the dispersal of emerging organic contaminants in different aquatic ecosystems could have detrimental long-term effects on the global environmental safety (Kumar et al., 2023).

This Research Topic focuses on biological nitrogen removal and emerging contaminants degradation technologies, including ANAMMOX process, AGS process and emerging contaminants removal process. In order to provide readers with an up-to-date understanding of the most fascinating themes, a total of nine articles written by fifty authors were published.

In this topic, Huang et al. systematically reviewed several innovative integrated biological nitrogen removing processes. The performance of short-cut nitrifying and denitrifying, ANAMMOX, simultaneous nitrifying and denitrifying, heterotrophic nitrifying-aerobic denitrifying, AGS, sulfur autotrophic denitrifying, iron autotrophic denitrifying, hydrogen autotrophic denitrifying and bio-electrochemical processes were analyzed in detail. In future, it is worthwhile to take into account the application of cutting-edge bio-denitrifying technology in upgrading urban sewage treatment plants, reducing the greenhouse gases emission and promoting smart water management.

White et al. found that ANAMMOX bacteria could interact with heterotrophic bacteria in a range of competitive and mutualistic ways. Using metagenomic assembly genome analysis, they examined the effects of influent NH_4^+-N:NO_2^--N ratios on the microbial population in a laboratory-size ANAMMOX reactor. The NH_4^+-N:NO_2^--N ratio was reduced from 1.32 to 1.1, which led to the decrease of ANAMMOX bacterial abundance. Meanwhile, metagenomic sequencing technology revealed that the abundance of bacteria using nrfAH gene related with dissimilatory nitrate reduction to ammonium (DNRA) increased.

Yang et al. evaluated the low concentration of readily biodegradable chemical oxygen demand (COD) on the mainstream ANAMMOX process. In long-term operation, the nitrite oxidation bacteria (NOB) abundance rose to 0.56%. Advanced nitrogen removal was achieved by introducing readily biodegradable organic matter with a COD/nitrogen ratio of 0.9. As a result, the NOB activity was greatly suppressed and high ANAMMOX bacterial abundance (2.48%) was determined.

Aqeel et al. described the settling properties, extracellular polymeric substances components and microbiological community dynamics of activated sludge under the action of organic matter. In autotrophic phase, pin-point granular sludge was obtained in R1 and the SVI_{30} gradually increased to 29 mL/g, indicating the improvement of settling properties. However, the settlement properties and PN:PS ratio of flocs decreased in the heterotrophic phase. Molecular approaches indicated that the pin-point granular sludge's major nitrifying bacteria was *Nitrospira*. Moreover, the predominant ammonium oxidization bacteria in seeding sludge and low ammonium cultivation conditions was *Comammox Nitrospira*.

Xu et al. analyzed the impact of lignocellulose on the AGS's granulation evolution process, structural stability and contaminants removing efficacy. It was shown that lignocellulose served as a skeleton within granules, promoting the development of AGS and improving structural strength, in addition to enhancing the secretion of polysaccharides components in tight extracellular-polymeric materials. Besides, lignocellulose had minimal effect on the removing efficiencies of COD, NH_4^+ -N and PO_4^{3-}-P, which were more than 95%, 99%, and 92%, respectively. Lignocellulose facilitated the significant proliferation of functional microbes such as *Nitrosomonas*, *Nitrospira*, *Candidatus Accumulibacter*, and *Candidatus Competibacter*.

Long et al. revealed the degradation performance of Ag-Bi_3O_4Cl plasma photocatalysts for emerging contaminants. The quantity of oxygen-deficient on the surface of catalyst first rose and subsequently dropped as the silver metal level increased. In addition, the light absorption efficiency was increased due to the plasmon resonance effect on the catalyst's surface, which decreased electron-hole pair recombination and increased the migration ability of electron-hole pair. Under optimal Ag-Bi_3O_4Cl dose, the removing efficiencies of ciprofloxacin and tetrabromo bisphenol A were 93.8% and 94.9%, respectively.

In the study of Zhang et al., a fungi-algae particle was assembled using *Fusarium* sp. and *Chlorella* sp. to break down polyacrylamide (PAM) and fix inorganic carbon (IC) in synthetic wastewater. It was demonstrated that a mixture of *Fusarium* sp. and *Chlorella* sp. was superior than the single species in terms of PAM degradation and carbon removal. For IC removal performance, the removing rate of the fungal-algal mixture was 38.5% ± 0.08% higher than that of microalgae.

Feng et al. evaluated the impact of synthetic polymers and agricultural wastes on the denitrification performance of seawater circulating treatment. It was found that the carbon releasing ability of agricultural waste was larger than that of synthetic polymers. Corn cobs in agricultural waste is a perfect carbon source for removing nitrogen from seawater aquaculture under low C/N ratio condition.

Wang et al. developed a real-time and unpolluted model for COD detection, which played an important contribution to the early detection of novel organic pollutants. As the organic contaminants and turbidity were commonly absorbed in the ultraviolet wavelength range, the accuracy of detection was inevitably affected. In their study, the superposition principle was used to deduct the turbidity-induced absorbance from the overlapping spectra.

This Research Topic addressed the most recent advancements on the nitrogen removing and emerging contaminants degradation technologies for low C/N ratio sewage treatment. The suitable operating parameters, treatment efficiency and microbial collaboration mechanism were well elucidated through laboratory experiments. It is necessary to further conduct new biological nitrogen removal technology research combined with practical engineering in the future.

Author contributions

JL: Writing—original draft, Writing—review & editing. ZZ: Writing—original draft, Writing—review & editing. YM: Writing—review & editing. DL: Writing—review & editing. HD: Writing—review & editing. LZ: Writing—review & editing. ML: Writing—review & editing.

Funding

The author(s) declare financial support was received for the research, authorship, and/or publication of this article. ZZ was funded by the National Natural Science Foundation of China (52100022) and Beijing Natural Science Foundation (8222039). HD was funded by the National Natural Science Foundation of China (42007359). LZ was funded by the Guangdong Basic and Applied Basic Research Foundation (2023A1515012556 and 2021A1515011750), the Key Project of Department of Education of Guangdong Province (2023KTSCX117), and Shenzhen

Science and Technology Program (the Stable Support Plan Program 20220804153845001).

Conflict of interest

The authors declare that the research was conducted in the absence of any commercial or financial relationships that could be construed as a potential conflict of interest.

Publisher's note

References

Al-Hazmi, H. E., Maktabifard, M., Grubba, D., Majtacz, J., Hassan, G. K., Lu, X., et al. (2023). An advanced synergy of partial denitrification-anammox for optimizing nitrogen removal from wastewater: A review. *Biores. Technol.* 381, 129168. doi: 10.1016/j.biortech.2023.129168

Chen, Y. J., Guo, G. Z., and Li, Y. Y. (2022). A review on upgrading of the anammox-based nitrogen removal processes: Performance, stability, and control strategies. *Biores. Technol.* 364, 127992. doi: 10.1016/j.biortech.2022.127992

Kumar, V., Singh, E., Singh, S., Pandey, A., and Bhargava, P. C. (2023). Micro- and nano-plastics (MNPs) as emerging pollutant in ground water: environmental impact, potential risks, limitations and way forward towards sustainable management. *Chem. Eng. J.* 459, 141568. doi: 10.1016/j.cej.2023.141568

Li, J., Wang, Z. W., and Wang, Y. Y. (2023). Integrating membrane aerated biofilm reactors with biological nitrogen removal processes: a new paradigm for achieving sustainable wastewater treatment plants. *Chem. Eng. J.* 475, 146025. doi: 10.1016/j.cej.2023.146025

Wu, H., Li, A. J., Gao, S. C., Xing, Z. L., and Zhao, P. (2023). The performance, mechanism and greenhouse gas emission potential of nitrogen removal technology for low carbon source wastewater. *Sci. Total Environ.* 903, 166491. doi: 10.1016/j.scitotenv.2023.166491

frontiers | Frontiers in Microbiology

TYPE Original Research
PUBLISHED 20 February 2023
DOI 10.3389/fmicb.2023.1141362

OPEN ACCESS

EDITED BY
Yuanyuan Miao,
Qingdao University,
China

REVIEWED BY
Weiqiang Zhu,
University of Antwerp,
Belgium
Dong Wei,
University of Jinan,
China
Xiaona Ma,
Jiangsu Ocean Universiity,
China

*CORRESPONDENCE
Hongwu Cui
✉ cuihw@ysfri.ac.cn

SPECIALTY SECTION
This article was submitted to Microbiotechnology, a section of the journal Frontiers in Microbiology

RECEIVED 10 January 2023
ACCEPTED 31 January 2023
PUBLISHED 20 February 2023

CITATION
Feng Y, Wang L, Yin Z, Cui Z, Qu K, Wang D, Wang Z, Zhu S and Cui H (2023) Comparative investigation on heterotrophic denitrification driven by different biodegradable polymers for nitrate removal in mariculture wastewater: Organic carbon release, denitrification performance, and microbial community. *Front. Microbiol.* 14:1141362. doi: 10.3389/fmicb.2023.1141362

Comparative investigation on heterotrophic denitrification driven by different biodegradable polymers for nitrate removal in mariculture wastewater: Organic carbon release, denitrification performance, and microbial community

Yuna Feng[1,2], Lu Wang[3], Zhendong Yin[2,4], Zhengguo Cui[2,3], Keming Qu[2,3], Dawei Wang[1,2], Zhanying Wang[1,2], Shengmin Zhu[2,4] and Hongwu Cui[2,3]*

[1]National Experimental Teaching Demonstration Center for Aquatic Science, National Demonstration Center for Experimental Fisheries Science Education, Shanghai Ocean University, Shanghai, China, [2]Key Laboratory of Sustainable Development of Marine Fisheries, Ministry of Agriculture and Rural Affairs, Yellow Sea Fisheries Research Institute, Chinese Academy of Fishery Sciences, Qingdao, China, [3]Marine Life Research Center, Laoshan Laboratory, Qingdao, China, [4]College of Chemistry and Chemical Engineering, Ocean University of China, Qingdao, China

Heterotrophic denitrification is widely studied to purify freshwater wastewater, but its application to seawater wastewater is rarely reported. In this study, two types of agricultural wastes and two types of synthetic polymers were selected as solid carbon sources in denitrification process to explore their effects on the purification capacity of low-C/N marine recirculating aquaculture wastewater (NO_3^--N 30mg/L, salinity 32‰). The surface properties of reed straw (RS), corn cob (CC), polycaprolactone (PCL) and poly3-hydroxybutyrate-hydroxypropionate (PHBV) were evaluated by Brunauer–Emmett–Teller, Scanning electron microscope and Fourier-transform infrared spectroscopy. Short-chain fatty acids, dissolved organic carbon (DOC), and chemical oxygen demand (COD) equivalents were used to analyze the carbon release capacity. Results showed that agricultural waste had higher carbon release capacity than PCL and PHBV. The cumulative DOC and COD of agricultural waste were 0.56–12.65 and 1.15–18.75mg/g, respectively, while those for synthetic polymers were 0.07–1.473 and 0.045–1.425mg/g, respectively. The removal efficiency of nitrate nitrogen (NO_3^--N) was CC 70.80%, PCL 53.64%, RS 42.51%, and PHBV 41.35%. Microbial community analysis showed that Proteobacteria and Firmicutes were the most abundant phyla in agricultural wastes and biodegradable natural or synthetic polymers. Quantitative real-time PCR indicated the conversion from nitrate to nitrogen was achieved in all four carbon source systems, and all six genes had the highest copy number in CC. The contents of medium nitrate reductase, nitrite reductase and nitrous oxide reductase genes in agricultural wastes were higher than those in synthetic polymers. In summary, CC is an ideal carbon source for denitrification technology to purify low C/N recirculating mariculture wastewater.

KEYWORDS

solid carbon source, slow-release, nitrate removal, mariculture wastewater, low C/N

Introduction

Compared to the traditional aquaculture system, the recirculating aquaculture system (RAS) plays an increasingly important role in the production model of aquaculture because of its small floor area, controllable breeding conditions, potential to effectively reduce the waste of water resources and ability to realize the advantages of high-density cultivation (Zou et al., 2018). Wastewater treatment is a key issue for RAS, and ammonia nitrogen (NH_4^+-N) and nitrite nitrogen (NO_2^--N) produced by residual bait and feces were toxic to aquaculture organisms. Therefore, NH_4^+-N and NO_2^--N must be transformed into nitrate nitrogen (NO_3^--N) having less toxicity through biological filters. With NO_3^--N pollution in water getting increased attention, numerous studies have shown that NO_3^--N in marine RAS has become one of the major sources of water environment pollution, and the accumulation of NO_3^--N will have long-term negative effects on aquaculture organisms (Davidson et al., 2017). The concentration of NO_3^--N is usually controlled by water exchange, which not only increases the wastewater generation but also threatens the ecological environment (Martins et al., 2010). Denitrification technology is an effective way to reduce NO_3^--N pollution in RAS wastewater (Johann et al., 2018). As with most mariculture wastewater, a low carbon-to-nitrogen ratio (C/N) is the main factor limiting the denitrification process because of its very low concentration of organic pollutants. Therefore, RAS wastewater treatment usually relies on the supplementation of additional carbon sources to ensure high efficiency and adequacy of denitrification (Zhao et al., 2012).

Common types of carbon sources in denitrification can be divided into water-soluble organic carbon and solid carbon. In practical applications, the addition of water-soluble organic carbon sources to the influent in the denitrification unit was studied earlier, mainly including alcohols such as methanol and ethanol (Fajardo et al., 2012), fatty acids such as acetate and propionic acid, and sugars such as glucose (Nyberg et al., 1996). However, relevant studies have found that water-soluble carbon source dosage is difficult to control and is prone to NO_2^--N accumulation and other secondary pollution problems (De Schryver et al., 2008). Therefore, some biodegradable polymers have been studied extensively because of their good long-term denitrification effect and controllable effluent chemical oxygen demand (COD). Many water-insoluble but biodegradable natural material and synthetic biodegradable polymers (BDPs) can be used as carriers for microorganisms in wastewater (Epsztein et al., 2016). Agricultural wastes, such as reed straw (RS), straw (SA), and corn cob (CC) are reported to have a good nitrogen removal effect and low price compared to other carbon sources (Rosales et al., 2017). BDPs (such as polyhydroxy chain alkylate (PHA), poly3-hydroxybutyrate-hydroxypropionate (PHBV), polycaprolactone (PCL), polybutanediol succinate (PBS), etc.) have been extensively studied for their good resistance to impact loading, while they are not economical compared to natural plants (Zhu et al., 2015). Therefore, the selection of additional carbon source is critical for the complete denitrification, so as not to reduce the nitrogen removal efficiency of denitrification or bring secondary pollution.

At present, the relevant research with solid carbon resource addition mainly focuses on the treatment of urban groundwater and industrial wastewater, and found that the denitrification efficiency can be effectively improved. Jia et al. (2019) explored the feasibility of using wheat straw, apricot pits, and walnut shells for nitrogen removal from low C/N synthetic wastewater in constructed wetland, and found that the total nitrogen removal efficiency was as high as 66.75%–93.67%. Cui et al. (2022) used wastepaper to purify wastewater from sewage treatment plants, it was found that the denitrification efficiency could reach 94.17%. However, the solid carbon source-driven denitrification technology to purify marine recirculating aquaculture wastewater is rarely studied. The main pollutant in marine recirculating aquaculture wastewater is nitrate nitrogen. Different from other wastewater, it has the characteristics of low C/N and high salinity. These characteristics may affect the growth of denitrifying bacteria, which is not conducive to denitrification. It is not clear whether solid carbon sources used for freshwater denitrification can maintain their carbon source release capacity in mariculture wastewater. And whether the high salinity and low-C/N characteristics of mariculture wastewater will reduce denitrification efficiency or produce other concerns. In this study, two agricultural wastes (RS and CC) and two BDPs (PCL and PHBV) were selected as the additional carbon sources. The surface characteristics, carbon release performance, and denitrification capacity of each solid carbon source were comprehensively investigated by conducting carbon source release and nitrate removal experiments. Based on the research results, the best solid carbon source was selected, and the feasibility of the four selected carbon sources as additional carbon sources for denitrification was evaluated, providing a reference for the selection of carbon sources for denitrification treatment of marine recirculating aquaculture wastewater.

Materials and methods

Materials

Four external carbon sources were used in this experiment. Agricultural waste RS and CC were purchased from Henan Gongyi Hengrun Water Treatment Materials Co., Ltd. (China). Before the experiment, the agricultural waste was washed with deionized water and dried in a drying oven at 60°C until constant weight. PCL and PHBV were purchased from the Dongguan Camphor Wood Suyuan Plastic Raw Materials Business Department (China). The physical properties of the selected materials are presented in Table 1. The Brunauer–Emmett–Teller surface area, pore-volume, and pore size were obtained by using fresh carbon source materials placed in static tubes, pumped to vacuum and degassed with Micromeritics Tristar II 3020 (USA), and measured in liquid nitrogen after depressurization and cooling.

Carbon source screening experiment

Carbon source release experiment

Add 40 grams of each carbon source into a 1,000 mL wide mouth bottle, and mixed with 800 ml natural seawater (salinity 31 ± 1 ‰, pH 7.72 ± 0.15, DO 5.56 ± 0.41, COD 2.32 ± 1.17). The bottle was then sealed with a plastic cap to prevent evaporation and contamination. The experimental temperature was 25°C and the experimental period was 30 days. The water in the bottle was collected every 2 days for determination of COD, TOC, and, DOC. Analysis of CODs was done

TABLE 1 The physical properties of the four types of carbon sources.

Carbon source	Appearance shape	Particle size (mm)	Brunauer–Emmett–Teller surface area (m^2/g)	Pore volume (cm^3/g)	Pore size (nm)
RS	Schistose	4–5	0.6388	0.001737	26.3734
CC	Schistose	4–5	0.2043	0.000479	10.9531
PCL	Cylinder	4–5	0.0487	0.000029	45.2805
PHBV	Pellet	4–5	0.0206	0.000028	3.2825

according to the method described in the Standard Method for Examination of Water and Wastewater GB 17378.7-1998 (1999). TOC and DOC were measured using a TOC analyzer (Shimadzu, TOC-L) with an automatic sampler (Shimadzu, ASI-V). At the end of this experiment, the contents of short-chain fatty acids (SCFAs) in water were measured. SCFAs, including acetic acid (AC), propionic acid (PA), butyric acid (BA), and other types (isobutyric acid, valeric acid, isovaleric acid, and hexanoic acid) were measured by ion chromatography-mass spectrometry (Shimadzu GCMS QP2010-ULTRA, Japan). After each sampling, an equal amount of sterilized seawater was added to the mouth-wide mouth bottle to keep the volume constant. Before and after the experiment, the carbon source samples were analyzed by Scanning electron microscopy (SEM) and Fourier transform infrared (FT-IR) spectroscopy. The carbon sources were crushed and randomly sampled to observed using SEM (ZEISS Gemini SEM 300, Germany), and the carbon distribution on the surface of the solid carbon source was analyzed using SEM-energy dispersive X-ray spectroscopy (EDS) (ZEISS Gemini SEM 300, Germany). The functional group information of carbon sources was identified by FTIR using a FTIR spectrometer (Thermo Scientific Nicolet iS20, USA). The physical properties of the three repeated tests are shown in Table 1.

Nitrate removal experiment

The apparatus used for nitrate removal experiment is shown in Figure 1. Each experimental group included a column reactor, peristaltic pump, inlet pool (180 L) and outlet pool (10 L). The column reactor was made of completely transparent acrylic sheet, with an internal diameter of 50 mm and a height of 900 mm, and the reactor was filled with 1.2 L wastewater without adding carbon source material. The reactor was divided into a water distribution layer, a support layer (pore diameter of 3 mm, to prevent carbon sources from falling into the water distribution layer), and filling layer from bottom to top, with four outlets on the column. The experimental inlet water was artificially simulated by recirculating mariculture wastewater with a salinity of 31 ± 1 ‰, NO_3^--N concentration of 30 mg/L (adjusted by KNO_3), phosphate (PO_4^{3-}-P) concentration of 1 mg/L (adjusted by KH_2PO_4), pH of 7.0–7.5 (adjusted by HCl), and the temperature was controlled at 25 ± 1°C during the experiment.

In order to improve the membrane hanging start-up efficiency of the reactor, the denitrifiers adapted to high salinity were acclimated and enriched before the experiment, and detailed steps are as follows: solid wastes discharged from marine recirculating aquaculture system were used as seeding sludge and inoculated into nutrient solution (30 mg/L NO_3^--N, 1 mg/L PO_4^{3-}-P, salinity 32‰), and reached mixed liquor suspended solids (MLSS) for 3 g/L. MLSS concentrations were measured according to the Standard Methods (APHA et al., 2012). Before the experiment, four types of carbon source materials were added into the reactor, and then seeding sludge was evenly inoculated into the column reactor. The carbon source fill rate was 50% and the hydraulic retention time (HRT) was set to 5 h. The NO_3^--N and NO_2^--N content in the outlet were sampled and measured, and the start-up operation finished as the biofilm reactor reached a steady-state with the effluent NO_3^--N less than 1.5 mg/L, and this process lasts about 2 months.

The experimental phase was 180 h. The wastewater in the inlet pool was pumped into the inlet through a peristaltic pump and discharged from the outlet to the outlet pool through the reactor. The NO_3^--N, NO_2^--N, NH_4^+-N, total nitrogen (TN), and COD concentrations at the outlet were measured every 8 h. Water samples were filtered first using a 0.45 μm membrane, and then NO_3^--N, NO_2^--N, TN (no membrane filtration), and NH_4^+-N were determined using an automatic nutrient analyzer (QuAAtro, SEAL, Germany). The nitrate removal efficiency (NRE) was calculated as follows:

$$NRE = \frac{\left(NO_3^- - \mathrm{N}\right)_{\mathrm{inf}} - \left(NO_3^- - \mathrm{N}\right)_{eff}}{\left(NO_3^- - \mathrm{N}\right)_{\mathrm{inf}}} \times 100\% \quad (1)$$

Bacterial community

Four carbon sources were taken for 16S rRNA high-throughput sequencing after the nitrate removal experiment. Microbial community genomic DNA was extracted from the carbon sources using the FastDNA® Spin Kit for Soil (MP Biomedicals, Norcross, GA, U.S.) according to the manufacturer's instructions. The hypervariable region V5-V7 of the bacterial 16S rRNA gene was amplified with primer pairs 799F (5'-AACMGGATTAGATACCCKG-3′) and 1193R (5'-ACGTCATCCCCACCTTCC-3′) using an ABI GeneAmp® 9700 PCR thermocycler (ABI, CA, USA) (Bulgarelli et al., 2012). In order to analyze the structure of microbial community, the Illumina MiSeq sequencing was conducted at the Shanghai Majorbio Bio-pharm Biotechnology Co., Ltd. (Shanghai, China). The raw reads were deposited in the NCBI Sequence Read Archive (SRA) database (Accession Number: PRJNA864076).

Operational taxonomic units (OTUs) were clustered with a 97% similarity cutoff (Stackebrandt and Goebel, 1994; Edgar, 2013) using UPARSE version 7.1(Edgar, 2013), and chimeric sequences were identified and removed. The taxonomy of each OTU representative sequence was analyzed using the RDP Classifier version 2.2 (Wang et al., 2007) against the Silva v138 16S rRNA database using a confidence threshold of 70%. Detailed method has been in Supplementary material Data Sheet 1.

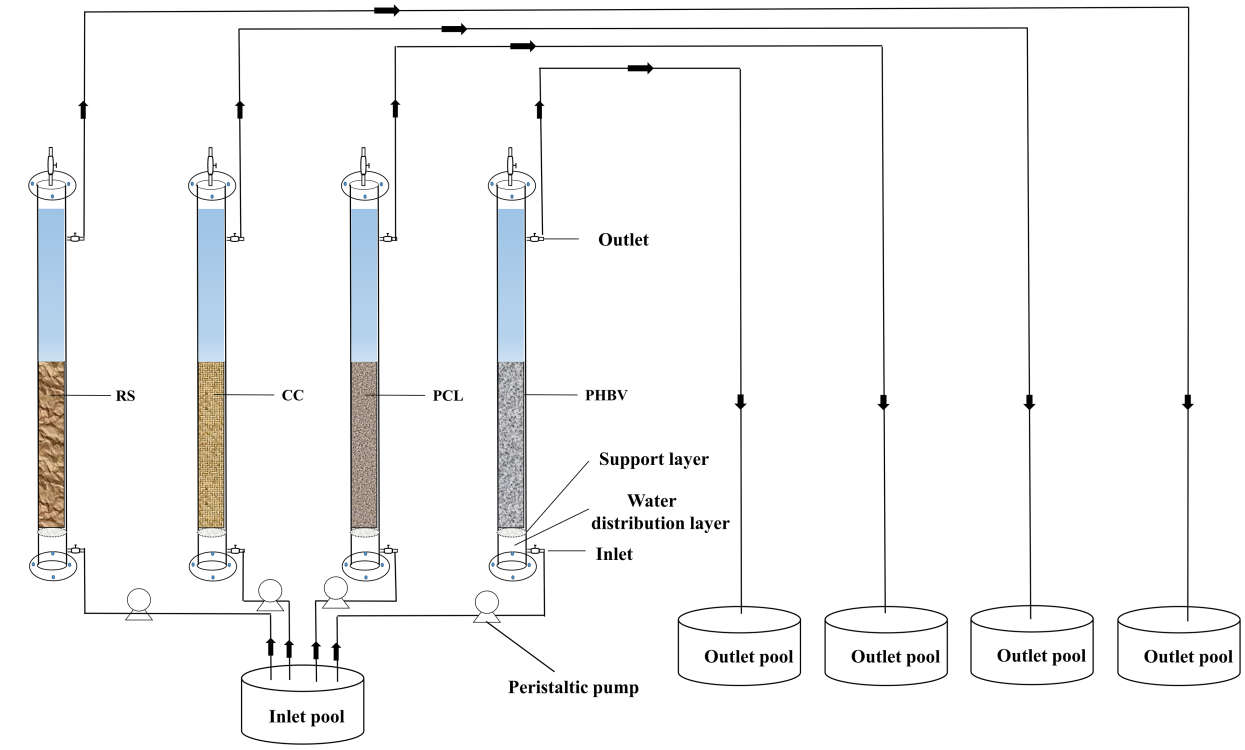

FIGURE 1
Schematic of the denitrification biofilm reactors.

Abundance of functional genes

The remaining DNA samples used for sequencing in Section 2.3 were used for quantitative real-time PCR (q-PCR) analysis. The key genes, including *narG* (encoding the membrane-bound nitrate reductase), *napA* (encoding the periplasmic nitrate reductase), *nirK* (encoding the copper-containing nitrite reductase), *nirS* (encoding the haem-containing nitrite reductases), *norB* (encoding nitric oxide reductase), and *nosZ* (encoding nitrous oxide reductase), were further quantified by q-PCR using a ChamQ SYBR Color qPCR Master Mix (2X) with an ABI PRISM 7300 Sequence Detection System (Applied Biosystems, USA), and were conducted in triplicate in different experimental groups. Each PCR tube (20 μl) contained 10 μl 2X ChamQ SYBR Color qPCR Master Mix (Nanjing Novizan Biotechnology Co., LTD, China), 2 μl DNA, 0.8 μl each of forward and reverse primer, 0.4 μl ROX Reference Dye II (50×), and sterile ddH_2O to a total volume of 20 μl. The primers used for the PCR amplification of each gene are listed in Table 2.

Statistical analysis

Statistical analysis and plotting were performed using Origin 2018 software (Origin Lab Corporation, USA). For SCFAs and gene abundance, one-way ANOVA combined with a t-test ($p < 0.05$) was conducted using SPSS Statistics 26 (SPSS, Chicago, IL, USA) to detect significant differences between the systems.

Results and discussion

Carbon release performance

Organic carbon release capacity

As can be seen from Figure 2A, the carbon sources of the four groups all showed an increasing trend in the early stage of the experiment, while the DOC content of the four experimental groups all decreased and tended to be stable in the later stage. The DOC contents of agricultural waste CC and RS were much higher than those of PCL and PHBV, and the average contents were CC (9.34 mg/g), RS (2.32 mg/g), PCL (0.92 mg/g), and PHBV (0.19 mg/g). Xiong et al. (2020) also observed the phenomenon of low DOC content in PCL. This is because agricultural wastes are natural cellulosic materials that contain a large number of water-soluble small molecules on the surface and inside of the materials (Zhao et al., 2020). Therefore, carbon from RS and CC was released rapidly in the early stage of the experiment under the action of the concentration difference, and the increase in the release rate was more obvious than that of PCL and PHBV. Wu et al. (2012) suggested that the growth of microorganisms affects the biodegradation of polymers, thus affecting the release of DOC. The rapid increase in DOC content due to the release of soluble products during microbial metabolism (Chu and Wang, 2013). As the carbon release experiment proceeded, the biofilm attached to the carbon source stabilized and matured gradually, showing that the content of DOC was gradually stable. In addition, higher content of DOC is beneficial to microbial growth (Chu and Wang, 2016). In the later stage, the internal concentration of the immediately releasing small molecules was low, and the remaining cellulose and hemicellulose were difficult to dissolve in

TABLE 2 Primers for quantitative real-time PCR assays.

Functional gene	Primer	Primer sequence (5′-3′)	Amplification size (bp)	Source
narG	LIY-narGf	TCGCCSATYCCGGCSATGTC	173 bp	Chen et al. (2012)
	LIY-narGr	GAGTTGTACCAGTCRGCSGAYTCSG		
napA	napAF	AAYATGGCVGARATGCACCC	518 bp	Li et al. (2022)
	napAR	GRTTRAARCCCATSGTCCA		
nirK	nirKR3CuR	GCCTCGATCAGRTTGTGGTT	473 bp	Palmer et al. (2011)
	nirK1aCuF	ATCATGGTSCTGCCGCG		
nirS	cd3aF	GTSAACGTSAAGGARACSGG	400 bp	Palmer et al. (2011)
	R3cdR	GASTTCGGRTGSGTCTTGA		
norB	LIY-norBf	AAATGGCTTTACGTCATCGTCG	313 bp	Jiang et al. (2019)
	LIY-norBr	TCTGCGTGCCGTGGGTCT		
nosZ	nosZ2F	CGCRACGGCAASAAGGTSMSSGT	267 bp	Henry et al. (2006)
	nosZ2R	CAKRTGCAKSGCRTGGCAGAA		

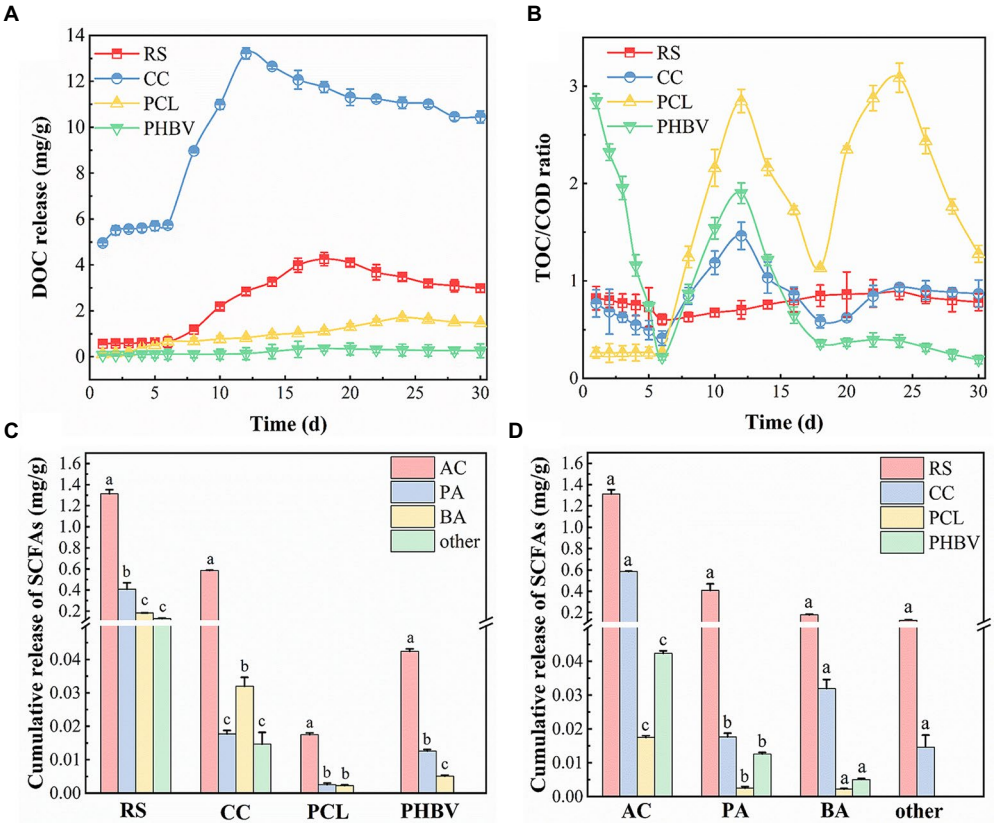

FIGURE 2
Release of different carbon sources. **(A)** Dissolved organic carbon (DOC); **(B)** Total organic carbon/Chemical oxygen demand (TOC/COD); **(C)** Differences in Short-chain fatty acids (SCFA) of the same carbon source; **(D)** Cumulative release of same SCFA with different carbon sources.

water, decomposing slowly under the action of microorganisms, resulting in a decreased carbon release rate gradually. Compared to agricultural wastes, BDPs have a higher degree of polymerization and a smaller surface area, which are not conducive to microbial growth; therefore, the DOC content is low.

Agricultural waste rapidly released carbon sources in the early stage, showing that their COD contents were much higher than those of BDPs. TOC refers to the total organic carbon content in water and can be used to express the organic carbon release rate from materials into the water. The TOC/COD ratio in the leaching solution could more directly indicate the release of organic carbon from agricultural waste (Xiong et al., 2020). Carbon source release results are mainly measured by DOC index, and TOC/COD can evaluate carbon source release performance from different angles. The TOC/COD levels of

the leached solutions of the four carbon sources within 30 days are shown in Figure 2B. The average ratios decreased in the order of PCL, PHBV, CC, and RS, which were 1.48, 0.98, 0.81, and 0.77, respectively. Contrary to the DOC contents, TOC/COD in the leaching solution of BDPs was higher, indicating that PCL and PHBV had higher carbon release utilization than agricultural waste. This is because agricultural waste is more likely to expand after soaking, and the small molecules inside are more likely to be released into water, resulting in a higher COD content and lower TOC/COD ratio. However, PCL and PHBV have higher degrees of polymerization, thus slower release of internal substances, lower COD concentrations, and higher TOC/COD. The use of agricultural waste-based carbon sources is relatively low, and there is a risk of exceeding COD standards and wasting carbon sources. This phenomenon was also reported by Ling et al. (2021).

SCFAs components of released carbon

SCFAs are commonly used as nitrogen and carbon sources for denitrification (Atasoy et al., 2018; Xiong et al., 2019; Wang et al., 2021). Different SCFA contents and combinations had different effects on denitrification performance. In this experiment, SCFAs from four carbon sources were measured (Figures 2C,D). The results showed that the contents of AC, PA, BA, and other SCFA in agricultural waste were higher than those of BDPs (Figure 2D). The cumulative released amounts of SCFAs in descending order is as follows: RS (2.08 mg/g) > CC (0.65 mg/g) > PHBV (0.06 mg/g) > PCL (0.02 mg/g). In agricultural waste, the AC content of RS (1.330 mg/g) was significantly higher than that of CC (0.588 mg/g), whereas, in BDPs, the AC content of PHBV (0.043 mg/g) was higher than that of PCL (0.018 mg/g). Reports have pointed out that when using acetate as a carbon source and electron donor, nitrate and nitrite reduction rates are faster, and AC has a simple biodegradation pathway and can be directly used in denitrifying bacterial systems (Constantin and Fick, 1997). The carbon source with a higher AC content is more conducive to denitrifying bacteria transformation and decomposition (Elefsiniotis et al., 2004), and nitrite is reduced simultaneously when acetate remains sufficient. When the AC content is insufficient, nitrate can be converted into nitrite due to the influence of substrate competition.

However, the BA content is also a factor affecting denitrification. In descending order, the BA contents in RS, CC, PHBV, and PCL were 0.18, 0.03, 0.005, and 0.002 mg/g, respectively. In the agricultural waste, RS contained much more BA than CC, which was six times that of CC. PHBV contained 2.5 times more BA than PCL in the BDPs. These results suggest that RS and PHBV may limit denitrification efficiency because of their high BA content. The PA content was similar to that of the BA. Studies have found that the removal efficiency of nitrate is very low when only butyrate is used as a carbon source (Li et al., 2015). Chen et al. (2016) found that when butyrate content increased from 5% to 30%, the NRE decreased from the highest value of 95.75% to the lowest of 42.5%. This indicates that a high concentration of BA inhibits nitrate removal, resulting in a reduced denitrification efficiency.

Chen et al. (2016) also found that a higher concentration of propionate leads to an excessive accumulation of NO_2^--N during denitrification. When the acetate/propionate ratio changed from >1 to <1, the accumulation of nitrite increased by 5 mg/L. The acetate/propionate ratios of the four carbon sources were > 1, among which that of CC was the first (33.57), followed by PCL (7.00), PHBV (3.40), and RS (2.99). Therefore, the use of CC and PCL may produce less NO_2^--N.

Surface characteristics of carbon source

Changes in the molecular bonds and functional groups were detected by FT-IR spectroscopy before and after the carbon source release experiment (Figure 3). FT-IR showed the organic components in different carbon sources at the functional group level. The comparison of the functional groups between agricultural waste and BDPs was quite distinct. BDPs contained more C single bonds and more complex spectra than agricultural waste. However, the FT-IR spectra of the carbon sources of the same type were similar, this suggests the presence of similar organic components in the same type of carbon source, which is similar to the results of Liang et al. (2009). The strong absorption peaks of fresh RS and CC at 3404 and 3,331 cm^{-1} were assigned to the N-H stretching vibration, and the peak shape pair was wider (Figures 4A,B), indicating that RS and CC contained many free hydroxyl groups. The absorption peaks of RS, CC, PCL, and PHBV at 1,735, 1,731, 1,721, and 1,710 cm^{-1} represent C=O stretching (Wei et al., 2012), among which PCL and PHBV had the strongest absorption peaks. The absorption peaks of RS and CC at 1,513 and 1,514 cm^{-1}, respectively, belong to amide bands I and II of cellular proteins (Munir and Jamil, 2018). The absorption peaks of fresh RS and CC at 1,374 cm^{-1} were attributed to the bending vibration of-CH3. Comparing the fresh and used carbon sources, the spectral morphology of FT-IR between RS and CC is more similar than that between PCL and PHBV, RS and CC with little change in peak position. However, the weak peak at 832 cm^{-1} disappeared in RS-used, indicating that many ring structures of fresh RS were destroyed during the carbon release experiment. The spectral shapes of fresh PCL and PCL-used samples were similar (Figures 3C,D), and the shapes and positions of the characteristic peaks did not change remarkably. PCL-used showed a decline in peak at 2,943 cm^{-1}, and a peak of PHBV-used at 3,401 cm^{-1} belonged to the weak peak O-H, showing that metabolites containing hydroxyl groups were generated as a result of hydrolytic degradation (Chu and Wang, 2011). The significant peaks of PCL and PHBV located at 1,416 and 1,408 cm^{-1}, respectively, indicate the presence of proteins, and Guo et al. (2022) also observed the same phenomenon. When using PCL as carbon source, Chu and Wang (2011) found that the effluent contained proteins and soluble microbial by-products, namely organic compounds derived from microbial metabolites.

Figure 4 shows the SEM images of the four carbon sources and the distribution of C before and after the carbon source release experiment (Since BDPs cannot be observed clearly at 5, 100 μm was chosen). The surfaces of agricultural waste were rougher than those of BDPs, with more convex and porous structures, both before and after the experiment. This is consistent with the results of the specific surface area and pore volume of the fresh carbon sources, which were higher for agricultural waste than for BDPs (Table 1). Carbon sources with a larger specific surface area may accelerate the denitrification process and allow more bacteria to attach to it, as reported in the study by Ovez (2006). The surfaces of the PCL and PHBV were relatively smooth (Figures 4C,D). The pore structure and pore size of RS and CC increased significantly after carbon source release (Figures 4A,B). Gao et al. (2022) also observed the same phenomenon. This change is caused by the fact that agricultural waste contains crude fiber or lignin, which makes it difficult to degrade, and provides more pore structure with soluble substances, which may also be the reason for the large amount of carbon released from agricultural waste. The structure of RS-used is slightly loose, but the surface structure of CC-used is uniform and relatively compact, and still maintains a stable physical

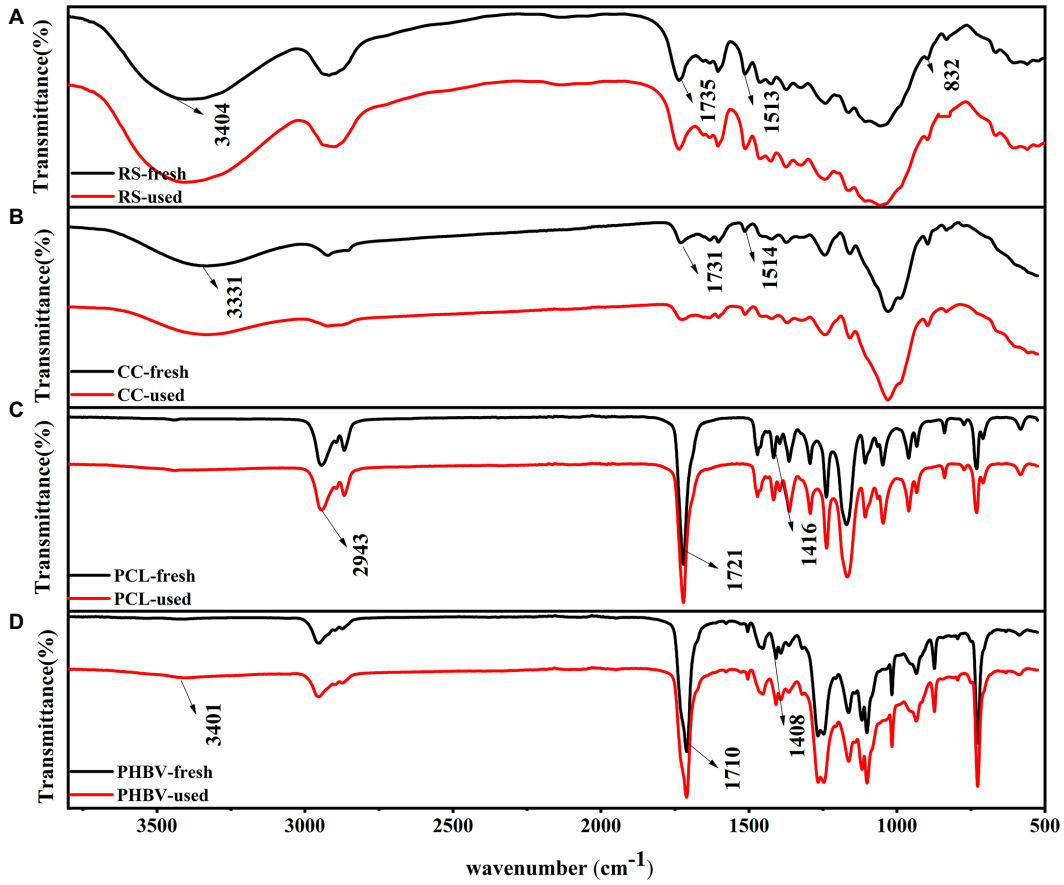

FIGURE 3
Comparison of FT-IR spectra of fresh and used carbon sources. **(A)** RS; **(B)** CC; **(C)** PCL; **(D)** PHBV.

structure, which indicates that the RS structure is not strong enough. The PCL and PHBV showed significant traces of corrosion shedding and partial protrusions; similar to the result observed by Chu and Wang (2013). The green dots represent the elemental C on the surface of the carbon source. It can be argued that, compared to the fresh carbon sources, the distribution intensity of the C element in the carbon source post release increased to varying degrees. Fresh RS and CC accounted for 45.71% and 65.72%, respectively of the total atomic distribution, which significantly increased to 77.62% and 72.90%, respectively, post release. The atomic ratios of PCL-fresh and PHBV-fresh C were 76.04% and 73.44%, respectively, which increased to 79.13% and 76.51%, respectively, post release. RS and CC were more densely distributed C elements than PCL and PHBV, possibly because RS and CC were partially decomposed during carbon release, resulting in an increased surface area (Zhang et al., 2007).

Operation performance of denitrification process based on carbon sources

Nitrogen removal performance

The nitrate removal performance of the continuous flow systems filled with different carbon sources within 180 h is shown in Figure 5. During the entire experiment, influent NO_3^--N remained at approximately 30 mg/L, while the effluent NO_3^--N concentration exhibited a downward trend, indicating that all four carbon sources could provide electron donors for the denitrification process (Figure 5A). The average NREs of CC, PCL, RS, and PHBV was 70.80%, 53.64%, 42.51%, and 41.35%, respectively (Figure 5B), CC had the highest denitrification efficiency. The lower NRE of RS and PHBV may be related to their high butyrate levels, which limit the denitrification rate (Figure 2C). The FT-IR (Figure 3A) and SEM (Figure 4A) results also indicated that the structure of RS was damaged after the carbon source release experiment, which could lead to its lower NRE. The high NRE results for CC and PCL corresponded to their higher DOC release in the immersion experiment (Figure 2A). In all experimental groups, the NRE showed a trend of a rapid increase in the first 40 h, followed by a decreasing trend during 40–160 h, and high NRE was maintained from 160 h to 180 h. The maximum NRE of the four reactors were RS 67.13% (160 h), CC 84.12% (176 h), PCL 73.26% (168 h) and PHBV 56.39% (168 h), respectively. CC always had the highest NRE within 180 h, this may be because the CC structure was more compact and rich in pore structures as indicated by SEM (Figure 4C). This indicated that CC was more conducive to the adaptation and sustainable action of denitrifiers in the environment. In addition, the NRE of CC reached more than 60% faster than that of several other systems (CC 24 h; PCL 80 h; RS 144 h; and PHBV never reached). This may be because the higher AC content and lower butyrate content after CC immersion were more conducive to improving denitrification efficiency. In the RS and PHBV systems, the

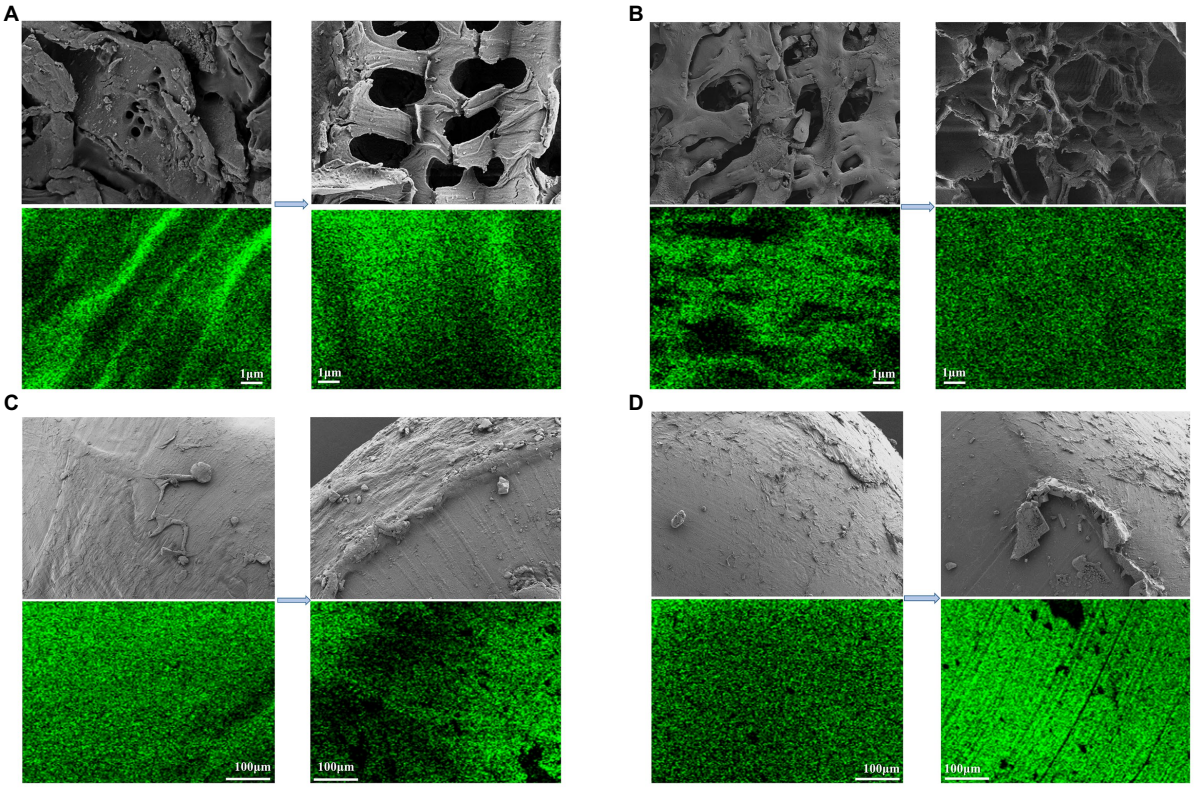

FIGURE 4
Distribution of SEM images and C of each carbon source before and after carbon released. **(A)** RS; **(B)** CC; **(C)** PCL; **(D)** PHBV.

residual amount of NO_3^--N increased, and the NRE removal trend fluctuated during the experiment, which may be partly due to the partial disintegration of RS and PHBV during use. The SEM results (Figures 4A,D) also confirmed this result. Corrosion of RS and PHBV also affects microbial attachment and biofilm integrity, which may further inhibit denitrification rates. The disintegration of RS and PHBV will contribute to the discharge of denitrifying bacteria out of the system, affecting the continuous and efficient removal of nitrate nitrogen, which may indicate that CC and PCL have more advantages when the system is used for a long time.

The generation of NO_2^--N in all the systems during the entire experimental period is shown in Figure 5C. The production of NO_2^--N was lower than 0.5 mg/L, and no accumulation occurred. Among the four experimental groups, the average NO_2^--N production in RS was the highest (0.274 mg/L), which may be related to the high PA content in RS (Figure 2C). NO_2^--N concentration in CC was 0.217 mg/L lower than that in RS. Compared to PCL, PHBV had a slightly higher average NO_2^--N residual concentration (PHBV 0.204 mg/L; PCL 0.197 mg/L), which is consistent with the results of PA in SCFAs. This corresponds to the results of the AC/BA ratio. Agricultural waste CC with a higher AC/PA ratio produced less NO_2^--N than RS. This was also confirmed by the BDPs. PHBV with a lower AC/PA ratio produced more NO_2^--N than PCL. The production of NO_2^--N has also been reported in previous studies (Xia et al., 2022). This might be because, in the process of denitrification, nitrite reductase is inhibited due to the electron competition with NO_3^--N reductase, resulting in lower respiration of nitrite and thus a lower reduction rate of nitrite (Ge et al., 2012).

A decrease in TN was observed in all four experimental groups (Figure 5D). The effluent TN content slightly differed among all four groups. NO_3^--N occupies a large proportion in TN (78.86%–97.55%). The TN removal effect in the CC group was more significant (67.33%), followed by PCL, PHBV, and RS (51.23%, 41.1%, and 39.34%, respectively), which was consistent with the NRE results. As shown in Figure 5E, all four systems achieved good NH_4^+-N removal, and the average concentrations were < 0.01 mg/L with a descending order of PCL (73.12%) > CC (61.98%) > PHBV (34.20%) > RS (23.45%). This indicated that almost no dissimilatory nitrate reduction to ammonia occurred in any of the denitrification processes.

Utilization of organic matter

The COD content was high in the early stage of the experiment, and the decline rate was rapid in the first 80 h and tended to be low in the later stage (Figure 5F). Yang et al. (2015) also reported similar results. The denitrification efficiency was low at the beginning of the experiment, and the complete denitrification process was not carried out, and consequently, non-utilization of the released carbon sources led to the high accumulation of COD in the effluent water. With the growth of the denitrifying bacteria, the denitrification rate increased and the COD removal efficiency also increased rapidly. Subsequently, the systems maintained a high NRE, the release of the solid carbon source and consumption by denitrifying bacteria reached a balance, and the COD content of the effluent reached a stable state. The experimental effluent COD of the system with agricultural waste as the carbon source was higher than that of the system with BDPs. The average effluent COD content of each system was the highest with CC (9.52 mg/L),

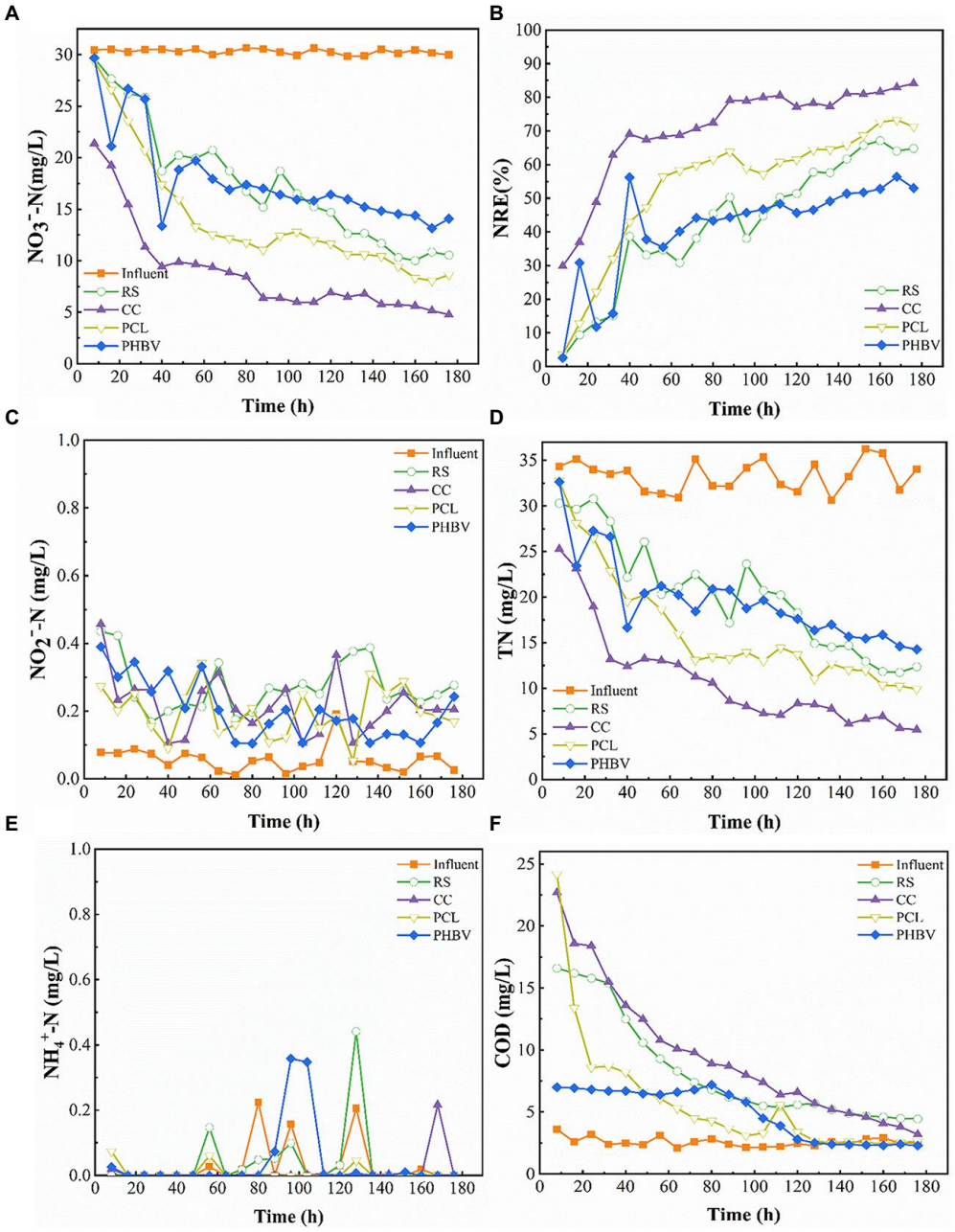

FIGURE 5
Nitrate removal performance of different carbon sources. **(A)** NO_3^--N concentrations; **(B)** Nitrate removal efficiency (NRE); **(C)** NO_2^--N accumulation; **(D)** Total nitrogen (TN) concentrations; **(E)** NH_4^+-N accumulation; **(F)** Chemical oxygen demand (COD) accumulation.

followed by RS (8.25 mg/L), PCL (5.78 mg/L), and PHBV (4.90 mg/L). The effluent COD of the four systems in the experiment was stable within the range 2.30–4.45 mg/L at the later stage of the experiment, which met the primary discharge standard of mariculture water (<10 mg/; SC/T 9103-2007, 2007).

Microbial community analysis

Analysis of bacterial community diversity and structure

The alpha diversity index results are shown in Figure 6B. A total of 58,054–60,965 effective sequences were obtained after the quality control process of raw sequence data (RS 60635, CC 58054, PCL 59365, and PHBV 60965), and the coverage rates of the four samples were greater than 0.99, indicating the high reliability and representativeness of the determination results. The Sobs index showed that the number of microorganisms observed in RS and CC was higher than that in PCL and PHBV. Chao and Ace indices in agricultural waste were higher than those in BDPs, indicating that higher cell flora proliferated by the use of RS and CC, and agricultural waste had higher species richness. The Simpson index showed that the species uniformity of BDPs was higher than that of agricultural waste.

According to linear discriminant analysis (LDA), Figure 6A shows that Firmicutes, Bacteroidetes, and Proteobacteria were the dominant

phyla in RS, while Desulfobacterota and Spirochaeota were the dominant phyla in CC. The dominant phyla in PCL and PHBV were the Verrucomicrobiota and Planctomycetota, respectively. The relative abundances of Proteobacteria in RS (74.39%) and CC (75.44%) were higher than those in PCL (1.59%) and PHBV (0.44%) (Figure 6B). Proteobacteria that include many denitrifying bacteria is the most important phylum in the biological denitrification system (Si et al., 2018), which might be the reason for the high NRE of agricultural wastes. Firmicutes were more abundant in PCL (96.84%) and PHBV (99.36%) than in RS (7.20%) and CC (7.11%). Some strains of Firmicutes produce extracellular enzymes that decompose biodegradable polymers (Chu and Wang, 2016), contributing significantly to hydrolysis and acidification (He et al., 2018), which might indicate that BDPs are beneficial for carbon source supplementation and nitrogen removal in denitrification. The primary difference in Proteobacteria between agricultural waste and BDPs was seen in the population of *Pseudomonas* (Figure 6D). Its contents in PCL and PHBV were 0.08% and 0.02%, respectively, which increased to 74.39% and 75.44% in RS and CC, respectively. The high *Pseudomonas* content in CC was consistent with the high NRE results

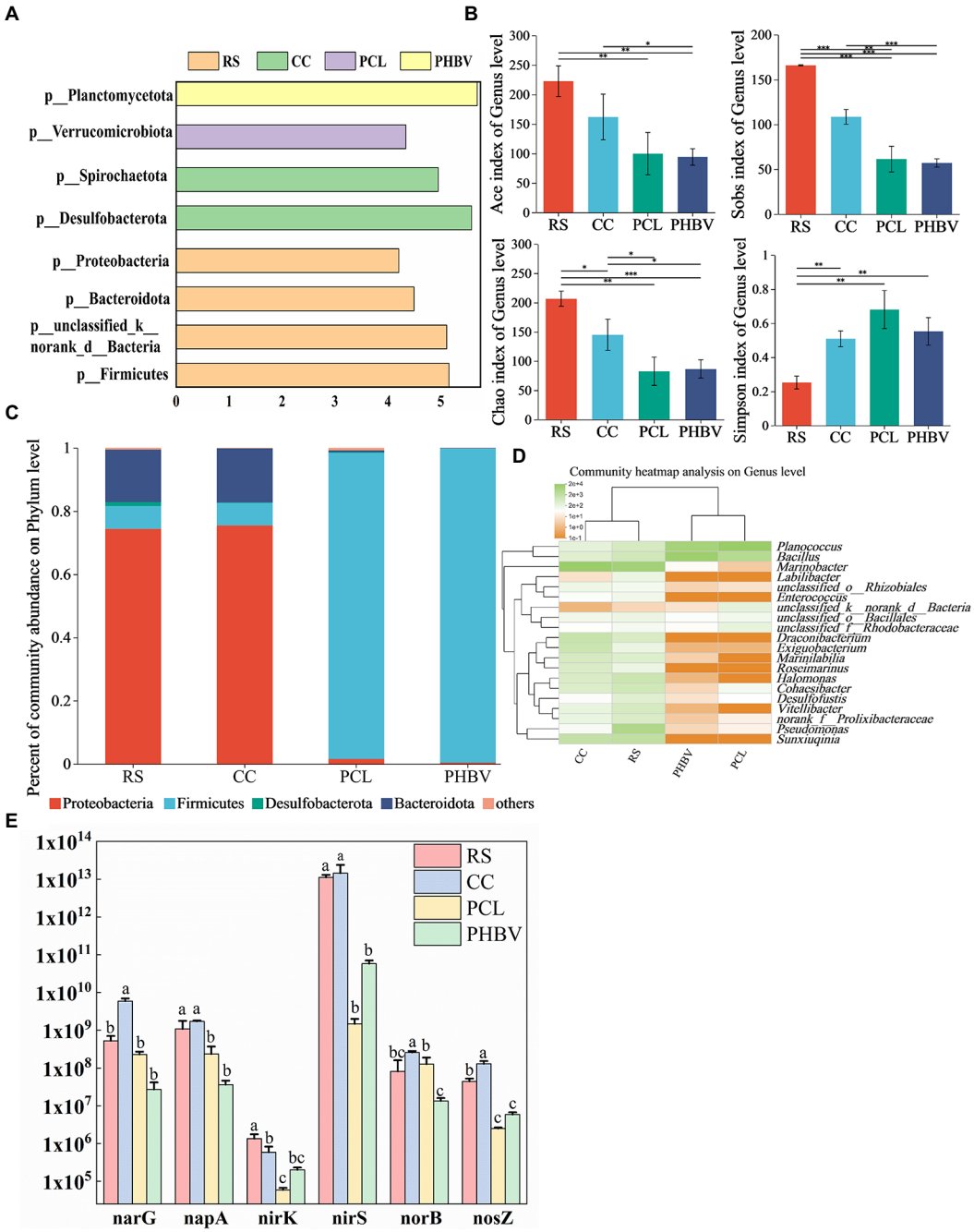

FIGURE 6
Composition and structure of microbial and abundance of nitrogen-functional genes. **(A)** The linear discriminant analysis (LDA) analysis at phylum level; **(B)** Relative abundance at phylum level; **(C)** Alpha diversity index of microbial community at genus level; **(D)** Clustering heat maps at the level of the first 20 genera; **(E)** Differences in the abundance of the same gene with different carbon sources.

of CC. Studies have shown that *Pseudomonas* can use soluble organic matter for denitrification (Mergaert et al., 2001). The difference in Firmicutes between agricultural waste and BDPs was in *Bacillus* population. Its concentrations in system with PCL and PHBV were 15.62% and 60.90%, respectively, but reduced to only 2.89% and 1.14% with RS and CC, respectively (Figure 6D). The relative abundances of Bacteroidetes in systems with RS, CC, PCL, and PHBV were 6.60, 17.07%, 0.53%, and 0.08%, respectively (Figure 6C). Studies have shown that Bacteroidetes are related to the degradation of macromolecular organic matter, such as starch, fiber, and protein (Fang et al., 2020). A higher Bacteroidetes content is beneficial for organic matter degradation (Jiang et al., 2021) and COD removal efficiency (Liang et al., 2020). These results indicate that compared to BDPs, the microbial community function in agricultural waste was more focused on nitrate removal and organic matter degradation.

Nitrogen functional genes of the denitrification bioreactor

Ji et al. (2012) reported that *narG* and *napA* were key functional genes involved in nitrate to nitrite transformation and participated in the first step of denitrification. *nirK* and *nirS* are the marker genes from nitrite to nitric oxide, which is the second step of denitrification. *NorB* is involved in the third step of denitrification, which is the functional gene of nitric oxide to nitrous oxide. *NosZ* is the signature gene for nitrous oxide to nitrogen, the final step in denitrification. Therefore, the q-PCR method was used to measure the absolute abundance of nitrogen functional genes in different experimental groups. The abundance of different genes varied greatly among the four carbon sources (Figure 6E). Six genes showed the highest expression in CC, among which *narG*, *norB* and *nosZ* were significantly higher than other groups. With the exception of *norB*, the other genes were expressed in RS second to CC, indicating the advantage of agricultural waste in reducing nitrate nitrogen concentration. The absolute abundance of *nosZ* in agricultural waste is higher than that of BDPs, which may be related to the high abundance of *Pseudomonas* sp. in CC and *Marinobacter* sp. in RS (Krishnani, 2010). *NorB* gene had the highest copy number in CC, higher than RS in PCL, while PHBV content was the lowest. *NirS* showed the highest abundance in the four systems, *nirK* was lower than other genes in all systems. The lower oxygen and higher organic matter in the reactor may be the reasons for the adverse growth of *nirK* (Chen et al., 2021). This may indicate that CC and PCL can reduce nitrite nitrogen accumulation in more pairs. In general, the abundance of nitrogen-functional genes with different carbon sources was consistent with the results of nitrogen removal performance among biological systems.

Conclusion

In this study, carbon release process and denitrification performance of agricultural waste (reed straw (RS), corn cob (CC)) and biodegradable natural or synthetic polymers (BDPs) (polycaprolactone (PCL) and poly3-hydroxybutyrate-hydroxypropionate (PHBV)) in synthetic marine recirculating quaculture wastewater were studied comprehensively. Agricultural waste released more organic matter than BDPs, and acetic acid was the largest component of the SCFA release. The four carbon sources can significantly enhance denitrification, and CC has the strongest denitrification removal effect. The primary microbial community in agricultural waste was Proteobacteria, whereas in BDPs, it was Firmicutes. Among the six genes, *nirS* and *nirK* were the most abundant and least abundant functional genes among the four carbon sources, respectively. Therefore, CC is found to be more feasible as additional carbon source for denitrification treatment of marine recirculating aquaculture wastewater.

Data availability statement

The datasets presented in this study can be found in online repositories. The names of the repository/repositories and accession number (s) can be found at: https://www.ncbi.nlm.nih.gov/genbank/, SRP864076.

Author contributions

YF: investigation, writing-original draft, and data curation. LW: resources, writing-review and editing. ZY: investigation and formal analysis. ZC: conceptualization, methodology, and funding acquisition. KQ: methodology, writing-review and editing. DW: software and data curation. ZW: methodology and resources. SZ: formal analysis and data curation. HC: software, writing-original draft, writing-review and editing. All authors contributed to the article and approved the submitted version.

Funding

This work was supported by the National Key Research and Development Program of China (2020YFD0900603 and 2020YFD0900600); Central Public-interest Scientific Institution Basal Research Fund, CAFS (No. 2020TD49 and 2021XT0604); and Marine S&T Fund of Shandong Province for Pilot National Laboratory for Marine Science and Technology (Qingdao) (No.2021QNLM050103-3).

Conflict of interest

The authors declare that the research was conducted in the absence of any commercial or financial relationships that could be construed as a potential conflict of interest.

Publisher's note

Supplementary material

The Supplementary material for this article can be found online at: https://www.frontiersin.org/articles/10.3389/fmicb.2023.1141362/full#supplementary-material

References

APHA, AWWA, and WEF (2012). *Standard Methods for the Examination of Water and Wastewater*, *22nd ed.*, Washington DC: American Public Health Association.

Atasoy, M., Owusu-Agyeman, I., Plaza, E., and Cetecioglu, Z. (2018). Bio-based volatile fatty acid production and recovery from waste streams: current status and future challenges. *Bioresour. Technol.* 268, 773–786. doi: 10.1016/j.biortech.2018.07.042

Bulgarelli, D., Rott, M., Schlaeppi, K., ver Loren van Themaat, E., Ahmadinejad, N., Assenza, F., et al. (2012). Revealing structure and assembly cues for Arabidopsis root-inhabiting bacterial microbiota. *Nat.* 488, 91–95. doi: 10.1038/nature11336

Chen, Z., Chang, Z., Qiao, L., Wang, J., Liu, Y., Song, X., et al. (2021). Effect of hydraulic retention time on solid-phase denitrification reactor in recirculating aquaculture system. *Aquac.* 543:736928. doi: 10.1016/j.aquaculture.2021.736928

Chen, Y., Guo, L., Zhang, J., Zhao, Y., Gao, M., and She, Z. (2016). Interaction of short-chain fatty acids carbon source on denitrification. *Environ. Technol.* 15, 1–11. doi: 10.1080/09593330.2016.1240714

Chen, Z., Liu, J., Wu, M., Xie, X., Wu, J., and Wei, W. (2012). Differentiated response of denitrifying communities to fertilization regime in Paddy soil. *Microb. Ecol.* 63, 446–459. doi: 10.1007/s00248-011-9909-5

Chu, L., and Wang, J. (2011). Comparison of polyurethane foam and biodegradable polymer as carriers in moving bed biofilm reactor for treating wastewater with a low C/N ratio. *Chemosphere* 83, 63–68. doi: 10.1016/j.chemosphere.2010.12.077

Chu, L., and Wang, J. (2013). Denitrification performance and biofilm characteristics using biodegradable polymers PCL as carriers and carbon source. *Chemosphere* 91, 1310–1316. doi: 10.1016/j.chemosphere.2013.02.064

Chu, L., and Wang, J. (2016). Denitrification of groundwater using PHBV blends in packed bed reactors and the microbial diversity. *Chemosphere* 155, 463–470. doi: 10.1016/j.chemosphere.2016.04.090

Constantin, H., and Fick, M. (1997). Influence of C-sources on the denitrification rate of a high-nitrate concentrated industrial wastewater. *Water Res.* 31, 583–589. doi: 10.1016/S0043-1354(96)00268-0

Cui, Y., Zhao, B., Xie, F., Zhang, X., Zhou, A., Wang, S., et al. (2022). Study on the preparation and feasibility of a novel adding-type biological slow-release carbon source. *J. Environ. Manag.* 316:115236. doi: 10.1016/j.jenvman.2022.115236

Davidson, J., Good, C., Williams, C., and Summerfelt, S. T. (2017). Evaluating the chronic effects of nitrate on the health and performance of post-smolt Atlantic salmon Salmo salar in freshwater recirculation aquaculture systems. *Aquac. Eng.* 79, 1–8.

De Schryver, P., Crab, R., Defoirdt, T., Boon, N., and Verstraete, W. (2008). The basics of bio-flocs technology: the added value for aquaculture. *Aquac.* 277, 125–137. doi: 10.1016/j.aquaculture.2008.02.019

Edgar, R. C. (2013). UPARSE: highly accurate OTU sequences from microbial amplicon reads. *Nat. Methods* 10, 996–998. doi: 10.1038/nmeth.2604

Elefsiniotis, P., Wareham, D. G., and Smith, M. O. (2004). Use of volatile fatty acids from an acid-phase digester for denitrification. *J. Biotechnol.* 114, 289–297. doi: 10.1016/j.jbiotec.2004.02.016

Epsztein, R., Beliavski, M., Tarre, S., and Green, M. (2016). High-rate hydrogenotrophic denitrification in a pressurized reactor. *Chem. Eng. J.* 286, 578–584. doi: 10.1016/j.cej.2015.11.004

Fajardo, C., Mosquera-Corral, A., Campos, J. L., and Méndez, R. (2012). Autotrophic denitrification with sulphide in a sequencing batch reactor. *J. Environ. Manag.* 113, 552–556. doi: 10.1016/j.jenvman.2012.03.018

Fang, D., Wu, A., Huang, L., Shen, Q., Zhang, Q., Jiang, L., et al. (2020). Polymer substrate reshapes the microbial assemblage and metabolic patterns within a biofilm denitrification system. *Chem. Eng. J.* 387, 124–128.

Gao, S., Gong, W., Zhang, K., Li, Z., Wang, G., Yu, E., et al. (2022). Effectiveness of agricultural waste in the enhancement of biological denitrification of aquaculture wastewater. *PeerJ* 28:13339. doi: 10.7717/peerj.13339

GB 17378.7-1998 (1999). *Specification for Marine Monitoring. Part 4, Seawater Analysis*. Beijing: Standards Press of China.

Ge, S., Peng, Y., Wang, S., Lu, C., Cao, X., and Zhu, Y. (2012). Nitrite accumulation under constant temperature in anoxic denitrification process: the effects of carbon sources and COD/NO_3-N. *Bioresour. Technol.* 114, 137–143. doi: 10.1016/j.biortech.2012.03.016

Guo, Y., Guo, L., Jin, C., Zhao, Y., Gao, M., Ji, J., et al. (2022). Comparison of primary and secondary sludge carbon sources derived from hydrolysis or acidogenesis for nitrate reduction and denitrification kinetics: organics utilization and microbial community shift. *Environ. Res.* 212:113403. doi: 10.1016/j.envres.2022.113403

He, Q., Zhang, D., Main, K., Feng, C., and Ergas, S. J. (2018). Biological denitrification in marine aquaculture systems: A multiple electron donor microcosm study. *Bioresour. Technol.* 263, 340–349. doi: 10.1016/j.biortech.2018.05.018

Henry, S., Bru, D., Stres, B., Hallet, S., and Philippot, L. (2006). Quantitative detection of the nosZ gene, encoding nitrous oxide reductase, and comparison of the abundances of 16S rRNA, narG, nirK, and nosZ genes in soils. *Appl. Env. Microbiol.* 72, 5181–5189. doi: 10.1128/AEM.00231-06

Ji, G. D., Wang, R. J., Zhi, W., et al. (2012). Distribution patpatterns ofnitrification functional genes and microbial floras in multimedia constructed wetlands. *Ecol. Eng.* 44, 179–188. doi: 10.1016/j.ecoleng.2012.03.015

Jia, L., Gou, E., Liu, H., Lu, S., Wu, S., and Wu, H. (2019). Exploring utilization of recycled agricultural biomass in constructed wetlands: characterization of the driving force for high-rate nitrogen removal. *Environ. Sci. Technol.* 53, 1258–1268. doi: 10.1021/acs.est.8b04871

Jiang, C., Xu, S., Wang, R., Feng, S., Zhou, S., Wu, S., et al. (2019). Achieving efficient nitrogen removal from real sewage via nitrite pathway in a continuous nitrogen removal process by combining free nitrous acid sludge treatment and DO control. *Water Res.* 161, 590–600. doi: 10.1016/j.watres.2019.06.040

Jiang, L., Zhang, Y., Shen, Q., Mao, Y., Zhang, Q., and Ji, F. (2021). The metabolic patterns of the complete nitrates removal in the biofilm denitrification systems supported by polymer and water-soluble carbon sources as the electron donors. *Bioresour. Technol.* 342:126002. doi: 10.1016/j.biortech.2021.126002

Johann, T., Christopher, N., and Schroeder, J. P. (2018). Impact of hydraulic retention time, backflushing intervals, and C/N ratio on the SID-reactor denitrification performance in marine RAS. *Aquac.* 496, 112–122. doi: 10.1016/j.aquaculture.2018.07.004

Krishnani, K. K. (2010). Detection and diversity of nitrifying and denitrifying functional genes in coastal aquaculture. *Aquac.* 302, 57–70. doi: 10.1016/j.aquaculture.2010.01.024

Li, C., Cao, J., Ren, H., Li, Y., and Tang, S. (2015). Comparison on kinetics and microbial community among denitrification process fed by different kinds of volatile fatty acids. *Process Biochem.* 50, 447–455. doi: 10.1016/j.procbio.2015.01.005

Li, P., Wang, C., Liu, G., Luo, X., Rauan, A., Zhang, C., et al. (2022). A hydroponic plants and biofilm combined treatment system efficiently purified wastewater from cold flowing water aquaculture. *Sci. Total Environ.* 821:153534. doi: 10.1016/j.scitotenv.2022.153534

Liang, Y., Wang, Q., Huang, L., Liu, M., Wang, N., and Chen, Y. (2020). Insight into the mechanisms of biochar addition on pollutant removal enhancement and nitrous oxide emission reduction in subsurface flow constructed wetlands: microbial community structure, functional genes and enzyme activity. *Bioresour. Technol.* 307:123249. doi: 10.1016/j.biortech.2020.123249

Liang, R., Yuan, H., Xi, G., and Zhou, Q. (2009). Synthesis of wheat straw-g-poly (acrylic acid) superabsorbent composites and release of urea from it. *Carbohydr. Polym.* 77, 181–187. doi: 10.1016/j.carbpol.2008.12.018

Ling, Y., Yan, G. K., Wang, H. Y., Dong, W. Y., Wang, H., Chang, Y., et al. (2021). Preliminary carbon sources and release mechanism of dissolved organic compounds from six agricultural wastes. *Environ. Sci.* 5, 2422–2431. (in Chinese)

Martins, C. I. M., Eding, E. H., Verdegem, M. C. J., Heinsbroek, L. T. N., Schneider, O., Blancheton, J. P., et al. (2010). New developments in recirculating aquaculture systems in Europe: a perspective on environmental sustainability. *Aquac. Eng.* 43, 83–93. doi: 10.1016/j.aquaeng.2010.09.002

Mergaert, J., Boley, A., Cnockaert, M. C., Müller, W. R., and Swings, J. (2001). Identity and potential functions of heterotrophic bacterial isolates from a continuous-Upflow fixed-bed reactor for denitrification of drinking water with bacterial polyester as source of carbon and electron donor. *Syst. Appl. Microbiol.* 24, 303–310. doi: 10.1078/0723-2020-00037

Munir, S., and Jamil, N. (2018). Polyhydroxyalkanoates (PHA) production in bacterial co-culture using glucose and volatile fatty acids as carbon source. *J. Basic Microbiol.* 58, 247–254. doi: 10.1002/jobm.201700276

Nyberg, U., Andersson, B., and Aspegren, H. (1996). Long-term experiences with external carbon sources for nitrogen removal. *Water Sci. Technol.* 33, 109–116. doi: 10.2166/wst.1996.0314

Ovez, B. (2006). Batch biological denitrification using Arundo donax, Glycyrrhiza glabra, and Gracilaria verrucosa as carbon source. *Process Biochem.* 41, 1289–1295. doi: 10.1016/j.procbio.2005.12.030

Palmer, K., Biasi, C., and Horn, M. A. (2011). Contrasting denitrifier communities relate to contrasting N_2O emission patterns from acidic peat soils in arctic tundra. *ISME J.* 6, 1058–1077. doi: 10.1038/ismej.2011.172

Rosales, E., Meijide, J., Pazos, M., and Sanromán, M. A. (2017). Challenges and recent advances in biochar as low-cost biosorbent: from batch assays to continuous-flow systems. *Bioresour. Technol.* S0960852417309884, 176–192. doi: 10.1016/j.biortech.2017.06.084

SC/T 9103-2007 (2007), *Water Discharge Requirements for Mariculture*. Ministry of Agriculture of the People's Republic of China. Water Drainage Standard for Water Drainage Standard for Sea Water Mariculture. SC/T 9103-2007, 2007. (in Chinese)

Si, Z., Song, X., Wang, Y., Cao, X., Zhao, Y., Wang, B., et al. (2018). Intensified heterotrophic denitrification in constructed wetlands using four solid carbon sources: denitrification efficiency and bacterial community structure. *Bioresour. Technol.* 267, 416–425. doi: 10.1016/j.biortech.2018.07.029

Stackebrandt, E., and Goebel, B. M. (1994). Taxonomic note: a place for DNA-DNA Reassociation and 16S rRNA sequence analysis in the present species definition in bacteriology. *Int. J. Syst. Bacteriol.* 44, 846–849.

Wang, H., Chen, N., Feng, C., and Deng, Y. (2021). Insights into heterotrophic denitrification diversity in wastewater treatment systems: Progress and future prospects

based on different carbon sources. *Sci. Total Environ.* 780:146521. doi: 10.1016/j.scitotenv.2021.146521

Wang, Q., Garrity, G. M., Tiedje, J. M., and Cole, J. R. (2007). Naive Bayesian classifier for rapid assignment of rRNA sequences into the new bacterial taxonomy. *Appl. Environ. Microbiol.* 73, 5261–5267. doi: 10.1128/AEM.00062-07

Wei, Z., Long, Y., Liu, X., et al. (2012). Effects of amylose/amylopectin ratio on starch-based superabsorbent polymers. *Carbohydr. Polym.* 87, 1583–1588. doi: 10.1016/j.carbpol.2011.09.060

Wu, W., Yang, F., and Yang, L. (2012). Biological denitrification with a novel biodegradable polymer as carbon source and biofilm carrier. *Bioresour. Technol.* 118, 136–140. doi: 10.1016/j.biortech.2012.04.066

Xia, L., Li, X., Fan, W., and Wang, J. (2022). Denitrification performance and microbial community of bioreactor packed with PHBV/PLA/rice hulls composite. *Sci. Total Environ.* 803:150033. doi: 10.1016/j.scitotenv.2021.150033

Xiong, R., Yu, X., Yu, L., Peng, Z., Cheng, L., Li, T., et al. (2019). Biological denitrification using polycaprolactone-peanut shell as slow-release carbon source treating drainage of municipal WWTP. *Chemosphere* 235, 434–439. doi: 10.1016/j.chemosphere.2019.06.198

Xiong, R., Yu, X., Zhang, Y., Peng, Z., Yu, L., Cheng, L., et al. (2020). Comparison of agricultural wastes and synthetic macromolecules as solid carbon source in treating low carbon nitrogen wastewater. *Sci. Total Environ.* 739:139885. doi: 10.1016/j.scitotenv.2020.139885

Yang, X. L., Jiang, Q., Song, H. L., Gu, T. T., and Xia, M. Q. (2015). Selection and application of agricultural wastes as solid carbon sources and biofilm carriers in MBR. *J. Hazard. Mater.* 283, 186–192. doi: 10.1016/j.jhazmat.2014.09.036

Zhang, L. S., Wu, W. Z., and Wang, J. L. (2007). Immobilization of activated sludge using improved polyvinyl alcohol (PVA) gel. *J. Environ. Sci.* 19, 1293–1297. doi: 10.1016/S1001-0742(07)60211-3

Zhao, Y., Wang, H., Dong, W., Chang, Y., Yan, G., Chu, Z., et al. (2020). Nitrogen removal and microbial community for the treatment of rural domestic sewage with low C/N ratio by a/O biofilter with Arundo donax as carbon source and filter media. *J. Water Process Eng.* 37:101509. doi: 10.1016/j.jwpe.2020.101509

Zhao, Y., Zhang, B., Feng, C., Huang, F., Zhang, P., Zhang, Z., et al. (2012). Behavior of autotrophic denitrification and heterotrophic denitrification in an intensified biofilm-electrode reactor for nitrate-contaminated drinking water treatment. *Bioresour. Technol.* 107, 159–165. doi: 10.1016/j.biortech.2011.12.118

Zhu, S. M., Deng, Y. L., Ruan, Y. J., Guo, X. S., Shi, M. M., and Shen, J. Z. (2015). Biological denitrification using poly (butylene succinate) as carbon source and biofilm carrier for recirculating aquaculture system effluent treatment. *Bioresour. Technol.* 192, 603–610. doi: 10.1016/j.biortech.2015.06.021

Zou, S., Guan, L., Taylor, D. P., Kuhn, D., and He, Z. (2018). Nitrogen removal from water of recirculating aquaculture system by a microbial fuel cell. *Aquac.* 497, 74–81. doi: 10.1016/j.aquaculture.2018.07.036

frontiers | Frontiers in Microbiology

TYPE Original Research
PUBLISHED 28 April 2023
DOI 10.3389/fmicb.2023.1186819

OPEN ACCESS

EDITED BY
Zhaoming Zheng,
Beijing University of Technology, China

REVIEWED BY
Bin Ma,
Hainan University, China
Xuliang Zhuang,
Chinese Academy of Sciences, China

*CORRESPONDENCE
Yandong Yang
✉ yangyandong@qut.edu.cn

RECEIVED 15 March 2023
ACCEPTED 10 April 2023
PUBLISHED 28 April 2023

CITATION
Yang Y, Long Y, Xu J, Liu S, Liu L, Liu C and Tian Y (2023) Achieving robust and highly efficient nitrogen removal in a mainstream anammox reactor by introducing low concentrations of readily biodegradable organics.
Front. Microbiol. 14:1186819.
doi: 10.3389/fmicb.2023.1186819

Achieving robust and highly efficient nitrogen removal in a mainstream anammox reactor by introducing low concentrations of readily biodegradable organics

Yandong Yang[1,2]*, Yanan Long[1], Jiarui Xu[1], Shichong Liu[1], Lei Liu[1], Changqing Liu[1] and Yong Tian[1]

[1]School of Environmental and Municipal Engineering, Qingdao University of Technology, Qingdao, China, [2]Engineering Research Center of Concrete Technology Under Marine Environment, Ministry of Education, Qingdao, China

In this study, an anammox reactor was operated to treat low-strength ($NH_4^+ + NO_2^-$, 25–35 mg/L) wastewater without (phase I) or with (phase II) readily biodegradable chemical oxygen demand (rbCOD). In phase I, although efficient nitrogen removal was achieved at the beginning, nitrate accumulated in the effluent after long-term operation (75 days), resulting in a decrease in the nitrogen removal efficiency to 30%. Microbial analysis revealed that the abundance of anammox bacteria decreased from 2.15 to 1.78%, whereas that of nitrite-oxidizing bacteria (NOB) increased from 0.14 to 0.56%. In phase II, rbCOD, in terms of acetate, was introduced into the reactor with a carbon/nitrogen ratio of 0.9. The nitrate concentration in the effluent decreased within 2days. Advanced nitrogen removal was achieved in the following operation, with an average effluent total nitrogen of 3.4mg/L. Despite the introduction of rbCOD, anammox pathway still dominated to the nitrogen loss. High-throughput sequencing indicated that high anammox abundance (2.48%) further supports its dominant position. The improvement in nitrogen removal was attributed to the enhanced suppression of NOB activity, simultaneous nitrate polishing through partial denitrification and anammox, and promotion of sludge granulation. Overall, the introduction of low concentrations of rbCOD is a feasible strategy for achieving robust and efficient nitrogen removal in mainstream anammox reactors.

KEYWORDS

anammox, partial denitrification, mainstream, nitrogen removal, readily biodegradable organics

1. Introduction

Autotrophic nitrogen removal from municipal wastewater through partial nitritation/anammox (PN/A) has gained considerable attention over the past decade as it can bring an energy-neutral wastewater treatment plant (WWTP) (Kartal et al., 2010; Cao et al., 2017). Different process types based on the number of stages (i.e., single- or two-stage) have been developed to employ PN/A in WWTPs. The two-stage PN/A system can optimize the partial nitritation (PN) and anammox processes in two separate reactors, which favor the enrichment of different microorganisms (Isanta et al., 2015; Cao et al., 2017; Chen et al.,

2020). Therefore, the two-stage PN/A process typically has a higher nitrogen removal rate than the single-stage PN/A process (Liu et al., 2018).

To date, the full-scale application of mainstream PN/As remains challenging. One of the major concerns is the high effluent nitrate concentration, which results in total nitrogen (TN) exceeding the discharge standard (Zhuang et al., 2022). In the two-stage PN/A process, nitrate can be generated both in the first-stage PN reactor owing to the activity of nitrite-oxidizing bacteria (NOB) and in the second-stage anammox reactor owing to the anammox and undesired NOB activities. According to the recent literature, nitrate production in the first-stage PN reactor can be minimized because of the development of various NOB suppression strategies, such as intermittent aeration, application of an ultra-low sludge retention time (SRT), and side-stream sludge treatment with inhibitors (Gilbert et al., 2014; Regmi et al., 2014; Wang et al., 2014, 2021). Whereas the second-stage anammox reactor became a major source of nitrate generation. Excessive nitrate production in anammox reactors due to undesired NOB activity has been reported in different reactor configurations, including sequencing batch reactors (SBR), completely stirred tank reactors, and expanded granular sludge blanket reactors (Sánchez Guillén et al., 2016; Liu et al., 2018; Zhang et al., 2019; Díaz et al., 2020; Li W. et al., 2020). Most of the NOB suppression methods developed in first-stage PN reactors are not applicable to second-stage anammox reactors because they may inhibit anammox activity. Therefore, strategies to reduce nitrate accumulation in anammox reactors must be investigated.

In early studies, readily biodegradable chemical oxygen demand (rbCOD) was considered a challenge for mainstream anammox processes, and hence, it should be eliminated by pretreatment as it can lead to the overgrowth of heterotrophs, which can outcompete anammox bacteria (Xu et al., 2015). However, recent studies have reported that the activities of anammox bacteria can be retained; in particular, nitrogen removal efficiencies can be improved to over 90% when anammox reactors were operated with an appropriate amount of rbCOD (C/N ratios of 0.5–1.5) (Li et al., 2016; Wang et al., 2019; Fu et al., 2021; Silveira et al., 2021; Chen et al., 2021a; He et al., 2023). However, most of these studies included wastewater treatment with high nitrogen concentrations (100–300 mg N/L), which can inhibit NOB growth due to the presences of free ammonia or free nitrous acid (Ge et al., 2015); consequently, excessive nitrate yield is negligible. It remains to be determined whether introducing rbCOD can resolve excessive nitrate production caused by NOB activity in mainstream anammox reactors. In addition, partial denitrification/anammox (PD/A) in anammox reactors can reduce the organic requirement for nitrogen removal and minimize the unfavorable effects of organics on anammox activity (Du et al., 2019). However, in most PD/A studies, ammonium and nitrate are the dominant nitrogen compounds in the influent (Du et al., 2019). In mainstream anammox reactors, nitrite is the main form of influent NO_x^- and nitrate is gradually produced by the anammox reaction. The status of PD/A in mainstream anammox reactors in presence of rbCOD has rarely been reported and requires further investigation (Chen et al., 2020; Zhuang et al., 2022).

In this study, a mainstream anammox reactor was established and operated, with and without rbCOD, in two phases. The nitrogen removal performance, process stability, microbial community, and sludge morphology of the two phases were compared. Based on these data, the influence of low concentrations of rbCOD on the mainstream anammox process was assessed, and the potential of nitrogen removal enhancement with low concentrations of rbCOD was evaluated.

2. Materials and methods

2.1. Experimental setup

Mainstream anammox treatment was performed in a 10 L SBR (Figure 1), which was seeded with sludge collected from a lab-scale anammox reactor treating high nitrogen wastewater. After inoculation, the initial biomass concentration in the reactor was 4.9 g/L. The SBR was operated for three cycles per day. Each cycle consisted of 10 min of feeding (volume exchange ratio of 50%), 360 min of anoxic mixing, 30 min of settling, 10 min of discharging, and 70 min of idling (Figure 1B). The reactor was operated at room temperature of 24–26°C. Except for effluent biomass washout and sludge sampling, sludge was not disposed during the operation of the reactor. The SRT was estimated to be longer than 30 days.

Depending on the influent characteristics, the operation of the mainstream anammox reactor can be divided to two phases (Figure 1A and Table 1). In phase I (days 1–75), the mainstream anammox reactor was fed with the effluent (5 L) of a PN reactor that treated synthetic municipal wastewater. Description of the PN reactor has been available in Supplementary material. The feeding of the mainstream anammox reactor had low COD (25.1 ± 8.8 mg/L), most of which would likely be refractory organic compounds as the wastewater had been biotreated. In phase II (days 76–135), a portion of the raw synthetic municipal wastewater (0.5 L) was bypassed, and mixed with the PN effluent (4.5 L) in the middle tank. The mixed stream was then fed into the anammox reactor. Therefore, rbCOD was introduced into the system in the form of acetate (24.2 mg COD/L). Except for the differences in the influent organic composition, the operational patterns and conditions of the reactor were identical in phases I and II.

2.2. Batch tests on the potential of PD/A in the reactor

Two *ex situ* batch tests were conducted to investigate the potential of the PD/A in the reactor. Sludge collected from the reactor was washed three times with deionized water, and then transferred to four separate 0.5-L conical flasks. After addition of organic and nitrogen substrates, the flasks were incubated in shaking incubators (200 rpm) at 25°C. During batch tests, the flasks were continuously stripped with nitrogen gas to provide an anoxic environment.

Batch Test I investigated whether nitrite could accumulate during denitrification. Therefore, only nitrate ($NaNO_3$) and acetate were added to the flasks. The initial nitrate concentration was constant at 15 mg/L, and acetate was added at different dosages. The initial COD/NO_3^--N ratios in four flasks were 0.5, 1.0, 1.5, and 2.0, respectively.

Batch Test II investigated whether denitrification could be integrated with the anammox process. In addition to nitrate ($NaNO_3$) and acetate, ammonium (NH_4Cl) was present in the feed.

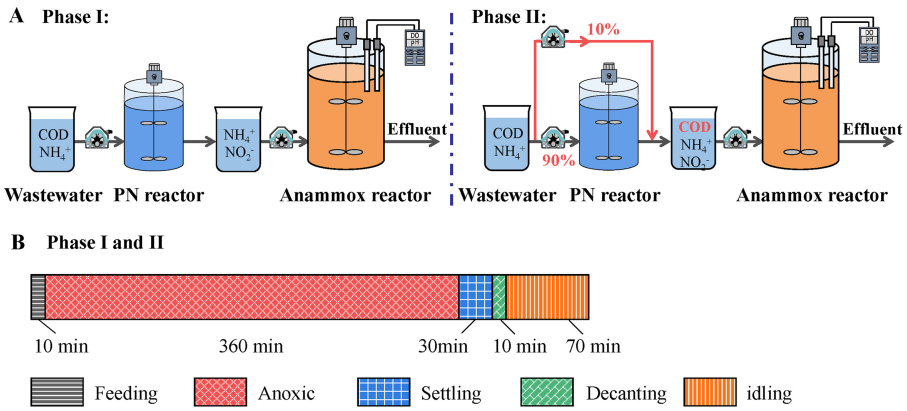

FIGURE 1
The schematic **(A)** and operational patterns **(B)** of the mainstream anammox reactor.

TABLE 1 Main characteristics of the influent of the mainstream anammox reactor.

	NH_4^+-N (mg/L)	NO_2^--N (mg/L)	NO_3^--N (mg/L)	TN (mg/L)	COD (mg/L)
Phase I	14.3 ± 2.5	14.1 ± 2.4	1.2 ± 0.8	29.4 ± 2.8	25.1 ± 8.8
Phase II	12.5 ± 1.8	12.3 ± 1.4	2.0 ± 0.6	26.8 ± 2.0	45.2 ± 11.2

The initial ammonium and nitrate concentrations were 10 mg/L and 15 mg/L, respectively. While different dosages of acetate were added to four flasks, resulting in COD/NO_3^--N ratios of 0.5, 1.0, 1.5, and 2.0, respectively.

2.3. Analytical methods

COD, NH_4^+-N, NO_2^--N, NO_3^--N, total nitrogen (TN), mixed liquor suspended solids, mixed liquor volatile suspended solids, and sludge volume index were measured using standard methods (APHA, 2005). The temperature, pH, and dissolved oxygen (DO) in the reactor were monitored on-line using a WTW Multi 3,620 instrument (WTW, Bavaria, Germany). Sludge size distribution was determined using a laser particle size analyzer (Malvern Mastersizer 2000, Malvern, United Kingdom).

2.4. Calculation of the nitrogen transformation pathways in typical cycles

Nitrogen transformation pathways in the reactor were computed based on the variations in nitrogen compounds concentrations in the typical cycles. The calculation only involves major nitrogen pathways. Different calculation methods are used in the two operating phases of the reactor. In phase I, the reactor was operated with negligible rbCOD input. Therefore, denitrification pathways were ignored in the calculation. Nitrogen conversions by anammox bacteria, ammonium-oxidizing bacteria (AOB) and NOB were calculated according to Eqs. 1–3.

$$\begin{aligned} TN_{anammox} = \Delta N = (NH_4^+ - N_{initial} + NO_2^- - N_{initial} \\ + NO_3^- - N_{initial}) - (NH_4^+ - N_{final} + NO_2^- \\ - N_{final} + NO_3^- - N_{final}) \end{aligned} \quad (1)$$

$$\begin{aligned} NH_4^+ - N_{AOB} = NH_4^+ - N_{initial} - NH_4^+ \\ - N_{final} - TN_{anammox} / 2.04 \end{aligned} \quad (2)$$

$$\begin{aligned} NO_3^- - N_{NOB} = NO_3^- - N_{final} - NO_3^- \\ - N_{initial} - TN_{anammox} \times 0.26 / 2.04 \end{aligned} \quad (3)$$

Where $TN_{anammox}$ represents TN removal by anammox bacteria, mg N/L; $NH_4^+ - N_{AOB}$ represents ammonium consumption by AOB, mg N/L; $NO_3^- - N_{NOB}$ represents nitrate production by NOB, mg N/L; $\varnothing N$ is the difference between the bulk total inorganic nitrogen concentrations at the start and end of the cycle, mg N/L; $NH_4^+ - N_{initial}$, $NO_2^- - N_{initial}$, and $NO_3^- - N_{initial}$ are the bulk ammonium, nitrite, and nitrate concentrations, respectively, at the start of the cycle, mg N/L; $NH_4^+ - N_{final}$, $NO_2^- - N_{final}$, and $NO_3^- - N_{final}$ are the bulk ammonium, nitrite, and nitrate concentrations, respectively, at the end of the cycle, mg N/L.

In phase II, the reactor was operated under stricter anoxic condition than phase I. An overall nitrate removal was achieved (Section 3.2). Therefore, nitrification pathway was ignored in the calculation. Nitrogen conversions *via* anammox, denitratation ($NO_3^- \rightarrow NO_2^-$), and denitritation ($NO_2^- \rightarrow N_2$) were calculated using Eqs. 4–6.

$$TN_{anammox} = \left(NH_4^+ - N_{initial} - NH_4^+ - N_{final}\right) \times 2.04 \quad (4)$$

$$\begin{aligned} NO_3^- - N_{denitratation} = NO_3^- - N_{initial} + TN_{anammox} \\ \times 0.26 / 2.04 - NO_3^- - N_{final} \end{aligned} \quad (5)$$

$$TN_{denitritation} = \Delta N - TN_{anammox} \quad (6)$$

Where $TN_{anammox}$ represents TN removal *via* anammox pathway, mg N/L; $NO_3^- - N_{denitratation}$ represents nitrate reduction *via* denitratation, mg N/L; $TN_{denitritation}$ represents TN removal *via* denitritation, mg N/L.

2.5. High-throughput sequencing analysis

Sludge samples collected from the reactor on day 1, day 75 and day 134 were freeze-dried (BT2KXL, Virtis, United States) and then stored at −20°C. Genomic DNA was extracted using the Fast DNA Kit (MPBiomedicals, CA, United States) according to the manufacture's instructions. The DNA concentration was measured using a Nanodrop Spectrophotometer (ND-1000, Isogen Life Science, Netherlands) to ensure the purity of the extract. The V3–V4 region of the 16S rRNA gene was amplified with bacterial primers 338F (5′-ACTCCTACG GGAGGCAGCAG-3′) and 806R (5′-GGACTAC HVGGGTWTCT AAT-3′). PCR products were sequenced on an Illumina MiSeq platform (Majorbio Bio-Pharm Technology Co., Ltd., Shanghai, China). Based on these data, the microbial composition was analyzed as described in our previous report (Yang et al., 2017). The raw reads have been deposited in the NCBI Sequence Read Archive (SRA) database (Accession Number: PRJNA942604).

3. Results

3.1. Nitrogen removal performance without and with rbCOD

In phase I, the mainstream anammox reactor was operated with negligible rbCOD input, as revealed by the insignificant COD removal (3.8 ± 2.1 mg/L) in the reactor (Figure 2A). Nitrogen removal performance was instable as shown in Figures 2B,C. Although good nitrogen removal performance was achieved at the beginning (days 1–40), the effluent nitrate concentration increased from 2.6 to 8.7 mg/L on day 41–75. In addition, ammonium and nitrite accumulated at the end of phase I, indicating a decline in the anammox activity in the reactor. Consequently, the nitrogen removal efficiency decreased from 83 to 30%.

In phase II, 24.2 mg COD/L acetate was introduced to the mainstream anammox reactor, increasing the rbCOD/TN ratio to 0.9. The average COD removal in the reactor was 27.7 mg/L, indicating a complete utilization of the rbCOD in the feeding (Figure 2A). Nitrate concentration in the effluent decreased from 8.7 mg/L to 2.1 mg/L within 2 days, and maintained at low level (1.1 ± 0.9 mg/L) in the following operation (Figure 2C). Overall, the nitrate removal was achieved. This suggested dentification in the reactor. In addition, the effluent ammonium and nitrite concentrations decreased simultaneously, indicating restoration of anammox activity. In phase II, advanced nitrogen removal was achieved with an average effluent TN of 3.4 mg/L and an average nitrogen removal efficiency of 87.2% (Figure 2B).

3.2. Changes in nitrogen transformation pathway after introducing rbCOD

The cycle analysis revealed changes in the nitrogen transformation pathway of the mainstream anammox reactor. In a typical phase I cycle (before introducing rbCOD), ammonium and nitrite were gradually removed, whereas nitrate accumulated considerably (Figure 3A). The ratio of NO_3^--N produced over NH_4^+-N removed (ΔNO_3^--N/ΔNH_4^+-N) was 0.92, which is much higher than the theoretical value of anammox reaction of 0.26 (Strous et al., 1998), indicating additional nitrate generation pathway. The nitrogen mass flow suggested that nitrification oxidized some ammonium to nitrite and oxidized part of the nitrite to nitrate in the anammox reactor (Figure 3B). Nitrification contributed to 79% of nitrate production, resulting in the insufficient nitrogen removal of the mainstream anammox reactor.

After introducing rbCOD in phase II, a simultaneous decrease in ammonium, nitrite and nitrate concentration was observed in a typical reaction cycle (Figure 3C). This indicates that not only the nitrate in the influent but also the nitrate generated by the anammox reaction were simultaneously removed by denitrification. Besides, nitrogen mass flow revealed partial denitrification (PD, $NO_3^- \rightarrow NO_2^-$) provided additional nitrite substrate for anammox (Figure 3D). As a result, *in situ* anammox activity was promoted. According to Figure 3D, anammox remained the dominant nitrogen removal pathway in the reactor with a contribution to nitrogen removal of 93%. Denitrification further improved the nitrogen removal efficiency, resulting in a low effluent TN concentration.

3.3. Potential of PD/A in anammox reactor revealed by batch tests

The potential of PD/A in the mainstream anammox reactor was further illustrated using *ex situ* batch tests. In Batch Test I, only nitrate and acetate were added to the feed to investigate denitrification. As shown in Figures 4A–D, nitrite accumulated at all COD/NO_3^--N ratios. The highest nitrate-to-nitrite transformation ratio of 50.0% was obtained with a COD/NO_3^--N ratio of 2.0. These results suggest that denitrification in the mainstream anammox reactor could provide additional nitrite for anammox.

In Batch Test II, ammonium was also added to the feed with nitrate and acetate. In the first hour, nitrate was removed significantly, whereas nitrite accumulated at all COD/NO_3^--N ratios, indicating the occurrence of PD (Figures 4E–H). Thereafter, ammonium, nitrite, and nitrate concentrations simultaneously decreased. Under the strict anoxic conditions in batch test, ammonium was removed through anammox pathway. The nitrite substrate for the anammox reaction was generated through PD. Therefore, the potential of PD/A in the mainstream anammox reactor is proved.

3.4. Microbial evolution in the mainstream anammox reactor

The effects of low-concentration rbCOD on the microbial community in the mainstream anammox reactor were investigated using high-throughput sequencing (Figure 5). In

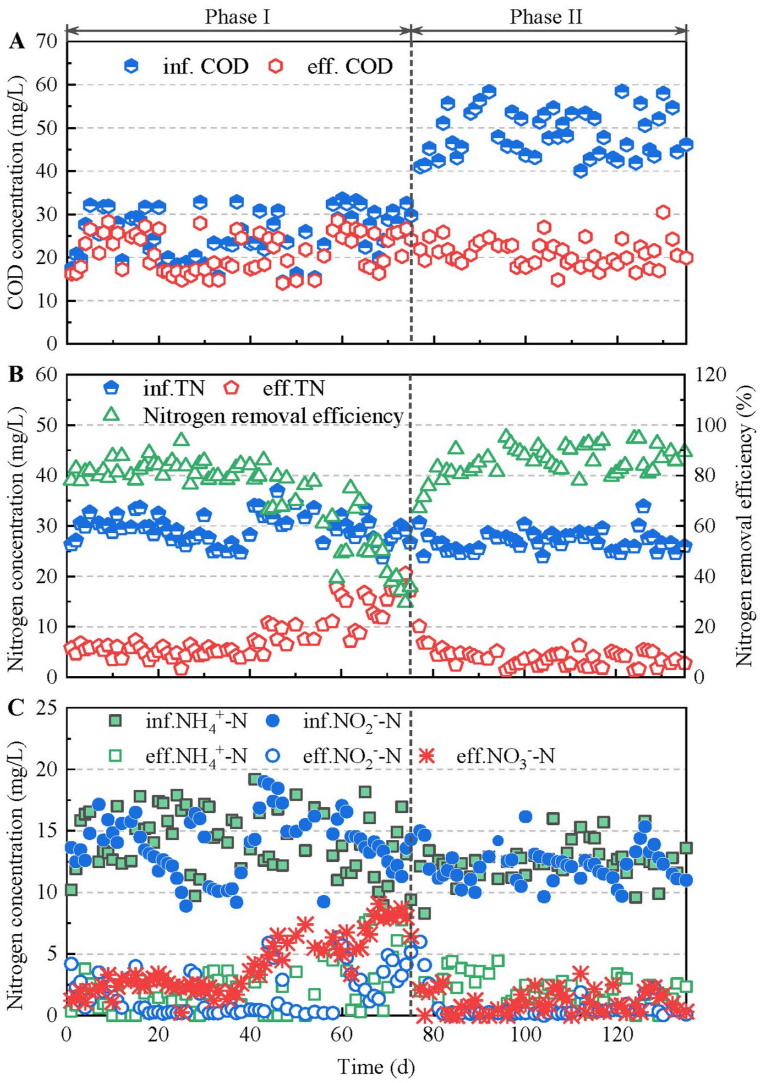

FIGURE 2
The COD (A) and TN (B) removal performance, as well as N-compound concentrations in the influent and effluent (C) of the mainstream anammox reactor.

phase I (without rbCOD), the abundance of anammox bacteria (dominated by *Candidatus Kuenenia*) declined from 2.08 to 1.73%, while the abundances of AOB (*Nitrosomonas*) and NOB (*Nitrospira*) increased significantly from 0.29 to 0.40% and from 0.14 to 0.56%, respectively. These trends are consistent with the nitrate accumulation and nitrogen removal deterioration during reactor operation. After introducing rbCOD in phase II, the abundance of anammox bacteria was restored to 2.48%, whereas the abundances of AOB and NOB decreased to 0.05 and 0.23%, respectively. These results suggest that the proper introduction of rbCOD benefits the enrichment of anammox bacteria and the suppression of nitrifying bacteria. Additionally, a transition in the denitrifying bacteria population was observed after the introduction of rbCOD. *Denitratisoma* with the capacity of complete denitrification ($NO_3^- \rightarrow N_2$) was the predominant denitrifying bacteria in phase I, and its abundance decreased from 3.91 to 2.00% in phase II. While *Thauera* and *Candidatus Competibacter*, which have been identified as the functional microorganisms for PD (Du et al., 2016; Shi et al., 2019; Ji et al., 2020), were considerably enriched in phase II with abundances increased from 0.18 to 2.15%, and from 0.15 to 1.35%, respectively. These results provided further evidence of PD/A in the reactor.

3.5. Granulation process in the mainstream anammox reactor

The seeding sludge of the mainstream anammox reactor contained a specific quantity of granular sludge (D > 200 μm, 17.4%) and had an average diameter of 130.8 μm (Figure 6). The sludge size was stable in phase I and increased significantly to 195.6 μm in phase II. Granular sludge eventually constituted 52.5% of the total biomass in the reactor, indicating that granulation was promoted after the introduction of rbCOD in phase II. Granulation in the reactor can facilitate the enrichment of anammox bacteria because they are more prone to grow in large aggregates (Vlaeminck et al., 2010; Laureni et al., 2019).

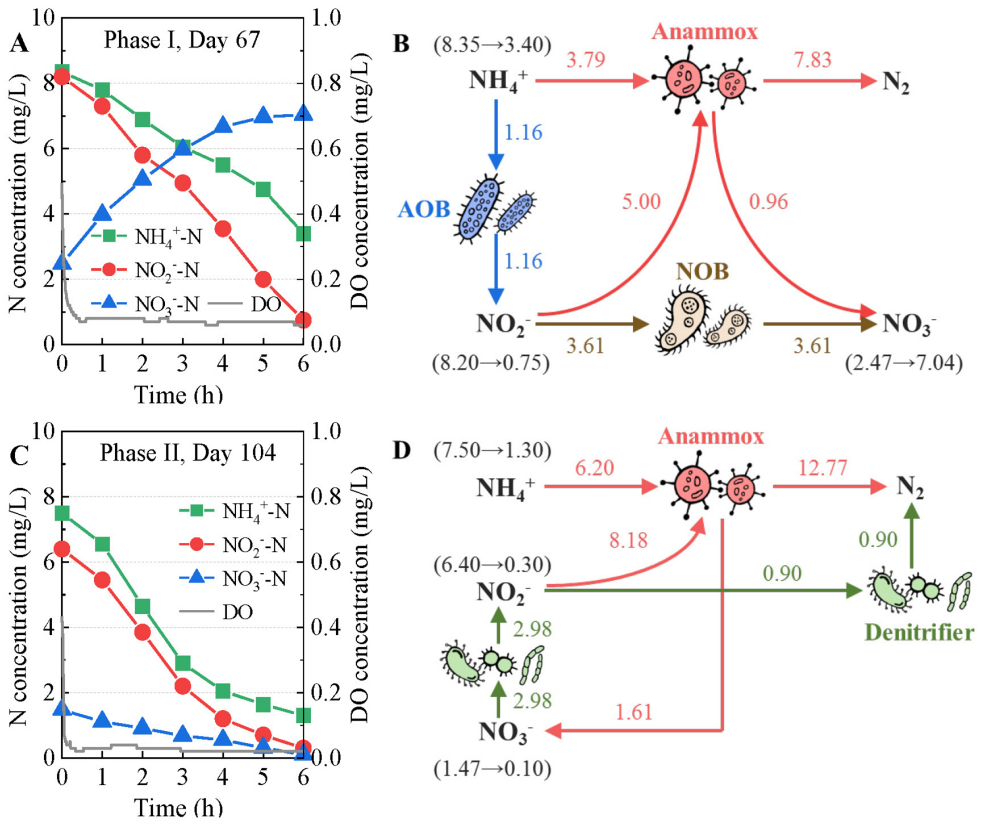

FIGURE 3
Variations in N-compound concentrations (**A**: phase I, **C**: phase II) and nitrogen transformation pathways (**B**: phase I, **D**: phase II) in the typical cycles of the mainstream anammox reactor.

4. Discussion

4.1. Mechanism of the nitrogen removal enhancement after introducing rbCOD

In the present study, the introduction of rbCOD quickly restored the mainstream anammox reactor from high nitrate accumulation (Figure 2). Advanced nitrogen removal was achieved in the presence of low concentrations of rbCOD. There may be multiple mechanisms behind the nitrogen removal enhancement in the mainstream anammox reactor after the introduction of rbCOD.

First, the suppression of nitrification was enhanced, which reduced *in situ* nitrate production. In phase I, the reactor was operated without rbCOD input. Relatively high nitrification activity results in an increase in nitrate production and a deterioration in nitrogen removal performance (Figures 2, 3), as demonstrated in the literature (Díaz et al., 2020; Li W. et al., 2020). The DO (0.06–0.08 mg/L) supporting nitrification transferred from influent and air at the top of the reactor during mechanical mixing (Figure 3A). Some nitrifier species, including complete ammonia oxidizer (comammox) and NOB in genus *Nitrospira*, exhibit high oxygen affinities (Liu and Wang, 2013; Akaboci et al., 2018; Roots et al., 2019). They may have contributed to nitrification in the reactor because the abundance of *Nitrospira* increased significantly (Figure 5). In contrast, the DO concentration in the reactor decreased to 0.02–0.04 mg/L in phase II after the introduction of rbCOD, possibly because of the activity of aerobic heterotrophic bacteria (Figure 3C). Therefore, stricter anoxic conditions were obtained in phase II than in phase I, which suppressed nitrification activity. Consequently, both AOB and NOB abundance decreased during phase II (Figure 5).

Second, PD/A was achieved in the reactor, which simultaneously removed the nitrate originating from the influent and produced by the anammox reaction. Batch tests have proved that nitrite can be accumulated during the denitrification of nitrate (Figures 4A–D). Besides, this part of nitrite can be utilized and removed by anammox bacteria with ammonium as the electron donor as revealed by cycle analysis (Figure 3D) and batch test (Figures 4E–H). In such ways, nitrate in the reactor was polished with a minor organic consumption, which improved the nitrogen removal efficiency of the reactor to a high level. In addition, although rbCOD was introduced with the influent at the beginning, nitrate was produced (*via* anammox) and reduced (*via* denitrification) continuously during the entire cycle (Figure 3). Therefore, endogenous denitrification was expected to occur. In this study, *Thauera* and *Candidatus Competibacter* were the functional bacteria responsible for PD during phase II (Figure 5). Both can restore rbCOD as endogenous carbon sources such as glycogen and polyhydroxyalkanoates (Lopez-Vazquez et al., 2009; Andreolli et al., 2022). Therefore, the rbCOD in the influent may have been transferred to endogenous carbon sources at the beginning and supported PD during the entire cycle.

Third, anammox activity and growth were promoted, which improves the process performance and stability. In this study, the

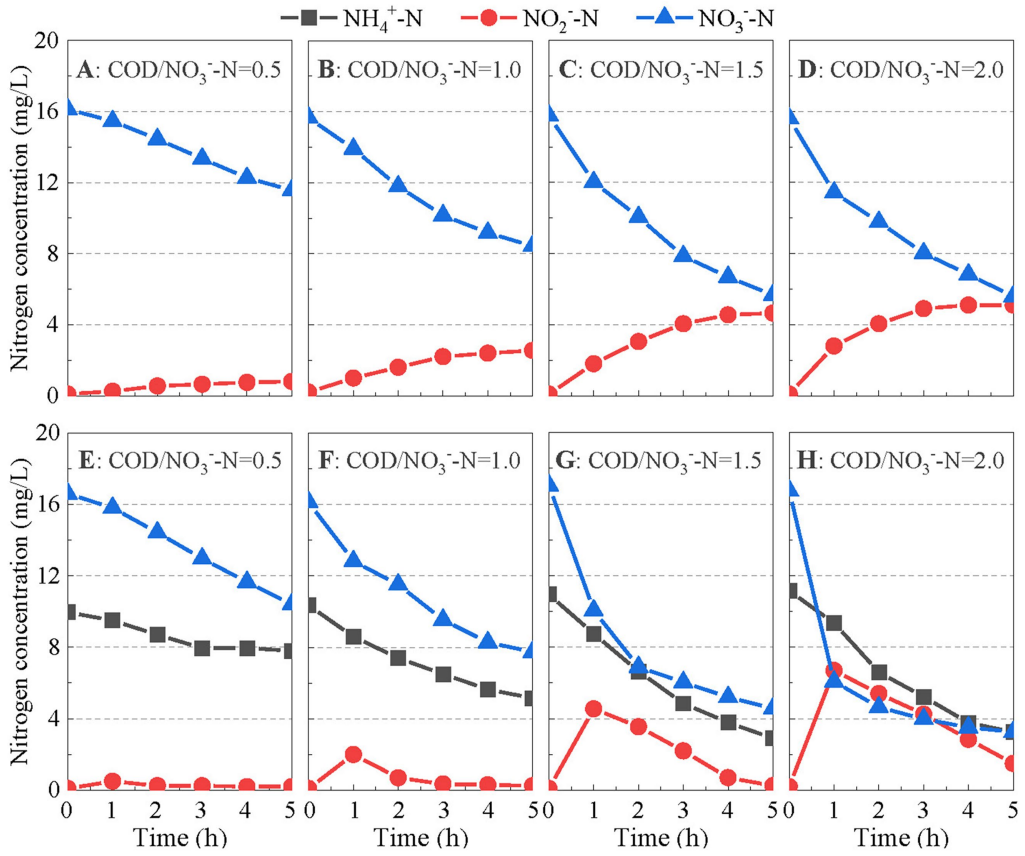

FIGURE 4
Variations in N-compound concentrations in Batch Tests I **(A–D)** and II **(E–H)**.

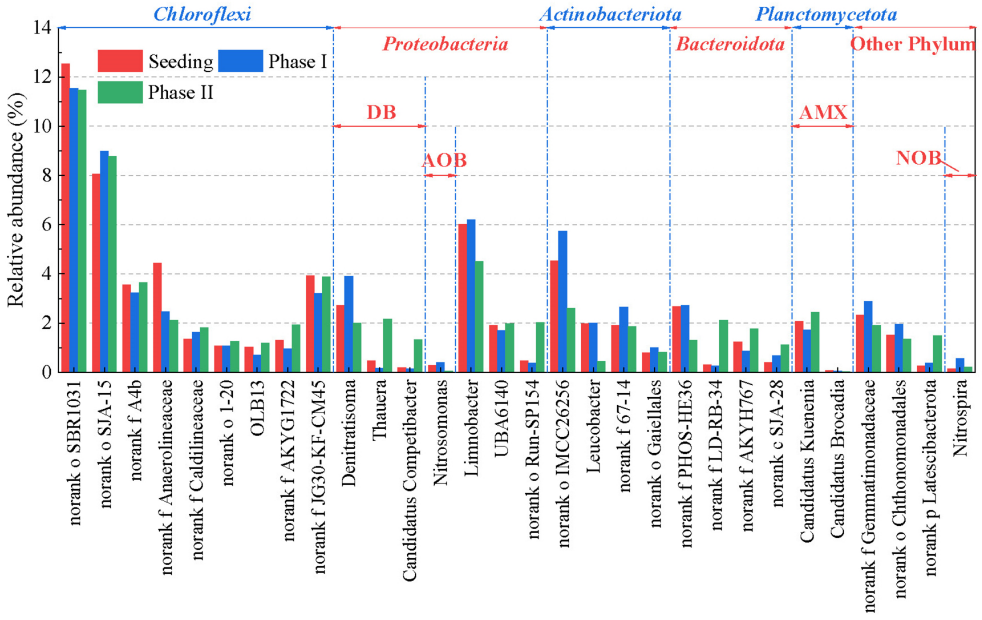

FIGURE 5
Variations in the microbial composition in the mainstream anammox reactor.

direct effects of rbCOD (acetate) on anammox activity may be limited. Low concentrations of acetate does not inhibit anammox activity (Huang et al., 2014). Some anammox species, such as *Candidatus Anammoxoglobus propionicus* and *Candidatus Brocadia*

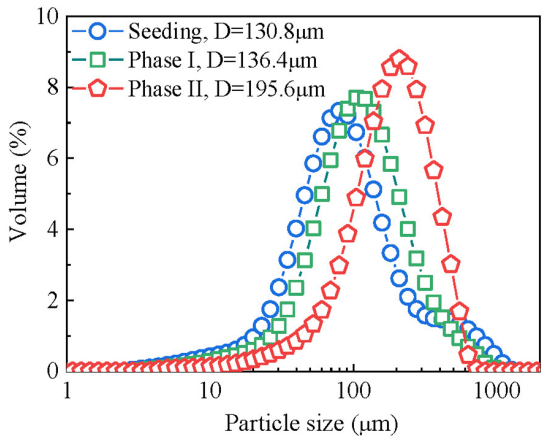

FIGURE 6
Variation in sludge size distribution in the mainstream anammox reactor.

fulgida can utilize short-chain fatty acids for energy generating (Kartal et al., 2007, 2008). However, this pathway may be insignificant in this study because anammox population in the reactor was dominated by genus *Candidatus Kuenenia* throughout the experiment. Therefore, rbCOD mainly promoted anammox activity in indirect ways. For example, the aerobic oxidation of rbCOD can consume the DO in bulk liquid and reduce its inhibitory effect on anammox activity (Strous et al., 1999). In addition, the anoxic utilization of rbCOD by PD of nitrate provided additional nitrite substrate for anammox bacteria and promoted anammox activity (Figure 3). Furthermore, the presence of rbCOD promoted extracellular polymers secretion and granulation in the mainstream anammox reactor (Figure 6) as demonstrated in the literature (Li et al., 2015; Chen et al., 2021a), which helped retain and enrich slow-growing anammox bacteria (Zhu et al., 2018; Chen et al., 2021b). Consequently, anammox abundance increased from 1.73 to 2.48% after introducing low concentrations of rbCOD (Figure 5). Meanwhile anammox pathway maintained its dominant position in nitrogen removal (Figure 3).

4.2. Application and further study

In this study, an effective and applicable strategy was employed to solve nitrate accumulation caused by undesired NOB activity in mainstream anammox reactors. Other strategies have been reported to reduce nitrate yield, including purging the oxygen in the influent with nitrogen gas, minimizing the surface area of the reactor in contact with the atmosphere by adopting a high height/diameter ratio, and providing protective covers in the anammox reactor (Díaz et al., 2020). However, these measures may not be economical or applicable in some cases, especially for upgrading existing WWTPs because they require major retrofitting of the reactor configuration. Hence, the present study included the strategy of introducing low concentration of rbCOD, which can reduce nitrate accumulation with a minor modification by redirecting part of the raw municipal wastewater to the anammox reactor or adding a small amount of external organic carbon (Le et al., 2019; Fofana et al., 2022). In addition, rbCOD can be provided using sludge fermentation liquid, if it is available in the WWTP (Cao et al., 2013; Basset et al., 2016; Ali et al., 2021). At last, it is noted that the proposed operating strategy for mainstream anammox process is also applicable to continuous flow reactors. However, additional measures may be required to enhance the retention of anammox bacteria, such as filling proper carriers and using cyclone to selective retain granular sludge (Wett et al., 2013; Yang et al., 2017).

Even when there is no excessive nitrate production by NOB, operating the mainstream anammox reactor with a low concentration of rbCOD is beneficial because of its potential to achieve complete nitrogen removal (Zhuang et al., 2022). Both PN/A and PD/A contributed to the nitrogen removal as reported in the literature (Li J. et al., 2020; Li et al., 2022). Specifically in this study, PN/A removed most of the nitrogen autotrophically, whereas PD/A removed the nitrate generated in the anammox reaction. A theoretical equation for this process is presented in Table 2 for Case III and compared with other anammox-based processes targeting complete nitrogen removal (Cases I and II). In Case I, PN/A removes nitrogen autotrophically, however 11% of ammonium is eventually converted to nitrate. The nitrate polishing through denitrification still consumes organic carbon. The overall organic requirement of Case I is 0.32 mg COD/mg N. In Case II, nitrite substrate for anammox is generated through the complete nitrification of ammonium and subsequent PD of nitrate. This approach requires additional oxygen and organic carbon than the nitrite generation pathway of PN. Overall, 2.35 mg O_2/mg N and 0.73 mg COD/mg N are consumed in Case II. Case III has theoretical advantages over Cases I and II. First, nitrite is mainly generated through PN, therefore saving of oxygen and organic carbon is expected when compared with Case II. Second, nitrate polishing is achieved through PD/A, which consumes less organic carbon than Case I. In addition, the PD/A in Case III can remove a certain amount of ammonium without consuming oxygen, therefore oxygen demand can also be saved compared with Case I. Overall Case III can achieve 100% nitrogen removal with the least requirement for oxygen (1.76 mg O_2/mg N) and organic matter (0.14 mg COD/mg N) in the three cases.

Despite these theoretical and practical advantages, several issues need to be resolved before employing the proposed nitrate control strategy. First, nitrogen removal mechanism should be further investigated. In this study, some secondary nitrogen metabolism pathways were ignored when computing the nitrogen transformation in the reactor, which might have an impact on the accuracy of the calculation. The complex microbial nitrogen-recycling networks should be resolved in future studies using advanced technologies such as isotope labeling technique, metagenomics and metatranscriptomics (Wang et al., 2019; Yang et al., 2020). Second, the feasibility of the nitrate control strategy should be further verified using real municipal wastewater, although PD and PD/A using complex organic carbons in real municipal wastewater have been reported in the literature (Shi et al., 2019; Du et al., 2020; Ji et al., 2020). Besides, prolonged experiments are required to investigate the long-term effects of organic additions, particularly with seasonal temperature variations. Third, the optimal ranges of the rbCOD concentration and rbCOD/TN ratio

TABLE 2 Comparison of the theoretical oxygen and organic demand of different cases for complete nitrogen removal base on anammox.

	Reaction	Oxygen demand (mg O_2/mgN)	Organic demand (mg COD/mgN)
Case I: PN/A + denitrification	Partial nitrification: $NH_3 + 1.5O_2 \rightarrow NO_2^- + H_2O + H^+$ (i) Anammox: $NH_3 + 1.32NO_2^- + H^+ \rightarrow 1.02\,N_2 + 0.26NO_3^- + 2H_2O$ (ii) Denitrification: $NO_3^- + 0.625CH_3COO^- + 0.625H^+ \rightarrow 0.5\,N_2 + HCO_3^- + 0.25CO_2 + 0.75H_2O$ (iii) Total reaction by (i × 1.32 + ii)/2.32 + iii × 0.11: $NH_3 + 0.85O_2 + 0.07CH_3COO^- \rightarrow 0.5\,N_2 + 0.11HCO_3^- + 0.03CO_2 + 1.51H_2O + 0.07H^+$	1.94	0.32
Case II: Complete nitrification + PD/A	Complete nitrification: $NH_3 + 2O_2 \rightarrow NO_3^- + H_2O + H^+$ (i) Partial denitrification: $NO_3^- + 0.25CH_3COO^- \rightarrow NO_2^- + 0.25HCO_3^- + 0.25CO_2 + 0.25H_2O$ (ii) Anammox: $NH_3 + 1.32NO_2^- + H^+ \rightarrow 1.02\,N_2 + 0.26NO_3^- + 2H_2O$ (iii) Total reaction by ((ii × 1.32 + iii) + i × 1.06)/2.06: $NH_3 + 1.03O_2 + 0.16CH_3COO^- \rightarrow 0.5\,N_2 + 0.16HCO_3^- + 0.16CO_2 + 1.65H_2O + 0.03H^+$	2.35	0.73
Case III PN/A + PD/A	Partial nitrification: $NH_3 + 1.5O_2 \rightarrow NO_2^- + H_2O + H^+$ (i) Anammox: $NH_3 + 1.32NO_2^- + H^+ \rightarrow 1.02\,N_2 + 0.26NO_3^- + 2H_2O$ (ii) Partial denitrification: $NO_3^- + 0.25CH_3COO^- \rightarrow NO_2^- + 0.25HCO_3^- + 0.25CO_2 + 0.25H_2O$ (iii) Total reaction by ((iii × 0.26 + ii) + i × 1.06)/2.06: $NH_3 + 0.77O_2 + 0.03CH_3COO^- \rightarrow 0.5\,N_2 + 0.03HCO_3^- + 0.03CO_2 + 1.52H_2O + 0.03H^+$	1.76	0.14

should be determined in future studies to minimize organic consumption in real applications.

5. Conclusion

In this study, a mainstream anammox treatment was established in an SBR. When the reactor was operated with no rbCOD, high levels of nitrate accumulated in the effluent because of undesired NOB activity, resulting in reduced nitrogen removal efficiency. In contrast, operation with a low rbCOD concentration restored the anammox reactor from nitrate accumulation and achieved highly efficient nitrogen removal. At a low concentration of rbCOD, anammox remained the dominant nitrogen removal pathway, whereas PD/A removed the nitrate generated by the anammox reaction. Besides, NOB were effectively suppressed because of the stricter anoxic environment. In addition, granulation was promoted, which favored the enrichment of slow-growing anammox bacteria. Overall, the introduction of low concentrations of rbCOD is a feasible strategy for achieving robust and efficient nitrogen removal in mainstream anammox reactors.

Data availability statement

The datasets presented in this study can be found in online repositories. The names of the repository/repositories and accession number(s) can be found in the article/Supplementary material.

Author contributions

YY: funding acquisition, conceptualization, data curation, and writing—original draft. YL: formal analysis, validation, investigation, and writing—original draft. JX: formal analysis and data curation. SL: methodology and resources. LL: software and data curation. CL: project administration and writing—review and editing. YT: funding acquisition and writing—review and editing. All authors contributed to the article and approved the submitted version.

Funding

This research was financially supported by the Natural Science Foundation of Shandong Province, China (Grant No. ZR2019BEE070), the National Natural Science Foundation of China (Grant No. 22176106), the Shandong Province Higher Educational Program for Introduction and Cultivation of Young Innovative Talents (2021), and the Open Research Fund of Engineering Research Center of Concrete Technology under Marine Environment, Ministry of Education (Grant No. TMduracon2022041).

Conflict of interest

The authors declare that the research was conducted in the absence of any commercial or financial relationships that could be construed as a potential conflict of interest.

Publisher's note

Supplementary material

The Supplementary material for this article can be found online at: https://www.frontiersin.org/articles/10.3389/fmicb.2023.1186819/full#supplementary-material

References

Akaboci, T. R. V., Gich, F., Ruscalleda, M., Balaguer, M. D., and Colprim, J. (2018). Effects of extremely low bulk liquid DO on autotrophic nitrogen removal performance and NOB suppression in side- and mainstream one-stage PNA. *J. Chem. Technol. Biotechnol.* 93, 2931–2941. doi: 10.1002/jctb.5649

Ali, P., Zalivina, N., Le, T., Riffat, R., Ergas, S., Wett, B., et al. (2021). Primary sludge fermentate as carbon source for mainstream partial denitrification–anammox (PdNA). *Water Environ. Res.* 93, 1044–1059. doi: 10.1002/wer.1492

Andreolli, M., Scerbacov, V., Frison, N., Zaccone, C., and Lampis, S. (2022). *Thauera* sp. Sel9, a new bacterial strain for polyhydroxyalkanoates production from volatile fatty acids. *New Biotechnol.* 72, 71–79. doi: 10.1016/j.nbt.2022.09.004

APHA (2005). *Standard methods for the examination of water and wastewater*, *21st*. Washington DC: American Public Health Association.

Basset, N., Katsou, E., Frison, N., Malamis, S., Dosta, J., and Fatone, F. (2016). Integrating the selection of PHA storing biomass and nitrogen removal via nitrite in the main wastewater treatment line. *Bioresour. Technol.* 200, 820–829. doi: 10.1016/j.biortech.2015.10.063

Cao, Y., Van Loosdrecht, M. C. M., and Daigger, G. T. (2017). Mainstream partial nitritation–anammox in municipal wastewater treatment: status, bottlenecks, and further studies. *Appl. Microbiol. Biotechnol.* 101, 1365–1383. doi: 10.1007/s00253-016-8058-7

Cao, S., Wang, S., Peng, Y., Wu, C., Du, R., Gong, L., et al. (2013). Achieving partial denitrification with sludge fermentation liquid as carbon source: the effect of seeding sludge. *Bioresour. Technol.* 149, 570–574. doi: 10.1016/j.biortech.2013.09.072

Chen, C., Jiang, Y., Liu, J., Adams, M., Chang, Y., Guo, M., et al. (2021a). The structure of anammox granular sludge under varying long-term organic matter stress: performance, physiochemical and microbial community. *J. Clean. Prod.* 323:129117. doi: 10.1016/j.jclepro.2021.129117

Chen, C., Jiang, Y., Zou, X., Guo, M., Liu, H., Cui, M., et al. (2021b). Insight into the influence of particle sizes on characteristics and microbial community in the anammox granular sludge. *J. Water Process. Eng.* 39:101883. doi: 10.1016/j.jwpe.2020.101883

Chen, Y., Zhao, Z., Liu, H., Ma, Y., An, F., Huang, J., et al. (2020). Achieving stable two-stage mainstream partial-nitrification/anammox (PN/A) operation via intermittent aeration. *Chemosphere* 245:125650. doi: 10.1016/j.chemosphere.2019.125650

Díaz, C., Belmonte, M., Campos, J. L., Franchi, O., Faúndez, M., Vidal, G., et al. (2020). Limits of the anammox process in granular systems to remove nitrogen at low temperature and nitrogen concentration. *Process. Saf. Environ. Prot.* 138, 349–355. doi: 10.1016/j.psep.2020.03.025

Du, R., Cao, S., Zhang, H., Li, X., and Peng, Y. (2020). Flexible nitrite supply alternative for mainstream anammox: advances in enhancing process stability. *Environ. Sci. Technol.* 54, 6353–6364. doi: 10.1021/acs.est.9b06265

Du, R., Peng, Y., Cao, S., Li, B., Wang, S., and Niu, M. (2016). Mechanisms and microbial structure of partial denitrification with high nitrite accumulation. *Appl. Microbiol. Biotechnol.* 100, 2011–2021. doi: 10.1007/s00253-015-7052-9

Du, R., Peng, Y., Ji, J., Shi, L., Gao, R., and Li, X. (2019). Partial denitrification providing nitrite: opportunities of extending application for anammox. *Environ. Int.* 131:105001. doi: 10.1016/j.envint.2019.105001

Fofana, R., Parsons, M., Long, C., Chandran, K., Jones, K., Klaus, S., et al. (2022). Full-scale transition from denitrification to partial denitrification–anammox (PdNA) in deep-bed filters: operational strategies for and benefits of PdNA implementation. *Water Environ. Res.* 94:e10727. doi: 10.1002/wer.10727

Fu, W., Zhu, R., Lin, H., Zheng, Y., and Hu, Z. (2021). Effect of organic concentration on biological activity and nitrogen removal performance in an anammox biofilm system. *Water Sci. Technol.* 84, 725–736. doi: 10.2166/wst.2021.258

Ge, S., Wang, S., Yang, X., Qiu, S., Li, B., and Peng, Y. (2015). Detection of nitrifiers and evaluation of partial nitrification for wastewater treatment: a review. *Chemosphere* 140, 85–98. doi: 10.1016/j.chemosphere.2015.02.004

Gilbert, E. M., Agrawal, S., Brunner, F., Schwartz, T., Horn, H., and Lackner, S. (2014). Response of different *Nitrospira* species to anoxic periods depends on operational DO. *Environ. Sci. Technol.* 48, 2934–2941. doi: 10.1021/es404992g

He, Y., Mao, H., Makinia, J., Drewnowski, J., Wu, B., Xu, J., et al. (2023). Impact of soluble organic matter and particulate organic matter on anammox system: performance, microbial community and N_2O production. *J. Environ. Sci.* 124, 146–155. doi: 10.1016/j.jes.2021.11.007

Huang, X.-L., Gao, D.-W., Tao, Y., and Wang, X.-L. (2014). C2/C3 fatty acid stress on anammox consortia dominated by *Candidatus Jettenia asiatica*. *Chem. Eng. J.* 253, 402–407. doi: 10.1016/j.cej.2014.05.055

Isanta, E., Reino, C., Carrera, J., and Perez, J. (2015). Stable partial nitritation for low-strength wastewater at low temperature in an aerobic granular reactor. *Water Res.* 80, 149–158. doi: 10.1016/j.watres.2015.04.028

Ji, J., Peng, Y., Li, X., Zhang, Q., and Liu, X. (2020). A novel partial nitrification-synchronous anammox and endogenous partial denitrification (PN-SAEPD) process for advanced nitrogen removal from municipal wastewater at ambient temperatures. *Water Res.* 175:115690. doi: 10.1016/j.watres.2020.115690

Kartal, B., Kuenen, J. G., and Van Loosdrecht, M. C. M. (2010). Sewage treatment with anammox. *Science* 328, 702–703. doi: 10.1126/science.1185941

Kartal, B., Rattray, J., Van Niftrik, L. A., Van, D. V. J., Schmid, M. C., Webb, R. I., et al. (2007). *Candidatus* "Anammoxoglobus propionicus" a new propionate oxidizing species of anaerobic ammonium oxidizing bacteria. *Syst. Appl. Microbiol.* 30, 39–49. doi: 10.1016/j.syapm.2006.03.004

Kartal, B., Van Niftrik, L., Rattray, J., De Vossenberg, J., Schmid, M. C., Damste, J. S. S., et al. (2008). *Candidatus* 'Brocadia fulgida': an autofluorescent anaerobic ammonium oxidizing bacterium. *FEMS Microbiol. Ecol.* 63, 46–55. doi: 10.1111/j.1574-6941.2007.00408.x

Laureni, M., Weissbrodt, D. G., Villez, K., Robin, O., De Jonge, N., Rosenthal, A., et al. (2019). Biomass segregation between biofilm and flocs improves the control of nitrite-oxidizing bacteria in mainstream partial nitritation and anammox processes. *Water Res.* 154, 104–116. doi: 10.1016/j.watres.2018.12.051

Le, T., Peng, B., Su, C., Massoudieh, A., Torrents, A., Al-Omari, A., et al. (2019). Impact of carbon source and COD/N on the concurrent operation of partial denitrification and anammox. *Water Environ. Res.* 91, 185–197. doi: 10.1002/wer.1016

Li, Y., Huang, Z., Ruan, W., Ren, H., and Zhao, M. (2015). ANAMMOX performance, granulation, and microbial response under COD disturbance. *J. Chem. Technol. Biotechnol.* 90, 139–148. doi: 10.1002/jctb.4298

Li, J., Peng, Y., Yang, S., Li, S., Feng, W., Li, X., et al. (2022). Successful application of anammox using the hybrid autotrophic–heterotrophic denitrification process for low-strength wastewater treatment. *Environ. Sci. Technol.* 56, 13964–13974. doi: 10.1021/acs.est.2c02920

Li, J., Peng, Y., Zhang, L., Li, X., Zhang, Q., Yang, S., et al. (2020). Improving efficiency and stability of anammox through sequentially coupling nitritation and denitritation in a single-stage bioreactor. *Environ. Sci. Technol.* 54, 10859–10867. doi: 10.1021/acs.est.0c01314

Li, J., Qiang, Z., Yu, D., Wang, D., Zhang, P., and Li, Y. (2016). Performance and microbial community of simultaneous anammox and denitrification (SAD) process in a sequencing batch reactor. *Bioresour. Technol.* 218, 1064–1072. doi: 10.1016/j.biortech.2016.07.081

Li, W., Zhuang, J. L., Zhou, Y. Y., Meng, F. G., Kang, D., Zheng, P., et al. (2020). Metagenomics reveals microbial community differences lead to differential nitrate production in anammox reactors with differing nitrogen loading rates. *Water Res.* 169:115279. doi: 10.1016/j.watres.2019.115279

Liu, G., and Wang, J. (2013). Long-term low DO enriches and shifts nitrifier community in activated sludge. *Environ. Sci. Technol.* 47, 5109–5117. doi: 10.1021/es304647y

Liu, W., Yang, D., Shen, Y., and Wang, J. (2018). Two-stage partial nitritation-anammox process for high-rate mainstream deammonification. *Appl. Microbiol. Biotechnol.* 102, 8079–8091. doi: 10.1007/s00253-018-9207-y

Lopez-Vazquez, C. M., Oehmen, A., Hooijmans, C. M., Brdjanovic, D., Gijzen, H. J., Yuan, Z., et al. (2009). Modeling the PAO–GAO competition: effects of carbon source, pH and temperature. *Water Res.* 43, 450–462. doi: 10.1016/j.watres.2008.10.032

Regmi, P., Miller, M. W., Holgate, B., Bunce, R., Park, H., Chandran, K., et al. (2014). Control of aeration, aerobic SRT and COD input for mainstream nitritation/denitritation. *Water Res.* 57, 162–171. doi: 10.1016/j.watres.2014.03.035

Roots, P., Wang, Y., Rosenthal, A. F., Griffin, J. S., Sabba, F., Petrovich, M., et al. (2019). Comammox *Nitrospira* are the dominant ammonia oxidizers in a mainstream low dissolved oxygen nitrification reactor. *Water Res.* 157, 396–405. doi: 10.1016/j.watres.2019.03.060

Sánchez Guillén, J. A., Lopez Vazquez, C. M., De Oliveira Cruz, L. M., Brdjanovic, D., and Van Lier, J. B. (2016). Long-term performance of the anammox process under low nitrogen sludge loading rate and moderate to low temperature. *Biochem. Eng. J.* 110, 95–106. doi: 10.1016/j.bej.2016.02.004

Shi, L., Du, R., and Peng, Y. (2019). Achieving partial denitrification using carbon sources in domestic wastewater with waste-activated sludge as inoculum. *Bioresour. Technol.* 283, 18–27. doi: 10.1016/j.biortech.2019.03.063

Silveira, N. C., Oliveira, G. H. D., Damianovic, M. H. R. Z., and Foresti, E. (2021). Two-stage partial nitrification-anammox process for nitrogen removal from slaughterhouse wastewater: evaluation of the nitrogen loading rate and microbial community analysis. *J. Environ. Manag.* 296:113214. doi: 10.1016/j.jenvman.2021.113214

Strous, M., Heijnen, J. J., Kuenen, J. G., and Jetten, M. S. M. (1998). The sequencing batch reactor as a powerful tool for the study of slowly growing anaerobic ammonium-oxidizing microorganisms. *Appl. Microbiol. Biotechnol.* 50, 589–596. doi: 10.1007/s002530051340

Strous, M., Kuenen, J. G., and Jetten, M. S. M. (1999). Key physiology of anaerobic ammonium oxidation. *Appl. Environ. Microbiol.* 65, 3248–3250. doi: 10.1128/AEM.65.7.3248-3250.1999

Vlaeminck, S. E., Terada, A., Smets, B. F., De Clippeleir, H., Schaubroeck, T., Bolca, S., et al. (2010). Aggregate size and architecture determine microbial sctivity balance for one-stage partial nitritation and anammox. *Appl. Environ. Microbiol.* 76, 900–909. doi: 10.1128/aem.02337-09

Wang, Z., Peng, Y., Li, J., Liu, J., Zhang, Q., Li, X., et al. (2021). Rapid initiation and stable maintenance of municipal wastewater nitritation during the continuous flow anaerobic/oxic process with an ultra-low sludge retention time. *Water Res.* 197:117091. doi: 10.1016/j.watres.2021.117091

Wang, X., Yang, R., Guo, Y., Zhang, Z., Kao, C. M., and Chen, S. (2019). Investigation of COD and COD/N ratio for the dominance of anammox pathway for nitrogen removal via isotope labelling technique and the relevant bacteria. *J. Hazard. Mater.* 366, 606–614. doi: 10.1016/j.jhazmat.2018.12.036

Wang, Q. L., Ye, L., Jiang, G. M., Hu, S. H., and Yuan, Z. G. (2014). Side-stream sludge treatment using free nitrous acid selectively eliminates nitrite oxidizing bacteria and achieves the nitrite pathway. *Water Res.* 55, 245–255. doi: 10.1016/j.watres.2014.02.029

Wett, B., Omari, A., Podmirseg, S. M., Han, M., Akintayo, O., Gómez Brandón, M., et al. (2013). Going for mainstream deammonification from bench to full scale for maximized resource efficiency. *Water Sci. Technol.* 68, 283–289. doi: 10.2166/wst.2013.150

Xu, G. J., Zhou, Y., Yang, Q., Lee, Z. M. P., Gu, J., Lay, W. S., et al. (2015). The challenges of mainstream deammonification process for municipal used water treatment. *Appl. Microbiol. Biotechnol.* 99, 2485–2490. doi: 10.1007/s00253-015-6423-6

Yang, Y., Pan, J., Zhou, Z., Wu, J., Liu, Y., Lin, J.-G., et al. (2020). Complex microbial nitrogen-cycling networks in three distinct anammox-inoculated wastewater treatment systems. *Water Res.* 168:115142. doi: 10.1016/j.watres.2019.115142

Yang, Y., Zhang, L., Cheng, J., Zhang, S., Li, B., and Peng, Y. (2017). Achieve efficient nitrogen removal from real sewage in a plug-flow integrated fixed-film activated sludge (IFAS) reactor via partial nitritation/anammox pathway. *Bioresour. Technol.* 239, 294–301. doi: 10.1016/j.biortech.2017.05.041

Zhang, B., Zhao, J., Zuo, J., Shi, X., Gong, J., and Ren, H. (2019). Realizing stable operation of anaerobic ammonia oxidation at low temperatures treating low strength synthetic wastewater. *J. Environ. Sci.* 75, 193–200. doi: 10.1016/j.jes.2018.03.020

Zhu, G., Wang, S., Ma, B., Wang, X., Zhou, J., Zhao, S., et al. (2018). Anammox granular sludge in low-ammonium sewage treatment: not bigger size driving better performance. *Water Res.* 142, 147–158. doi: 10.1016/j.watres.2018.05.048

Zhuang, J.-L., Sun, X., Zhao, W.-Q., Zhang, X., Zhou, J.-J., Ni, B.-J., et al. (2022). The anammox coupled partial-denitrification process in an integrated granular sludge and fixed-biofilm reactor developed for mainstream wastewater treatment: performance and community structure. *Water Res.* 210:117964. doi: 10.1016/j.watres.2021.117964

frontiers | Frontiers in Microbiology

TYPE Original Research
PUBLISHED 09 June 2023
DOI 10.3389/fmicb.2023.1210790

OPEN ACCESS

EDITED BY
Huike Dong,
Chinese Academy of Sciences (CAS), China

REVIEWED BY
Hongbiao Du,
Tsinghua University, China
Hongliang Wang,
Hubei University of Science and Technology, China
Yuanzhi Hong,
Beihua University, China
Huinan Che,
Hohai University, China

*CORRESPONDENCE
Guangming Zhang
✉ 2020017@hebut.edu.cn
Jia Zhu
✉ zhujia@szpt.edu.cn

†These authors share first authorship

RECEIVED 23 April 2023
ACCEPTED 23 May 2023
PUBLISHED 09 June 2023

CITATION
Long Z, Guo T, Chen C, Zhang G and Zhu J (2023) Preparation and application of Ag plasmon Bi_3O_4Cl photocatalyst for removal of emerging contaminants under visible light. *Front. Microbiol.* 14:1210790. doi: 10.3389/fmicb.2023.1210790

Preparation and application of Ag plasmon Bi_3O_4Cl photocatalyst for removal of emerging contaminants under visible light

Zeqing Long[1†], Tingting Guo[2†], Chao Chen[2], Guangming Zhang[3*] and Jia Zhu[4*]

[1]Department of Public Health and Preventive Medicine, Changzhi Medical College, Changzhi, China, [2]Heping Hospital Affiliated to Changzhi Medical College, Changzhi, China, [3]School of Energy & Environmental Engineering, Hebei University of Technology, Tianjin, China, [4]School of Materials and Environmental Engineering, Shenzhen Polytechnic, Shenzhen, China

Photocatalytic degradation has been extensively investigated toward the removal emerging contaminants (ECs) from water. In this study, a series of Ag-Bi_3O_4Cl plasmon photocatalysts were synthesized through the photo-deposition of metallic Ag on the Bi_3O_4Cl surface. The effects of plasmon modification on the catalytic performance of bismuth oxychlorides were analyzed. Ag addition did not alter the morphology of Bi_3O_4Cl. With the increasing Ag content, the number of oxygen defects on the catalyst surface first increased and then decreased. Moreover, the surface plasmon resonance effect of Ag suppressed the recombination of electron–hole pairs, promoting the migration and separation of photocarriers and improving the light absorption efficiency. However, the addition of excessive Ag reduced the number of active sites on the Bi_3O_4Cl surface, hindering the catalytic degradation of pollutants. The optimal Ag-Bi_3O_4Cl photocatalyst (Ag ratio: 0.025; solution pH: 9; dosage: 0.8 g/L) achieved 93.8 and 94.9% removal of ciprofloxacin and tetrabromobisphenol A, respectively. The physicochemical and photoelectric properties of Ag-Bi_3O_4Cl were determined through various characterization techniques. This study demonstrates that introducing metallic Ag alters the electron transfer path of the catalyst, reduces the recombination rate of electron–hole pairs, and effectively improves the catalytic efficiency of Bi_3O_4Cl. Furthermore, the pathways of ciprofloxacin degradation products and their biotoxicity were revealed.

KEYWORDS

emerging contaminants (ECs), plasmon, Bi_3O_4Cl, environmental purification, visible light, biotoxicity

1. Introduction

Pharmaceutical and personal care products (PPCPs) and endocrine-disrupting chemicals (EDCs) are representative of emerging contaminants (ECs) that possess a bioaccumulation tendency and non-degradability (Liu et al., 2021; Wang et al., 2021); They are harmful to the nervous system of humans and other organisms, affect the function of the endocrine system, and endanger the reproductive capacity of humans and animals (Zhao et al., 2018). Ciprofloxacin (CIP), as a typical PPCP, has been widely used as a broad-spectrum antibiotic.

Tetrabromobisphenol A (TBBPA) is the most industrially consumed flame retardant and considered as an EDC (Law et al., 2006; Klein et al., 2020). The complete removal of these pollutants through conventional water treatment processes is difficult (Morin-Crini et al., 2022). Therefore, there is an urgent need to develop new and efficient processes for the removal of these ECs from water.

Photocatalytic technology has attracted increasing attention in recent years owing to its sustainability and high contaminant mineralization rate (Long et al., 2020a). Previous studies have shown that photocatalytic technology can effectively remove ECs from water (Jiang et al., 2019). However, traditional photocatalysts (such as TiO_2 and ZnO) have low solar light harvest efficiency and high charge recombination rate, limiting their activities and EC removal performance (Long et al., 2020b). Therefore, developing new and efficient visible-light-driven photocatalysts is necessary.

Recently, photocatalysts based on bismuth oxychlorides (BiOCl, Bi_3O_4Cl, $Bi_{12}O_{17}Cl_2$, and $Bi_{24}O_{31}Cl_{10}$) have been extensively studied (Xinping et al., 2006; Cui et al., 2016; Chang et al., 2017). The distinctive layered structure of bismuth oxychlorides is favorable to form an internal electric field, thereby accelerating electron–hole pair separation and imparting excellent optoelectronic properties (Long et al., 2020c). Researchers have worked extensively on modifying bismuth oxychlorides to further enhance their photocatalytic activities. Plasmon modification is currently one of the most important methods for catalyst modification (Zhang et al., 2019). Its principle is to exploit the plasmon resonance effect of noble metals to form a Schottky barrier on the interface with the catalyst, thus accelerating charge transfer, promoting electron–hole pairs separation, and enhancing light absorption by the catalyst. In addition, the increased current density can heat the metal particles, thereby accelerating the photochemical reaction (Hou et al., 2011). Yu et al. (2013) reported a series of (Rh, Pd, Pt)-BiOCl plasmon photocatalysts exhibiting excellent photocatalytic performance in visible light because the plasmon resonance generated by the noble metal nanoparticles improved the charge separation efficiency through electron capture. Xu et al. (2019) prepared a novel Ag@BiOCl plasmon photocatalyst, wherein the Schottky barrier formed by the BiOCl semiconductor and Ag nanoparticles served as a photoelectron capture center to to separate the photogenerated charges. Hence, the photocatalytic performance of the bismuth-oxychloride-based system was significantly improved through plasmon modification.

According to previous studies, among various bismuth-oxychloride-based photocatalysts, Bi_3O_4Cl has a more positive oxidation potential to oxidize pollutants, and its bandgap is suitable for visible-light-driven photocatalysis (Long et al., 2022a). Moreover, Bi_3O_4Cl has a desirable oxygen defect concentration to accelerate electron–hole pair separation (Cui et al., 2018). Therefore, Bi_3O_4Cl was used as the base material in this study, and relatively low-cost metallic Ag was used for plasmon modification. The performance of the Ag-Bi_3O_4Cl photocatalyst toward the removal of CIP and TBBPA was evaluated. A series of characterization techniques to analyze the physicochemical and photoelectric properties of the photocatalyst were conducted in order to reveal the modification and electron migration mechanisms. The results provide insights into the development of plasmon-modified bismuth oxychloride photocatalysts and their application in the removal of ECs from water.

2. Experimental

2.1. Materials and methods

(**Supplementary material**).

2.2. Synthesis of Ag-Bi_3O_4Cl plasmonic photocatalysts

To synthesize the Bi_3O_4Cl nanoflakes, KCl (4 mmol) powder and deionized water (60 ml) were added to a 200 ml beaker. Subsequently, $Bi(NO_3)_3{\cdot}5H_2O$ (4 mmol) was added, and the mixture was thoroughly stirred for 30 min to obtain a white suspension. The suspension was ultrasonicated for 5 min to achieve a uniform dispersion. Next, a NaOH (1 mol/L) solution was added dropwise, and the pH of the suspension was adjusted to 12.0 upon vigorous stirring. Subsequently, the suspension was transferred to a 100 ml Teflon hydrothermal reactor and maintained at 160°C for 12 h. The precipitate was separated and washed three times with deionized water and ethanol. Finally, Bi_3O_4Cl nanoflakes were obtained by drying the product in an air oven at 80°C for 4 h.

To synthesize Ag-Bi_3O_4Cl plasmonic photocatalysts, the prepared Bi_3O_4Cl nanoflakes (0.736 g, 1 mmol) and deionized water (60 ml) were placed in a beaker and stirred for 30 min. Then, the standard $AgNO_3$ standard solution (0.01, 0.025, 0.05, and 0.1 mmol) was added, and the mixture was stirred for 2 h under a 500 W xenon lamp. Subsequently, the product was washed three times with water and alcohol and dried in an oven at 80°C for 4 h. The prepared photocatalysts were denoted as 0.01-Ag-Bi_3O_4Cl, 0.025-Ag-Bi_3O_4Cl, 0.05-Ag-Bi_3O_4Cl, and 0.1-Ag-Bi_3O_4Cl, wherein 0.01, 0.025, 0.05, and 0.1 represent the molar concentration of the $AgNO_3$ solution.

2.3. Characterization

(**Supplementary material**).

2.4. Photocatalytic tests and data analysis

In this study, the catalytic activity of the catalyst was assessed by the photocatalytic decomposition of ECs. A certain amount of photocatalysts and CIP (50 ml; 10 mg/L) or TBBPA (50 ml; 10 mg/L) solution were added to a quartz reactor and sonicated for 30 s. Next, the quartz reactor was placed in a PCX50C Discover photocatalytic reaction system equipped with a 5 W white LED lamp as a visible light source (400 nm $\leq \lambda \leq$ 800 nm, Perfect Light Co., Ltd., Beijing, China).

Before irradiation, the mixture of the photocatalyst and contaminant solution (CIP or TBBPA, 10 mg/L) in the quartz reactor was stirred under dark conditions for 30 min to achieve

the adsorption–desorption equilibrium. Then, the light source was turned on, and samples were extracted at specific intervals using a syringe. Next, the extracted solution was filtered through a 0.22 μm nitrocellulose filter to remove the suspended catalyst. The CIP concentration was measured at 277 nm using a UH5300 UV-vis spectrometer (Hitachi), and the TBBPA concentration was measured at 209 nm using an LC 3000 HPLC system (Agilent Technology Co., Ltd., Santa Clara, CA, United States) with a Thermo Fisher C18 column. The mobile phase in the HPLC column was 0.1 % acetic acid aqueous solution (solution A) and methanol (solution B). The v/v ratio of solution A to B was 2:8. The flow rate was 1 ml/min, and the column temperature was 35°C.

The main active species generated in the photocatalytic process were investigated to determine the possible mechanism. Sodium oxalate (SO, 1 mmol/L), tert-butyl alcohol (TBA, 10 mmol/L), and benzoquinone (BQ, 1 mmol/L) were added to scavenge holes (h^+), hydroxyl radicals ($^{\cdot}OH$), and superoxide radicals ($^{\cdot}O_2^-$), respectively (Bi et al., 2016).

All experiments were repeated three times, and the mean values were reported.

3. Results and discussion

3.1. Characterization of photocatalysts

3.1.1. Crystal structures and morphologies

The crystal structures of the catalysts were analyzed using X-ray diffraction (XRD). Figure 1 shows the XRD patterns of a series of Ag-Bi_3O_4Cl samples prepared with different Ag contents. The diffraction patterns of all Ag-Bi_3O_4Cl catalysts agree well with that of the monoclinic crystal Bi_3O_4Cl (JCPDS 36-0760). Compared with pure Bi_3O_4Cl, the peaks and lattice parameters of the Ag-Bi_3O_4Cl catalysts remain unchanged, confirming that Ag is deposited on the Bi_3O_4Cl surface rather than entering its lattice. In addition, the intensity ratio of the (600)/(411) peaks change slightly, suggesting that the Ag content can impact the preferred orientation and the crystallinity of Bi_3O_4Cl to a certain extent (Li J. et al., 2014). The diffraction peak of metallic Ag is not detected possibly because of its low content and good dispersion on the Bi_3O_4Cl surface. Moreover, no impurities or other phases are detected, indicating the high purity of the synthesized photocatalysts.

Figures 2A–D show the scanning electron microscopy (SEM) images of the Ag-Bi_3O_4Cl plasmonic photocatalysts with different Ag loadings. All samples exhibit the nanoflake morphology identical to that of Bi_3O_4Cl, indicating that Ag addition does not change the morphology of Bi_3O_4Cl. However, the surfaces of the nanoflakes become rough with increasing Ag content, implying that their crystallinity has changed, consistent with the XRD results.

Figures 2E–I show the results of the energy-dispersive X-ray spectroscopy (EDS) surface elemental analysis of the 0.025-Ag-Bi_3O_4Cl. The spectra reveal that Bi, O, Cl, and Ag are uniformly distributed on the surface. This is consistent with the XRD results that Ag is not incorporated into the lattice of Bi_3O_4Cl but deposited on its surface. Moreover, the uniform elemental distribution facilitates the electron transfer in the photocatalytic degradation (Niu et al., 2020b).

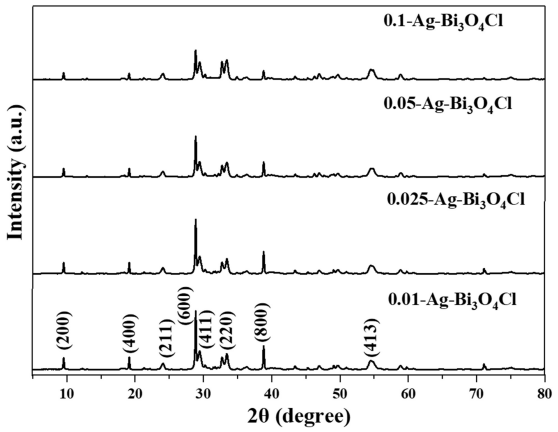

FIGURE 1
X-ray diffraction (XRD) patterns of Ag-Bi_3O_4Cl photocatalysts with different ratios.

To further investigate the crystal structure of Ag-Bi_3O_4Cl, 0.025-Ag-Bi_3O_4Cl was selected as a representative sample for transmission electron microscopy (TEM) analysis. As shown in Figure 3A, it exhibits a nanoflake shape, consistent with the SEM images. In Figure 3B, the lattice spacings of 0.2702 and 0.1561 nm correspond to the (220) and (105) crystal planes of Bi_3O_4Cl and Ag, respectively. These results agree with the XRD and SEM observations and demonstrate that Ag is deposited on the surface of Bi_3O_4Cl and does not dissolve in the lattice.

The specific surface areas and porous structures of pure Bi_3O_4Cl and Ag-Bi_3O_4Cl with different Ag loadings are summarized in Table 1. As the Ag loading increases, the specific surface area and pore volume first increase and then decrease, with 0.025-Ag-Bi_3O_4Cl exhibiting the maximum specific surface area (19.971 m^2/g) and highest pore volume (0.083 cm^3/g). These results indicate that adding an appropriate amount of Ag to Bi_3O_4Cl can increase the surface area and pore volume, thereby enhancing the adsorption capacity. As the adsorption capacity increases, more pollutants can accumulate on the surface. The larger the specific surface area, the more active components are exposed, promoting the catalytic degradation of organic pollutants (Niu et al., 2020a).

3.1.2. Chemical compositions and valence state

Figure 4 shows the chemical compositions and valence states of Ag-Bi_3O_4Cl plasmon photocatalysts synthesized with different Ag ratios. As shown in Figure 4A, Bi, Cl, O, and C elements are found in all samples and no impurity peaks are observed. The characteristic peak of Ag is not detected for 0.01-Ag-Bi_3O_4Cl because of its low Ag content. With the increasing Ag loading, this peak emerges in the spectra of 0.025-Ag-Bi_3O_4Cl and 0.05-Ag-Bi_3O_4Cl.

Figure 4B shows the Bi 4f characteristic peaks of the samples. In pure Bi_3O_4Cl, two characteristic peaks at 159.3 eV and 164.6 eV were detected, corresponding to the Bi $4f_{5/2}$ and Bi $4f_{7/2}$ orbitals of the Bi trivalent chemical state, respectively (Zhang et al., 2020). In addition, with an increase in the Ag content, the diffraction peak shifted toward a low binding energy, indicating the presence of low-charged Bi ions at the external sites of the Bi_3O_4Cl

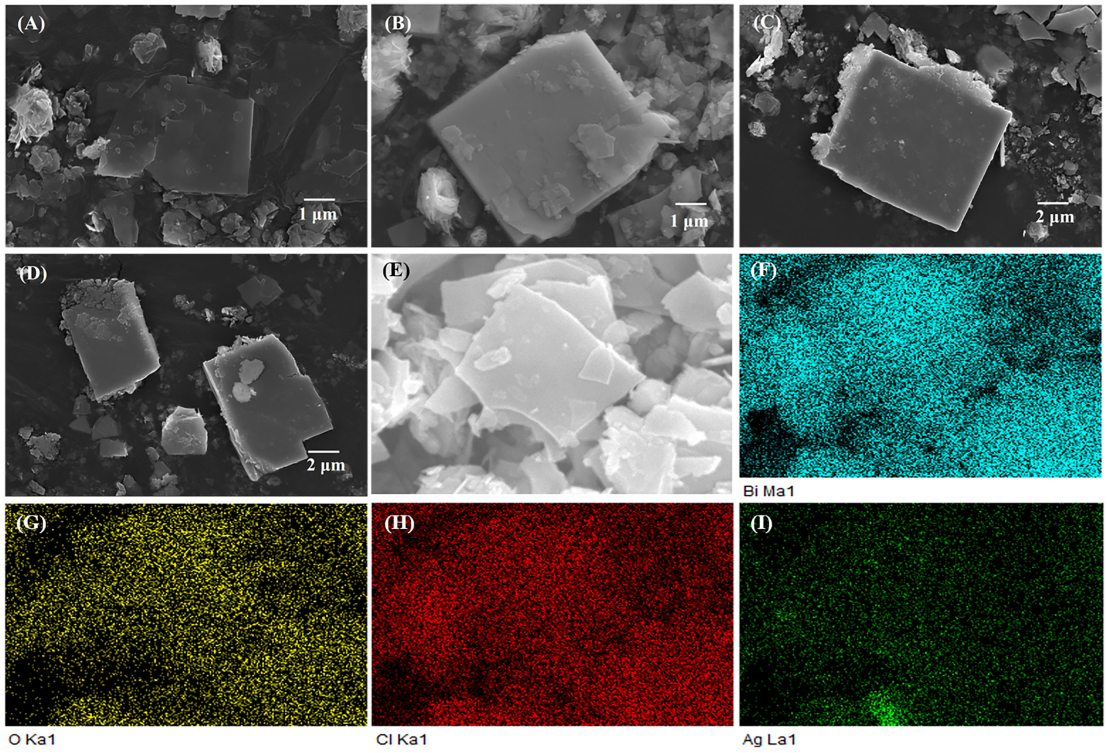

FIGURE 2
The SEM image and surface elements distribution of samples: **(A–D)** The SEM image of 0.01-Ag-Bi_3O_4Cl–0.1-Ag-Bi_3O_4Cl. **(E–I)** The surface elements distribution of 0.025-Ag-Bi_3O_4Cl.

nanosheet. Sun et al. (2019) reported similar observations, which were attributed to the introduction of Ag metal, leading to the generation of oxygen defects (Apelgren et al., 2019).

In **Figure 4C**, there are two characteristic peaks of O 1s at approximately 531.5–531.7 eV and 529.7–530.1 eV, corresponding to the O_2^- in oxygen-deficient regions and lattice oxygen, respectively (Long et al., 2022b). Moreover, the oxygen defect content first increased and then decreased with increasing Ag content, and the presence of oxygen defects promoted electron-hole pairs separation in the photocatalysts (Zou et al., 2021). The presence of oxygen defects was further confirmed using electron spin resonance (ESR). In **Supplementary Figure 1**, the oxygen vacancies increase with the introduction of metallic Ag.

In **Figure 4D**, the two characteristic peaks of Bi_3O_4Cl are at approximately 199.8 and 198.3 eV, corresponding to Cl $2p_{1/2}$ and Cl $2p_{3/2}$, respectively (Wang et al., 2019). The characteristic peak of Cl 2p corresponding to Ag-Bi_3O_4Cl exhibits a trend of transition from a low binding energy to a high binding energy. The shift and transition of the Cl 2p characteristic peak in Ag-Bi_3O_4Cl may be due to the change in the Cl-O distance caused by oxygen defects; similar results have been observed in the study of Bi-BiOI (Sun et al., 2019).

In **Figure 4E**, the presence of elemental Ag in the 0.025-Ag-Bi_3O_4Cl and 0.05-Ag-Bi_3O_4Cl samples can be clearly observed, with two characteristic peaks of Ag 3d at approximately 373.9 and 367.8 eV, corresponding to Ag $3d_{3/2}$ and Ag $3d_{5/2}$, respectively (Phuruangrat et al., 2021). The intensities of the diffraction peaks tended to be increase with increasing Ag metal content. However, no characteristic Ag peak was observed in the 0.01-Ag-Bi_3O_4Cl sample, which may be because of the low content of Ag.

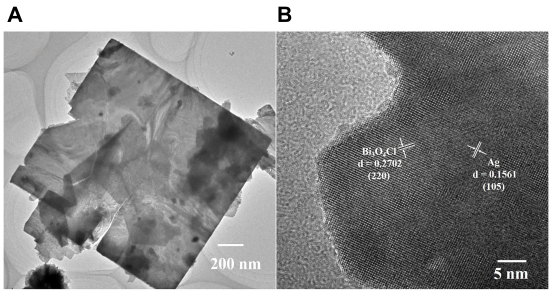

FIGURE 3
The TEM analysis of 0.025-Ag-Bi_3O_4Cl: **(A)** TEM image, **(B)** high resolution transmission electron microscopy (HRTEM) of the sample.

TABLE 1 The BET surface areas, pore volume, and pore diameter of Bi_3O_4Cl, 0.025-Ag-Bi_3O_4Cl, and 0.05-Ag-Bi_3O_4Cl.

Sample	S_{BET} (m^2/g)	Pore volume (cm^3g^{-1})	Pore diameter (nm)
Bi_3O_4Cl	10.841	0.047	1.677
0.025-Ag-Bi_3O_4Cl	19.971	0.083	1.923
0.05-Ag-Bi_3O_4Cl	12.092	0.039	1.675

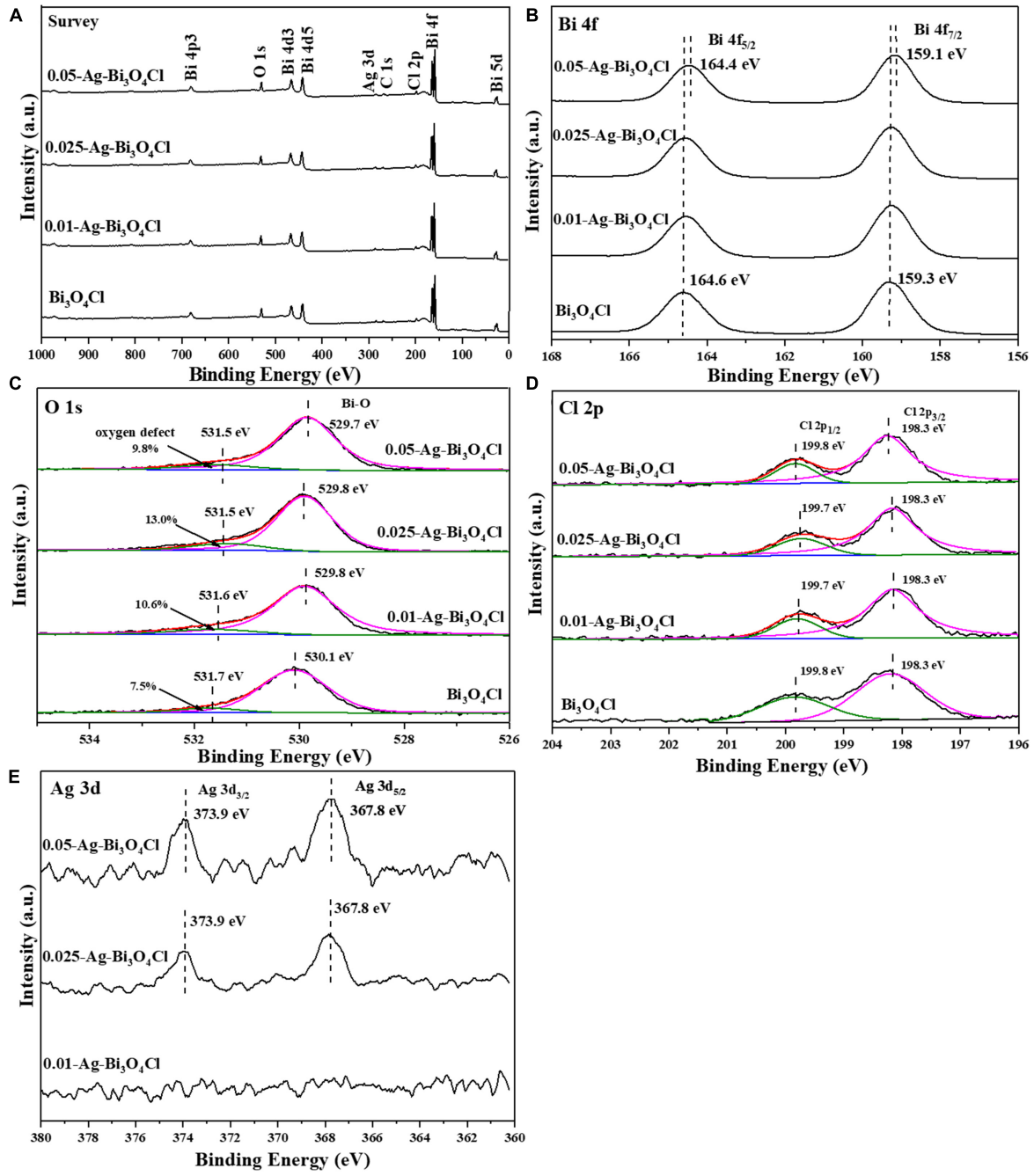

FIGURE 4
The X-ray photoelectron spectroscopy (XPS) spectra of photocatalysts: **(A)** survey; **(B)** Bi 4f; **(C)** O 1s; **(D)** Cl 2p; **(E)** Ag 3d.

3.1.3. Optical and electrochemical properties

The UV-vis diffuse reflectance spectroscopy results for the Bi_3O_4Cl and Ag-Bi_3O_4Cl plasmon photocatalysts are shown in Figure 5A. The maximum optical absorption wavelength of pure Bi_3O_4Cl is approximately 540 nm. The series of Ag-Bi_3O_4Cl plasmon photocatalysts exhibited absorption at all visible wavelengths from 500 to 800 nm, which increased with increasing Ag content. This result indicates that the Ag metal on the surface of Bi_3O_4Cl undergoes a plasmon resonance phenomenon under visible-light irradiation, which greatly increases its light absorption ability and broadens its light absorption range. From the plot of $(\alpha h\nu)^{1/2}$ versus energy ($h\nu$) (Liu et al., 2017), the band gap of the Bi_3O_4Cl photocatalyst was determined to be 2.38 eV (Figure 5B). These results indicate that the Ag-Bi_3O_4Cl photocatalyst has superior visible-light absorption ability, which is beneficial for the utilization of sunlight.

As shown in Figure 5C, the photoluminescence (PL) peak intensities of the Ag-Bi_3O_4Cl samples are weaker than those of Bi_3O_4Cl, indicating that the introduction of Ag reduced the electron-hole recombination rate of the photocatalyst. As the Ag content increased, the PL peak intensity of the samples gradually decreased. This is because excessive Ag metal hinders electron-hole

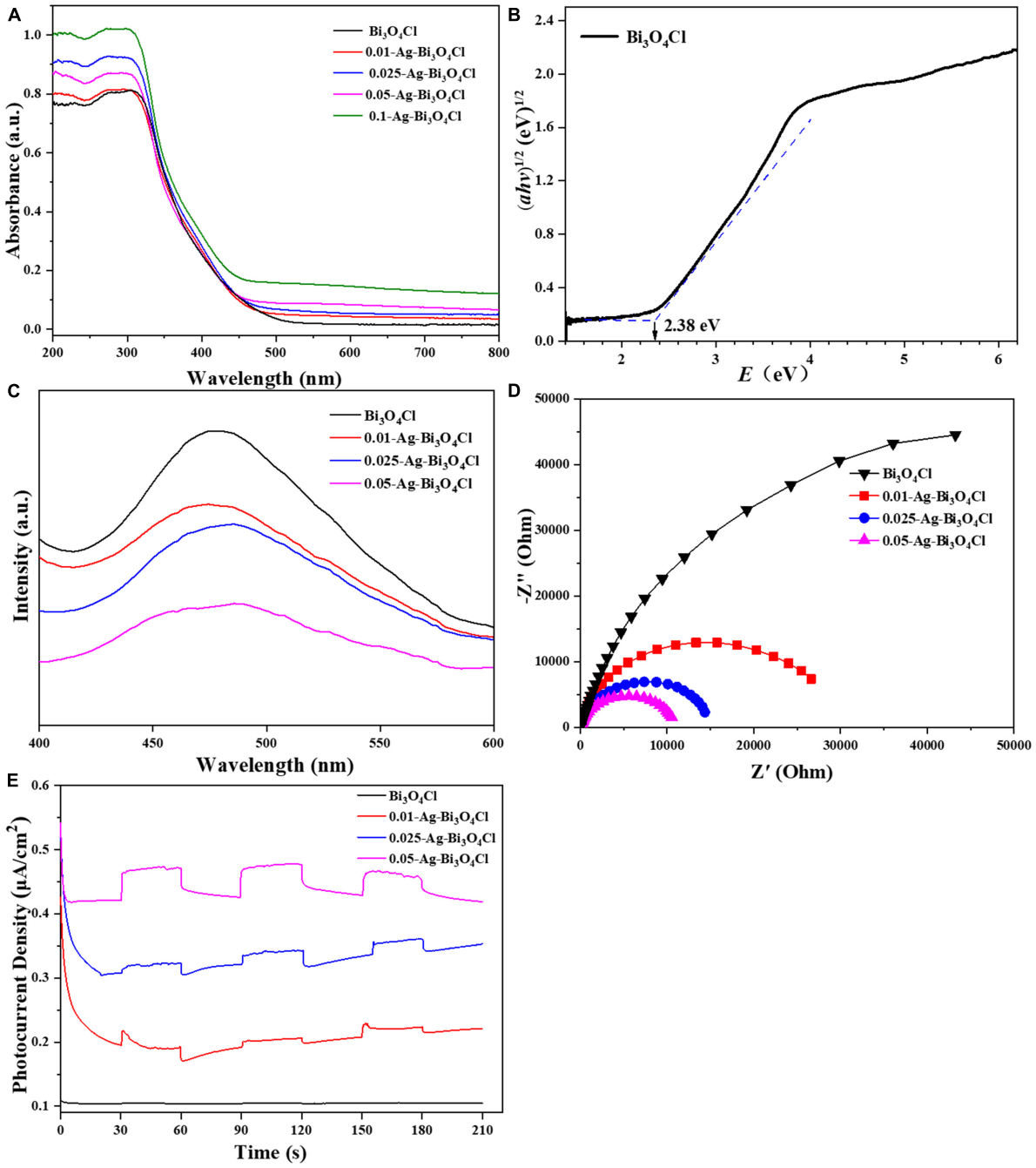

FIGURE 5
(A) UV–Vis diffuse reflection spectrum (DRS), **(B)** bandgap energies, **(C)** photoluminescence (PL) spectra, **(D)** EIS Nyquist plots, and **(E)** TPRs of the investigated catalysts.

pairs recombination and promotes carrier migration (Jiang et al., 2020).

The migration, conversion, and separation of electron-hole pairs in the Ag-Bi_3O_4Cl plasmon photocatalysts were evaluated using electrochemical impedance spectroscopy (EIS) and transient current response (TPR). A smaller arc radius of the Nyquist curve of the photocatalyst indicates faster charge transfer. The trend of the influence of the Ag content on the radius of the curved arc is consistent with that of the PL spectrum and also presents a gradually decreasing trend (**Figure 5D**). The photocurrent response of the photocatalyst (**Figure 5E**) exhibited a gradually increasing trend as the Ag content increased. This result is consistent with the PL and EIS results, indicating that the presence of Ag metal promotes the migration, conversion, and separation of the electron-hole pairs of Bi_3O_4Cl (Hong et al., 2023).

Based on the optical and electrochemical characteristics of the photocatalysts, it can be concluded that the Ag content significantly affects the photoelectric performance of Ag-Bi_3O_4Cl plasmon photocatalysts; with the increase in Ag content, the recombination of photogenerated electron-hole pairs is reduced,

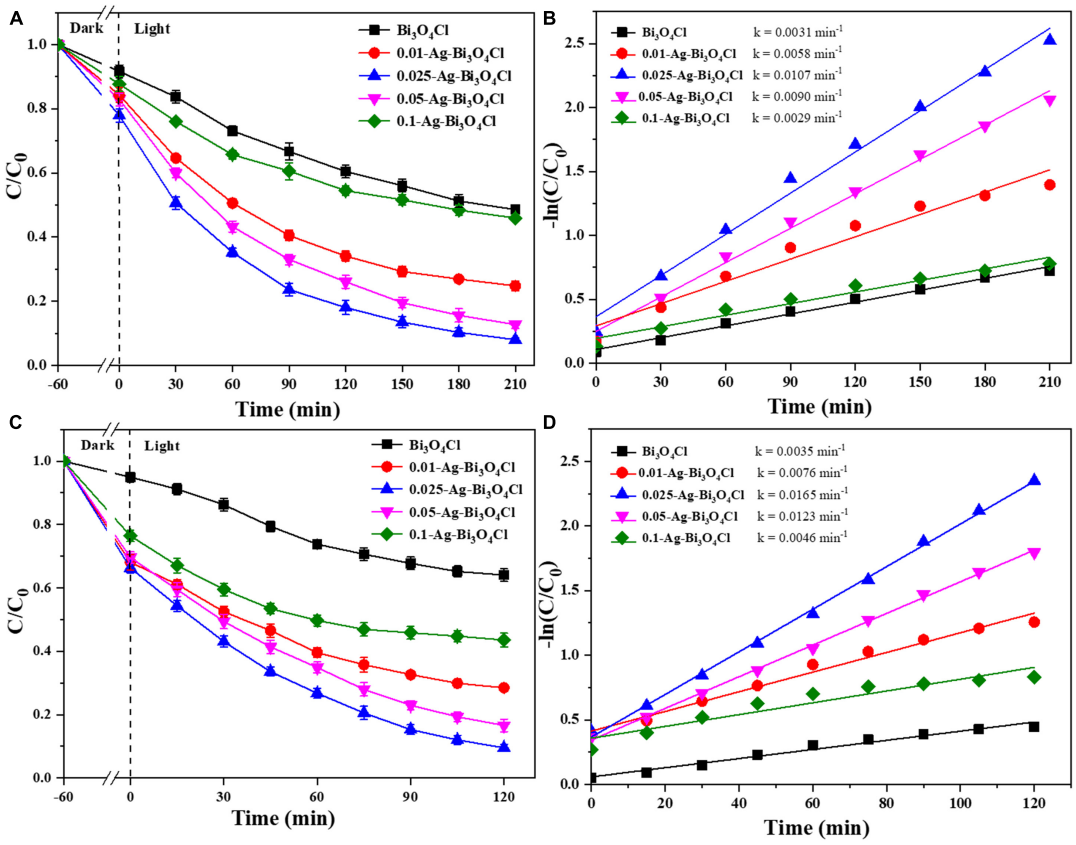

FIGURE 6
Ciprofloxacin (CIP) and TBBPA removal in different photocatalysts: **(A)** removal efficiency of CIP; **(B)** kinetics of CIP removal; **(C)** removal efficiency of TBBPA; **(D)** kinetics of TBBPA removal; conditions: the concentration of CIP and TBBPA = 10 mg/L, initial pH, catalyst dosage = 0.8 g/L.

and the migration and separation capabilities of electrons and holes are enhanced, which is conducive to improving the performance of photocatalysts. However, in the photocatalytic oxidation of pollutants, the active substance that still plays the main role is Bi_3O_4Cl, and the presence of excessive Ag reduces the number of active sites of Bi_3O_4Cl, which may hinder the catalytic degradation of pollutants (Chen et al., 2014).

According to the above research, the morphology of Bi_3O_4Cl does not change after Ag deposition. Ag content affects the photoelectric performance of Bi_3O_4Cl, and an appropriate concentration of Ag can maximize the catalytic activity of Bi_3O_4Cl.

3.2. Performance of Ag-Bi_3O_4Cl photocatalyst toward EC degradation

3.2.1. Applicability of Ag-Bi_3O_4Cl for CIP and TBBPA removal

As discussed in section "3.1. Characterization of photocatalysts," Ag addition changes the physical and chemical properties of Bi_3O_4Cl, which in turn affects its catalytic activity. In this section, the applicability of Ag-Bi_3O_4Cl toward the removal of CIP and TBBPA (as the target contaminants) is verified by analyzing the degradation performance of Ag-Bi_3O_4Cl plasmonic photocatalysts with different Ag loadings.

As shown in Figures 6A, C, the adsorption capacities of the different photocatalysts for both CIP and TBBPA are ranked as follows: 0.025-Ag-Bi_3O_4Cl > 0.05-Ag-Bi_3O_4Cl > 0.01-Ag-Bi_3O_4Cl > 0.1-Ag-Bi_3O_4Cl > Bi_3O_4Cl. Moreover, a single Bi_3O_4Cl photocatalyst had a poor effect on the treatment of ECs. After 210 min, the removal rate of pure Bi_3O_4Cl for CIP was only 51.4%, whereas after 120 min, the removal rate of TBBPA was only 36.0%.

In comparison, the effect of the Ag-Bi_3O_4Cl plasmon photocatalysts on the treatment of CIP and TBBPA was better than that of single Bi_3O_4Cl, but the effect of samples prepared with different Ag contents was still different. For samples (0.01–0.1)-Ag-Bi_3O_4Cl, their photocatalytic degradation efficiencies for CIP were 75.2, 92.0, 87.3, and 54.1% after 210 min, respectively. After 120 min, their photocatalytic degradation efficiencies of TBBPA were 71.5, 90.5, 83.4, and 56.5%, respectively. As shown in Figures 6B, D, 0.025-Ag-Bi_3O_4Cl exhibits the highest degradation rates of CIP (0.0107 min^{-1}) and TBBPA (0.0165 min^{-1}). The degradation of CIP/TBBPA was 1.8/2.2, 1.2/1.3, 3.7/3.6, and 3.5/3.6 times higher than those of 0.01-Ag-Bi_3O_4Cl, 0.05-Ag-Bi_3O_4Cl, 0.1-Ag-Bi_3O_4Cl, and Bi_3O_4Cl, respectively.

These results indicate that the efficiency of the Ag-Bi_3O_4Cl plasmon photocatalyst prepared by adding an appropriate amount of Ag to treat ECs in the water is much higher than that of a single

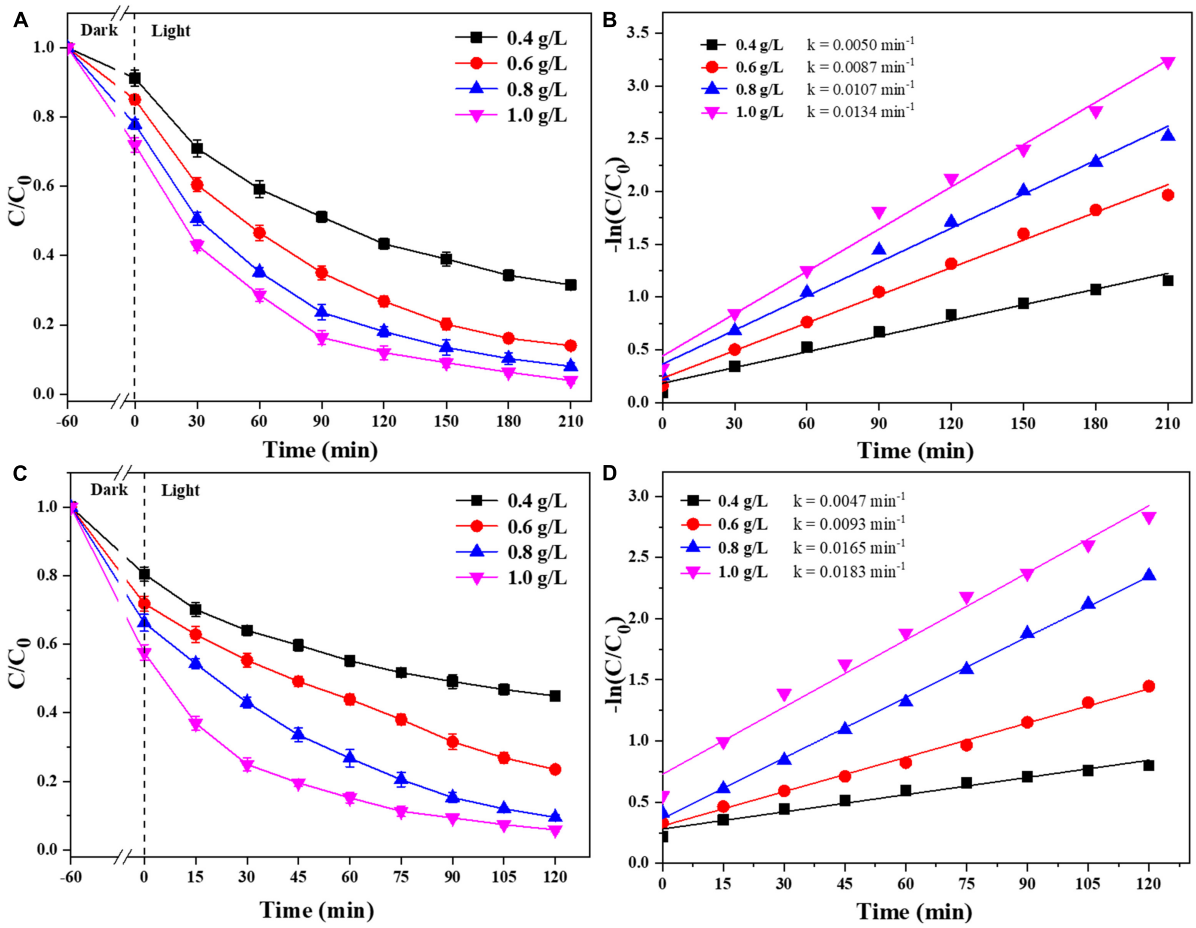

FIGURE 7
Removal efficiency of CIP and TBBPA by 0.025-Ag-Bi_3O_4Cl with different catalyst dosages: **(A)** removal efficiency of CIP; **(B)** kinetics of CIP removal; **(C)** removal efficiency of TBBPA; **(D)** kinetics of TBBPA removal.

Bi_3O_4Cl photocatalyst. Moreover, during the preparation process, the variation in the Ag metal content affected the photocatalytic performance of Ag-Bi_3O_4Cl, which showed a trend of increasing and then decreasing with increasing Ag metal content.

Based on the characterization analysis results discussed in section "3.1. Characterization of photocatalysts," the Ag content significantly affects the photoelectric performance of the Ag-Bi_3O_4Cl plasmon photocatalysts. The increase in Ag content reduces the recombination of photogenerated electron-hole pairs and enhances the migration and separation capabilities of electrons and holes, which is conducive to improving the performance of the photocatalyst. However, the active substance that plays the main role in the photocatalytic oxidation of pollutants is Bi_3O_4Cl. Excessive Ag metal content reduced the number of Bi_3O_4Cl active sites, which hindered the catalytic degradation of pollutants. Therefore, it is necessary to select an appropriate Ag content. The experiments described in this section show that 0.025-Ag-Bi_3O_4Cl is the optimal ratio.

3.2.2. Effect of catalyst dosage and solution pH on EC removal

We were selected that 0.025-Ag-Bi_3O_4Cl was used to study the effects of the photocatalyst dosage and reaction pH on the degradation of CIP and TBBPA. As shown in Figure 7, when the dosage of 0.025-Ag-Bi_3O_4Cl was increased from 0.4 to 1.0 g/L, the adsorption performance, removal efficiency, and reaction rate constant of CIP and TBBPA gradually increase with the increase of the catalyst dosage. This is because by adding more photocatalyst, more active sites were obtained, thus improving the adsorption and catalytic efficiency of CIP and TBBPA. Moreover, the dosage of 0.8 g/L of photocatalyst is sufficient to fully degrade CIP and TBBPA. Therefore, considering both cost and degradation efficiency, a catalyst dosage of 0.8 g/L was selected as the optimal dosage condition in this study, and 0.8 g/L is selected for the following experiments.

In addition, the effect of the initial pH of the pollutants on the photocatalyst degradation was studied. As shown in Figure 8, the photocatalysts were effectively degraded both CIP and TBBPA in weakly acidic and alkaline environments. When the initial pH of CIP and TBBPA is in a weak alkaline environment, 0.025-Ag-Bi_3O_4Cl exhibited the optimal adsorption and degradation effects (CIP: 93.8%; TBBPA: 94.9%) and the highest reaction rate constants (CIP: 0.02259 min^{-1}; TBBPA: 0.0195 min^{-1}). In contrast, the adsorption and treatment effects of the photocatalyst on pollutants are significantly reduced under strongly acidic conditions. Some studies have shown that the solubility of CIP is significantly affected

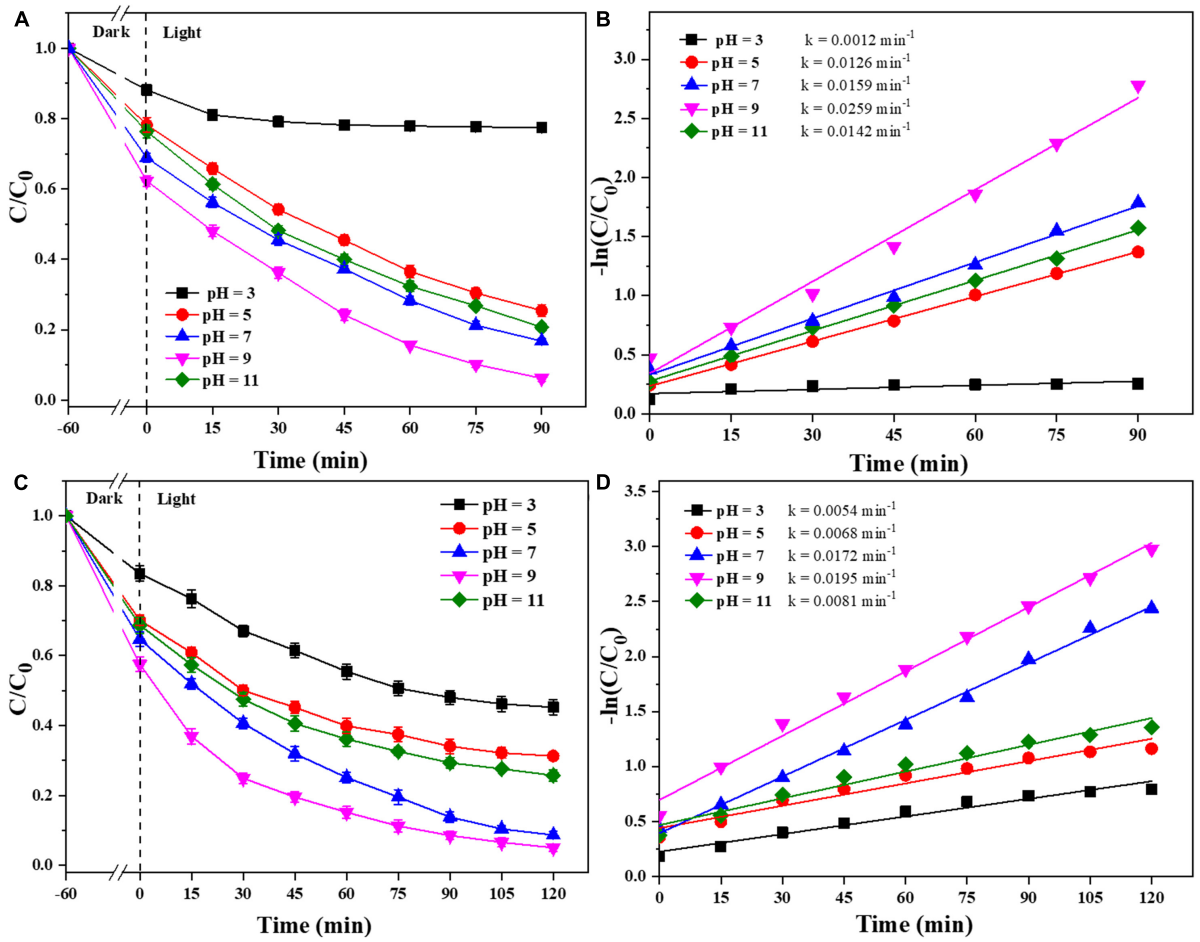

FIGURE 8
Removal efficiency of CIP and TBBPA by 0.025-Ag-Bi_3O_4Cl with different initial pH values of solution: **(A)** removal efficiency of CIP; **(B)** kinetics of CIP removal; **(C)** removal efficiency of TBBPA; **(D)** kinetics of TBBPA removal.

by pH and can form cationic, anionic, or amphoteric species, which mainly depends on its different pK_a (6.1 and 8.7) (Mao et al., 2016). Among them, amphoteric CIP ions have the lowest solubility and highest hydrophobicity, which results in a higher adsorption of CIP on the photocatalyst when the pH is between 6.1 and 8.7, thus indirectly improving the reaction rate. When the pH is higher than the TBBPA pK_a (~7.4), the degradation and debromination rates of TBBPA also increase sharply with an increase in pH, which contributes to easier degradation of TBBPA (Han et al., 2016). This also indicates that the Ag-Bi_3O_4Cl plasmon photocatalyst can adsorb and remove CIP and TBBPA in both weakly acidic and alkaline environments, which is a good practical application.

3.2.3. Reusability and stability of Ag-Bi_3O_4Cl

A reusability test of 0.025-Ag-Bi_3O_4Cl was performed; the results are shown in **Figure 9**. In **Figure 9A**, the SEM image of 0.025-Ag-Bi_3O_4Cl shows that its morphology did not change significantly before and after the reaction (**Figure 2**). Bi_3O_4Cl as the substrate is well preserved, and no Ag aggregation is observed on the photocatalyst surface. **Figure 9B** shows the XRD patterns of 0.025-Ag-Bi_3O_4Cl before and after the reaction, wherein the diffraction peaks are in the same position and the intensities remain unchanged, indicating that the photocatalyst has good stability.

Figures 9C, D show the photocatalytic degradation results of 0.025-Ag-Bi_3O_4Cl in five cycles. The CIP and TBBPA removal rates reach 70.6 and 71.2%, respectively, after five utilization cycles, suggesting the good reusability of the photocatalyst.

3.3. Photocatalytic mechanisms

3.3.1. Radical quenching experiments and total organic carbon removal

To explore the reaction mechanism of the Ag-Bi_3O_4Cl plasmonic photocatalyst system, radical-quenching experiments were conducted on the free radicals generated in the catalytic system (**Figure 10**).

The addition of TBA, as a quencher of $^{\cdot}OH$, had only a slight effect on the 0.025-Ag-Bi_3O_4Cl photocatalytic degradation of CIP and TBBPA, indicating that $^{\cdot}OH$ did not play a decisive role in the photocatalytic degradation of CIP and TBBPA (Jiang et al., 2018).

The addition of SO, as a quencher of h^+, significantly inhibited the 0.025-Ag-Bi_3O_4Cl photocatalytic degradation of both CIP and TBBPA. This result indicated that h^+ was the active species that played a dominant role in the photocatalytic degradation of CIP and TBBPA. This is because of the high valence-band (VB) position

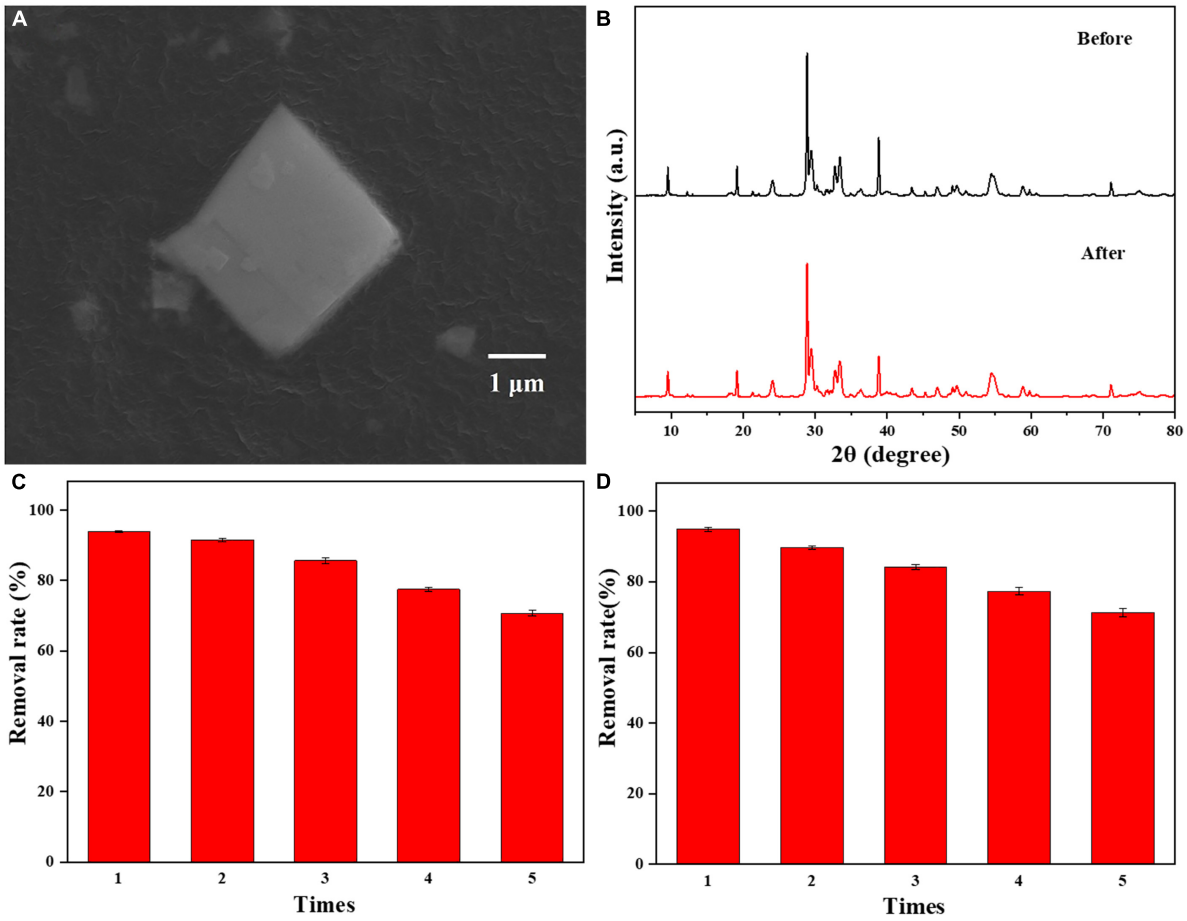

FIGURE 9
(A) SEM images of 0.025-Ag-Bi_3O_4Cl after use; **(B)** the XRD patterns of 0.025-Ag-Bi_3O_4Cl before and after use; reusability of 0.025-Ag-Bi_3O_4Cl in **(C)** CIP and **(D)** TBBPA degradation.

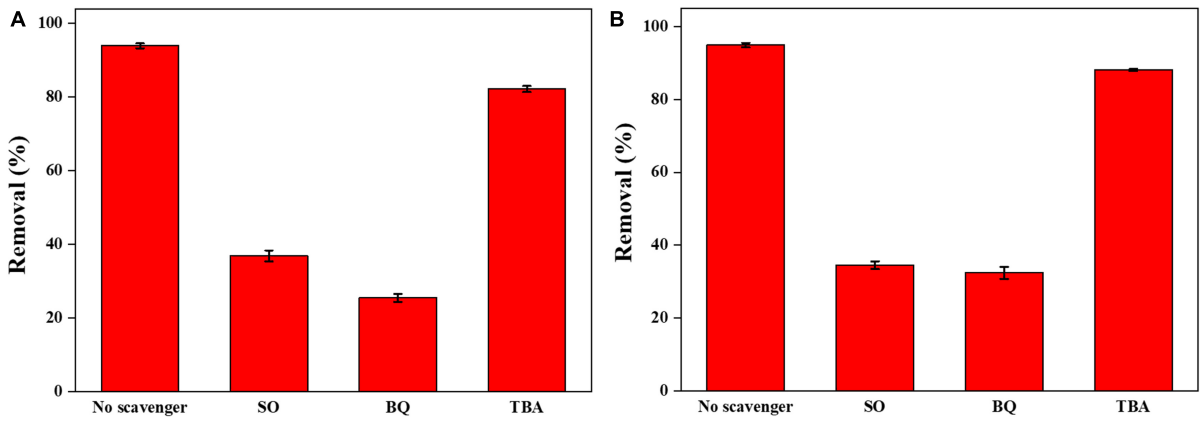

FIGURE 10
(A) Effects of various scavengers on the photocatalytic degradation of CIP; **(B)** effects of various scavengers on the photocatalytic degradation of TBBPA.

of Ag-Bi_3O_4Cl, and h^+ can directly oxidize organic pollutants (Long et al., 2022a).

The addition of BQ, as a quencher of $\cdot O_2^-$, also had a significant inhibitory effect on the photocatalytic degradation of CIP and TBBPA by 0.025-Ag Bi_3O_4Cl. This is due to the plasmon resonance phenomenon of Ag metal elements with light illumination, which greatly promotes the separation of electron-hole pairs and the generation of $\cdot O_2^-$, which can effectively oxidize and decompose pollutants in water (Li F. et al., 2014).

10.3389/fmicb.2023.1210790

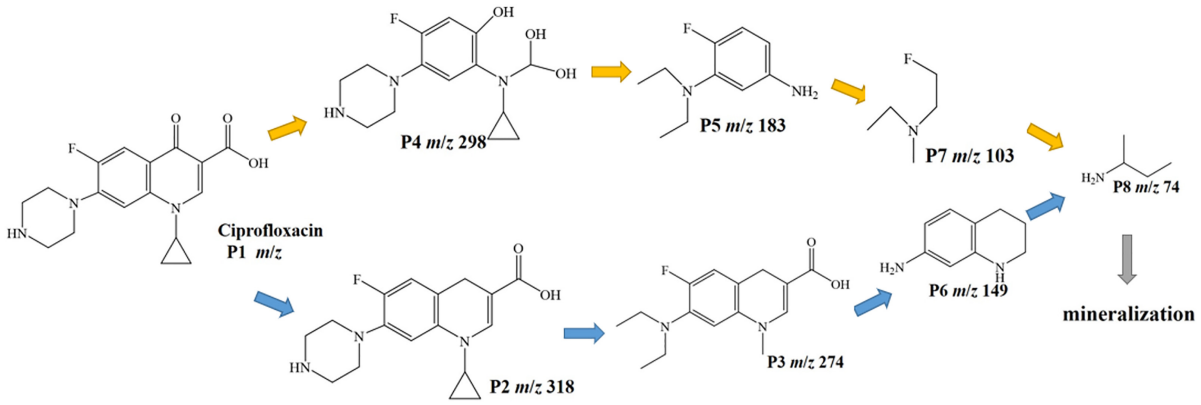

FIGURE 11
Suggested photocatalytic degradation pathways of CIP.

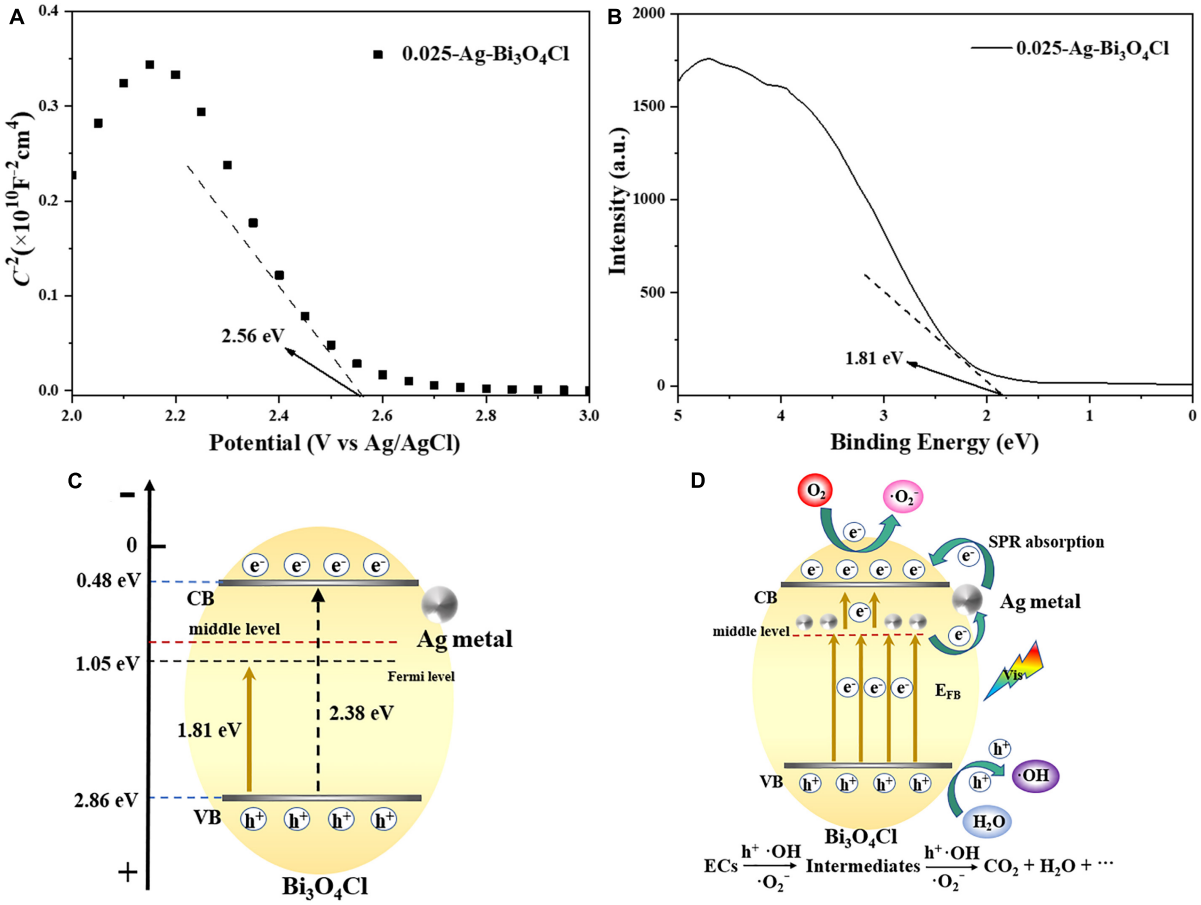

FIGURE 12
(A) Mott–Schottky plots of 0.025-Ag-Bi_3O_4Cl; **(B)** valence band (VB) XPS spectra of 0.025-Ag-Bi_3O_4Cl; **(C)** structural shifts of 0.025-Ag-Bi_3O_4Cl plasmon photocatalyst; **(D)** possible mechanism of Ag-Bi_3O_4Cl degrading ECs.

From the above results, it is clear that photo-generated holes (h^+) and superoxide radicals ($\cdot O_2^-$) play the dominant role in the photocatalytic degradation of CIP and TBBPA.

The photocatalytic degradation of CIP and TBBPA using total organic carbon (TOC) was investigated. After 210 min (CIP) and 120 min (TBBPA) of visible light irradiation, the removal rates of TOC reached 40.7 and 47.2%, respectively. Further removal of these intermediates was achieved by increasing the reaction time. These results indicate that the Ag-Bi_3O_4Cl plasmon photocatalysts are effective for the treatment of ECs and exhibit good pollutant mineralization ability.

3.3.2. Degradation pathways of CIP and biotoxicity analysis of intermediate products

The intermediates of CIP photodegradation on 0.025-Ag Bi_3O_4Cl were detected by LC-MS (**Supplementary Figure 2** and **Supplementary Table 1**). Based on these fragments and previous reports, two different degradation pathways were inferred in **Figure 11** (Dewitte et al., 2008; Gao et al., 2021). In pathway I, CIP was attacked by the strong oxidizing radical and deoxygenated to produce the product P2 (m/z = 318). Next, the piperazine ring was broken and the ternary ring was further damaged by oxidation to produce products P3 (m/z = 274), P6 (m/z = 149), and P8 (m/z = 74). In pathway II, CIP was attacked by the oxide species and substituted with hydroxyl groups to generate product P4 (m/z = 298). Next, the C-N bond of the piperazine ring was broken and the ternary ring is removed, producing intermediate P5 (m/z = 183) and through a series of cleavage processes intermediates P7 (m/z = 103), P8 (m/z = 74) were generated. Finally, the above intermediate products could be decomposed into CO_2 and H_2O.

The biological toxicity of CIP degradation products was analyzed using EPI-ECOSAR software. There were two possible pathways for the degradation of CIP by 0.025-Ag-Bi_3O_4Cl plasmon photocatalysts, namely CIP-P2-P3-P6-P8 and CIP-P4-P5-P7-P8. As shown in **Supplementary Table 2**, the biotoxicity of the intermediate products of CIP showed a trend of first significantly increasing in toxicity and then gradually decreasing. The biotoxicity of some intermediate products (P3 and P5) were much higher than that of CIP. Therefore, more attention should be paid to the detection of biotoxicity of degradation products in the treatment of ECs.

3.3.3. Possible mechanism of CIP and TBBPA removal over Ag-Bi_3O_4Cl

To illustrate the mechanism of the Ag metal-modified Bi_3O_4Cl at the electronic structure level, the flat band potential (E_{FB}) of 0.025-Ag-Bi_3O_4Cl was measured using Mott–Schottky plots. As shown in **Figure 12A**, the negative slope of the tangent line in the Mott–Schottky plot of 0.025-Ag Bi_3O_4Cl, which is a typical p-type semiconductor (Abe et al., 2015), indicates that the introduction of Ag metal did not change the semiconductor type of Bi_3O_4Cl. The flat band potential (E_{FB}) of 0.025-Ag Bi_3O_4Cl was 2.56 eV [2.76 eV versus normal hydrogen electrode (NHE)]. The E_{VB} position of the p-type semiconductor is close to its E_{FB} potential, which is approximately positive for E_{FB} (0.1 eV) (Zheng and Lei, 2018). From this, it can be seen that in this work, the corresponding potential of E_{VB} of 0.025-Ag Bi_3O_4Cl is approximately 2.86 eV versus NHE. **Figure 12B** shows the X-ray photoelectron spectroscopy (XPS)-VB spectrum of 0.025-Ag-Bi_3O_4Cl, and the potential difference between VB of 0.025-Ag-Bi_3O_4Cl and its Fermi energy level is 1.81 eV as can be seen from the figure. Moreover, according to the formula $E_{CB} = E_{VB} - E_g$ (Long et al., 2020c) and UV-vis results (The bandwidth E_g for Bi_3O_4Cl is 2.38 eV), the E_{CB} and E_{VB} value of 0.025-Ag-Bi_3O_4Cl were calculated as 0.48 and 2.86 eV, respectively (**Figure 12C**).

Based on the above analysis and related literature reports (Ma et al., 2015), potential photocatalytic mechanisms involving electron migration pathways and the catalytic degradation of pollutants by Ag-Bi_3O_4Cl plasmon photocatalysts were proposed (**Figure 12D**). During the photocatalytic reaction, the charge carriers in the VB of Bi_3O_4Cl were excited by visible light. When Ag metal is deposited on the surface of Bi_3O_4Cl, it increases the concentration of oxygen defects, resulting in the formation of an intermediate energy level in the semiconductors (Pan and Heagy, 2019). In addition, the plasmon resonance effect generated by the Ag metal under illumination greatly increased the light absorption ability of the photocatalyst (Shi et al., 2018). The coexistence of oxygen defects and Ag metals promotes electron transfer (Gao et al., 2014). Moreover, before Bi_3O_4Cl was modified, its electrons were directly excited from the VB to the conduction band (CB), making it prone to electron-hole pair recombination. In contrast, after plasmon modification, the electron migration path of the photocatalyst shifts to the intermediate energy level formed by Ag-Bi_3O_4Cl, where electrons from the VB in Bi_3O_4Cl are first excited, and then some of them are stored by Ag metal. Another part of the electron transitions from the Ag metal to the CB of Bi_3O_4Cl, which greatly hinders the probability of electron-hole recombination and can effectively improve the performance of the photocatalyst. Since the redox potential of $O_2/{}^{\cdot}O_2^-$ is −0.33 eV, which is more negative than the CB position of 0.025-Ag-Bi_3O_4Cl (0.48 eV), it is theoretically impossible to generate ${}^{\cdot}O_2^-$. However, due to the plasmon resonance effect of Ag metal, the electrons excited to the CB of Bi_3O_4Cl via Ag metal can react with O_2, thus generating ${}^{\cdot}O_2^-$ free radicals, which is consistent with the phenomenon reported by Jiang et al. (2018). The carrier charge separation led to the generation of a large number of h^+ ions in the VB of Ag-Bi_3O_4Cl. And the h^+ can also react with water to generate strong oxidizing radicals ${}^{\cdot}OH$. Finally, the generated h^+, ${}^{\cdot}O_2^-$, and ${}^{\cdot}OH$ have strong oxidation ability, gradually degrading emerging contaminants into small molecule organic compounds, CO_2, and H_2O.

The potential reaction process for the Ag-Bi_3O_4Cl photocatalytic degradation of the ECs is shown in Eqs. (1–7).

$$Ag{-}Bi_3O_4Cl_{(s)} + hv \rightarrow e_{CB}^- + h_{VB}^+ \quad (1)$$

$$ECs + hv \rightarrow ECs^* + e_{CB}^- \quad (2)$$

$$O_2 + e_{CB}^- \rightarrow \cdot O_2^- \quad (3)$$

$$H_2O + h_{VB}^+ \rightarrow \cdot OH + OH^- \quad (4)$$

$$OH^- + h_{VB}^+ \rightarrow \cdot OH \quad (5)$$

$$h_{VB}^+ + ECs \rightarrow \text{intermediates} \rightarrow CO_2 + H_2O \quad (6)$$

$$\cdot O_2^- + ECs \rightarrow \text{intermediates} \rightarrow CO_2 + H_2O \quad (7)$$

4. Conclusion

In this study, a series of Ag-Bi_3O_4Cl plasmonic photocatalysts were synthesized using a photodeposition method and

characterized in detail. The introduction of Ag does not alter the morphology of Bi_3O_4Cl. With an increase in the Ag content, the oxygen defects on the photocatalyst surface first increase and then decrease. An appropriate Ag content of Ag-Bi_3O_4Cl can effectively enhance the photoelectric performance. The presence of Ag and oxygen defects promote the electron transfer in the photocatalyst. Under the optimal conditions (Ag content: 0.025, catalyst dosage: 0.8 g/L, and solution pH: 9), the Ag-Bi_3O_4Cl plasmonic photocatalyst can remove 93.8% of CIP and 94.9% of TBBPA, under visible light. Photogenerated holes (h^+) and superoxide radicals ($^{\cdot}O_2^-$) are strongly oxidative radicals that play major roles in the photocatalytic reactions. The CIP degradation pathway was analyzed; the biological toxicity of CIP degradation products showed a trend of first increasing and then decreasing. In this study, a green, and stable plasmonic photocatalyst was developed and applied for the efficient removal of ECs from water and the biological toxicity of the degradation products was analyzed.

Data availability statement

The original contributions presented in this study are included in the article/**Supplementary material**, further inquiries can be directed to the corresponding authors.

Author contributions

ZL: conceptualization, methodology, and writing—original draft preparation. TG: data curation, investigation, and validation. CC: data curation and validation. GZ: supervision, visualization, investigation, writing—review, and editing. JZ: visualization, writing—review and editing, and funding acquisition. All authors contributed to the article and approved the submitted version.

Funding

This work was supported by the Science and Technology Innovation Project of Colleges and Universities in Shanxi Province (2022L361), the Youth Scientific Research Project of Shanxi Basic Research Program (202203021222311), the Doctoral Research Foundation of Changzhi Medical College (BS202204), the Project of Shenzhen Science and Technology Innovation Commission (No. KCXFZ20211020163817025), and the University-level Supporting Projects by Shenzhen polytechnic (No. 6020320003K).

Acknowledgments

We thank Shiyanjia Lab (www.shiyanjia.com) for the material testing service.

Conflict of interest

The authors declare that the research was conducted in the absence of any commercial or financial relationships that could be construed as a potential conflict of interest.

Publisher's note

All claims expressed in this article are solely those of the authors and do not necessarily represent those of their affiliated organizations, or those of the publisher, the editors and the reviewers. Any product that may be evaluated in this article, or claim that may be made by its manufacturer, is not guaranteed or endorsed by the publisher.

Supplementary material

The Supplementary Material for this article can be found online at: https://www.frontiersin.org/articles/10.3389/fmicb.2023.1210790/full#supplementary-material

References

Abe, T., Tanno, Y., Taira, N., and Nagai, K. (2015). Efficient organo-photocatalysis system of an n-type perylene derivative/p-type cobalt phthalocyanine bilayer for the production of molecular hydrogen from hydrazine. *RSC Adv.* 5, 46325–46329. doi: 10.1039/C5RA03842A

Apelgren, P., Amoroso, M., Säljö, K., Montelius, M., Lindahl, A., Stridh Orrhult, L., et al. (2019). Reversibly tuning the surface state of Ag via the assistance of photocatalysis in Ag/BiOCl. *Nanotechnology* 30:305601. doi: 10.1088/1361-6528/ab192e

Bi, C., Cao, J., Lina, H., Wang, Y., and Chen, S. (2016). Applied catalysis B : environmental enhanced photocatalytic activity of $Bi_{12}O_{17}Cl_2$ through loading Pt quantum dots as a highly efficient electron capturer. *Appl. Catal. B, Environ.* 195, 132–140. doi: 10.1016/j.apcatb.2016.05.011

Chang, F., Wang, X., Luo, J., Wang, J., Xie, Y., Deng, B., et al. (2017). Ag/$Bi_{12}O_{17}Cl_2$ composite: a case study of visible-light-driven plasmonic photocatalyst. *Mol. Catal.* 427, 45–53. doi: 10.1016/j.molcata.2016.11.028

Chen, Y., Huang, W., He, D., Situ, Y., and Huang, H. (2014). Construction of heterostructured g-C_3N_4/Ag/TiO_2 microspheres with enhanced photocatalysis performance under visible-light irradiation. *ACS Appl. Mater. Interfaces* 6, 14405–14414. doi: 10.1021/am503674e

Cui, P., Wang, J., Wang, Z., Chen, J., Xing, X., Wang, L., et al. (2016). Bismuth oxychloride hollow microspheres with high visible light photocatalytic activity. *Nano Res.* 9, 593–601. doi: 10.1007/s12274-015-0939-z

Cui, Z., Dong, X., Sun, Y., Zhou, Y., Zhang, Y., and Dong, F. (2018). Simultaneous introduction of oxygen vacancies and Bi metal onto the {001} facet of Bi_3O_4Cl woven nanobelts for synergistically enhanced photocatalysis. *Nanoscale* 10, 16928–16934. doi: 10.1039/C8NR05322G

Dewitte, B., Dewulf, J., Demeestere, K., Van De Vyvere, V., De Wispelaere, P., and Van Langenhove, H. (2008). Ozonation of ciprofloxacin in water: HRMS identification of reaction products and pathways. *Environ. Sci. Technol.* 42, 4889–4895. doi: 10.1021/es8000689

Gao, W., Wang, M., Ran, C., Yao, X., Yang, H., Liu, J., et al. (2014). One-pot synthesis of Ag/r-GO/TiO_2 nanocomposites with high solar absorption and enhanced anti-recombination in photocatalytic applications. *Nanoscale* 6, 5498–5508. doi: 10.1039/c3nr05466g

Gao, Y., Cong, S., Yu, H., and Zou, D. (2021). Investigation on microwave absorbing properties of 3D C@$ZnCo_2O_4$ as a highly active heterogenous catalyst and the degradation of ciprofloxacin by activated persulfate process. *Sep. Purif. Technol.* 262:118330. doi: 10.1016/j.seppur.2021.118330

Han, S. K., Yamasaki, T., and Yamada, K. (2016). Photodecomposition of tetrabromobisphenol A in aqueous humic acid suspension by irradiation with light of various wavelengths. *Chemosphere* 147, 124–130. doi: 10.1016/j.chemosphere.2015.12.072

Hong, Y. Z., Yang, L., and Tian, Y. W. (2023). Rational design 2D/3D MoS_2/In_2O_3 composites for great boosting photocatalytic H_2 production coupled with dye degradation. *J. Taiwan Inst. Chem. E.* 146:104862. doi: 10.1016/j.jtice.2023.104862

Hou, W., Liu, Z., Pavaskar, P., Hung, W. H., and Cronin, S. B. (2011). Plasmonic enhancement of photocatalytic decomposition of methyl orange under visible light. *J. Catal.* 277, 149–153. doi: 10.1016/j.jcat.2010.11.001

Jiang, E., Liu, X., Che, H., Liu, C., Dong, H., and Che, G. (2018). Visible-light-driven Ag/Bi_3O_4Cl nanocomposite photocatalyst with enhanced photocatalytic activity for degradation of tetracycline. *RSC Adv.* 8, 37200–37207. doi: 10.1039/C8RA07482H

Jiang, R., Lu, G., Nkoom, M., Yan, Z., Wu, D., Liu, J., et al. (2020). Mineralization and toxicity reduction of the benzophenone-1 using 2D/2D Cu_2WS_4/BiOCl Z-scheme system: simultaneously improved visible-light absorption and charge transfer efficiency. *Chem. Eng. J.* 400:125913. doi: 10.1016/j.cej.2020.125913

Jiang, R., Lu, G., Yan, Z., Wu, D., Liu, J., and Zhang, X. (2019). Enhanced photocatalytic activity of a hydrogen bond-assisted 2D/2D Z-scheme $SnNb_2O_6/Bi_2WO_6$ system: highly efficient separation of photoinduced carriers. *J. Colloid Interface Sci.* 552, 678–688. doi: 10.1016/j.jcis.2019.05.104

Klein, E., Milkowska-Shibata, M., Tseng, K., Sharland, M., Gandra, S., Pulcini, C., et al. (2020). Assessment of WHO antibiotic consumption and access targets in 76 countries, 2000-15: an analysis of pharmaceutical sales data. *Lancet Infect. Dis.* 21, 107–115. doi: 10.1016/S1473-3099(20)30332-7

Law, R., Allchin, C., Boer, J., Covaci, A., Herzke, D., Lepom, P., et al. (2006). Levels and trends of brominated flame retardants in the European environment. *Chemosphere* 64, 187–208. doi: 10.1016/j.chemosphere.2005.12.007

Li, F., Wang, Q., Wang, X., Li, B., Hao, Y., Liu, R., et al. (2014). In-situ one-step synthesis of novel BiOCl/$Bi_{24}O_{31}Cl_{10}$ heterojunctions via self-combustion of ionic liquid with enhanced visible-light photocatalytic activities. *Appl. Catal. B Environ.* 150–151, 574–584. doi: 10.1016/j.apcatb.2014.01.009

Li, J., Zhang, L., Li, Y., and Yu, Y. (2014). Synthesis and internal electric field dependent photoreactivity of Bi_3O_4Cl single-crystalline nanosheets with high {001} facet exposure percentages. *Nanoscale* 6, 167–171. doi: 10.1039/C3NR05246J

Liu, Y., Zhu, G., Gao, J., Zhu, R., Hojamberdiev, M., Wang, C., et al. (2017). A novel synergy of Er^{3+}/Fe^{3+}co-doped porous Bi_5O_7I microspheres with enhanced photocatalytic activity under visible-light irradiation. *Appl. Catal. B Environ.* 205, 421–432. doi: 10.1016/j.apcatb.2016.12.061

Liu, Z. H., Dang, Z., Yin, H., and Liu, Y. (2021). Making waves: improving removal performance of conventional wastewater treatment plants on endocrine disrupting compounds (EDCs): their conjugates matter. *Water Res.* 188:116469. doi: 10.1016/j.watres.2020.116469

Long, Z., Li, Q., Wei, T., Zhang, G., and Ren, Z. (2020a). Historical development and prospects of photocatalysts for pollutant removal in water. *J. Hazard. Mater.* 395:122599. doi: 10.1016/j.jhazmat.2020.122599

Long, Z., Xian, G., Zhang, G., Zhang, T., and Li, X. (2020b). BiOCl-$Bi_{12}O_{17}Cl_2$ nanocomposite with high visible-light photocatalytic activity prepared by an ultrasonic hydrothermal method for removing dye and pharmaceutical. *Chinese J. Catal.* 41, 464–473. doi: 10.1016/S1872-2067(19)63474-1

Long, Z., Zhang, G., Wei, T., Niu, L., Zhu, J., and Li, J. (2020c). Tuning of Bi_xO_yCl formation with sonication time during ultrasound-hydrothermal preparation. *J. Ind. Eng. Chem.* 84, 322–331. doi: 10.1016/j.jiec.2020.01.014

Long, Z., Song, H., Zhang, G., Gao, J., and Zhu, J. (2022a). Fabrication of Bi-Bi_3O_4Cl plasmon photocatalysts for removal of aqueous emerging contaminants under visible light. *J. Environ. Sci.* 118, 87–100. doi: 10.1016/j.jes.2021.08.026

Long, Z., Wang, H., Huang, K., Zhang, G., and Xie, H. (2022b). Di-functional Cu^{2+}-doped BiOCl photocatalyst for degradation of organic pollutant and inhibition of cyanobacterial growth. *J. Hazard. Mater.* 424:127554. doi: 10.1016/j.jhazmat.2021.127554

Ma, L., Sun, T., Cai, H., Zhou, Z. Q., Sun, J., and Lu, M. (2015). Enhancing photocatalysis in $SrTiO_3$ by using Ag nanoparticles: a two-step excitation model for surface plasmon-enhanced photocatalysis. *J. Chem. Phys.* 143:084706. doi: 10.1063/1.4929910

Mao, D., Yu, A., Ding, S., Wang, F., Yang, S., Sun, C., et al. (2016). One-pot synthesis of BiOCl half-shells using microemulsion droplets as templates with highly photocatalytic performance for the degradation of ciprofloxacin. *Appl. Surf. Sci.* 389, 742–750. doi: 10.1016/j.apsusc.2016.07.178

Morin-Crini, N., Lichtfouse, E., Fourmentin, M., Ribeiro, A. R. L., Noutsopoulos, C., Mapelli, F., et al. (2022). Removal of emerging contaminants from wastewater using advanced treatments. a review. *Nanotechnology* 30:305601.

Niu, L., Xian, G., Long, Z., Zhang, G., and Zhou, N. (2020a). MnCeOx/diatomite catalyst for persulfate activation to degrade organic pollutants. *J. Environ. Sci.* 89, 206–217. doi: 10.1016/j.jes.2019.09.020

Niu, L., Xian, G., Long, Z., Zhang, G., Zhu, J., and Li, J. (2020b). $MnCeO_X$ with high efficiency and stability for activating persulfate to degrade AO7 and ofloxacin. *Ecotoxicol. Environ. Saf.* 191:110228. doi: 10.1016/j.ecoenv.2020.110228

Pan, H., and Heagy, M. D. (2019). Plasmon-enhanced photocatalysis: Ag/TiO_2 nanocomposite for the photochemical reduction of bicarbonate to formic acid. *MRS Adv.* 4, 425–433. doi: 10.1557/adv.2018.677

Phuruangrat, A., Thongtem, T., and Thongtem, S. (2021). Microwave-assisted deposition synthesis, characterization and photocatalytic activities of UV-light-driven Ag/BiOCl nanocomposites. *Inorg. Nano-Metal Chem.* 51, 1813–1821. doi: 10.1080/24701556.2020.1855198

Shi, C., Dong, X., Wang, X., Ma, H., and Zhang, X. (2018). Ag nanoparticles deposited on oxygen-vacancy-containing $BiVO_4$ for enhanced near-infrared photocatalytic activity. *Chinese J. Catal.* 39, 128–137. doi: 10.1016/S1872-2067(17)62990-5

Sun, M., Zhang, W., Sun, Y., Zhang, Y., and Dong, F. (2019). Synergistic integration of metallic Bi and defects on BiOI: enhanced photocatalytic NO removal and conversion pathway. *Chinese J. Catal.* 40, 826–836. doi: 10.1016/S1872-2067(18)63195-X

Wang, H., Xi, H., Xu, L., Jin, M., Zhao, W., and Liu, H. (2021). Ecotoxicological effects, environmental fate and risks of pharmaceutical and personal care products in the water environment: a review. *Sci. Total Environ.* 788:147819. doi: 10.1016/j.scitotenv.2021.147819

Wang, X., Liu, X., Liu, G., Zhang, C., Liu, G., Xu, S., et al. (2019). Rapid synthesis of BiOCl graded microspheres with highly exposed (110) facets and oxygen vacancies at room temperature to enhance visible light photocatalytic activity. *Catal. Commun.* 130:105769. doi: 10.1016/j.catcom.2019.105769

Xinping, L., Tao, H., Fuqiang, H., Wendeng, W., and Jianlin, S. (2006). Photocatalytic activity of a Bi-based oxychloride Bi_3O_4Cl. *J. Phys. Chem. B* 110, 24629–24634. doi: 10.1021/jp065373m

Xu, X., Yan, Q., Gu, X., and Luo, Y. (2019). The preparation and photocatalytic performance of BiOCl@Ag, a visible-light responsive catalyst. *J. Mater. Sci. Mater. Electron.* 30, 8892–8902. doi: 10.1007/s10854-019-01217-z

Yu, C., Cao, F., Li, G., Wei, R., Yu, J. C., Jin, R., et al. (2013). Novel noble metal (Rh, Pd, Pt)/BiOX(Cl, Br, I) composite photocatalysts with enhanced photocatalytic performance in dye degradation. *Sep. Purif. Technol.* 120, 110–122 doi: 10.1016/j.seppur.2013.09.036

Zhang, D., Tan, G., Wang, M., Li, B., Dang, M., Wang, Y., et al. (2020). The formation of direct Z-scheme Ag/BiOCl/$AgIO_3$ heterojunction and its degradation stability. *Appl. Surf. Sci.* 530:147228. doi: 10.1016/j.apsusc.2020.147228

Zhang, L., Liang, C., Guo, H., Niu, C. G., Zhao, X. F., Wen, X. J., et al. (2019). Construction of a high-performance photocatalytic fuel cell (PFC) based on plasmonic silver modified Cr-BiOCl nanosheets for simultaneous electricity production and pollutant removal. *Nanoscale* 11, 6662–6676. doi: 10.1039/C8NR09616C

Zhao, L., Deng, J., Sun, P., Liu, J., Ji, Y., Nakada, N., et al. (2018). Nanomaterials for treating emerging contaminants in water by adsorption and photocatalysis: systematic review and bibliometric analysis. *Sci. Total Environ.* 627, 1253–1263. doi: 10.1016/j.scitotenv.2018.02.006

Zheng, J., and Lei, Z. (2018). Incorporation of CoO nanoparticles in 3D marigold flower-like hierarchical architecture MnCo2O4 for highly boosting solar light photo-oxidation and reduction ability. *Appl. Catal. B Environ.* 237, 1–8. doi: 10.1016/j.apcatb.2018.05.060

Zou, P., Li, Z., Jia, P., Luo, G., and Wang, C. (2021). Enhanced photocatalytic activity of bismuth oxychloride by in-situ introducing oxygen vacancy. *Colloids Surfaces Physicochem. Eng. Asp.* 623:126705. doi: 10.1016/j.colsurfa.2021.126705

frontiers | Frontiers in Microbiology

TYPE Original Research
PUBLISHED 10 July 2023
DOI 10.3389/fmicb.2023.1224207

OPEN ACCESS

EDITED BY
Dingchang Li,
East China Jiaotong University,
China

REVIEWED BY
Xu Hui,
Research Center for Eco-environmental Sciences (CAS), China
Hongbiao Du,
Tsinghua University, China
Hongxia Zhang,
Chinese Academy of Sciences (CAS), China

*CORRESPONDENCE
Xuemei Li
✉ 20150023@ruc.edu.cn

†These authors have contributed equally to this work

RECEIVED 17 May 2023
ACCEPTED 26 June 2023
PUBLISHED 10 July 2023

CITATION
Wang H, Xiang H, Xiong T, Feng J, Zhang J and Li X (2023) A straightforward approach utilizing an exponential model to compensate for turbidity in chemical oxygen demand measurements using UV-vis spectrometry. *Front. Microbiol.* 14:1224207. doi: 10.3389/fmicb.2023.1224207

A straightforward approach utilizing an exponential model to compensate for turbidity in chemical oxygen demand measurements using UV-vis spectrometry

Hongliang Wang[1], Houkui Xiang[1†], Tongqiang Xiong[1†], Jinping Feng[1†], Jianquan Zhang[1] and Xuemei Li[2*]

[1]School of Automation, Hubei University of Science and Technology, Xianning, China, [2]Office of Laboratory Management and Teaching Facilities Development, Renmin University of China, Beijing, China

Recently, ultraviolet-visible (UV-vis) absorption spectrometry has garnered considerable attention because it enables real-time and unpolluted detection of chemical oxygen demand (COD) and plays a crucial role in the early warning of emerging organic contaminants. However, the accuracy of detection is inevitably constrained by the co-absorption of organic pollutants and turbidity at UV wavelengths. To ensure accurate detection of COD, it is necessary to directly subtract the absorbance caused by turbidity from the overlaid spectrum using the principle of superposition. The absorbance of COD is confined to the UV range, whereas that of turbidity extends across the entire UV-vis spectrum. Therefore, based on its visible absorbance, the UV absorbance of turbidity can be predicted. In this way, the compensation for turbidity is achieved by subtracting the predicted absorbance from the overlaid spectrum. Herein, a straightforward yet robust exponential model was employed based on this principle to predict the corresponding absorbance of turbidity at UV wavelengths. The model was used to analyze the overlaid absorption spectra of synthetic water samples containing COD and turbidity. The partial least squares (PLS) method was employed to predict the COD concentrations in synthetic water samples based on the compensated spectra, and the corresponding root mean square error (RMSE) values were recorded. The results indicated that the processed spectra yielded a considerably lower RMSE value (9.51) than the unprocessed spectra (29.9). Furthermore, the exponential model outperformed existing turbidity compensation models, including the Lambert-Beer law-based model (RMSE=12.53) and multiple-scattering cluster method (RMSE=79.34). Several wastewater samples were also analyzed to evaluate the applicability of the exponential model to natural water. UV analysis yielded undesirable results owing to filtration procedures. However, the consistency between the compensated spectra and filtered wastewater samples in the visible range demonstrated that the model is applicable to natural water. Therefore, this proposed method is advantageous for improving the accuracy of COD measurement in turbid water.

KEYWORDS

chemical oxygen demand, turbidity compensation, ultraviolet-visible spectrometry, turbid water, exponential model

1. Introduction

With the rapid development of industries and explosive population growth, considerable amounts of emerging organic contaminants are being discharged into natural water bodies, causing severe environmental issues in the world today (Lapworth et al., 2012; Pal et al., 2014). Chemical oxygen demand (COD), which represents the level of organic pollutants in water, is a crucial indicator of the impact of emerging organic contaminants on water quality. Having reliable COD analysis methods is essential for effective water quality monitoring in wastewater treatment, a prerequisite for controlling water pollution. Currently, methods for measuring COD include the potassium permanganate method, the dichromate method, the flow-injection analysis method, the electrochemical analysis method, and ultraviolet-visible (UV-vis) spectroscopy (Li et al., 2018). Among these methods, UV-vis spectroscopy is the most commonly used optical technique for assessing the COD concentration in water (Hu and Wang, 2017; Xu et al., 2023). This approach indirectly measures the absorption of UV-vis light by organic matter to determine COD levels.

UV-vis spectroscopy is widely utilized for COD measurement due to its rapid measurement time, lack of secondary pollution, reagent-free nature, and ability to provide real-time determination (Carré et al., 2017; Ma et al., 2018). However, UV-vis spectroscopy is typically limited by the interference of suspended particles; thus, effective methods must be adopted to suppress the influence of interfering factors and improve prediction accuracy (Wu et al., 2017; Chen et al., 2021). Turbidity compensation has become a research focus in the area of COD measurement based on UV-vis spectroscopy (Hu et al., 2016; Li et al., 2019; Hu et al., 2020; Kang et al., 2022; Zhang et al., 2022). Nevertheless, the turbidity compensation algorithm for COD measurement has not been extensively researched.

Presently, there are primarily two categories of turbidity compensation methods (Li et al., 2019). In one category, the COD value is corrected by using a model of the COD prediction error versus turbidity; however, such a model cannot completely eliminate the impact of turbidity, leading to poor versatility. In the second category, the absorption spectrum is determined by subtracting the absorbance caused by turbidity, requiring a complex model to calculate the turbidity absorbance. Apart from exhibiting large deviations, these complex models pose challenges for embedded programming and local calibration, rendering them unsuitable for online sensors. To address these limitations, the main objectives of this study were as follows: (1) develop an effective turbidity compensation method for COD measurement using UV-vis spectrometry, (2) investigate the applicability of embedded programming and local calibration as well as the possibility of online spectrometers to the model, (3) evaluate the accuracy of COD prediction in mixtures containing COD and turbidity, and (4) explore the feasibility of measuring COD in natural water using this model.

2. Materials and methods

2.1. Experimental device

The spectral measuring system primarily comprises four parts: a light source, quartz cell, micro UV-vis spectrometer, and computer (Figure 1). The xenon lamp source (42 mm × 42 mm × 37 mm, L13651-01, HAMAMATSU) produced a light of 185 to 2000 nm, which was collimated by a lens and passed through the quartz cell. The attenuated light emanating from the quartz cell was gathered by a 256-pixel microspectrometer (15 mm × 22 mm × 35 mm, UV20 UV-vis, Horiba) through a converging lens. The operation and data collection of the spectrometer were controlled using an additional computer. The xenon lamp and spectrometer used in this study were compact enough to be enclosed within a cylinder, enabling the development of streamlined spectral probes. Ensuring that the optical system exhibits sufficient stability is crucial, because irregular factors can easily disrupt the absorption law of turbidity across the entire spectrum.

2.2. Water samples and materials

The absorption behavior of turbidity was investigated using formazine owing to its excellent optical stability. The formazine suspensions were prepared via a chemical reaction between hydrazine sulfate and hexamethylenetetramine, following the method outlined in ISO 7027-2016. To establish a mathematical model for turbidity compensation, 15 formazine suspensions of 10–200 FNU (formazine nephelometric units) were prepared. Further, a series of mixtures containing COD and turbidity were measured to validate the performance of the established model. Subsequently, 30 different mixtures with specific concentrations of COD and turbidity were prepared using a COD stock solution and formazine suspension. The COD stock solution was prepared by dissolving potassium hydrogen phthalate in water. All reagents were purchased from Maclin (China), and all solutions were prepared using ultrapure water (18.2 MΩ cm at 25°C) obtained from a Millipore Milli-Q system.

Several wastewater samples were also analyzed to assess the applicability of the model to natural water. The samples were collected at the inlet of an A/A/O municipal wastewater treatment system located in the Low Carbon Water Environmental Technology Center at Renmin University in China. The turbidity absorbance of wastewater was determined by calculating the difference spectra between filtered and unfiltered samples, with the filtration process utilizing 0.45 μm membranes (Haining Kewel Company, China). Finally, the feasibility of the model was assessed through a comparison of the compensated and measured spectra from the filtered water samples.

2.3. Measurement procedures

All water samples were analyzed using the experimental apparatus depicted in Figure 1, which employs a single optical path design and utilizes a quartz cell with an optical path length of 10 mm. To ensure high stability in acquiring spectra, the integration time and average signal of the spectrometer were set to 2000 ms and three times, respectively. Prior to measurement, all water samples underwent thorough agitation through rapid particle precipitation. Each water sample was measured five times and the obtained spectra were averaged to reduce the influence of random errors. The transmitted spectrum of the ultrapure water was used as a reference to calculate the sample absorbance.

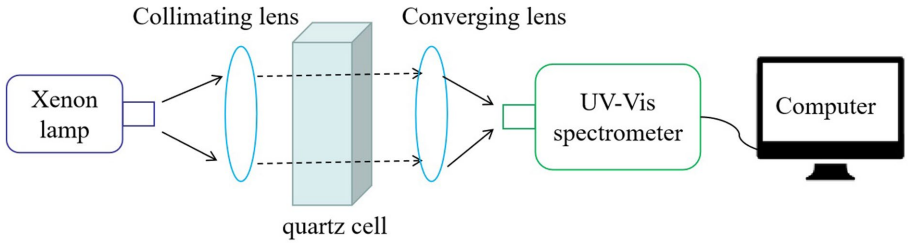

FIGURE 1
Schematic illustration of spectral acquisition system.

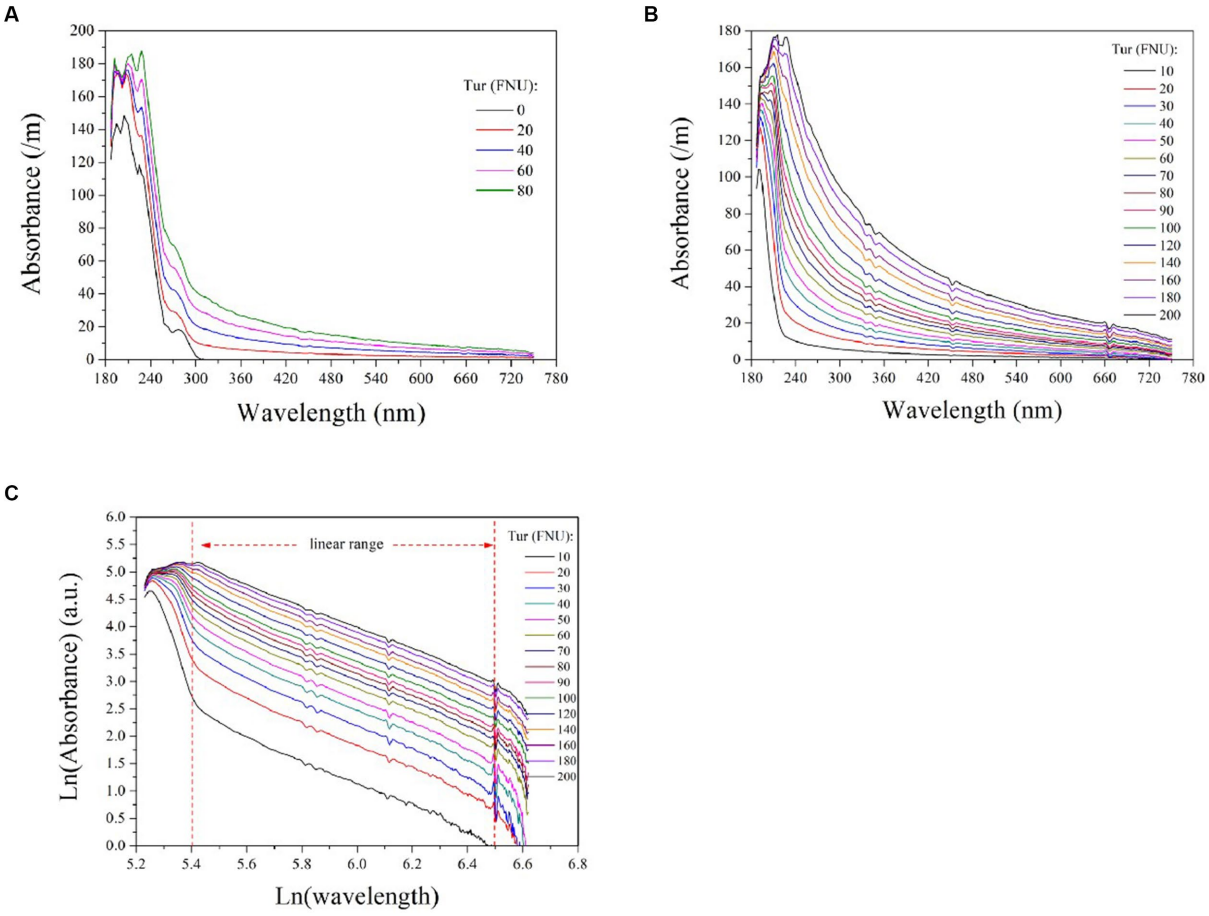

FIGURE 2
The absorption spectra of 50mg/L COD solutions mixed with varying turbidity concentrations **(A)**; the absorption spectra of formazine suspensions at different concentrations **(B)**; the logarithmic UV-vis spectra of formazine suspensions **(C)**. The two vertical dashed lines indicate the linear range of the curves, which is between 5.4<Ln (wavelength) <6.5 or 220nm<wavelength<660nm.

3. Results and discussion

3.1. UV-vis absorption behavior of turbidity and proposed exponential model

To investigate the impact of turbidity on COD detection via UV-vis spectrometry, we measured the absorption spectra of 50 mg/L COD solutions mixed with varying concentrations of turbidity, as depicted in Figure 2A. Absorption by the pure COD solution occurred predominantly within the UV range (180 ~ 320 nm) and increased with increasing turbidity concentration. This confirms that water turbidity poses a significant challenge to measuring COD using UV-vis spectrometry. Therefore, it is imperative to establish an efficient model for predicting the equivalent absorbance of turbidity at each UV wavelength to obtain the absorbance of COD alone by subtracting the overlapping spectrum. This method enables accurate detection of COD through the compensated ultraviolet spectrum.

TABLE 1 The results of linear regression analysis on the logarithmic spectra of formazine suspensions.

Turbidity (FNU)	Slope *k*	Intercept *b*	R^2
10	−2.13	2.21	0.988
20	−2.16	2.92	0.995
30	−2.10	3.35	0.993
40	−2.12	3.59	0.995
50	−2.10	3.77	0.996
60	−2.09	3.93	0.997
70	−2.07	4.06	0.997
80	−2.09	4.19	0.998
90	−2.10	4.30	0.998
100	−2.02	4.37	0.998
120	−2.03	4.54	0.998
140	−2.04	4.70	0.998
160	−2.06	4.81	0.998
180	−2.01	4.91	0.998
200	−2.00	4.99	0.998

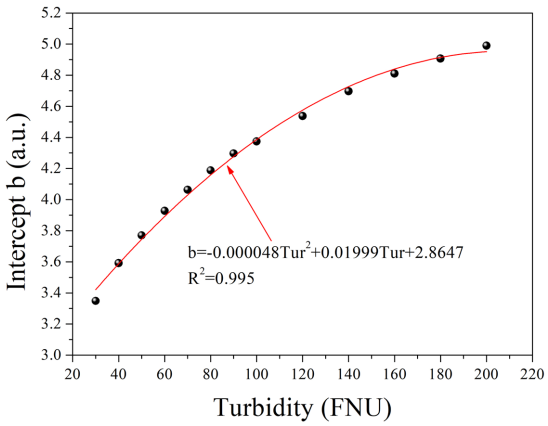

FIGURE 3
The relationship between intercept *b* and the concentration of turbidity.

To establish a model for predicting the equivalent absorbance of turbidity at different wavelengths, further investigation into its absorption behavior across the entire spectrum is required. For this purpose, we measured the absorbance of formazine suspensions with varying concentrations ranging from 10 to 200 FNU and presented the resulting spectra in Figure 2B. Turbidity exhibits absorbance over the entire spectrum owing to light scattering caused by suspended particles, with higher turbidity corresponding to stronger absorbance at each wavelength. For each absorption spectrum, the absorbance decreases rapidly initially and then gradually with longer wavelengths. Several studies have reported an exponential increase in particle absorbance at shorter wavelengths, which is visually consistent with the absorption spectra of formazine suspensions (Langergraber et al., 2003; Berho et al., 2004). We hypothesized that an exponential model could be utilized to predict the absorbance of turbidity at each wavelength, enabling effective turbidity compensation.

Based on the aforementioned hypothesis, the logarithmic UV-vis spectra of the formazine suspensions were transformed to linear form, as illustrated in Figure 2C. It is noteworthy that the logarithmic spectra exhibit a visually linear trend within the range of 220 to 660 nm (5.4 < Ln (wavelength) < 6.5). The logarithmic spectra were subjected to linear regression analysis, with the resulting data presented in Table 1. The high values of R^2 (>0.98) indicate a strong linear correlation between the variables under investigation. However, there are nonlinear regions within the logarithmic spectra, particularly at shorter and longer wavelengths. The nonlinearity observed at shorter wavelengths (<220 nm) may be attributed to the presence of co-absorptive substances, such as organic compounds and nitrates. As absorbances at longer wavelengths (>660 nm) are relatively small, they are susceptible to random noise interference, causing nonlinearity. In summary, the relationship between turbidity absorbance and wavelength can be expressed by Eq. (1) below:

$$Ln\left(A_{Tur}\right) = k \cdot Ln\left(\lambda\right) + b \tag{1}$$

The absorbance of turbidity at wavelength λ is denoted by A_{Tur}, and k and b represent the slope and intercept of the logarithmic spectra, respectively. However, the linearity of Equation (1) may be affected by the stability of the experimental system, with an unstable system often resulting in a downward trend in the logarithmic spectra. The instability of the system is primarily attributed to the impact of the spectrometer and xenon lamp. Specifically, the highly sensitive charge-coupled device detector in the spectrometer is susceptible to noise, ambient light, and dark-current interference. In contrast, the spectrometer utilized in this study was equipped with a less sensitive complementary metal-oxide-semiconductor detector (e.g., UV20, Horiba), which tends to be less susceptible to these impact factors. Additionally, the light intensity of the xenon lamp must be sufficiently strong to ensure a high signal-to-noise ratio in the system.

Table 1 clearly shows that parameter b gradually increases with increasing turbidity, while parameter k remains relatively constant. Furthermore, an investigation into the relationship between parameter b and turbidity was conducted, as depicted in Figure 3. To simplify the local calibration, a polynomial function was utilized to fit the curve with an R^2 value of 0.995. A quadratic relationship between parameter b and turbidity was demonstrated, allowing for the determination of parameter b as a function of turbidity based on Eq. (2) as follows:

$$b = m \cdot \mathrm{Tur}^2 + n \cdot Tur + p \tag{2}$$

The quadratic function is represented by the coefficients m, n, and p, while Tur denotes the turbidity concentration. Substituting Eq. (2) into Eq. (1) allows the prediction of the absorbance of any given turbidity concentration at each wavelength using Eq. (3):

$$A_{Tur} = \exp\left(m \cdot Tur^2 + n \cdot Tur + p\right) \cdot \lambda^k \tag{3}$$

By applying the superposition principle between COD absorbance and equivalent turbidity absorbance, compensation of the entire UV-vis spectrum can be achieved by subtracting the equivalent

turbidity absorbance. Subsequently, the absorbance of COD alone can be obtained using Eq. 4 as follows:

$$A_{COD} = A_{raw} - A_{Tur} = A_{raw} - \exp\left(m \cdot Tur^2 + n \cdot Tur + p\right) \cdot \lambda^k \quad (4)$$

where A_{raw} represents the absorbance of the raw spectrum at a specific wavelength λ and A_{COD} denotes the compensated absorbance of COD at the same wavelength. The latter can be transformed into a COD concentration by utilizing multivariate analysis tools. Measuring the turbidity prior to measuring COD is recommended because COD absorbance occurs in the UV range rather than in the visible range of the spectrum (Figure 2A). Turbidity can be measured by utilizing the absorbance at visible wavelengths, such as the wavelength band of 500 to 750 nm (Fleischmann et al., 2002). As depicted in Figure 2B, a proportional relationship exists between turbidity and the absorbance of visible wavelengths; thus, multivariate analysis tools (e.g., partial least squares method; PLS) can also be employed for turbidity measurement.

3.2. Validation of the proposed exponential model

3.2.1. Chemical oxygen demand prediction by exponential model and its comparison with the Lambert-Beer law and multiple-scattering cluster method

To verify the compensation performance of the exponential model, a series of mixtures containing COD and turbidity were measured, and the corresponding raw spectra are presented in Figure 4A. Subsequently, these raw spectra underwent processing using Eq. (4), resulting in compensated absorption spectra, as shown in Figure 4B. Other turbidity compensation models, such as the Lambert-Beer law-based (LBL) and multiple-scattering cluster (MSC) models mentioned in the literature, were also examined for comparison with the exponential model presented here (Wu et al., 2017; Li et al., 2019; Chen et al., 2021). The compensated spectra from the LBL and MSC models are shown in Figures 4C,D, respectively. The compensated spectra of MSC exhibit distinct deviations from those of the exponential and LBL models. Specifically, after compensation by the MSC model, the absorbance of water samples at visible wavelengths remains nonzero, whereas it approaches zero in the compensated spectra of the LBL and exponential models. This discrepancy can be attributed to turbidity in the water samples, which the MSC model cannot effectively eliminate. Moreover, the majority of the UV spectra tend to cluster together in the MSC model, which disrupts the proportional relationship between UV absorption and COD concentration, leading to decreasing COD measurement accuracy. In contrast, the LBL and exponential models provide highly dispersed UV spectra that enable more accurate predictions of COD.

The PLS method has been demonstrated to provide the most robust multivariate calibrations for addressing concentration-spectra relationships. As such, it is employed herein to retrieve the COD concentration based on the compensated absorption spectra (Wold et al., 2001; Lepot et al., 2016; Li et al., 2020). Figure 5A displays the predictions of the PLS models based on four types of compensated spectra, with their corresponding R^2 and RMSE values listed in Table 2. The results obtained from the LBL and exponential models are generally consistent with the actual COD values, exhibiting small RMSE values. In contrast, the MSC predictions deviate greatly from the actual values, resulting in larger RMSE values. Therefore, the MSC model is comparatively less effective in compensating for turbidity than the exponential and LBL models.

Although the accuracy of the COD prediction in turbid water was significantly enhanced by the LBL and exponential models, a lower RMSE value was achieved only with the exponential model. This outcome may be attributed to the LBL model employing Lambert-Beer's law to simulate the turbidity absorbance at each wavelength. It is well known that the Lambert-Beer law establishes a linear correlation between absorbance and solute concentration. However, this linearity is only observed at low concentrations at which the absorbance of the solute remains below a certain threshold. As previously stated, the absorbance of the turbidity increases exponentially as the wavelength decreases. Therefore, the relationship between absorbance and turbidity becomes less linear at shorter wavelengths, as shown in Figure 5B. Owing to this nonlinearity in the UV region, the LBL method performs worse in the UV than in the visible region. In contrast, the turbidity absorption conforms almost entirely to the exponential law across the entire spectrum. Therefore, the performance of the exponential model is consistent from the UV to the visible regions. As UV absorption provides more informative data for COD prediction, the RMSE value obtained by the exponential model was lower than that obtained with the LBL model.

3.2.2. Verification of the COD measurement in natural water using the exponential model

Turbidity in natural water is caused by the presence of numerous particles of varying properties, resulting in multiple scattering (Huber and Frost, 1998). To assess the applicability of the exponential model in natural water, several wastewater samples were also analyzed. The turbidity absorption in wastewater can be determined by calculating the difference spectra between filtered and unfiltered samples, as illustrated in plots (A) and (B) of Figure 6. Subsequently, the logarithmic spectra of turbidity can be obtained, as shown in Figure 6C. Here, the logarithmic spectra exhibit a visually linear and uniform trend at ln(wavelength) >5.8 (wavelength > 320 nm). An exponential model can be established based on the linear portions of the spectra to predict the equivalent absorbance of turbidity at each wavelength. The elimination of cross-sensitivity in the UV range is achieved by subtracting the equivalent absorbance. By comparing Figures 2C, 6C, it is evident that the logarithmic spectra slopes of formazine suspensions exhibits a significantly greater magnitude than that of turbidity in wastewater. The disparity in particle size between the formazine suspension and wastewater turbidity is the primary cause of this phenomenon. Several studies have indicated that particulates with smaller diameters tend to exhibit a steep absorption spectrum, whereas those with larger diameters typically display a more gradual absorption spectrum (Huber and Frost, 1998; Berho et al., 2004). Therefore, the smaller particle size of formazine particles results in a steeper logarithmic spectrum compared to wastewater turbidity.

Artificial filtration can also eliminate the cross-sensitivity of turbidity, allowing for a visual evaluation of the performance of the exponential model through comparison with filtered samples, as shown in Figure 6D. The compensated spectra are highly consistent with the filtered spectra within the wavelength band of 320 ~ 720 nm. However, the compensated spectra exhibit higher values than the filtered spectra at the 200 ~ 320 nm range, potentially resulting in positive deviations during the COD measurements.

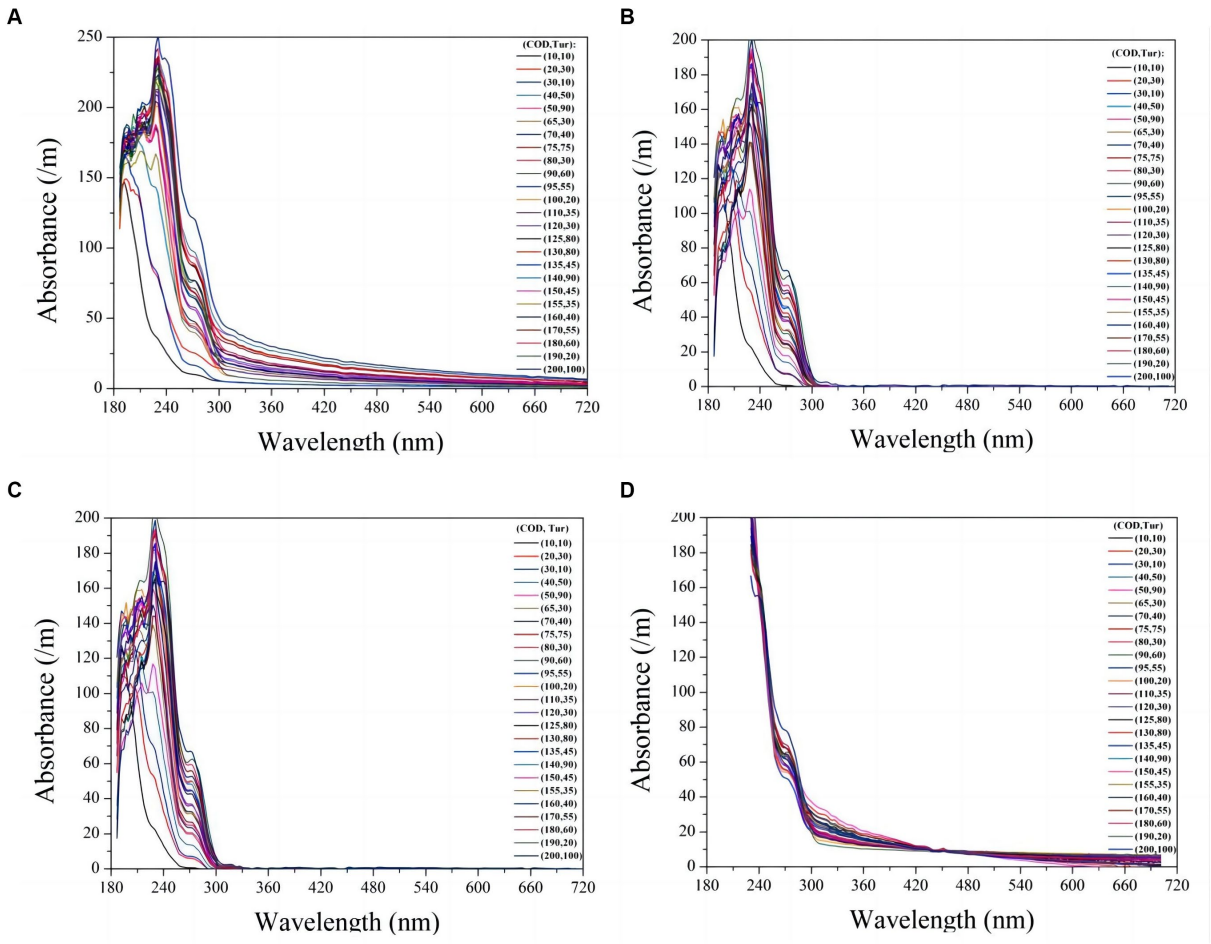

FIGURE 4
The raw UV-vis spectra of 30 mixtures containing COD and turbidity are presented **(A)**. The compensated spectra of the mixtures using exponential model, LBL, and MSC model are shown in **(B)**, **(C)**, and **(D)** respectively.

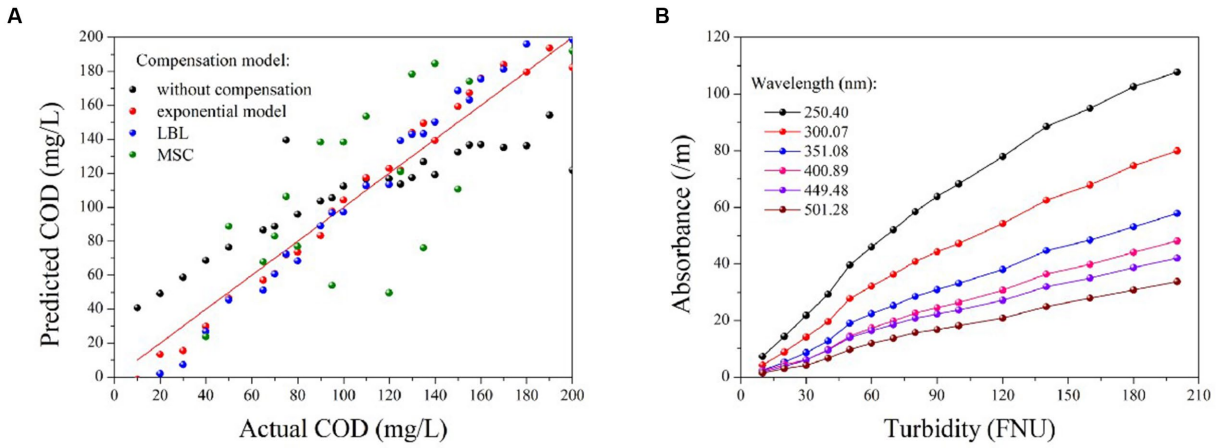

FIGURE 5
The prediction results of COD based on the compensated spectra provided by different methods **(A)**; the correlation between turbidity and absorbance at various wavelengths **(B)**.

TABLE 2 The predictive outcomes of PLS models based on diverse compensated spectra.

Compensation method	Without compensation	Exponential model	LBL	MSC
R^2	0.79	0.98	0.98	0.72
RMSE	29.90	9.51	12.53	79.34

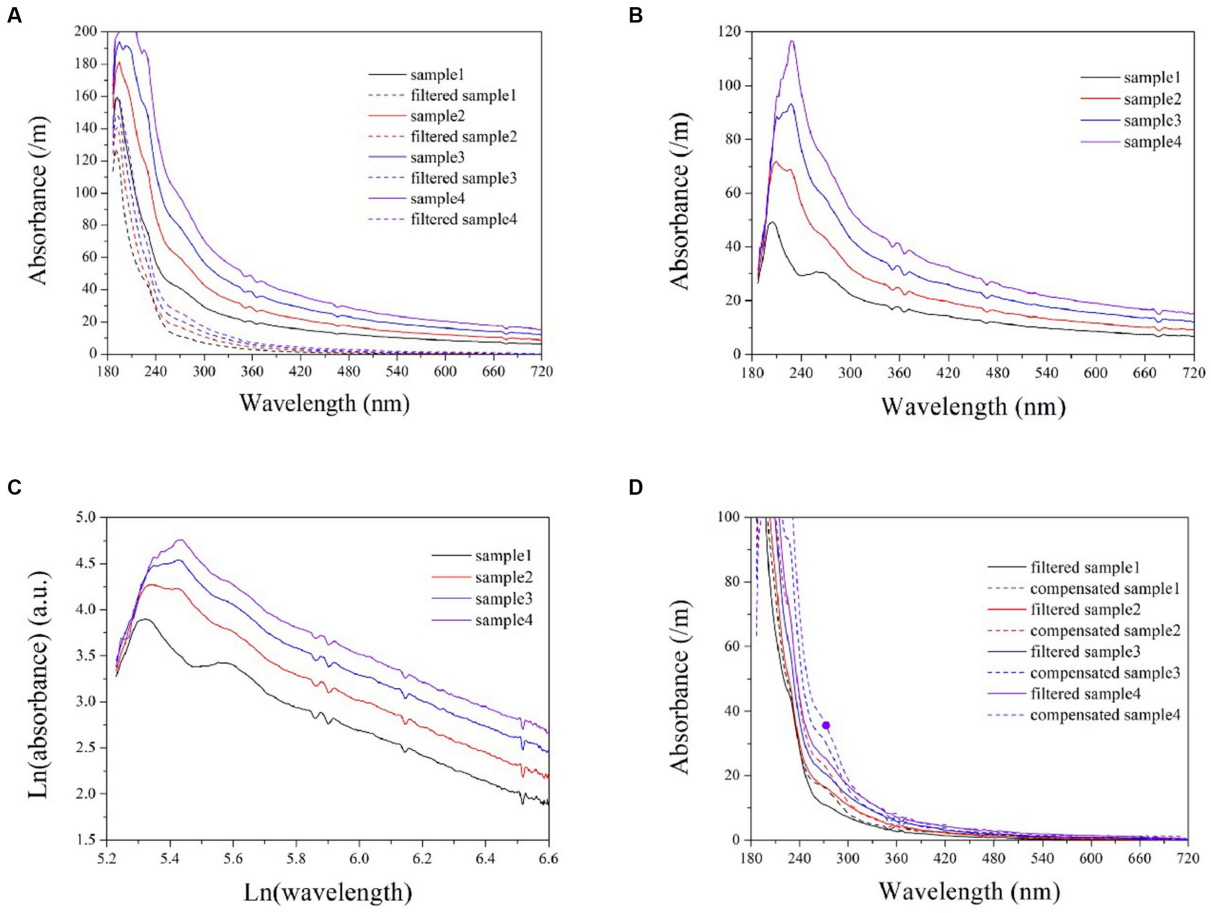

FIGURE 6
The UV-vis spectra of wastewater samples, both filtered and unfiltered **(A)**; turbidity spectra in wastewater obtained by calculating the difference between filtered and unfiltered samples **(B)**; logarithmic turbidity spectra in wastewater samples **(C)**; a comparison between compensated spectra and filtered sample spectra **(D)**.

Although the compensated spectra exhibited inconsistencies with those of the filtered samples in the UV region, these discrepancies are primarily attributable to the filtration process itself, which results in a loss of COD and subsequently lower filtered spectra in this wavelength range. Therefore, it can be concluded that the deviation observed within the UV range is not due to any shortcomings inherent within the exponential model. In achieving a high level of consistency between the compensated spectra and the filtered spectra in the visible range, the exponential model demonstrates that it remains applicable for simulating turbidity absorption behavior in natural water. The validation results indicate that the proposed exponential model is superior to the LBL and MSC methods for compensating turbidity, rendering it suitable for use in online spectrometers to enhance COD measurement accuracy in turbid water. The light scattering caused by particles in water is influenced by various factors, such as the concentration, diameter, and refractive index of the particle, as well as the measuring angle and wavelength of incident light (Huber and Frost, 1998). It is important to acknowledge that these factors may also impact the turbidity compensation model, thus necessitating recalibration of the model in response to changes in application conditions.

4. Conclusion

Presently, the presence of turbidity in water poses a significant challenge for accurate COD measurements based on UV-vis spectrometry. Therefore, implementing turbidity compensation techniques is necessary to ensure data validation and precision. However, current methods for such compensation are too intricate to be automated for online spectrometers. Herein, an exponential model with two parameters was established for turbidity compensation. One parameter was kept constant, while the other was varied quadratically with turbidity. This simple model satisfies the requirements of

embedded programming and local calibration of online sensors. Based on the model, the equivalent turbidity absorbance at each wavelength can be obtained. Compensation across the entire spectrum is then achieved by subtracting the equivalent absorbance to obtain the COD-specific absorbance. Finally, accurate detection of COD can be achieved using the compensated spectra. Compared with existing models, such as the LBL and MSC models, the exponential model demonstrates significantly superior performance. Although its performance in the UV region is unsatisfactory owing to filtration procedures, the consistency between the compensated spectra and filtered wastewater samples in the visible range suggests that the exponential model remains applicable for natural water analysis. In summary, the exponential model is demonstrated to be a highly effective approach for enhancing the precision of COD measurement by online spectrometers, offering valuable support for compensation techniques aimed at eliminating turbidity interference.

Data availability statement

The original contributions presented in the study are included in the article/Supplementary material, further inquiries can be directed to the corresponding author.

Author contributions

HW, HX, and TX performing all the experiments and writing the manuscript. JF and JZ drawing and summarizing figures. XL designing, managing the project, and editing. HW, HX, TX, JF, JZ, and XL discuss the results and commented on the manuscript. All authors contributed to the article and approved the submitted version.

Funding

This work was supported by the doctoral research foundation of Hubei university of Science and Technology (BK202321) and Major Project of Scientific and Technological Innovation in Hubei (Grant No. 2020BGC028, 2019AAA057).

Conflict of interest

The authors declare that the research was conducted in the absence of any commercial or financial relationships that could be construed as a potential conflict of interest.

References

Berho, C., Pouet, M., Bayle, S., Azema, N., and Thomas, O. (2004). Study of UV-vis responses of mineral suspensions in water. *Colloids Surf. A Physicochem. Eng. Asp.* 248, 9–16. doi: 10.1016/j.colsurfa.2004.08.046

Carré, E., Pérot, J., Jauzein, V., Lin, L., and Lopez-Ferber, M. (2017). Estimation of water quality by UV-vis spectrometry in the framework of treated wastewater reuse. *Water Sci. Technol.* 76, 633–641. doi: 10.2166/wst.2017.096

Chen, X., Yin, G., Zhao, N., Yang, R., Xia, M., Feng, C., et al. (2021). Turbidity compensation method based on Mie scattering theory for water chemical oxygen demand determination by UV-vis spectrometry. *Anal. Bioanal. Chem.* 413, 877–883. doi: 10.1007/s00216-020-03042-4

Fleischmann, N., Staubmann, K., and Langergraber, G. (2002). Management of sensible water uses with real-time measurements. *Water Sci. Technol.* 46, 33–40. doi: 10.2166/wst.2002.0048

Hu, Y., and Wang, X. (2017). Application of surrogate parameters in characteristic UV-vis absorption bands for rapid analysis of water contaminants. *Sens. Actuators B: Chem.* 239, 718–726. doi: 10.1016/j.snb.2016.08.072

Hu, Y., Wen, Y., and Wang, X. (2016). Novel method of turbidity compensation for chemical oxygen demand measurements by using UV-vis spectrometry. *Sens. Actuators B: Chem.* 227, 393–398. doi: 10.1016/j.snb.2015.12.078

Hu, Y., Zhao, D., Qin, Y., and Wang, X. (2020). An order determination method in direct derivative absorption spectroscopy for correction of turbidity effects on COD measurements without baseline required. *Spectrochim. Acta A* 226:117646. doi: 10.1016/j.saa.2019.117646

Huber, E., and Frost, M. (1998). Light scattering by small particles. *J. Water Supply Res. Technol. – Aqua.* 47, 87–94. doi: 10.2166/aqua.1998.14

Kang, Z., He, Z., Wen, Y., Chen, H., and Zhang, Q. (2022). Smart COD sensor using UV-vis spectroscopy against optical window surface contamination. *Measurement* 187:110125. doi: 10.1016/j.measurement.2021.110125

Langergraber, G., Fleischmann, N., and Hofstädter, F. (2003). A multivariate calibration procedure for UV/VIS spectrometric quantification of organic matter and nitrate in wastewater. *Water Sci. Technol.* 47, 63–71. doi: 10.2166/wst.2003.0086

Lapworth, D., Baran, N., Stuart, M., and Ward, R. (2012). Emerging organic contaminants in groundwater: a review of sources, fate and occurrence. *Environ. Pollut.* 163, 287–303. doi: 10.1016/j.envpol.2011.12.034

Lepot, M., Torres, A., Hofer, T., Caradot, N., Gruber, G., Aubin, J., et al. (2016). Calibration of UV-vis spectrophotometers: a review and comparison of different methods to estimate TSS and total and dissolved COD concentrations in sewers, WWTPs and rivers. *Water Res.* 101, 519–534. doi: 10.1016/j.watres.2016.05.070

Li, J., Luo, G. B., He, L., Xu, J., and Lyu, J. (2018). Analytical approaches for determining chemical oxygen demand in water bodies: a review. *J. Crit. Rev. Anal. Chem.* 48, 47–65. doi: 10.1080/10408347.2017.1370670

Li, P., Qu, J., He, Y., Bo, Z., and Pei, M. (2020). Global calibration model of UV-vis spectroscopy for COD estimation in the effluent of rural sewage treatment facilities. *RSC Adv.* 10, 20691–20700. doi: 10.1039/C9RA10732K

Li, J., Tong, Y., Guan, L., Wu, S., and Li, D. (2019). A turbidity compensation method for COD measurements by UV-vis spectroscopy. *Optik* 186, 129–136. doi: 10.1016/j.ijleo.2019.04.096

Ma, J., Meng, F., Zhou, Y., Wang, Y., and Shi, P. (2018). Distributed water pollution source localization with Mobile UV-visible spectrometer probes in wireless sensor networks. *Sensors* 18, 606–625. doi: 10.3390/s18020606

Pal, A., He, Y., Jekel, M., Reinhard, M., and Gin, K. Y. (2014). Emerging contaminants of public health significance as water quality indicator compounds in the urban water cycle. *Environ. Int.* 71, 46–62. doi: 10.1016/j.envint.2014.05.025

Wold, S., Sjöström, M., and Eriksson, L. (2001). PLS-regression: a basic tool of chemometrics. *Chemom. Intell. Lab. Syst.* 58, 109–130. doi: 10.1016/S0169-7439(01)00155-1

Wu, D., Wei, B., Tang, G., Feng, P., Tang, Y., Liu, J., et al. (2017). Turbidity disturbance compensation for UV-vis spectrum of waterbody based Mie scattering. *Acta Opt. Sin.* 37, 234–355. doi: 10.3788/aos201737.0230007

Xu, X., Wang, J., Li, J., Fan, A., Zhang, Y., Chang, X., et al. (2023). Research on COD measurement method based on UV-vis absorption spectra of transmissive and reflective detection systems. *Front. Environ. Sci.* 11:1175363. doi: 10.3389/fenvs.2023.1175363

Zhang, H., Zhou, X., Tao, Z., Lv, T., and Wang, J. (2022). Deep learning-based turbidity compensation for ultraviolet-visible spectrum correction in monitoring water parameters. *Front. Environ. Sci.* 10:986913. doi: 10.3389/fenvs.2022.986913

frontiers | Frontiers in Microbiology

TYPE Original Research
PUBLISHED 09 August 2023
DOI 10.3389/fmicb.2023.1243410

OPEN ACCESS

EDITED BY
Zhaoming Zheng,
Beijing University of Technology, China

REVIEWED BY
Xiaoxia Wang,
Qingdao University, China
Liangliang Shi,
Hainan University, China
Da Kang,
Beijing University of Technology, China

*CORRESPONDENCE
Lisa Alvarez-Cohen
✉ lisaac@berkeley.edu

RECEIVED 20 June 2023
ACCEPTED 13 July 2023
PUBLISHED 09 August 2023

CITATION
White C, Antell E, Schwartz SL, Lawrence JE, Keren R, Zhou L, Yu K, Zhuang W and Alvarez-Cohen L (2023) Synergistic interactions between anammox and dissimilatory nitrate reducing bacteria sustains reactor performance across variable nitrogen loading ratios. *Front. Microbiol.* 14:1243410. doi: 10.3389/fmicb.2023.1243410

Synergistic interactions between anammox and dissimilatory nitrate reducing bacteria sustains reactor performance across variable nitrogen loading ratios

Christian White[1], Edmund Antell[1], Sarah L. Schwartz[1], Jennifer E. Lawrence[2], Ray Keren[1], Lijie Zhou[3], Ke Yu[4], Weiqin Zhuang[5] and Lisa Alvarez-Cohen[1,6]*

[1]Department of Civil & Environmental Engineering, University of California, Berkeley, Berkeley, CA, United States, [2]CDM Smith, Boston, MA, United States, [3]College of Chemistry and Environmental Engineering, Shenzhen University, Shenzhen, China, [4]School of Environment and Energy, Shenzhen Graduate School, Peking University, Shenzhen, China, [5]Department of Civil & Environmental Engineering, University of Auckland, Auckland, New Zealand, [6]Earth and Environmental Sciences Division, Lawrence Berkeley National Laboratory, Berkeley, CA, United States

Anaerobic ammonium oxidizing (anammox) bacteria are utilized for high efficiency nitrogen removal from nitrogen-laden sidestreams in wastewater treatment plants. The anammox bacteria form a variety of competitive and mutualistic interactions with heterotrophic bacteria that often employ denitrification or dissimilatory nitrate reduction to ammonium (DNRA) for energy generation. These interactions can be heavily influenced by the influent ratio of ammonium to nitrite, NH_4^+:NO_2^-, where deviations from the widely acknowledged stoichiometric ratio (1:1.32) have been demonstrated to have deleterious effects on anammox efficiency. Thus, it is important to understand how variable NH_4^+:NO_2^- ratios impact the microbial ecology of anammox reactors. We observed the response of the microbial community in a lab scale anammox membrane bioreactor (MBR) to changes in the influent NH_4^+:NO_2^- ratio using both 16S rRNA gene and shotgun metagenomic sequencing. Ammonium removal efficiency decreased from 99.77±0.04% when the ratio was 1:1.32 (prior to day 89) to 90.85±0.29% when the ratio was decreased to 1:1.1 (day 89–202) and 90.14±0.09% when the ratio was changed to 1:1.13 (day 169–200). Over this same timespan, the overall nitrogen removal efficiency (NRE) remained relatively unchanged (85.26±0.01% from day 0–89, compared to 85.49±0.01% from day 89–169, and 83.04±0.01% from day 169–200). When the ratio was slightly increased to 1:1.17–1:1.2 (day 202–253), the ammonium removal efficiency increased to 97.28±0.45% and the NRE increased to 88.21±0.01%. Analysis of 16S rRNA gene sequences demonstrated increased relative abundance of taxa belonging to Bacteroidetes, Chloroflexi, and Ignavibacteriae over the course of the experiment. The relative abundance of Planctomycetes, the phylum to which anammox bacteria belong, decreased from 77.19% at the beginning of the experiment to 12.24% by the end of the experiment. Analysis of metagenome assembled genomes (MAGs) indicated increased abundance of bacteria with *nrfAH* genes used for DNRA after the introduction of lower influent NH_4^+:NO_2^- ratios. The high relative abundance of DNRA bacteria coinciding with sustained bioreactor performance indicates a mutualistic relationship between the anammox and DNRA bacteria. Understanding these interactions could support more robust bioreactor operation at variable nitrogen loading ratios.

KEYWORDS

anammox, DNRA, denitrification, metagenome, stoichiometric ratio, bioreactor, wastewater

1. Introduction

Nitrogen removal from wastewater is paramount to the remediation of anthropogenic nutrient pollution and the protection of sensitive aquatic environments (USEPA, 2007; Smith and Schindler, 2009; Davidson et al., 2014). One strategy to remove nitrogen from wastewater is anaerobic ammonium oxidation (anammox), in which ammonium (NH_4^+) is anaerobically oxidized using nitrite (NO_2^-) as an electron acceptor (Mulder et al., 1995; van de Graaf et al., 1995; Strous et al., 1998). Anammox is a biogeochemical process facilitated by chemolithoautotrophic bacteria in the Phylum Planctomycetes (Strous et al., 1999; Schmid et al., 2000) and is estimated to account for up to 70% of fixed nitrogen removal in marine environments (Kuypers et al., 2003; Devol, 2015). The anammox process has shown great potential for robust sidestream nitrogen removal, with full scale installations demonstrating nitrogen removal efficiencies up to 90% and ammonium removal rates up to 9.5 kg NH_4^+-N/L·d (Abma et al., 2007; Joss et al., 2009; Lackner et al., 2014) while using 60% less energy and producing 90% less sludge than conventional nitrification–denitrification systems (Jetten et al., 1997; Lackner et al., 2014; Cho et al., 2019). Despite these benefits, anammox-based water treatment faces multiple challenges including long start up periods (6 months-2 years) (Jetten et al., 2001; Kuenen, 2008; Kartal et al., 2013) and process instability due to inhibitory compounds (Jin et al., 2012; Lotti et al., 2012), operational fluctuations, and microbially-provoked destabilizations (Ali and Okabe, 2015). Thus, prior anammox research has sought to better-understand microbial community dynamics in order to design, maintain, and operate more resilient reactors.

Anammox reactors harbor phylogenetically and functionally diverse bacteria that engage in a variety of synergistic, competitive, and mutualistic interactions (Guo et al., 2016; Bhattacharjee et al., 2017; Lawson et al., 2017; Pereira et al., 2017). The presence of a core microbial community identified alongside anammox bacteria—which have never been isolated in pure culture—suggests an ecological niche specific to the conditions found inside of the reactor. Previous research consistently identifies bacteria belonging to the phyla Proteobacteria, Chloroflexi, Ignavibacteria, and Bacteroidetes as part of this core community (Gonzalez-Martinez et al., 2015; Keren et al., 2020). Many of the interactions occurring among different anammox community members are predicated on an exchange of organic carbon substrates, secondary metabolites, and various nitrogen species (Jenni et al., 2014; Zhao et al., 2018; Cao et al., 2020; Zhang et al., 2020, 2021). These complex relationships are key to improving nitrogen removal efficiency and sustaining microbial growth within bioreactors. For example, heterotrophic bacteria performing nitrate reduction through *nar* or *nap* nitrate reductases can reduce nitrate (NO_3^-) to nitrite, providing a substrate for anammox; anammox bacteria then produce organic carbon that feeds heterotrophic partners, forming a nitrite loop. However, other nitrogen metabolisms can disrupt this loop. Bacteria performing dissimilatory nitrate reduction to ammonium (DNRA) with *nrfA* or *nrfH* cytochrome nitrite reductases convert nitrite back to ammonium, forming antagonistic relationships with anammox bacteria that can disrupt reactor performance (Einsle et al., 2002; Speth et al., 2016; Wang et al., 2019). Heterotrophs performing DNRA actively compete with denitrifiers for organic carbon substrates and both nitrate and nitrite, a competition that has been shown to depend on C/N ratio, carbon source availability, and hydraulic retention time (van den Berg et al., 2016, 2017a,b).

The competition between bacteria performing DNRA and denitrification can also be altered by influent resource concentrations (Jia et al., 2020). In full scale systems, anammox is coupled with nitritation to provide a nitrite source, generally resulting in a nitrogen influent stream of approximately 50% ammonium (NH_4^+) and 50% nitrite (NO_2^-), or a NH_4^+:NO_2^- molar ratio of 1:1 (Joss et al., 2009; Lackner et al., 2014). Because of the competition between denitrifying bacteria and DNRA for nitrite, the NH_4^+:NO_2^- ratio needed within an anammox reactor tends to be higher. Highly enriched anammox cultures remove ammonium and nitrite at a ratio between 1:1.2 and 1:1.32 (Zhu et al., 2017). Any divergence from this ratio can lead to poor reactor performance, or in extreme cases, reactor crashes. While changes to reactor performance during ratio changes has been well documented, the underlying changes to the microbial community that drive performance changes are poorly understood.

Given that full-scale anammox reactors are susceptible to performance destabilization due to variable nitrogen loading (Joss et al., 2011), it is important to evaluate the effects of fluctuating nitrogen species ratios on the complex network of metabolic interdependencies between anammox, DNRA, and denitrification bacteria. Here we constrain the microbial community response to perturbations induced by influent nitrogen loading ratio changes in a lab scale anammox reactor. We evaluate the effects of variable nitrogen loading ratios on reactor performance, anammox activity, and microbial community dynamics; we also assess the changes in microbial interactions as a result of changing influent conditions using 16S rRNA amplicon sequencing and shotgun metagenomic sequencing analysis. The results provide insight into the competitive and synergistic relationships between bacteria employing different nitrogen metabolisms, and how these complex relationships affect reactor performance, stability, and resiliency.

2. Methods

2.1. Bioreactor operation

A 1 L anaerobic membrane bioreactor (MBR) was operated for 1 year prior to the experiment. The reactor was enriched for anammox bacteria from anaerobic digester solids. The specific details of initial inoculation and operation can be found in (Keren et al., 2020). A polyvinylidene fluoride membrane with a pore size of 0.22 μm was mounted to the inside of the reactor and a gas mix (Argon:CO_2 = 95:5; 50 mL/min) was continuously supplied to purge the system of oxygen and maintain circumneutral pH (6.9–7.2) (Supplementary Figure S2). Temperature was maintained at 37°C using a heating jacket (Eppendorf, Hauppauge, NY) and mixing was provided through an impeller at a rate of 200 rpm. A synthetic media containing ammonium, nitrite,

bicarbonate, and trace nutrients prepared anaerobically under nitrogen was continuously fed to the reactor; the exact composition can be found in Supplementary Table S1. Influent and effluent samples were collected every other day to monitor concentrations of ammonium, nitrite, and nitrate using HACH test kits (HACH, Loveland, CO), as described in the manufacturer's methods 10031, 10019, and 10020, respectively. Mixed liquor suspended solids (MLSS) and mixed liquor volatile suspended solids (MLVSS) were measured according to standard methods (USEPA, 2001).

The experiment took place over 252 days during which the hydraulic retention time (HRT) of the reactor was maintained at 12 h (via an effluent pump) and the solids retention time (SRT) was maintained at 50 days (via biomass wasting). For the first 88 days of the experiment, $NH_4^+$and NO_2^-were loaded at the conventional 1:1.32 ratio at concentrations of 500 mg-N/L and 660 mg-N/L, respectively. On day 89, the influent ammonium concentration was raised to 600 mg-N/L, decreasing the NH_4^+:NO_2^- ratio to 1:1.1. On day 169, the influent nitrite concentration was raised to 680 mg-N/L, increasing the NH_4^+:NO_2^- ratio to 1:1.13. From day 200 to 252, the total nitrogen loading was slowly increased while also increasing the NH_4^+:NO_2 ratio from 1:1.13 to 1:1.2 as shown in Table 1. This range of NH_4^+:NO_2^- ratios was selected for the experiment in order to maintain stable operation of the reactor, as lower ratios (<1:1) have been demonstrated to lead to the accumulation of free ammonia (FA) (Fernández et al., 2012) and higher ratios (>1:1.3) have been shown to lead to nitrite inhibition (Jin et al., 2013). The dominant anammox strain in our MBR (*Brocadia sinica*) has also been shown to have higher sensitivity to nitrite inhibition than other strains such as *Kuenenia* (Oshiki et al., 2011). Thus the influent nitrogen ratios tested in this experiment were selected to avoid these issues.

2.2. DNA extraction

Biomass samples were collected every 2–10 days via syringe through an extraction port, flash frozen in liquid nitrogen, and stored at −80°C until further use. Genomic DNA was extracted from the samples using the DNeasy PowerSoil Kit (Qiagen, Carlsbad, CA) as described in the manufacturer's protocol. DNA quality was assessed using a NanoDrop Spectrophotometer (Thermo Scientific, Waltham, MA) and Bioanalyzer 2100 (Agilent Technologies, Santa Clara, CA). DNA was quantified using a Qubit fluorometer (Thermofisher Scientific, Walthan, MA), diluted to 10 ng/μl with nuclease free water (Thermo Scientific, Waltham, MA), and stored at −20°C until further use. Shotgun metagenomic sequencing samples were sent to the Joint Genome Institute (JGI) in Walnut Creek, CA. There, DNA was sequenced (150 bp paired-end) on an Illumina HiSeq 2500 1 T sequencer (Ilumina, San Diego, CA). 16S rRNA sequencing for samples collected from day 1 to 45 were sequenced at the Institute for Environmental Genomics at the University of Oklahoma and the remaining samples were sequenced at JGI on an Illumina MiSeq sequencer (Illumina, San Diego, CA).

TABLE 1 Influent nitrogen loading and NH_4^+:NO_2^- ratio data.

Day	Influent ammonium (mg-N/L)	Influent nitrite (mg-N/L)	NH_4^+:NO_2^- ratio	Nitrogen loading rate (g N/L-d)
0	500	660	1.32	2.32
89	600	660	1.1	2.52
169	600	680	1.13	2.52
200	600	700	1.17	2.6
217	600	710	1.18	2.62
218	600	720	1.2	2.64
235	640	768	1.2	2.82
243	660	792	1.2	2.9
250	680	816	1.2	2.99

2.3. 16S rRNA gene analysis

The microbial community composition was evaluated by 16S ribosomal RNA sequencing of 28 DNA samples collected throughout the experiment. The V4 region was amplified using primers 515F (5′-GTGCCAGCMGCCGCGG-3′) and 806R (3′-TAATCTWTGG VHCATCAG-5′), with barcodes attached to the reverse primer. Amplicons were pooled at equal molarity and purified with the QIAquick Gel Extraction Kit (QIAGEN Sciences, Germantown, MD). Paired-end sequencing (250 bp paired-end) was then performed on the Illumina MiSeq sequencer (Illumina, San Diego, CA). The full protocol is provided by Wu et al. (2015). Sequence processing and data analysis was conducted using MOTHUR v.1.39.5, following the MiSeq Standard Operating Procedure (SOP) (Schloss et al., 2009), and OTUs were assigned based on a 97% sequence similarity threshold.

2.4. Metagenomic sequencing, assembly, and binning

Three DNA samples were used for metagenomic sequencing, two from single timepoints on day 37 and 140 and one bulked from samples taken on days 232, 235, and 237. Resulting sequences from each time point were processed separately according to the procedure previously reported in Keren et al. (2020). KEGG Automated Annotation Service (KAAS) was used to annotate predicted gene sequences using Hidden Markov Models (HMMs). Single time point genome abundances were calculated using reads per kilobase per million (RPKM). The log ratio change for each genome was calculated based on the procedure previously reported in Keren et al. (2020). Briefly, three genomes with stable coverage across the three time points were selected as reference frame genomes. The coverage of each genome was then divided by the coverage of the three reference frame genomes. These ratios were then used to calculate the log ratio changes between samples yielding three values, one for each reference frame genome. This was done in order to account/adjust for differences in sequencing depth between samples, which can otherwise lead to biased results. Relative replication rates were calculated using iRep (Brown et al., 2016). Briefly, the replication rates of bacteria were estimated by calculating the coverage ratio between the origin of replication and the terminus of replication. In a population that is not actively replicating, the coverage at the ratio and terminus will be the same, and the ratio will be one. For populations that are actively replicating the coverage will be greater around the origin of replication

TABLE 2 Membrane bioreactor (MBR) performance and effluent data.

Day	NH_4^+ Removal Efficiency	NO_2^- Removal efficiency	Nitrogen removal efficiency	Nitrogen removal rate (g N/L-d)	Nitrate production rate (g N/L-d)	ΔNO_3^- :ΔNH_4^+
0–89	99.77 ± 0.04%	96.85 ± 2.34%	85.26 ± 0.01%	1.98 ± 0.03	0.08 ± 0.01	0.30 ± 0.01
89–169	90.85 ± 0.29%	99.56 ± 0.05%	85.49 ± 0.01%	2.15 ± 0.01	0.06 ± 0.01	0.23 ± 0.01
169–200	90.14 ± 0.09%	99.65 ± 0.02%	83.04 ± 0.01%	2.13 ± 0.01	0.08 ± 0.01	0.29 ± 0.01
200–252	97.28 ± 0.45%	99.76 ± 0.03%	88.21 ± 0.01%	2.37 ± 0.03	0.07 ± 0.01	0.24 ± 0.05

because of replication forks that have not finished replicating. Thus, the higher this ratio the higher the proportion of the population that is actively replicating.

2.5. Statistical analysis

Principal component analysis (PCA) was applied to evaluate the correlation between taxa abundance for different pathways (anammox, denitrification, and DNRA) and reactor performance parameters. In order to assign pathways to specific taxa, 16S rRNA sequences obtained from metagenomes with genes encoding for each pathway were aligned to representative sequences from amplicon sequencing following the procedure described in Keren et al. (2020). For MAGs not containing 16S rRNA sequences but classified down to the species level, sequences were obtained from NCBI. PCA analysis was conducted using R[1] with the "factoextra" package in RStudio.[2]

3. Results

3.1. Bioreactor performance

Under the initial NH_4^+:NO_2^- ratio of 1:1.32, the average ammonium and nitrite removal efficiencies were 99.77 ± 0.04% and 96.85 ± 2.31%, respectively (Table 2), and the average nitrogen removal rate (NRR) taking into consideration the generation of nitrate from nitrite by anammox bacteria to generate reducing equivalents for carbon fixation was 1.98 ± 0.03 g-N/L·d. This resulted in a nitrate production rate of 0.075 ± 0.002 g-N/L·d and a NO_3^-:NH_4^+ ratio of 0.298 ± 0.0007:1, which is slightly above the conventional ratio of 0.26:1 (Strous et al., 1998). Following the influent ratio shift on day 89, the average ammonium concentration in the effluent increased from 1.14 ± 0.22 mg-N/L to 55.19 ± 1.68 mg-N/L, which was expected due to the increased NH_4^+ in the influent. Of the 100 mg-N/L NH_4^+ added to the influent, about half was emitted in the effluent, while the remaining ammonium was likely removed through the anammox reaction or was assimilated for biomass synthesis. After increasing the NO_2^- influent concentration, the nitrogen loading rate (NLR) was steadily increased from 2.60 g-N/L·d on day 200 to 2.99 g-N/L·d on day 250 (Table 1). From day 89 to day 202 the average ammonium removal efficiency fell to 90.74 ± 0.25% and the nitrite removal efficiency increased to 99.57 ± 0.04%; the NRR increased to 2.16 ± 0.01 g-N/L·d. This resulted in a nitrate production rate of 0.066 ± 0.002 g-N/L·d and a NO_3^-:NH_4^+ ratio of 0.24 ± 0.005:1. From day 202 to day 253, ammonium removal efficiency increased back to 97.28 ± 0.45%, and the NO_3^-:NH_4^+ ratio decreased again to 0.237 ± 0.005:1 (Figure 1).

3.2. Microbial community in MBR through 16S amplicon sequencing

16S rRNA amplicon sequencing was conducted to ascertain changes in abundance of taxonomic groups throughout the reactor lifecycle. Figure 2 shows the relative abundance of 16S rRNA genes at the phylum level. At the beginning of the experiment, the dominant phylum in the reactor was Planctomycetes, accounting for 77.19% of total reads. Other significant phyla included Chloroflexi, Ignavibacteria, and Proteobacteria accounting for 7.73, 4.57, and 8.67% of total reads respectively, which is consistent with previously reported results (Pereira et al., 2017). Of the reads belonging to Chloroflexi, over 99% belonged to the class Anaerolineae and of the reads belonging to Proteobacteria, 50.40% belonged to the class Alphaproteobacteria. Over the course of the experiment, the relative abundance of Planctomycetes decreased from 77.19 to 12.24%. Meanwhile, the relative abundance of Chloroflexi and Ignavibacteria increased from 7.73 and 4.57% to 23.36 and 38.22%, respectively. The relative abundance of the phylum *Bacteroidetes* also increased from <0.05% at the beginning of the experiment to 7.30% by the end. The Shannon, Simpson, and Chao indices were calculated using relative abundance data from sequenced amplicons, which indicated that the microbial diversity of the community increased over the course of the experiment. Further information on diversity calculations and results can be found in the Supplementary Table S3.

The abundance of taxonomic groups was also aggregated at the genus level (Figure 3). These results are consistent with relative abundances at the phylum level, demonstrating high abundance genera in Chloroflexi, Ignavibacteria, Proteobacteria, and Bacteroidetes phyla. Several genera associated with the families Anaerolineaceae, Rhodocylacea, Burkholderiaceae and the order Ignavibacteriales were consistently abundant throughout the experiment, which was consistent with previously reported results (Du et al., 2017; Hu et al., 2018; Pereira et al., 2019; Xiao et al., 2021). Several of the genera from Anaerolineaceae and Ignavibacteriales increased by at least one order of magnitude following the initial ratio change made on day 89. Multiple genera from Rhodospiralles, Flavobacteriales, Sphingobacteriales, and Chitinophagales that were previously undetected or low abundance increased by at least two orders of magnitude post-ratio change.

1 https://www.r-project.org/

2 https://www.rstudio.com/

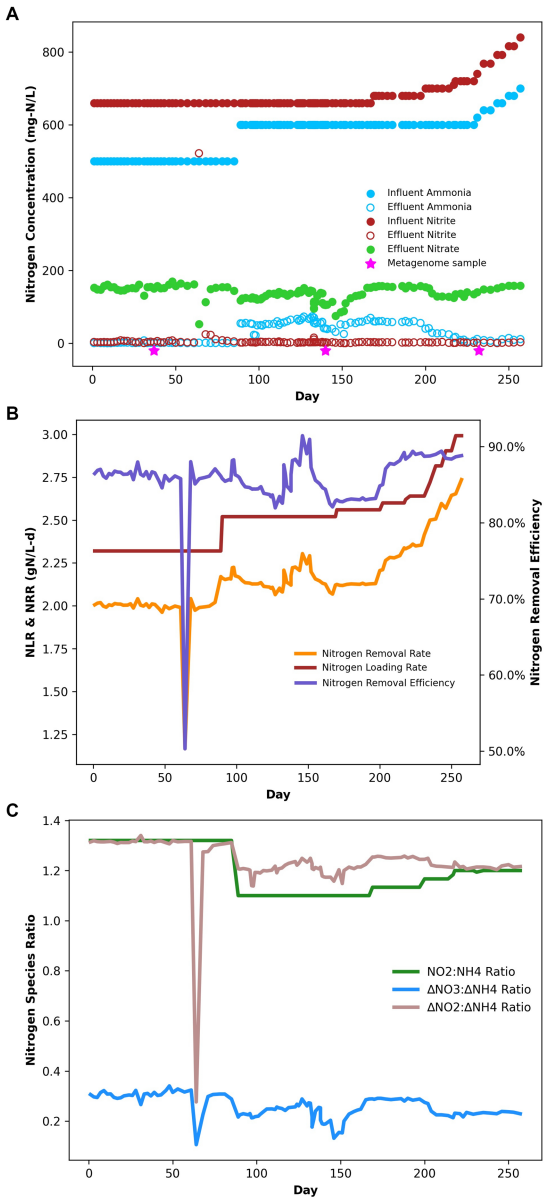

FIGURE 1
(A) Bioreactor performance nitrogen speciation data. **(B)** Bioreactor performance during the experiment in terms of NRR, NLR, and NRE. **(C)** Bioreactor performance stoichiometric ratios of nitrogen species.

3.3. Metagenome sequencing results

After read quality control 342,892,526 reads were obtained from all three metagenome samples. Reads were assembled into Metagenome Assembled Genomes (MAG), resulting in 27,836 contigs with a median N50 of 2,138 bp. Contigs were binned to draft genomes resulting in 129 draft genomes accounting for 74.62% of quality filtered reads on average across all three samples (Supplementary Table S4). These MAGs represented 20 bacterial phyla and one archaeal phylum, as shown in Figure 4. The most abundant genomes based on coverage were affiliated with Planctomycetes, Proteobacteria, Ignavibacteriae, Chloroflexi, and the super-phylum Candidate Phyla Radiation (CPR). A full list of genomes is available in Supplementary Table S5. AMX1 (*Brocadia sinica*), the only anammox MAG recovered, accounted for 44.97% of all reads on average across all three metagenome samples. AMX1 had an average GC content of 42.29%, a genome size of 3.1 Mbp, and 2,859 open reading frames (ORFs) which was consistent with other previously reported anammox genomes for this strain (Oshiki et al., 2015; Feng et al., 2019).

3.4. Nitrogen cycle gene abundances

To assess the changes in abundance of nitrogen metabolic genes, the relative abundance of these genes was calculated for each metagenomic sampling timepoint (Figure 5). The metabolic genes with the highest abundance throughout the duration of the experiment included hydrazine dehydrogenase (*hdh*), hydrazine synthase (*hzsA/B/C*), hydroxylamine oxidoreductase (*hao*), respiratory nitrate reductase (*narGH*), nitrous oxide reductase (*nosZ*), and cytochrome c membrane associated nitrite reductases (*nrfAH*) with relative abundances ranging from 4.3 to 32.3%. For the purposes of this study, we are utilizing *nrfAH*, the gene encoding the one-step reduction of nitrite to ammonium as a proxy for DNRA. Likewise, we are employing *nirK* and *nirS*, both used for nitrite reduction to nitric oxide, as proxies for denitrification. The abundance of functional analogs *nirK* and *nirS*, were only 0.9 and 0.1%, respectively; however, the relative abundance of respiratory nitrate reductases *narGH* was 30.99% on average, indicating the wide prevalence of nitrate reduction capacity. The nitrogen gene relative abundances for samples from day 37 and 140 were nearly identical; by day 232, the relative abundance of *nrfAH* nitrite reductases and *narGH* nitrate reductases increased slightly and the relative abundance of anammox associated hydrazine synthase and hydrazine dehydrogenase decreased slightly (Figure 5). The taxonomic variability and relatively stable metabolic composition suggest high levels of functional redundancy amongst bacteria in the reactor.

To understand how different nitrogen metabolisms influenced microbial competition throughout the duration of the experiment, the abundance of key individual MAGs was calculated for each timepoint as shown in Figure 6. *narGH* nitrate reductases were the most abundant of any nitrogen metabolic gene and widely distributed amongst MAGs. The next most abundant nitrogen metabolism gene identified in key MAGs was *nrfAH*. The top 5 most abundant MAGs including AMX01 (*Brocadia*), IGN01 (*Ignavibacterium*), CFLX01 (Chloroflexi), PROT01 (Burkholderiales), and BAC01 all contained *narGH*. AMX01, CFLX01, and IGN01 also contained *nrfAH*. The abundance of AMX01 decreased from 9.67 RPKM on day 37 to 7.81 RPKM on day 232, while the abundances of CFLX01 and IGN01 increased from 14.11 and 9.18 RPKM on day 37 to 23.02 and 15.98 RPKM on day 232. Many of the MAGs that encoded for *narGH* also lacked the remaining genes necessary for the full denitrification pathway, which could result in the accumulation of nitrite. This is consistent with previously reported results (Speth et al., 2016) supporting the presence of a nitrite loop, in which nitrate is recycled back to anammox bacteria via partial denitrification of nitrate to nitrite (Kartal et al., 2011). Many genomes encoding for DNRA also encode genes for partial denitrification but for the purposes of our

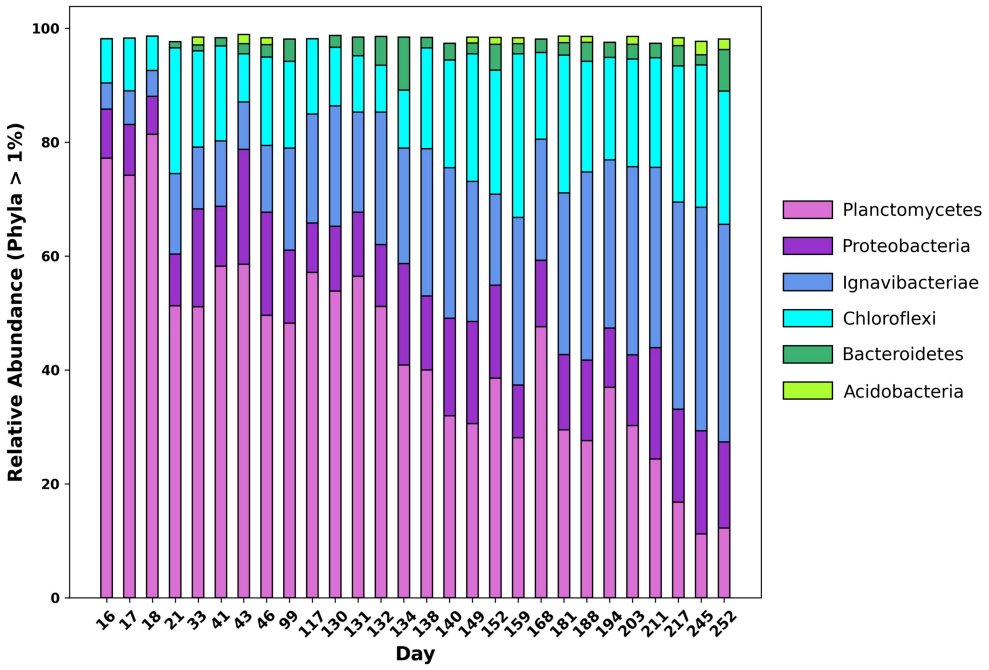

FIGURE 2
Changes in relative abundance at the phylum level of 16 S rRNA amplicon sequences over time from day 16 of the experiment to day 252.

analysis, we assume these bacteria will carry out DNRA as the most energetically favorable pathway.

Nitrogen transport and sensing genes, which can be used to infer substrate affinity, were identified in the top 14 most abundant MAGs by coverage (Figure 7), and all MAGs with genome coverage above 40% (Supplementary Figure S4). This analysis was performed to assess how effectively different organisms compete for various nitrogen substrates. Nitrate, a byproduct of anammox biosynthesis, is frequently abundant in anammox reactors, while nitrite is kept limiting to prevent nitrite toxicity. Therefore, the bacteria with the greatest affinity for nitrite will have a competitive advantage. Most genomes contained transporters belonging to the Nitrate/Nitrite Porter (NNP) family, including *narK*, *nrtP*, and *nasA* for nitrate and nitrite membrane transport (Moir and Wood, 2001). Consistent with previously reported anammox metagenomes (Ji et al., 2022; Wang et al., 2022), AMX01 contained Nitrate Transporter superfamily (NRT) nitrate/nitrite transporters, the high affinity nitrate/nitrite transporter *nrtB*, and a polytopic membrane transporter specifically for nitrite, *nirC*. Several genomes, excluding those of anammox bacteria, also encoded genes for putative formate-nitrite transporters from the formate-nitrate transporter (FNT) superfamily, including formate channel *focA* and formate permease *fdhC*. Previous research has shown that some denitrifying bacteria have a higher affinity for nitrite than nitrate (Kraft et al., 2014). This was supported by the presence of FNT transporters in a higher proportion of MAGs without *nrfAH* than those with these nitrate-metabolizing genes. The majority of genomes also encoded nitrate/nitrite sensor protein complexes *narX/L* and *nar Q/P*. These genes, which are often colocated on the *nar* operon, have been demonstrated to regulate expression of nitrate/nitrite reductases as well as other respiratory proteins (Browning et al., 2006).

3.5. Microbial community dynamics

Log-ratio (LR) changes between day 232 and day 37 were calculated using each MAG's coverage normalized to three reference genomes (Figure 8A). Of the 50 MAGs that experienced LR changes above the upper 95% confidence interval (CI) (Supplementary Table S7), 25 had RPKM abundances lower than the 95% CI (Supplementary Table S9) and 32 contained *narGH*, 15 contained *nirKS*, and 17 contained *nrfAH*. Of the 57 MAGs that experienced LR changes below the lower 95% CI, 36 had RPKM abundances lower than the lower 95% CI, and 35 contained *narGH*, 21 contained *nirKS*, and 13 contained *nrfAH*. Significant log-ratio changes in coverage did not have a strong correlation with taxonomy (Supplementary Table S6).

iRep values, which estimate each MAG's replication rate, ranged between 1.12 and 2.29 (Figure 8B). As expected, *Brocadia* had the lowest replication rates at all three time points with an average of 1.14. CFLX13 (Chloroflexi) had the highest replication rates with an average of 2.15. PROT03 (Rhodocyclales) experienced the most substantial decrease in replication rates during the course of the experiment, falling from 1.85 at day 37 to 1.43 at day 232 (a 23% decrease); CPR01 experienced the most significant increase, from 1.39 on day 37 to 2.15 on day 232 (a 55% increase). With the exception of CPR01, all of the MAGs that demonstrated increased replication rates between time points had negative log-ratio changes between day 37 and 232. This observation could be an indication of higher mortality rates suggestive of r-type strategists, or organisms well adapted to optimize growth during unstable environmental conditions. These types of organisms have shorter life cycles but very high reproduction rates associated with low efficiency substrate utilization (Grime, 1977; Andrews and Harris, 1986; Ho et al., 2017).

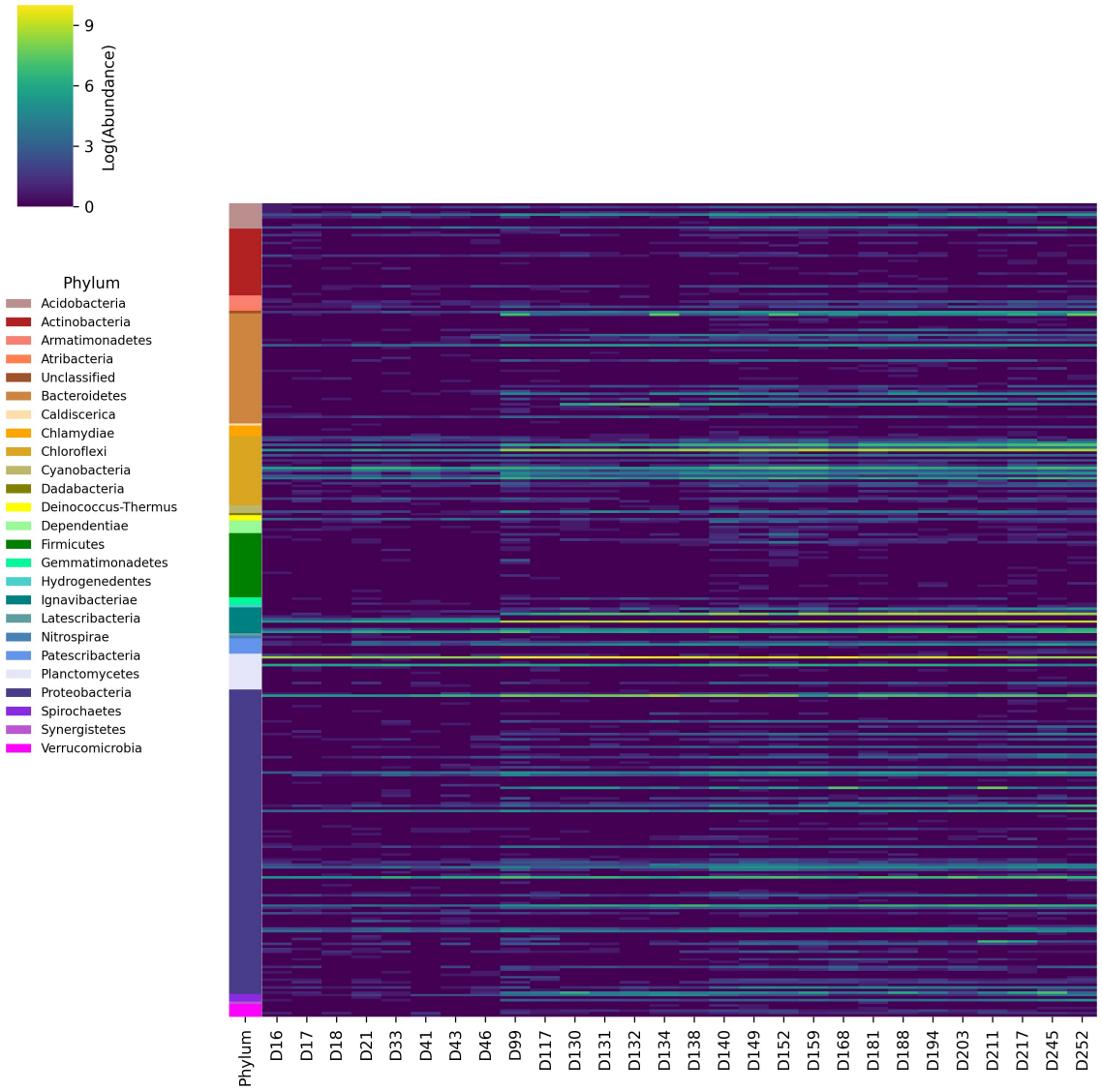

FIGURE 3
Changes in logarithmic abundances of 16 S rRNA amplicon reads aggregated at the genus level over time from day 16 of the experiment to day 252.

3.6. Taxon abundance and reactor operational parameters

To evaluate the effects of different nitrogen pathways on reactor performance, PCA analysis was conducted for the abundance of anammox, *nirKS* (denitrifying), and *nrfAH* (DNRA) associated taxa (Figure 9). The abundance of anammox bacteria is positively correlated with ammonium removal efficiency and the nitrate production rate, indicating the anammox bacteria are primarily responsible for ammonium removal and nitrate production as expected. The abundance of DNRA and denitrifying bacteria is positively correlated with nitrogen removal efficiency, nitrite removal efficiency, and the nitrogen removal rate, and negatively correlated with the ammonium removal efficiency, nitrate production rate, and effluent nitrite concentrations. However, the abundance of DNRA bacteria is more strongly associated with nitrite removal efficiency than denitrification. These results are consistent with the performance of the MBR throughout the course of the experiment, as the abundance of anammox bacteria decreased after the ratio change on day 89, while the ammonium removal efficiency decreased as well. Nevertheless, the overall nitrogen removal rate and nitrogen removal efficiency increased along with the increased growth of DNRA bacteria.

4. Discussion

4.1. Microbial community shifts in reactor

While previous studies have examined the performance of anammox reactors under variable influent loading ratios, analyses of the effects on the microbial community are limited. After the introduction of decreased NH_4^+:NO_2^- ratios, we observed an increase in the microbial diversity of the system. Of the 317 genera identified

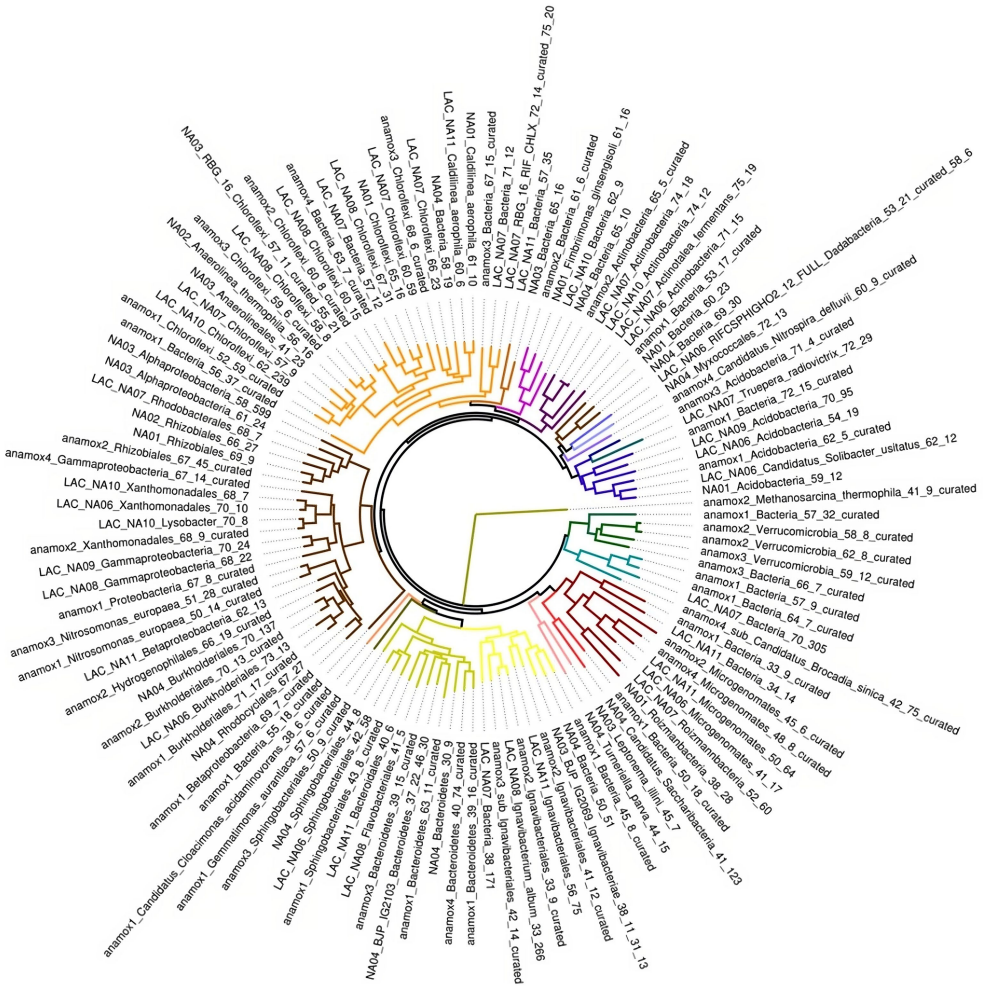

FIGURE 4
Maximum likelihood phylogenetic tree from concatenated ribosomal proteins of three metagenomic samples taken during the experiment.

through amplicon sequencing, 36% increased by at least one order of magnitude after the ratio change, and the alpha diversity also increased steadily. This increased diversity may correspond to increased availability of ammonium as a growth-limiting nitrogen source. Of the 129 MAGs identified, only 25 contained canonical assimilatory nitrate/nitrite reductases to utilize nitrate or nitrite as nitrogen sources; this suggests that most of the microbial community may require ammonium as a fixed nitrogen source for cell growth. During the initial nitrogen loading ratio, effluent ammonium concentrations remained low, within the range of 0–0.143 mM. Anammox bacteria are known to have high affinities for ammonium, as evidenced by the presence of multiple ammonium transporters in their genomes (Hu et al., 2012; Kartal et al., 2012; Van Niftrik and Jetten, 2012). This gives anammox microbes a competitive advantage for ammonium uptake, even at low concentrations. When the ratio of nitrogen substrates changed, the low fixed nitrite concentration would have limited ammonium oxidation, leading to an increased concentration of ammonium in the reactor, in excess of what anammox bacteria could use. This resulted in increased reactor ammonium concentrations (Figure 1), which may have supported the growth of other organisms with lower affinities for ammonium uptake to support biosynthesis.

Increased microbial diversity could also be explained by the interaction of diversifying stochastic drift constrained by deterministic homogenous selection. Based on theory supporting these processes, a microbial community will trend towards functional homogeneity during static environmental conditions (homogenous selection), but will also undergo variable changes in composition due to weak selection pressures (drift) (Stegen et al., 2015; Zhou and Ning, 2017). In anammox reactors, these processes would result in the selection of bacteria well-adapted to the conditions created by reactor operational parameters and the dominance of anammox bacteria, independent of taxonomy, as shown through the log-ratio changes (Figure 8A). However, when the reactor maintains these environmental conditions for extended periods of time, weak selection can promote fluctuations in the microbial community composition. Throughout the duration of the experiment, the reactor maintained relatively stable performance, except for effluent ammonium concentrations rising post-ratio change. Despite this consistency, populations of bacterial taxa from Ignavibacteriae, Chloroflexi, and Bacteroidetes still fluctuated. This is similar to results presented by Ya et al. (2023) where increased abundance of Chloroflexi and Proteobacteria was observed despite stable reactor operation. Functional redundancy amongst these bacterial groups could contribute to their increased abundance,

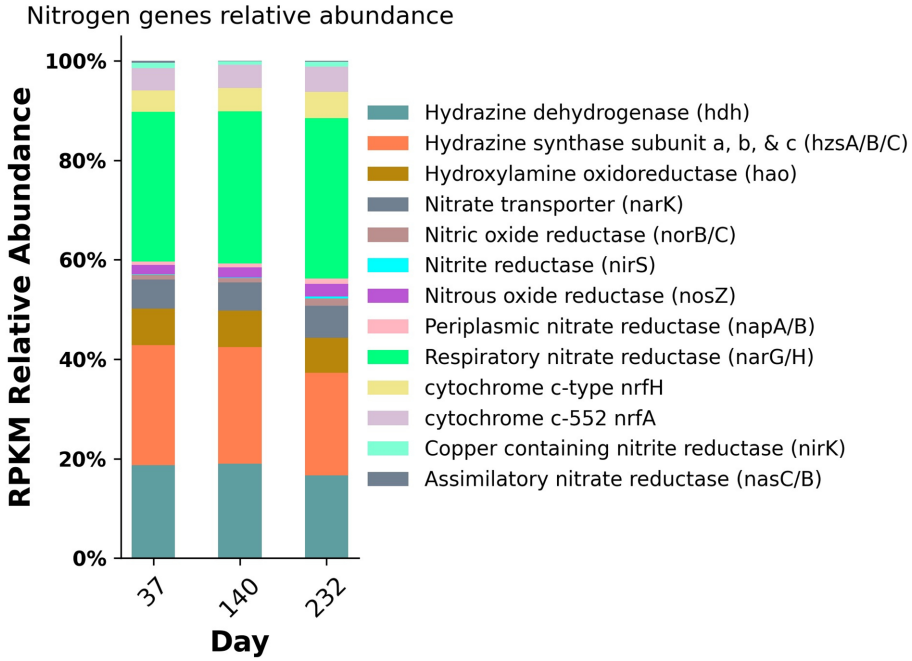

FIGURE 5
Nitrogen gene relative abundances from metagenomic sequencing from three time points during the experiment.

despite the lack of any operational or natural perturbations. This hypothesis, combined with the sustained high activity of anammox bacteria despite low abundance, could provide an explanation for the maintenance of efficient bioreactor performance (>85% nitrogen removal) despite significant changes to the microbial community.

4.2. Synergistic interactions between DNRA and anammox

After the influent NH_4^+:NO_2^- ratio change, we observed increased abundance of bacteria capable of performing DNRA. Amplicon sequencing and shotgun metagenomic sequencing revealed increased abundance of bacteria belonging to Ignavibacteriae, Chloroflexi, and Bacteroidetes, phyla previously associated with DNRA in anammox reactors (Wang et al., 2019; Keren et al., 2020; Bryson et al., 2022). While there is not sufficient evidence to conclude that the ratio change directly led to increased abundance of DNRA bacteria in this reactor system, the co-occurrence of this trend with stable reactor operation is an intriguing observation worth consideration. Previous studies have reported the presence and increased replication of DNRA bacteria to coincide with decreased reactor performance (Keren et al., 2020). However, DNRA bacteria have also been shown to form symbiotic interactions with anammox bacteria, promoting robust reactor performance (Li et al., 2020; Sheng et al., 2021). Many anammox species can also perform DNRA using simple organic acids as substrates (Castro-Barros et al., 2017), further complicating the characterization of the interplay between these metabolisms. Zhou et al. (2023) reported very similar results to those observed in this work, demonstrating increased abundance of DNRA bacteria with improved nitrogen removal efficiency (NRE) at lower NH_4^+:NO_2^- ratios, but deleterious effects on NRE at higher NH_4^+:NO_2^-(Zhou et al., 2023). The results from that study illustrate the delicate balance between anammox and DNRA, and how the complexity of these interactions is impacted by influent loading rates, organic carbon concentrations, and anammox species niche differentiation.

The observation of increased abundance of bacteria utilizing DNRA post-ratio change could be explained using a few key considerations. Previous research on the competitive balance between DNRA and denitrification suggests that DNRA is generally favored over denitrification at higher C/N ratios (van den Berg et al., 2016). This observation has also been purported to apply for both nitrate and nitrite and under dual limitation conditions when both the supply of electron donor and electron acceptor are limited in the environment (van den Berg et al., 2017a). Organic carbon concentrations, estimated from the biodegradable fraction of biomass measured through MLVSS (Supplementary Figure S3) remained substantially higher than effluent nitrate and nitrite concentrations throughout the duration of the experiment indicating conditions favorable for DNRA. From day 0 up until day 89 when the influent NH_4^+:NO_2^- ratio was 1:1.32, anammox bacteria, DNRA bacteria, and denitrifiers actively competed for nitrite and anammox bacteria were able to sustain relative dominance likely due to a higher affinity for nitrite as evidenced by multiple nitrite transporters (Figure 7). However, on day 89 when the NH_4^+:NO_2^- ratio was shifted to 1:1.1, the influent ammonium concentration was increased, and this would have required more nitrite to undergo the anammox reaction to completely oxidize ammonium to dinitrogen gas. Lowering the NH_4^+:NO_2^- ratio could have intensified the competition for nitrite, and this increased competition could select for bacteria that are capable of utilizing already limited substrates more efficiently. From a thermodynamic perspective, the theoretical amount of energy produced per mole of nitrite for DNRA and anammox is comparable (Castro-Barros et al., 2017). However, the yield of biomass produced per mole of nitrite through DNRA is effectively higher than through anammox, and bacterial growth rates are also significantly higher under DNRA (Figure 8B). Thus, when the ratio shift occurred

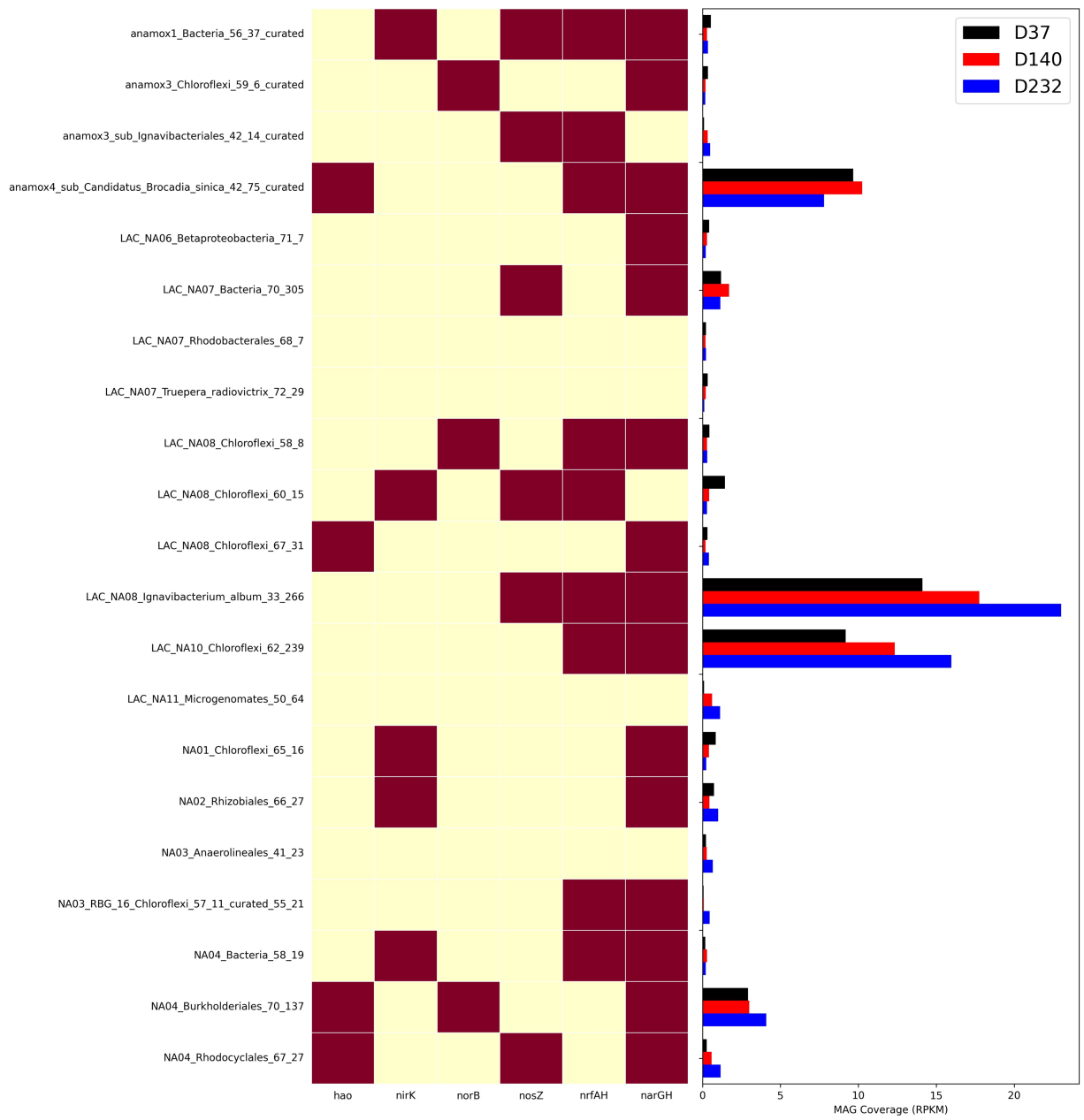

FIGURE 6
Heatmap showing presence of nitrogen genes in MAGs and abundance of MAGs from three timepoints with metagenome samples measured as RPKM.

and nitrite limitation was intensified, DNRA bacteria could have been poised to proliferate because of their ability to grow and biosynthesize more efficiently. It is important to consider that anammox bacteria also convert nitrite to nitrate to generate reducing equivalents for carbon fixation and biomass production (Strous et al., 2006). Additional competition for nitrite could lead to anammox bacteria diverting more nitrite towards energy generation than carbon fixation. This could result in decreased biomass production, which could offer a possible explanation for the decrease in cell abundance observed throughout the duration of the experiment. This explanation neglects the capability of anammox bacteria to utilize partial DNRA to convert nitrate back to nitrite to use for the anammox reaction. However, this reaction has only explicitly been identified to support the oxidation of volatile fatty acids (VFAs) (Castro-Barros et al., 2017) and is uncharacterized for alternative carbon substrates.

Reactor configuration and biomass growth type adds another dimension of complexity to the dynamics between anammox, DNRA, and denitrifying bacteria. Bryson et al. (2022) reported higher abundance of Ignavibacteriae and Phycisphaerae with *nrfAH* genes used for DNRA in two stage anammox configurations as compared with one stage configurations, citing a negative selection pressure on facultatively aerobic denitrifiers in a strictly anaerobic environment (Bryson et al., 2022). Our findings are consistent with those observations given that the strict anaerobic conditions provide a niche for fermentative bacteria (Gonzalez-Gil et al., 2015; Speth et al., 2016; Bhattacharjee et al., 2017). These observations could provide insight into the conditions that favor

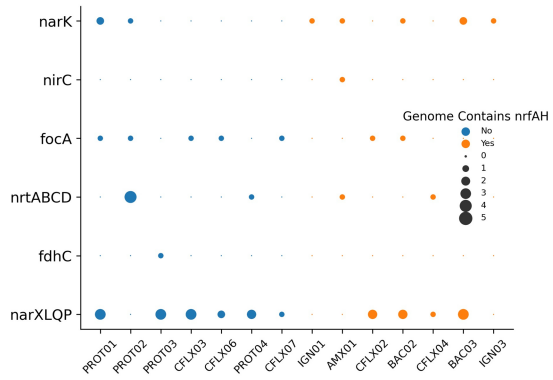

FIGURE 7
Putative nitrate/nitrite transporters and sensors encoded in MAGs.

DNRA in anammox systems. Many of the bacteria with *nrfAH* could be coupling DNRA to the fermentation of extracellular amino acids and exogenous carbon substrates. This reaction is more bioenergetically favorable than pure fermentation (Kraft et al., 2011), and could be even more competitive than alternative nitrogen pathways when the carbon substrate is more reduced. IGN01 and IGN03 both contain genes encoding for acetate kinase, and CFLX01 encodes genes for acetate ligase, suggesting that these strains have the ability to ferment acetate or propionate. This would be especially advantageous under the conditions found in the MBR where the concentrations of fermentable substrates, such as extracellular amino acids and polysaccharides, are likely much higher than non-fermentable substrates such as acetate, ethanol, or methanol. Fermentable sugars such as D-Arabinose, D-Ribose, and D-Mannose and sialic acids such as neuraminic acid, commonly found in anammox extracellular polysaccharides (Yin et al., 2015; Boleij et al., 2020; Wang et al., 2020), have also been shown to selectively enrich

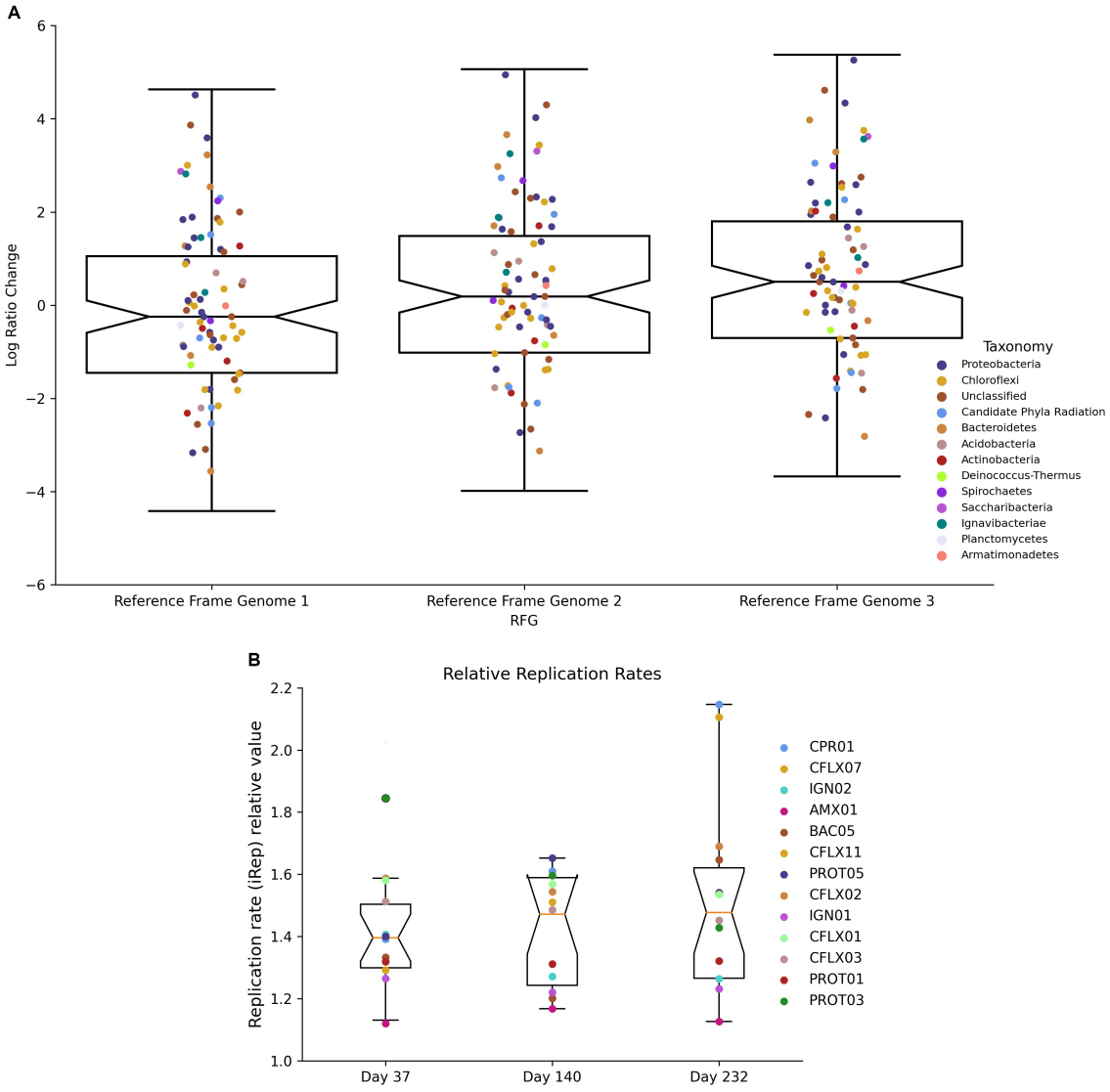

FIGURE 8
(A) Log ratio changes between D37 and D232 using different genomes as reference frames. **(B)** Replication rate values on D37, D140, and D232.

10.3389/fmicb.2023.1243410

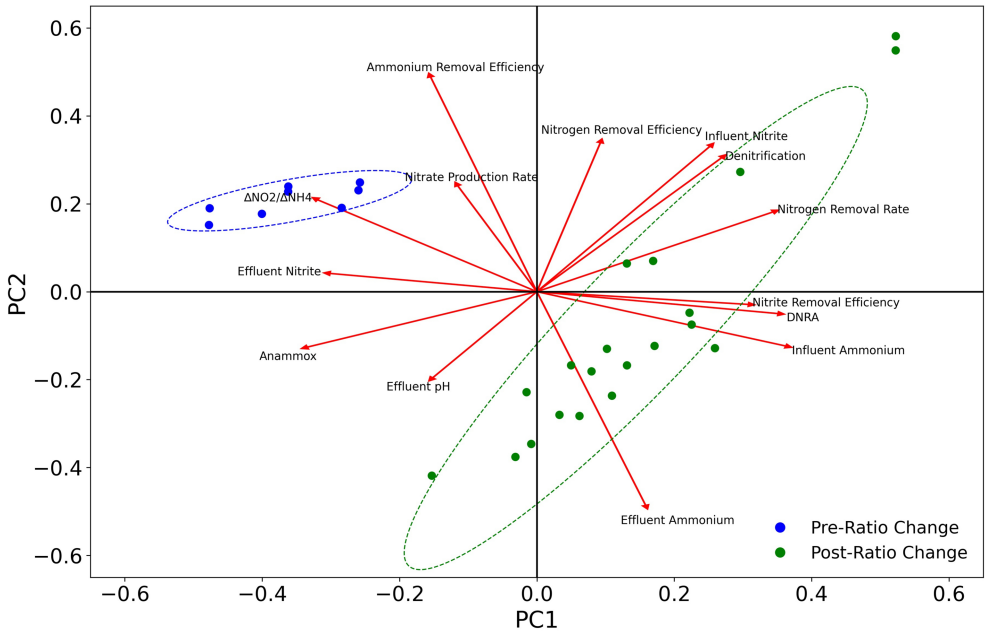

FIGURE 9
PCA plot of changes in taxa abundance for anammox, denitrification, and DNRA with reactor operational parameters. Ellipses represent 95% confidence intervals.

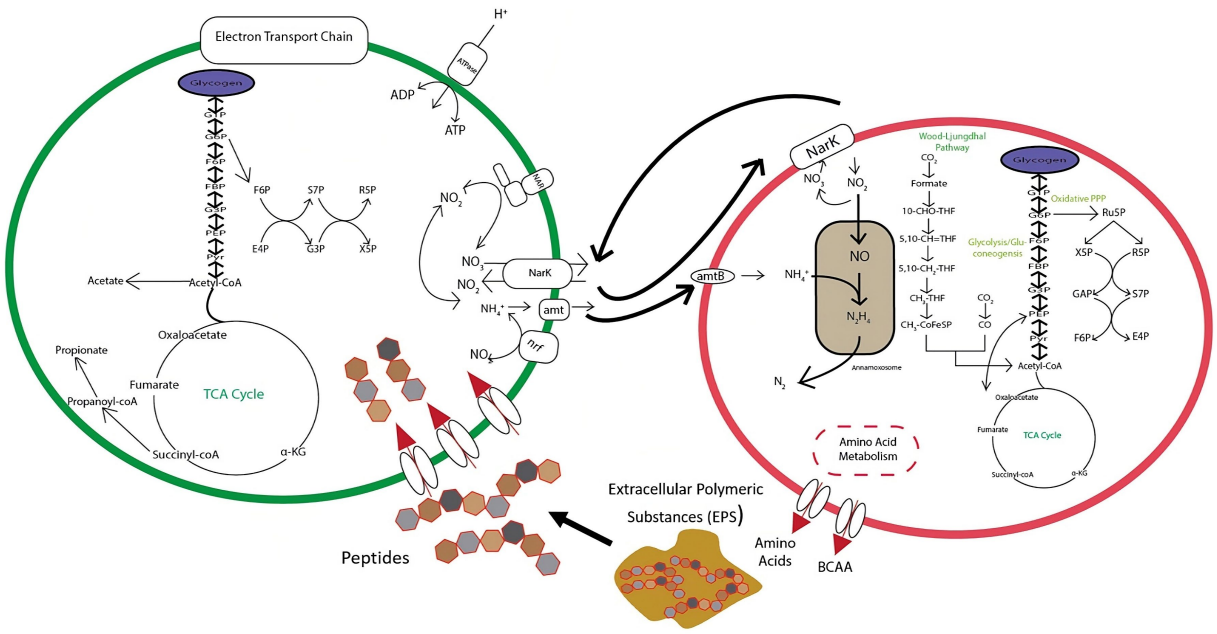

FIGURE 10
Conceptual diagram of metabolic exchanges occurring between anammox and DNRA bacteria within the tested bioreactor.

DNRA bacteria over denitrifiers (Carlson et al., 2020). When the ratio shift occurred, and the competition for nitrite intensified, the ability to couple nitrite reduction to fermentation of highly reduced carbon substrates could have also contributed to the enrichment of DNRA. Thus, the type of carbon source and the oxidative conditions in anammox systems also has a substantial impact on the competitive balance between anammox, denitrifiers, and DNRA bacteria.

The balance between DNRA and anammox is predicated on an exchange of nitrate, ammonium, and organic carbon substrates as shown in Figure 10. DNRA bacteria are thought to utilize substrates derived

from extracellular polymeric substances (EPS) produced by anammox bacteria (Keren et al., 2020), which would necessitate a symbiotic relationship between these two pathways. DNRA can provide anammox bacteria with nitrite through the reduction of nitrate via *nar* and *nap* nitrate reductases, or ammonium through the reduction of nitrite with *nrfAH* nitrite reductases. This steady flow of material exchanges can result in enhanced nitrogen removal in a variety of ecosystems (Ahmad et al., 2021; Sheng et al., 2021). Despite this, DNRA can still actively compete with anammox for nitrite, and even potentially destabilize aggregates through overconsumption of EPS, leading to anammox cell death (Keren et al., 2020). This tipping point is a pivotal junction to distinguish in order to optimize reactor efficiency and resiliency. It is also important to evaluate how this relationship changes at more extreme NH_4^+:NO_2^- ratios (<1:1.1 and >1:1.3). Thus, further research is needed to identify and parameterize the equilibrium of this dynamic.

4.3. Reactor performance implications

Anammox reactors are known to be sensitive to operational conditions and are susceptible to destabilizations after perturbation. These systems are particularly sensitive to nitrite fluctuations (Bettazzi et al., 2010; Puyol et al., 2014). The formation of synergistic relationships between anammox and DNRA can help to alleviate the deleterious effects of nitrite inhibition by keeping nitrite concentrations low. These interactions have been demonstrated to assist in the recovery of anammox reactor performance following nitrite inhibition (Qiao et al., 2022; Zhou et al., 2023), and to help stimulate the recovery of anammox bacteria from dormancy (Zhu et al., 2019). Promoting synergy between anammox and DNRA bacteria could be even more important at higher nitrogen loading rates, which cause the reactor to be more susceptible to nitrite inhibition (Tang et al., 2010). Throughout the duration of this study, nitrite concentrations rarely rose above detectable levels in the effluent, which can be attributed to the abundance of excess ammonium for the anammox reaction (1 mole of NH_4^+ requires 1.32 moles of NO_2^- to be fully oxidized) but also to the reduction of nitrite to ammonium by DNRA bacteria and, to a lesser extent, nitrite reduction to dinitrogen gas by denitrifying bacteria. The abundance of DNRA bacteria was also positively correlated with the nitrite removal efficiency, nitrogen removal efficiency, and nitrogen removal rates (Figure 9). These results provide evidence for the positive contributions of DNRA towards robust reactor performance. The interactions between anammox and DNRA bacteria can be enhanced by organic carbon amendments to encourage the growth of DNRA microbes, which has been previously reported to have beneficial effects on reactor performance (Jenni et al., 2014; Zhang et al., 2021; Fan et al., 2022). Taking advantage of the synergy between anammox and DNRA could be especially advantageous during reactor startup, where anammox activity is vulnerable to performance disruptions due to nitrite inhibition. These interactions could also be leveraged during periods of elevated nitrite concentrations by dosing with organic carbon to stimulate the growth of DNRA bacteria.

5. Conclusion

In a single-stage anammox MBR, adjusting influent NH_4^+:NO_2^- from the conventional ratio of 1:1.32 to 1:1.1 led to a significant change in the microbial community. Despite relatively minor changes in total nitrogen removal efficiency (85.26 ± 0.01% pre-ratio change vs. 85.833 ± 0.002% post-ratio change), the relative abundance of anammox bacteria in the system decreased from 77.19 to 12.24% by 16 S rRNA amplicon sequencing. This coincided with the growth of bacteria capable of performing DNRA; the phyla Ignavibacteriae and Chloroflexi increased from 7.73 and 4.57%, respectively, to 23.36 and 38.22%. These results demonstrate the positive effects of a stable dynamic between anammox and DNRA, which can result in robust reactor performance and enhanced nitrogen removal.

Data availability statement

The datasets presented in this study can be found in online repositories. The names of the repository/repositories and accession number(s) can be found in the article/Supplementary material.

Author contributions

EA and JL supervised the study. EA, JL, and LA-C designed the study. EA and JL maintained the bioreactor. CW analyzed the bioreactor performance, 16S rRNA gene data, metagenomics data, and wrote the manuscript. SS contributed to data analysis and visualization. RK contributed to metagenomic data analysis. LJ, KY, and WZ assisted with study design and manuscript revision. All authors read the manuscript and contributed with their input.

Funding

This research was supported by the National Natural Science Foundation of China (Nos. 51709005 and 51708362), and the National Science Foundation through the Engineering Research Center for ReInventing the Nation's Water Infrastructure (ReNUWIt) ECC-1028962. This material is also based upon work supported by the National Science Foundation Graduate Research Fellowship under grant no. DGE 1106400.

Acknowledgments

The authors would like to acknowledge the Joint Genome Institute (JGI) and the Institute for Environmental Genomics at the University of Oklahoma for providing the DNA sequencing used to produce this study.

Conflict of interest

Author JL was employed by CDM Smith.

The remaining authors declare that the research was conducted in the absence of any commercial or financial relationships that could be construed as a potential conflict of interest.

Publisher's note

All claims expressed in this article are solely those of the authors and do not necessarily represent those of their affiliated organizations, or those of the publisher, the editors and the

reviewers. Any product that may be evaluated in this article, or claim that may be made by its manufacturer, is not guaranteed or endorsed by the publisher.

Author disclaimer

Any opinion, findings, and conclusions or recommendations expressed in this material are those of the authors and do not necessarily reflect the views of the National Science Foundation.

Supplementary material

The Supplementary material for this article can be found online at: https://www.frontiersin.org/articles/10.3389/fmicb.2023.1243410/full#supplementary-material

References

Abma, W. R., Ce, S., Mulder, J. W., van der Star, W. R. L., Strous, M., Tokutomi, T., et al. (2007). Full-scale granular sludge anammox process. *Water Sci. Technol.* 55, 27–33. doi: 10.2166/wst.2007.238

Ahmad, H. A., Guo, B., Zhuang, X., Zhao, Y., Ahmad, S., Lee, T., et al. (2021). A twilight for the complete nitrogen removal via synergistic partial-denitrification, anammox, and DNRA process. *Npj Clean Water* 4, 1–11. doi: 10.1038/s41545-021-00122-5

Ali, M., and Okabe, S. (2015). Anammox-based Technologies for Nitrogen Removal: advances in process start-up and remaining issues. *Chemosphere* 141, 144–153. doi: 10.1016/j.chemosphere.2015.06.094

Andrews, J. H., and Harris, R. F. (1986). "R- and K-selection and microbial ecology" in *Advances in microbial ecology*. ed. K. C. Marshall (Boston, MA: Springer US), 99–147.

Bettazzi, E., Caffaz, S., Vannini, C., and Lubello, C. (2010). Nitrite inhibition and intermediates effects on anammox Bacteria: a batch-scale experimental study. *Process Biochem.* 45, 573–580. doi: 10.1016/j.procbio.2009.12.003

Bhattacharjee, A. S., Sha, W., Lawson, C. E., Jetten, M. S. M., Kapoor, V., Santo, J. W., et al. (2017). Whole-community metagenomics in two different anammox configurations: process performance and community structure. *Environ. Sci. Technol.* 51, 4317–4327. doi: 10.1021/acs.est.6b05855

Boleij, M., Kleikamp, H., Pabst, M., Neu, T. R., van Loosdrecht, M.-a. C. M., and Lin, Y. (2020). Decorating the anammox house: sialic acids and Sulfated glycosaminoglycans in the extracellular polymeric substances of anammox granular sludge. *Environ. Sci. Technol.* 54, 5218–5226. doi: 10.1021/acs.est.9b07207

Brown, C. T., Olm, M. R., Thomas, B. C., and Banfield, J. F. (2016). Measurement of bacterial replication rates in microbial communities. *Nat. Biotechnol.* 34, 1256–1263. doi: 10.1038/nbt.3704

Browning, D. F., Lee, D. J., Wolfe, A. J., Cole, J. A., and Busby, S. J. W. (2006). The *Escherichia Coli* K-12 NarL and NarP proteins insulate the Nrf promoter from the effects of integration host factor. *J. Bacteriol.* 188, 7449–7456. doi: 10.1128/JB.00975-06

Bryson, S. J., Hunt, K. A., Stahl, D. A., Mari, K. H., and Winkler, M. K. H. (2022). Metagenomic insights into competition between denitrification and dissimilatory nitrate reduction to ammonia within one-stage and two-stage partial-nitritation anammox bioreactor configurations. *Front. Microbiol.* 13:1402. doi: 10.3389/fmicb.2022.825104

Cao, S., Rui, D., and Zhou, Y. (2020). Coupling anammox with heterotrophic denitrification for enhanced nitrogen removal: a review. *Crit. Rev. Environ. Sci. Technol.* 51, 2260–2293. doi: 10.1080/10643389.2020.1778394,

Carlson, H. K., Lui, L. M., Price, M. N., Kazakov, A. E., Carr, A. V., Kuehl, J. V., et al. (2020). Selective carbon sources influence the end products of microbial nitrate respiration. *ISME J.* 14, 2034–2045. doi: 10.1038/s41396-020-0666-7

Castro-Barros, C. M., Jia, M., van Loosdrecht, M. C. M., Volcke, E. I. P., and Winkler, M. K. H. (2017). Evaluating the potential for dissimilatory nitrate reduction by anammox bacteria for municipal wastewater treatment. *Bioresour. Technol.* 233, 363–372. doi: 10.1016/j.biortech.2017.02.063

Cho, S., Kambey, C., and Nguyen, V. K. (2019). Performance of anammox processes for wastewater treatment: a critical review on effects of operational conditions and environmental stresses. *Water* 12:20. doi: 10.3990/w12010020

Davidson, K., Gowen, R. J., Harrison, P. J., Fleming, L. E., Hoagland, P., and Moschonas, G. (2014). Anthropogenic nutrients and harmful algae in coastal waters. *J. Environ. Manag.* 146, 206–216. doi: 10.1016/j.jenvman.2014.07.002

Devol, A. H. (2015). Denitrification, anammox, and N2 production in marine sediments. *Ann. Rev. Mar. Sci.* 7, 403–423. doi: 10.1146/annurev-marine-010213-135040

Du, R., Cao, S., Li, B., Niu, M., Wang, S., and Peng, Y. (2017). Performance and microbial community analysis of a novel DEAMOX based on partial-denitrification and anammox treating ammonia and nitrate wastewaters. *Water Res.* 108, 46–56. doi: 10.1016/j.watres.2016.10.051

Einsle, O., Messerschmidt, A., Huber, R., Kroneck, P. M. H., and Neese, F. (2002). Mechanism of the six-electron reduction of nitrite to ammonia by cytochrome c nitrite reductase. *J. Am. Chem. Soc.* 124, 11737–11745. doi: 10.1021/ja0206487

Fan, J., Rui, D., Liu, Q., Li, C., and Peng, Y. (2022). Insight into the microbial interactions of anammox and heterotrophic Bacteria in different granular sludge systems: effect of size distribution and available organic carbon source. *Bioresour. Technol.* 364:128055. doi: 10.1016/j.biortech.2022.128055

Feng, Y., Zhao, Y., Jiang, B., Zhao, H., Wang, Q., and Liu, S. (2019). Discrepant gene functional potential and cross-feedings of anammox bacteria ca. Jettenia Caeni and ca. Brocadia Sinica in response to acetate. *Water Res.* 165:114974. doi: 10.1016/j.watres.2019.114974

Fernández, I., Dosta, J., Fajardo, C., Campos, J. L., Mosquera-Corral, A., and Méndez, R. (2012). Short- and long-term effects of ammonium and nitrite on the anammox process. *J. Environ. Manag.* 95, S170–S174. doi: 10.1016/j.jenvman.2010.10.044

Gonzalez-Gil, G., Sougrat, R., Behzad, A. R., Lens, P. N. L., and Saikaly, P. E. (2015). Microbial community composition and ultrastructure of granules from a full-scale anammox reactor. *Microb. Ecol.* 70, 118–131. doi: 10.1007/s00248-014-0546-7

Gonzalez-Martinez, A., Osorio, F., Morillo, J. A., Rodriguez-Sanchez, A., Gonzalez-Lopez, J., Abbas, B. A., et al. (2015). Comparison of bacterial diversity in full scale anammox bioreactors operated under different conditions. *Biotechnol. Prog.* 31, 1464–1472. doi: 10.1002/btpr.2151

Grime, J. P. (1977). Evidence for the existence of three primary strategies in plants and its relevance to ecological and evolutionary theory. *Am. Nat.* 111, 1169–1194. doi: 10.1086/283244

Guo, J., Yongzhen Peng, L., Fan, L. Z., Ni, B. J., Kartal, B., Feng, X., et al. (2016). Metagenomic analysis of anammox communities in three different microbial aggregates. *Environ. Microbiol.* 18, 2979–2993. doi: 10.1111/1462-2920.13132

Ho, A., Paolo Di Lonardo, D., and Bodelier, P. L. E. (2017). Revisiting life strategy concepts in environmental microbial ecology. *FEMS Microbiol. Ecol.* 93:fix006. doi: 10.1093/femsec/fix006

Hu, Q. Y., Da Kang, R., Wang, A. Q., Ding, G. A., Zhang, M., Qiu, L., et al. (2018). Characterization of oligotrophic AnAOB culture: morphological, physiological, and ecological features. *Appl. Microbiol. Biotechnol.* 102, 995–1003. doi: 10.1007/s00253-017-8587-8

Hu, Z., Speth, D. R., Francoijs, K. J., Quan, Z. X., and Jetten, M. S. M. (2012). Metagenome analysis of a complex community reveals the metabolic blueprint of anammox bacterium 'Candidatus Jettenia Asiatica'. *Front. Microbiol.* 3. doi: 10.3389/fmicb.2012.00366

Jenni, S., Vlaeminck, S. E., Morgenroth, E., and Udert, K. M. (2014). Successful application of nitritation/anammox to wastewater with elevated organic carbon to Ammonia ratios. *Water Res.* 49, 316–326. doi: 10.1016/j.watres.2013.10.073

Jetten, M. S. M., Horn, S. J., and Van Loosdrecht, M. C. M. (1997). Towards a more sustainable municipal wastewater treatment system. *Water Sci. Technol. J. Int. Assoc. Water Pollut. Res.* 35, 171–180. doi: 10.2166/wst.1997.0341

Jetten, Mike S. M., Wagner, Michael, Fuerst, John, Van Loosdrecht, Mark, Kuenen, Gijs, and Strous, Marc. (2001). Microbiology and application of the anaerobic ammonium oxidation ('anammox') process. *Curr. Opin. Biotechnol.* 283–288.

Ji, X. M., Wang, Y. L., Zhan, X., Zhuoying, W., and Lee, P. H. (2022). Meta-omics reveal the metabolic acclimation of freshwater anammox Bacteria for saline wastewater treatment. *J. Clean. Prod.* 362:132184. doi: 10.1016/j.jclepro.2022.132184

Jia, M., Winkler, M. K. H., and Volcke, E. I. P. (2020). Elucidating the competition between heterotrophic denitrification and DNRA using the resource-ratio theory. *Environ. Sci. Technol.* 54, 13953–13962. doi: 10.1021/acs.est.0c01776

Jin, R.-C., Xing, B.-S., Jin-Jin, Y., Qin, T.-Y., and Chen, S.-X. (2013). The importance of the substrate ratio in the operation of the anammox process in Upflow biofilter. *Ecol. Eng.* 53, 130–137. doi: 10.1016/j.ecoleng.2012.12.027

Jin, R. C., Yang, G. F., Jin Jin, Y., and Zheng, P. (2012). The inhibition of the anammox process: a review. *Chem. Eng. J.* 197, 67–79. doi: 10.1016/j.cej.2012.05.014

Joss, A., Derlon, N., Cyprien, C., Burger, S., Szivak, I., Traber, J., et al. (2011). Combined nitritation-anammox: advances in understanding process stability. *Environ. Sci. Technol.* 45, 9735–9742. doi: 10.1021/es202181v

Joss, A., Salzgeber, D., Eugster, J., König, R., Rottermann, K., Burger, S., et al. (2009). Full-scale nitrogen removal from digester liquid with partial nitritation and anammox in one SBR. *Environ. Sci. Technol.* 43, 5301–5306. doi: 10.1021/es900107w

Kartal, B., De Almeida, N. M., Maalcke, W. J., Huub, J. M., den Camp, O., Jetten, M. S. M., et al. (2013). How to make a living from anaerobic ammonium oxidation. *FEMS Microbiol. Rev.* 37, 428–461. doi: 10.1111/1574-6976.12014

Kartal, B., Maalcke, W. J., De Almeida, N. M., Cirpus, I., Gloerich, J., Geerts, W., et al. (2011). Molecular mechanism of anaerobic ammonium oxidation. *Nature* 5, 5–10. doi: 10.1038/nature10453

Kartal, B., van Niftrik, L., Keltjens, J. T., Huub, J. M., den Camp, O., and Jetten, M. S. M. (2012). Anammox—growth physiology, cell biology, and metabolism. *Adv. Microb. Physiol.* 60, 211–262. doi: 10.1016/B978-0-12-398264-3.00003-6

Keren, R., Lawrence, J. E., Zhuang, W., Jenkins, D., Banfield, J. F., Alvarez-Cohen, L., et al. (2020). Increased replication of dissimilatory nitrate-reducing Bacteria leads to decreased anammox bioreactor performance. *Microbiome* 8, 1–21. doi: 10.1186/s40168-020-0786-3

Kraft, B., Strous, M., and Tegetmeyer, H. E. (2011). Microbial nitrate respiration – genes, enzymes and environmental distribution. *J. Biotechnol.* 155, 104–117. doi: 10.1016/j.jbiotec.2010.12.025

Kraft, B., Tegetmeyer, H. E., Sharma, R., Klotz, M. G., Ferdelman, T. G., Hettich, R. L., et al. (2014). The environmental controls that govern the end product of bacterial nitrate respiration. *Science* 345, 676–679. doi: 10.1126/science.1254070

Kuenen, J. G. (2008). Anammox bacteria: from discovery to application. *Nat. Rev. Microbiol.* 6, 320–326. doi: 10.1038/nrmicro1857

Kuypers, M. M. M., Olav Sliekers, A., Lavik, G., and Schmid, M. (2003). Anaerobic ammonium oxidation by anammox Bacteria in the Black Sea. *Nature* 422, 608–611. doi: 10.1038/nature01472,

Lackner, S., Gilbert, E. M., Vlaeminck, S. E., Joss, A., Horn, H., and van Loosdrecht, M. C. M. (2014). Full-scale partial Nitritation/anammox experiences – an application survey. *Water Res.* 55, 292–303. doi: 10.1016/j.watres.2014.02.032

Lawson, C. E., Sha, W., Bhattacharjee, A. S., Hamilton, J. J., McMahon, K. D., Goel, R., et al. (2017). Metabolic network analysis reveals microbial community interactions in anammox granules. *Nat. Commun.* 8, 1–12. doi: 10.1038/ncomms15416

Li, Z., Peng, Y., and Gao, H. (2020). Enhanced long-term advanced denitrogenation from nitrate wastewater by anammox consortia: dissimilatory nitrate reduction to ammonium (DNRA) coupling with anammox in an upflow biofilter reactor equipped with EDTA-2Na/Fe(II) ratio and PH control. *Bioresour. Technol.* 305:123083. doi: 10.1016/j.biortech.2020.123083

Lotti, T., van der Star, W. R. L., Kleerebezem, R., Lubello, C., and van Loosdrecht, M. C. M. (2012). The effect of nitrite inhibition on the anammox process. *Water Res.* 46, 2559–2569. doi: 10.1016/j.watres.2012.02.011

Moir, J. W. B., and Wood, N. J. (2001). Nitrate and nitrite transport in Bacteria. *Cell. Mol. Life Sci.* 58, 215–224. doi: 10.1007/PL00000849

Mulder, A., van de Graaf, A. A., Robertson, L. A., and Kuenen, J. G. (1995). Anaerobic ammonium oxidation discovered in a denitrifying fluidized bed reactor. *FEMS Microbiol. Ecol.* 16, 177–184. doi: 10.1111/j.1574-6941.1995.tb00281.x

Oshiki, M., Shimokawa, M., Fujii, N., Satoh, H., and Okabe, S. (2011). Physiological characteristics of the anaerobic ammonium-oxidizing bacterium 'Candidatus Brocadia Sinica'. *Microbiology* 157, 1706–1713. doi: 10.1099/mic.0.048595-0

Oshiki, M., Shinyako-Hata, K., Satoh, H., and Okabe, S. (2015). Draft genome sequence of an anaerobic ammonium-oxidizing bacterium, 'Candidatus Brocadia Sinica'. *Genome Announc.* 3, e00267-15. doi: 10.1128/genomeA.00267-15

Pereira, A. D., Cabezas, A., Etchebehere, C., de Lemos Chernicharo, C. A., and de Araújo, J. C. (2017). Microbial communities in anammox reactors: a review. *Environ. Technol. Rev.* 6, 74–93. doi: 10.1080/21622515.2017.1304457

Pereira, A. D., de Almeida, L., Fernandes, H. M., Castro, C., Leal, C. D., Carvalho, B. G. P., et al. (2019). Nitrogen removal from food waste digestate using partial nitritation-anammox process: effect of different aeration strategies on performance and microbial community dynamics. *J. Environ. Manag.* 251:109562. doi: 10.1016/j.jenvman.2019.109562

Puyol, D., Carvajal-Arroyo, J. M., Sierra-Alvarez, R., and Field, J. A. (2014). Nitrite (not free nitrous acid) is the Main inhibitor of the anammox process at common PH conditions. *Biotechnol. Lett.* 36, 547–551. doi: 10.1007/s10529-013-1397-x

Qiao, X., Zhang, L., Qiu, Z., Wang, L., Wu, Y., Deng, C., et al. (2022). Specific denitrifying and dissimilatory nitrate reduction to ammonium Bacteria assisted the recovery of anammox community from nitrite inhibition. *Front. Microbiol.* 12:781156. doi: 10.3389/fmicb.2021.781156

Schloss, P. D., Westcott, S. L., Ryabin, T., Hall, J. R., Hartmann, M., Hollister, E. B., et al. (2009). Introducing Mothur: open-source, platform-independent, community-supported software for describing and comparing microbial communities. *Appl. Environ. Microbiol.* 75, 7537–7541. doi: 10.1128/AEM.01541-09

Schmid, M., Twachtmann, U. L. F., Klein, M., Strous, M., Juretschkoi, S., and Jetten, M. (2000). Molecular evidence for genus level diversity of Bacteria capable of catalyzing anaerobic ammonium oxidation. *Syst. Appl. Microbiol.* 23, 93–106. doi: 10.1016/S0723-2020(00)80050-8,

Sheng, H., Weng, R., He, Y., Wei, Z., Yang, Y., Chen, J., et al. (2021). The coupling of mixotrophic denitrification, dissimilatory nitrate reduction to ammonium (DNRA) and anaerobic ammonium oxidation (anammox) promoting the start-up of anammox by addition of calcium nitrate. *Bioresour. Technol.* 341:125822. doi: 10.1016/j.biortech.2021.125822

Smith, V. H., and Schindler, D. W. (2009). Eutrophication science: where do we go from Here? *Trends Ecol. Evol.* 24, 201–207. doi: 10.1016/j.tree.2008.11.009

Speth, D. R., Michiel, H., Zandt, I.' T., Guerrero-Cruz, S., Dutilh, B. E., and Jetten, M. S. M. (2016). Genome-based microbial ecology of anammox granules in a full-scale wastewater treatment system. *Nat. Commun.* 7. doi: 10.1038/ncomms11172

Stegen, J. C., Lin, X., Fredrickson, J. K., and Konopka, A. E. (2015). Estimating and mapping ecological processes influencing microbial community assembly. *Front. Microbiol.* 6:370. doi: 10.3389/fmicb.2015.00370

Strous, M., Heijnen, J. J., Kuenen, J. G., and Jetten, M. S. M. (1998). The sequencing batch reactor as a powerful tool for the study of slowly growing anaerobic ammonium-oxidizing microorganisms. *Appl. Microbiol. Biotechnol.* 50, 589–596.

Strous, M., Pelletier, E., Mangenot, S., Rattei, T., Lehner, A., Taylor, M. W., et al. (2006). Deciphering the evolution and metabolism of an anammox bacterium from a community genome. *Nature* 440, 790–794. doi: 10.1038/nature04647

Strous, M., Planet, E., The MechanicsAmerica, M., Appl, P., Island, A., et al. (1999). Missing lithotroph identified as new planctomycete. *Nature* 400, 446–449. doi: 10.1038/22749

Tang, C.-J., Zheng, P., Mahmood, Q., and Chen, J.-W. (2010). Effect of substrate concentration on stability of anammox biofilm reactors. *J. Cent. S. Univ. Technol.* 17, 79–84. doi: 10.1007/s11771-010-0014-6

USEPA (2007). Wastewater Technology Fact Sheet Side Stream Nutrient Removal. U.S. Environmental Protection Agency, EPA 832-F-07-017.

USEPA (2001). "Method 1684: Total, fixed, and volatile solids in water, solids, and biosolids. EPA-821-R-01-015", Office of Water, Office of Science and Technology. Engineering and Analysis Division, U.S. Washington, DC: Environmental Protection Agency.

van de Graaf, A. A., Mulder, A., Bruijn, P. D. E., Jetten, M. S. M., Robertson, L. A., and Gijs Kuenen, J. (1995). Anaerobic oxidation of ammonium is a biologically mediated process. *Appl Environ Microbiol.* 61, 1246–1251. doi: 10.1128/aem.61.4.1246-1251.1995

van den Berg, E. M., Rombouts, J. L., Kuenen, J. G., Kleerebezem, R., and Loosdrecht, M. C. M. v. (2017b). Role of nitrite in the competition between denitrification and DNRA in a chemostat enrichment culture. *AMB Express* 7, 1–7. doi: 10.1186/s13568-017-0398-x

van den Berg, E. M., Boleij, M., Kuenen, J. G., Kleerebezem, R., and Loosdrecht, M. C. M. v. (2016). DNRA and denitrification coexist over a broad range of acetate/N-NO3- ratios, in a chemostat enrichment culture. *Front. Microbiol.* 7:1842. doi: 10.3389/fmicb.2016.01842

van den Berg, E. M., Elisário, M. P., Kuenen, J. G., Kleerebezem, R., and Loosdrecht, M. C. M. v. (2017a). Fermentative Bacteria influence the competition between Denitrifiers and DNRA Bacteria. *Front. Microbiol.* 8:1684. doi: 10.3389/fmicb.2017.01684

Van Niftrik, L., and Jetten, M. S. M. (2012). Anaerobic ammonium-oxidizing Bacteria: unique microorganisms with exceptional properties. *Microbiol Mol Biol Rev* 76, 585–596. doi: 10.1128/MMBR.05025-11

Wang, S., Liu, L., Li, H., Fang, F., Yan, P., Chen, Y., et al. (2020). The branched chains and branching degree of exopolysaccharides affecting the stability of anammox granular sludge. *Water Res.* 178:115818. doi: 10.1016/j.watres.2020.115818

Wang, Y., Qigui Niu, X., Zhang, L. L., Wang, Y., Chen, Y., Negi, M., et al. (2019). Exploring the effects of operational mode and microbial interactions on bacterial community assembly in a one-stage partial-Nitritation anammox reactor using integrated multi-omics. *Microbiome* 7, 1–15. doi: 10.1186/s40168-019-0730-6

Wang, D., Wang, Y., Liu, L., Chen, Y., Chunxiao Wang, Y., Li, Y., et al. (2022). Response and resilience of anammox consortia to nutrient starvation. *Microbiome* 10, 1–14. doi: 10.1186/s40168-021-01212-9

Wu, L., Wen, C., Qin, Y., Yin, H., Qichao, T., Van Nostrand, J. D., et al. (2015). Phasing amplicon sequencing on Illumina Miseq for robust environmental microbial community analysis. *BMC Microbiol.* 15, 1–12. doi: 10.1186/s12866-015-0450-4

Xiao, R., Ni, B. J., Liu, S., and Huijie, L. (2021). Impacts of organics on the microbial ecology of wastewater anammox processes: recent advances and meta-analysis. *Water Res.* 191:116817. doi: 10.1016/j.watres.2021.116817

Ya, T., Huang, Y., Wang, K., Wang, J., Liu, J., Hai, R., et al. (2023). Functional stability correlates with dynamic microbial networks in anammox process. *Bioresour. Technol.* 370:128557. doi: 10.1016/j.biortech.2022.128557

Yin, C., Meng, F., and Chen, G. H. (2015). Spectroscopic characterization of extracellular polymeric substances from a mixed culture dominated by ammonia-oxidizing Bacteria. *Water Res.* 68, 740–749. doi: 10.1016/j.watres.2014.10.046

Zhang, T., Wei, N., and Guangxue, W. (2020). Autotrophic nitrogen removal and potential microbial interactions in anammox systems with different ammonia and organic carbon concentrations. *J. Water Process Engin.* 37:101493. doi: 10.1016/j.jwpe.2020.101493

Zhang, T., Yin, Q., Shi, Y., and Guangxue, W. (2021). Microbial physiology and interactions in anammox systems with the intermittent addition of organic carbons. *Bioresour. Technol.* 319:124226. doi: 10.1016/j.biortech.2020.124226

Zhao, Y., Liu, S., Jiang, B., Feng, Y., Zhu, T., Tao, H., et al. (2018). Genome-Centered metagenomics analysis reveals the symbiotic organisms possessing ability to cross-feed with anammox Bacteria in anammox consortia. *Environ. Sci. Technol.* 52, 11285–11296. doi: 10.1021/acs.est.8b02599

Zhou, J., and Ning, D. (2017). Stochastic community assembly: does it matter in microbial ecology? *Microbiol Mol Biol Rev* 81, e00002-17. doi: 10.1128/MMBR.00002-17

Zhou, L., Zhao, B., and Zhuang, W. Q. (2023). Double-edged sword effects of dissimilatory nitrate reduction to ammonium (DNRA) Bacteria on anammox Bacteria performance in an MBR reactor. *Water Res.* 233:119754. doi: 10.1016/j.watres.2023.119754

Zhu, W., Li, J., Dong, H., Wang, D., and Zhang, P. (2017). Effect of influent substrate ratio on anammox granular sludge: performance and kinetics. *Biodegradation* 28, 437–452. doi: 10.1007/s10532-017-9807-8

Zhu, G., Wang, S., Wang, C., Zhou, L., Zhao, S., Li, Y., et al. (2019). Resuscitation of anammox Bacteria after >10,000 years of dormancy. *ISME J.* 13, 1098–1109. doi: 10.1038/s41396-018-0316-5

frontiers | Frontiers in Microbiology

TYPE Original Research
PUBLISHED 21 August 2023
DOI 10.3389/fmicb.2023.1254152

OPEN ACCESS

EDITED BY
Yuanyuan Miao,
Qingdao University, China

REVIEWED BY
Yao Chen,
Chongqing Jiaotong University, China
Fangxu Jia,
Beijing Jiaotong University, China
Zhe Liu,
Xi'an University of Architecture and Technology, China

*CORRESPONDENCE
Jie Xu
xujie@qut.edu.cn

RECEIVED 06 July 2023
ACCEPTED 31 July 2023
PUBLISHED 21 August 2023

CITATION
Xu J, Gao Y, Bi X, Li L, Xiang W and Liu S (2023) Positive effects of lignocellulose on the formation and stability of aerobic granular sludge.
Front. Microbiol. 14:1254152.
doi: 10.3389/fmicb.2023.1254152

Positive effects of lignocellulose on the formation and stability of aerobic granular sludge

Jie Xu[1]*, Yuan Gao[1], Xuejun Bi[1], Lin Li[2], Wenjuan Xiang[1] and Shichang Liu[1]

[1]School of Environmental and Municipal Engineering, Qingdao University of Technology, Qingdao, China, [2]Key Laboratory of the Three Gorges Reservoir Region's Eco-Environment, Ministry of Education, College of Environment and Ecology, Chongqing University, Chongqing, China

Introduction: Lignocellulose is one of the major components of particulate organic matter in sewage, which has a significant influence on biological wastewater treatment process. However, the effect of lignocellulose on aerobic granular sludge (AGS) system is still unknown.

Methods: In this study, two reactors were operated over 5 months to investigate the effect of lignocellulose on granulation process, structure stability and pollutants removal of AGS.

Results and discussion: The results indicated that lignocellulose not only promoted the secretion of tightly bound polysaccharide in extracellular polymeric substances, but also acted as skeletons within granules, thereby facilitating AGS formation, and enhancing structural strength. Lignocellulose imposed little effect on the removal efficiency of pollutants, with more than 95, 99, and 92% of COD, NH_4^+-N, and PO_4^{3-}-P were removed in both reactors. However, it did exhibit a noticeable influence on pollutants conversion processes. This might be due to that the presence of lignocellulose promoted the enrichment of functional microorganisms, including *Candidatus_Accumulibacter*, *Candidatus_Competibacter*, *Nitrosomonas*, and *Nitrospira*, etc. These findings might provide valuable insights into the control strategy of lignocellulose in practical AGS systems.

KEYWORDS

aerobic granular sludge, lignocellulose, extracellular polymeric substances, wastewater treatment, microbial community structure

1. Introduction

Aerobic granular sludge (AGS) technology has gained widespread attention as an excellent replacement for conventional activated sludge (CAS) due to its significant advantages (Han, 2022). It has been proved that AGS could achieve excellent performance in the treatment of municipal wastewater as well as industrial wastewater from textiles (Lourenço et al., 2015), pharmaceuticals (Amorim et al., 2014), papermaking (Vashi et al., 2019), petrochemicals (Campo and Di Bella, 2019), etc. However, the application of AGS technology in practical engineering is significantly constrained by challenges such as prolonged granulation time and poor stability under unfavorable conditions (Franca et al., 2018).

The influent substrates have a significant influence on the formation and stability of AGS (Szabó, 2017; De Sousa Rollemberg et al., 2018; Adler and Holliger, 2020). For example, when glucose was applied as the sole carbon source, the cultivated AGS appeared as loose hairy

granules due to the excessive proliferation of filamentous bacteria (Moy et al., 2002); when applying sodium acetate (NaAc) as the carbon source, the dominant microorganisms in granules were cocci, resulting in a more compact structure (Nancharaiah and Kiran, 2018); however, when a mixture of glucose and NaAc was applied, the surface of AGS was dominated by brevibacterium, while the interior part was dominated by cocci, exhibiting a distinct hierarchical structure (Bao et al., 2009). Lashkarizadeh et al. (2015) investigated the impact of real domestic wastewater on AGS cultivated with synthetic wastewater. The results showed that a significant granule disintegration occurred when the influent was switched from synthetic wastewater to real domestic wastewater. Although regranulation occurred after 30 d, the morphology and performance of the newly formed granules differed significantly from the initial ones. This might be due to that the complex carbon source composition in actual domestic sewage affected the microbial community and extracellular polymeric substances (EPS) characteristics in granules, thereby influencing the properties of AGS (Lemaire et al., 2008).

Particulate Organic Matter (POM) is one of the primary components of organic matter in domestic wastewater, accounting for over 60% of the organic loading (Rickert and Hunter, 1967). Studies have shown that particle size had a significant impact on the removal process of POM. Most particles larger than 100 μm could be effectively removed through sedimentation (Morgenroth et al., 2002), but smaller particles tended to enter the biological treatment system and be removed through the adsorption and entrapment by bio-aggregates (Levine et al., 1991). Currently, researches on POM in sewage treatment were mostly focused on activated sludge process, while few related studies were conducted with AGS. Cetin et al. (2018) demonstrated that high influent suspended solids (SS) content after coarse screening resulted in smaller and more stable mature granules in AGS reactors treating domestic wastewater. However, in this experiment, the specific categorization of SS was absent. Schwarzenbeck et al. (2004) and Wagner et al. (2015) investigated the impact of barley flour and starch on AGS. It was found that the hydrolysis of barley flour and starch particles adsorbed on the surface of AGS resulted in the outward extension of filamentous bacteria, leading to a decrease in granule structural stability. Nevertheless, the content of barley flour and starch in domestic wastewater is relatively low and their hydrolysis rates are relatively fast. Compared to them, lignocellulose, which constitutes 30–50% of SS in domestic wastewater, is evidently more representative (Crutchik et al., 2018). The complex structure of lignocellulose, with varied bonding interactions among cellulose, hemicellulose, and lignin, renders it a challenging substrate for enzymatic degradation (Andlar et al., 2018). Generally, the removal efficiency of lignocellulose by primary clarification is less than 50%. Therefore, a considerable portion of lignocellulose will enter the biological treatment process. Ruiken et al. (2013) and Benneouala et al. (2017) reported that the hydrolysis of lignocellulose in activated sludge took at least 10 d, and the removal of lignocellulose could effectively reduce the energy consumption of wastewater treatment plant. However, the effects of removal or biodegradation of lignocellulose on the oxygen demand, sludge production, nutrient removal and dewaterability are clear knowledge gaps. Exploring the influence of lignocellulose on the formation and properties of AGS is of great significance for the long-term stable operation of AGS system in practical engineering, but the related research has not been reported as far as we know.

In this study, toilet paper was used as the source of lignocellulose. Two AGS-SBR reactors were operated in the absence (R1) and presence (R2) of lignocellulose to investigate its effects on the granules. During the experiment, the sludge morphology, microstructure, mechanical strength, EPS, as well as the removal efficiencies of pollutants, were detected to study the physicochemical variations of the granules. High-throughput sequencing technology was employed to analyze the succession of microbial community, aiming to clarify the influence mechanism of lignocellulose on the formation and properties of AGS.

2. Materials and methods

2.1. Preparation of lignocellulose

The source of lignocellulose in this study was toilet paper produced by Hengan International Group Co., Ltd. Firstly, the toilet paper was subjected to a 3 min crushing process in a grinder. After pulverization, it was mixed with tap water in a conical flask with magnetic stirring at 1,000 rpm for 2 h. This process allowed the toilet paper to disperse evenly in tap water under shear force, effectively simulating the state of lignocellulose in real domestic wastewater.

2.2. Reactors operation

The cultivation of AGS was carried out using two lab-scale SBR reactors, which were composed of reactor column, inlet system, aeration system, drainage system, automatic control system, and supporting pipelines. The effective volume of the reactors was 3 L, with 7 cm internal diameter, and 80 cm effective height (H/d = 11.4). During aeration, the gas flow rate was kept at 3 L/min using glass flowmeters, corresponding to a superficial gas velocity of 1.3 cm/s. The drainage solenoid valves were installed at the midpoint of the effective height of the reactors, allowing for a volume exchange ratio of 50%. The operating cycle was kept at 3 h, and consisted of the following stages: feeding (60 min), aeration (100–111 min), settling (15–4 min), and drainage (5 min). Dissolved oxygen (DO), temperature, and pH were not controlled during operation.

2.3. Seeding sludge and synthetic wastewater

The seeding sludge used in this experiment was obtained from the secondary sedimentation tank of the integrated fixed-film activated sludge (IFAS) process at Tuandao Wastewater Treatment Plant in Qingdao, China. The sludge diameter was measured to be 76.9 μm, and the initial sludge concentrations in the reactors after inoculation were 3.5 g/L. To avoid external interference caused by fluctuations in actual wastewater quality, this experiment utilized synthetic wastewater as the feeding. Glucose and NaAc were applied as the mainly carbon sources with a ratio of 1:2. Ammonium chloride (NH_4Cl) was applied as the sole nitrogen source. Phosphorus sources were provided by dipotassium phosphate (K_2HPO_4) and monopotassium phosphate (KH_2PO_4). The final concentrations of soluble COD (sCOD), NH_4^+-N, and PO_4^{3-}-P in the synthetic wastewater were 520 mg/L, 55 mg/L, and 9.7 mg/L, respectively.

Other components in the synthetic wastewater included 20 mg/L $FeSO_4{\cdot}7H_2O$, 100 mg/L $CaCl_2$, 15 mg/L $MgSO_4{\cdot}7H_2O$, 35 mg/L K_2HPO_4, 15 mg/L KH_2PO_4, and 1 mL/L trace elements (Vishniac and Santer, 1957). In R2, an additional 80 mg/L pretreated lignocellulose (40% of average SS concentrations, accounting for 112 mg/L of total COD) was added to the influent (Crutchik et al., 2018).

2.4. Analysis methods

The sludge characteristics (ML(V)SS, SVI), and water quality (COD, NH_4^+-N, nitrogen oxides (NO_3^--N, NO_2^--N), and PO_4^{3-}-P) were measured regularly according to standard methods (Eaton et al., 2005). The diameter of AGS at different periods was measured using laser particle size analyzer (Mastersizer-3000) and wet sieving method (Kishida et al., 2012). After homogenization treatment of AGS, the loosely bound EPS (LB-EPS) and tightly bound EPS (TB-EPS) were extracted using the thermal hydrolysis method (Laguna et al., 1999). The content of protein (PN) and polysaccharide (PS) in EPS was determined using the improved BCA protein assay kit from Sangon Biotech (Shanghai) Co., Ltd. and the phenol-sulfuric acid method (Gerhardt et al., 1994), respectively. The macroscopic morphology and microscopic structure of AGS were monitored using a stereomicroscope (Olympus Corporation SZX2-ILLK, Japan) and a scanning electron microscope (SEM, Carl Zeiss Gemini 300, Germany). The structural strength of the granules was qualitatively determined using ultrasonic disruption experiments, as described by Xu et al. (2019).

2.5. High-throughput sequencing

To characterize the microbial community, sludge samples were collected at day 0, 40, 70, and 150. The mixtures were centrifuged at 4,000 g and 4°C for 10 min, and the supernatant was discarded. Genomic DNA was extracted from samples using E.Z.N.ATM Mag-Bind Soil DNA Kit (M5635-02, OMEGA, United States) following the manufacturer's instructions. The extracted DNA was amplified using universal primers targeting the V3-V4 region of the bacterial 16S rDNA gene (forward primer 341F and reverse primer 805R). The polymerase chain reactions (PCR) were conducted for two rounds and the products above 400 bps were purified using Agencourt AMPure XP (Beckman, United States) and quantified using the Qubit 2.0 DNA detection kit (Life, United States). The final products were sequenced on the Illumina Miseq™ platform by Majorbio Company (Shanghai, China). The sequencing data were analyzed using the Majorbio cloud platform.

3. Results and discussion

3.1. Formation of aerobic granules

In order to investigate the influence of lignocellulose on the formation and stability of AGS, the diameter, MLSS, morphology, and mechanical strength of the sludge were measured during operation. Based on the overall trends observed in the two reactors, the entire experimental process could be divided into four stages.

The first stage was from day 1 to day 30. During this stage, the settling time was gradually reduced from 15 to 4 min within 15 d, providing the necessary selection pressure for granulation. It should be pointed out that most lignocellulose was trapped by the sludge layer during the influent stage, and its penetration depth was less than 10 cm. The mixing and contact between lignocellulose and sludge mainly occurred during aeration. As shown in Figure 1, the concentration of MLSS in R2 decreased to 2.93 g/L within 10 d and remained relatively stable thereafter. In contrast, it initially increased to 3.78 g/L and then gradually decreased to 3.32 g/L in R1. This might be attributed to the poor settling ability of lignocellulose, which entrapped and retained flocs during settling, leading to increased screening intensity. It should be noted that small granules appeared in R2 on day 15, which was about 5 d earlier than R1. Figures 2A,B are the stereo microscope images of the sludge on day 20. It can be seen that lignocellulose was wrapped around granules, like filamentous bacteria, resulting in a larger granule size and less free flocs in R2. Most flocs were gathered around lignocellulose, indicating that lignocellulose might promote the formation of AGS by acting as skeletons for sludge aggregating. However, starting from day 20, a rapid increase in the proportion of granular sludge in R1 occurred, and its average diameter reached 311 μm by the 30th day, which was higher than the 217 μm observed in R2. As shown in Supplementary Figure A1, the size distribution in R1 was more concentrated, and the proportion of granular sludge (diameter > 200 μm) reaching 74.2%, while the proportion of granular sludge in R2 was only 43.92%. Figures 2C,D show that granules in R1 at this point had a loose and irregular morphology, while granules in R2 exhibited more compact structure. However, due to the presence of the extended lignocellulose on the AGS surface, a significant amount of flocs were trapped around granules, which might be the main reason for the lower proportion of AGS in R2. SEM images reveal that the granules in R1 (Figure 2I) were formed on the basis of the skeleton structure of filamentous bacteria. However, the granules in R2 (Figure 2J) were primarily supported by lignocellulose, and there was no significant outward expansion of filamentous bacteria. This phenomenon contrasted with the results reported by Wagner et al. (2015) and Schwarzenbeck et al. (2004), which might be attributed to the relatively rapid hydrolysis rate of barley flour and starch by microorganisms, resulting in an increased substrate gradient in AGS, thereby inducing the outward proliferation of filamentous bacteria.

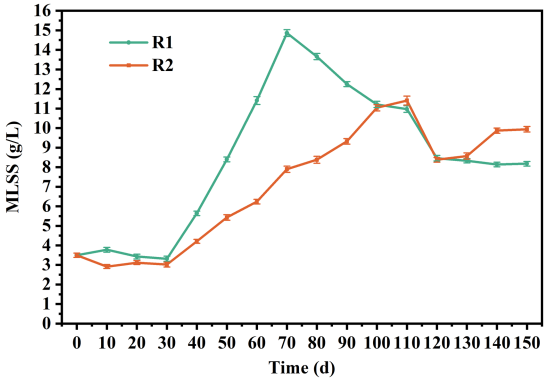

FIGURE 1
MLSS concentration in R1 and R2.

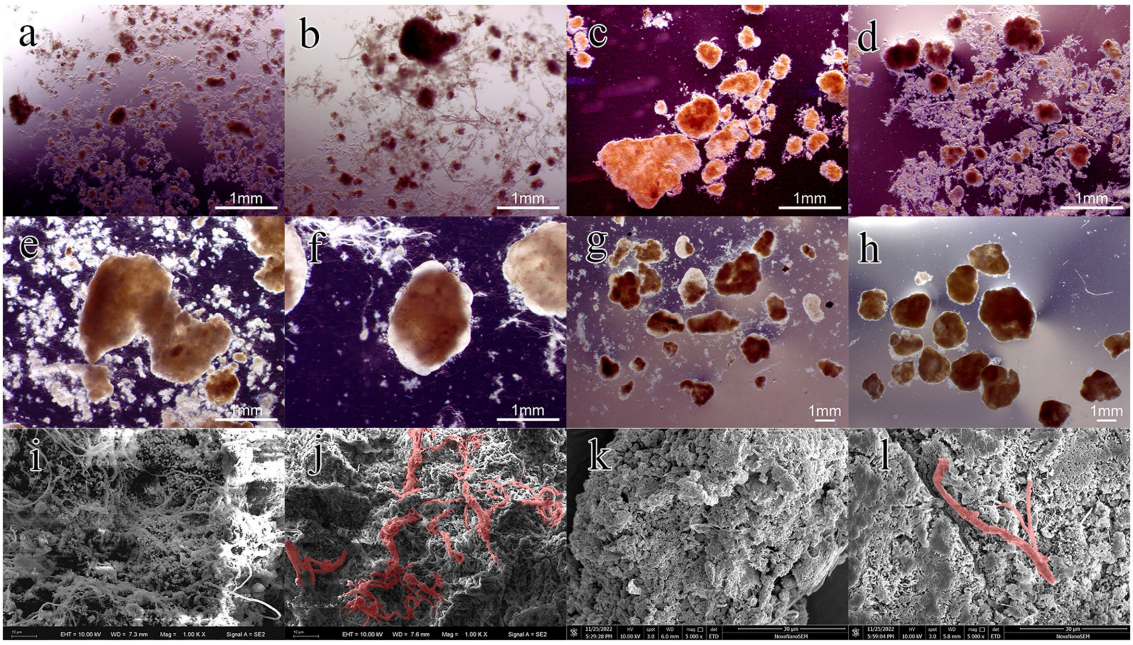

FIGURE 2
Images of granules at different stages of the granulation process: granules at day 20 (**A**, R1; **B**, R2), day 30 (**C**, R1; **D**, R2), day 100 (**E**, R1; **F**, R2) and day 150 (**G**, R1; **H**, R2); SEM of AGS at day 30 (**I**, R1; **J**, R2) and day 150 (**K**, R1; **L**, R2).

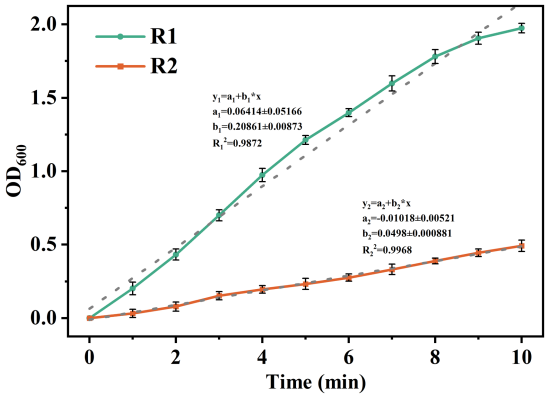

FIGURE 3
Variation of OD_{600} in supernatant of mature granules under 60 W ultrasound.

Nevertheless, the structure of lignocellulose is intricate, and the hydrolysis process requires the cooperation of multiple microorganisms (Berlin et al., 2010). Therefore, the hydrolysis rate was much slow and mainly occurred inside granules, which impeded the outwards proliferation of filamentous bacteria.

Phase II was from day 30–70. During this period, the biomass in both reactors increased rapidly, reaching 14.86 and 7.9 g/L on day 70, respectively. The average growth rate of MLSS in R1 was about 0.29 g/L/d, which was 2.42 times of that in R2. The reason for this result might be that AGS had a low interception efficiency of lignocellulose, which led to the discharge of the sludge with poor sedimentation performance along with lignocellulose, resulting in higher SS levels in the effluent of R2. Starting from day 70 (Phase III), disintegration of granules in R1 occurred. A part of fragmented granules was discharged with the drainage, resulting in a rapid decrease in MLSS of R1, reaching 11.21 g/L on day 110. As shown in Figure 2E, hollow structure and excessive proliferation of filamentous bacteria were observed in the granules, which might be the main reasons for granule disintegration (Adav et al., 2008). However, this phenomenon did not appear in R2, and the MLSS growth rate was close to that of phase II (Figure 2F), indicating that the presence of lignocellulose could improve the stability of AGS.

From day 110, the sludge discharge strategy was implemented to maintain a sludge retention time (SRT) of 30 d, which stabilized the MLSS concentrations in the two reactors at 8.2 and 9.9 g/L, respectively. The distribution of granule size was measured at day 120 and 150. As shown in Supplementary Figure A2, the average diameter of AGS in R1 decreased from 1.47 to 1.08 mm, indicating an ongoing granule disintegration. However, the size distribution in R1 became more concentrated by day 150, with the AGS percentage increasing from 74.77 to 97.57%, revealing a successful regranulation. As shown in Figures 2G,H, the granules in both reactors were irregular spheres, but the granules in R2 exhibited a higher degree of integrity and roundness. SEM images reveal that the AGS in R1 (Figure 2K) were mainly composed of cocci. In R2 (Figure 2L), the microbial species were more abundant, while bacilli, brevibacterium and cocci can all be found on the surface of granules. It should be noted that the proportion of lignocellulose in R2 was significantly reduced compared to phase I, which is consistent with the low retention efficiency of lignocellulose by granular sludge mentioned above.

To further evaluate the enhancement of lignocellulose on the structural stability of AGS, the mature granules were subjected to ultrasonic fragmentation at 60 W. As shown in Figure 3, the increasing rate of OD_{600} values in the supernatant represents the granule crushing rate. It can be found that the OD_{600} values in both reactors increased

continuously after the beginning of ultrasound treatment. The linear fitting showed that the granule crushing process in R2 was more gentle, and the crushing rate of AGS-R2 was only 23.8% of that of AGS-R1, indicating that the lignocellulose skeleton could effectively enhance the stability of AGS by providing a more uniform inter-granule compactness.

3.2. Pollutants removal performance

The pollutants removal performance in both reactors was analyzed throughout the experiment. As shown in Figure 4, the variations of pollutants removal efficiencies in both reactors were similar generally. As shown in Figure 4A, after a short adaptation period, the sCOD removal rate in R1 increased to above 97%, which was approximately 3% higher than R2. From day 19, there was a significant decrease in sCOD removal efficiency in both reactors, reaching 88.96 and 87.44% by day 23. This might be attributed to the loss of sludge and increased sieving strength caused by the presence of lignocellulose. Subsequently, as the granules grew, the sCOD removal efficiency in R2 gradually increased to over 95% and remained stable thereafter. However, a significant decrease of sCOD removal rate was observed in R1 on day 81, which might be due to the sludge loss caused by granule disintegration. As the broken sludge gradually adapted to the operating environment, its sCOD removal efficiency recovered within 6 d.

In terms of nitrogen removal, the differences also appeared in the first stage. As shown in Figures 4B,C, both reactors achieved over 98% NH_4^+-N removal efficiency within 15 d, but NO_2^--N was significantly accumulated in R2, which reached 5.74 mg/L on day 29. In contrast, the effluent NO_3^--N concentration was much higher in R1, indicating a higher nitrite oxidation rate. The different loss rate of nitrite oxidation bacteria (NOB) during sludge selecting might be the main reason for this phenomenon (Winkler et al., 2012). As the granules matured, the TN removal efficiencies in R1 and R2 were basically maintained at approximately 50% until the end of operation.

In the enhanced phosphorus removal system, the removal of phosphorus is primarily achieved by the excessive uptake by polyphosphate-accumulating organisms (PAOs), and SRT is one of the main influencing factors for phosphorus removal efficiency (Campo et al., 2020). Therefore, the significantly different sludge quantity and effluent SS concentrations between the two reactors

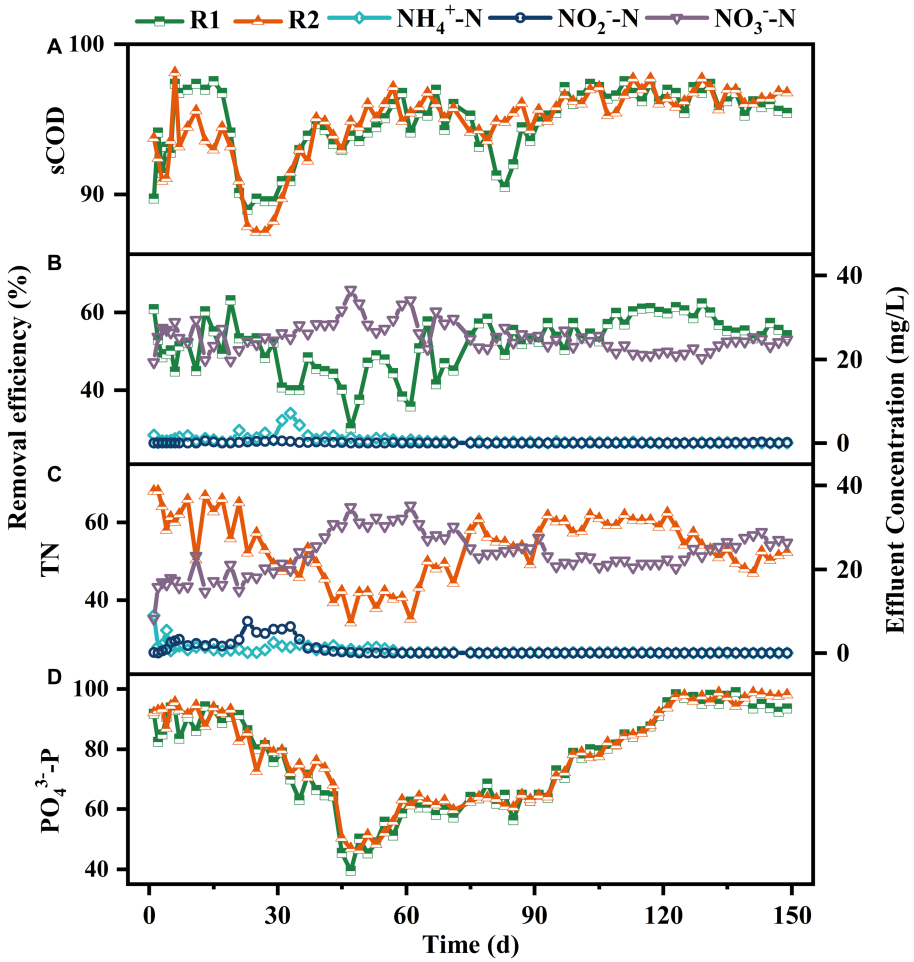

FIGURE 4
Removal performance on sCOD **(A)**, TN-R1 **(B)**, TN-R2 **(C)**, PO_4^{3-}-P **(D)** and effluent concentrations of NH_4^+-N, NO_2^--N and NO_3^--N in R1 **(B)** and R2 **(C)**.

were supposed to cause different PO_4^{3-}-P removal performance. Surprisingly, the two reactors displayed similar PO_4^{3-}-P removal performance throughout the experiment. As shown in Figure 4D, the PO_4^{3-}-P removal efficiency in both reactors remained above 80% during the first 23 d. After that, a rapid decrease occurred and the removal efficiency reduced to 39.48 and 46.8% within 20 d. Although there was a slight increase in the following 48 d, the PO_4^{3-}-P removal efficiency remained below 65%, even during the granule disintegration phase in R1. Temperature fluctuations might be the primary factor contributing to this result. As described by Ab Halim et al. (2016), high temperature could inhibit the uptake of carbon sources by PAOs, resulting in a disadvantage position of PAOs in the competition with glycogen-accumulating organisms (GAOs). Since the operating temperature was not controlled during the experiment, the temperature inside the reactors increased to above 25°C from day 27, and the highest temperature could reach 35°C (data not shown). As the environmental temperature decreased from day 95, the removal efficiency of PO_4^{3-}-P increased to around 80% gradually. Subsequently, with the implementation of the sludge discharge strategy, the PO_4^{3-}-P removal efficiency increased to over 92 and 97% within 10 d, respectively, and remained stable thereafter.

The pollutants conversion processes in typical cycle were detected on day 150 to further identify the effect of lignocellulose on AGS. As shown in Supplementary Figure A3, significant differences appeared in terms of N and PO_4^{3-}-P removal. After feeding, the NO_3^--N concentration in R1 decreased by 23.54% except for influent dilution, which was 13.81% higher than that in R2, implying a higher traditional denitrification efficiency. During the aeration phase, the concentration of NH_4^+-N in R2 decreased to below 5 mg/L within 60 min, corresponding to an ammonia oxidation rate of 1.87 mgNH_4^+-N/gMLSS/h, which was 1.56 times higher than that of R1. It is worth noting that during the first 20 min of aeration, the increase rate of NO_3^--N in R2 was much lower than that in R1, indicating that R2 had a higher simultaneous nitrification–denitrification efficiency. In terms of phosphorus removal, it can be observed that the phosphorus release and accumulation rates in R2 were 2.28 and 3.20 mgP/gMLSS, respectively, which were 2.57 and 3.14 times higher than that in R1, revealing that the presence of lignocellulose could effectively enhance the activity of PAOs.

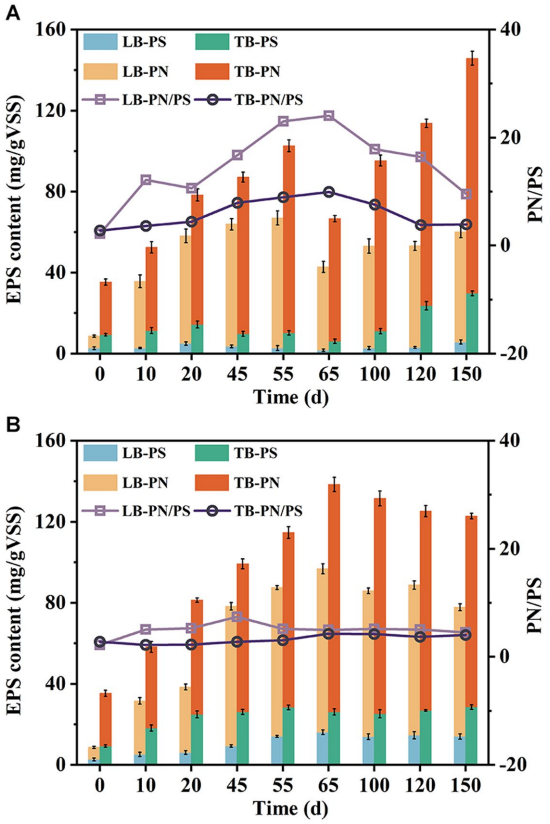

FIGURE 5
Variation of PN and PS content of LB-EPS and TB-EPS during the operation in R1 **(A)** and R2 **(B)**.

3.3. Characteristics of EPS

EPS are crucial components of AGS, playing a significant role in microbial aggregation, granule formation, and structural stability maintenance (McSwain et al., 2005). As shown in Figures 5A,B, the EPS content exhibited an upward trend in both systems during the early stages of operation. R1 showed a faster increase rate in TB-PN, while R2 exhibited a faster increase rate in TB-PS. By the 55th day, the TB-PS content in R2 had reached 28.38 mg/gVSS, which was 7.15 times higher than that in R1. There might be three hypotheses for this phenomenon. Firstly, the toilet paper used here contained a certain amount of cellulose, which might be extracted and detected as PS (Ruiken et al., 2013). Secondly, the lignocellulose present in the system could be hydrolyzed by microorganisms, releasing cellulose and hemicellulose from its structure (Chen et al., 2017). Lastly, the presence of lignocellulose stimulated microorganisms to secrete more PS. Additional research is required to further confirm the specific causes for this phenomenon. It should be noticed that the TB-PS in R1 showed an initial upward trend followed by a decline during the first two stages. At the end of phase II (day 65), a significant decrease in EPS content occurred, particularly in TB-PN and TB-PS, which reduced by 34.41 and 40.6%, respectively. By comparison, EPS in R2 continued to increase during this stage and reached a stable level after day 65. Studies have shown that PN and PS played different roles in the structure of AGS (McSwain et al., 2005). PS, especially β-PS, served as the skeleton for maintaining the structural stability of AGS, while PN acted as the fillings (Adav et al., 2010). In this study, the increase of PN content in R1 was consistent with the formation and amplification process of granular sludge, while the decrease of TB-PS content had indicated a decline in its supporting capacity. Simultaneously, the outward extension of filamentous bacteria resulted in increased granule irregularity, ultimately leading to the disintegration of AGS under the action of hydraulic shear force. In the later stages of the experiment, the PN and PS content in R1 gradually recovered, with a comparable TB-PS and 1.23 times higher TB-PN content than that of R2, which was consistent with its regranulation process.

The increase of PN/PS ratio has always been regarded as an important indicator of sludge granulation (Franca et al., 2018). In this study, the LB-PN/PS and TB-PN/PS ratios in R1 and R2 exhibited an increasing trend during granulation, but decreasing in mature

granules. Furthermore, despite the lower PN/PS values in AGS-R2, it exhibited significantly better performance in granule formation and higher structural stability, indicating that the content of EPS, especially TB-PS, played a more crucial role in AGS than PN/PS ratio.

3.4. Characteristics of microbial community

High-throughput sequencing technology was employed to investigate the differences in microbial community structure between R1 and R2. Sludge samples were collected at different stages, including Day 0 (SEED), Day 40 (R1-1 & R2-1), Day 70 (R1-2 & R2-2), and Day 150 (R1-3 & R2-3). As shown in Supplementary Table A1, the highest community richness and diversity were observed in SEED. As the reactors operated, the richness in R1 and R2 decreased continuously, which was approximately half of that in SEED at the end of the experiment, indicating a significant microbial selection effect during granulation. Besides, the values of Shannon, Ace and Chao index in R2-3 were higher compared to R1-3, indicating that the addition of lignocellulose could improve the microbial community richness and diversity in mature AGS.

Figure 6A shows the relative abundance of main phyla in different samples. It can be seen that the predominant phyla (relative abundance >5%) were Proteobacteria, Actinobacteriota, Bacteroidota, Chloroflexi, Patescibacteria, and Fibrobacterota. Both abundances of Proteobacteria and Bacteroidota increased initially and then decreased during granulation. Interestingly, Actinobacteriota showed an opposite trend, and its relative abundance in R1-3 was 59.5%, which was in an absolute dominant position. Chloroflexi is usually filamentary and mostly exists in EPS with PS as the substrate for metabolism (Kragelund et al., 2007). In this study, the relative abundance of Chloroflexi in R2 remained relatively stable around 6.5%, while it was negatively related to the TB-PS content in R1, suggesting that the excessive growth of Chloroflexi could be one reason for the instability of AGS-R1. It is worth mentioning that the relative abundance of Fibrobacterota in R2 increased from 0.03 to 7.6% during the first 40 d, but gradually decreased as the granules matured, while it was lower than the detection limit in R1. The study has shown that Fibrobacterota has the function of hydrolyzing cellulose (Xu et al., 2021). The enrichment of this phylum confirmed that the cellulose components in toilet paper could be intercepted and hydrolyzed by floc sludge. With the sludge granulation, the retention efficiency of AGS to lignocellulose reduced, therefore Fibrobacterota gradually lost its dominance position.

To further investigate the impact of lignocellulose on the microbial community succession, heat map at genus level is analyzed. As shown in Figure 6B, the dominant genera in SEED were *norank_f__Caldilineaceae*, *Nitrospira*, *Candidatus_Competibacter*, *norank_f__Caldilineaceae*, *norank_f__Saprospiraceae*, and *norank_f__A4b*. By the 40th day, the dominant bacterial genera in R1 turned to be *Thauera* (15.15%), *Thiothrix* (13%), *Tessaracoccus* (11.66%), *Zoogloea* (10.11%), and *Candidatus_Competibacter* (5.81%). However, in R2, the dominant genera were *Candidatus_Competibacter* (16.44%), *Zoogloea* (9.56%), and *norank_f__Fibrobacteraceae* (7.61%). *Thauera* is a traditional denitrifying bacteria, which can perform short-cut denitrification by reducing NO_3^--N to NO_2^--N under limited carbon source condition (Tao et al., 2023). The enrichment of *Thauera* in R1 might be related to

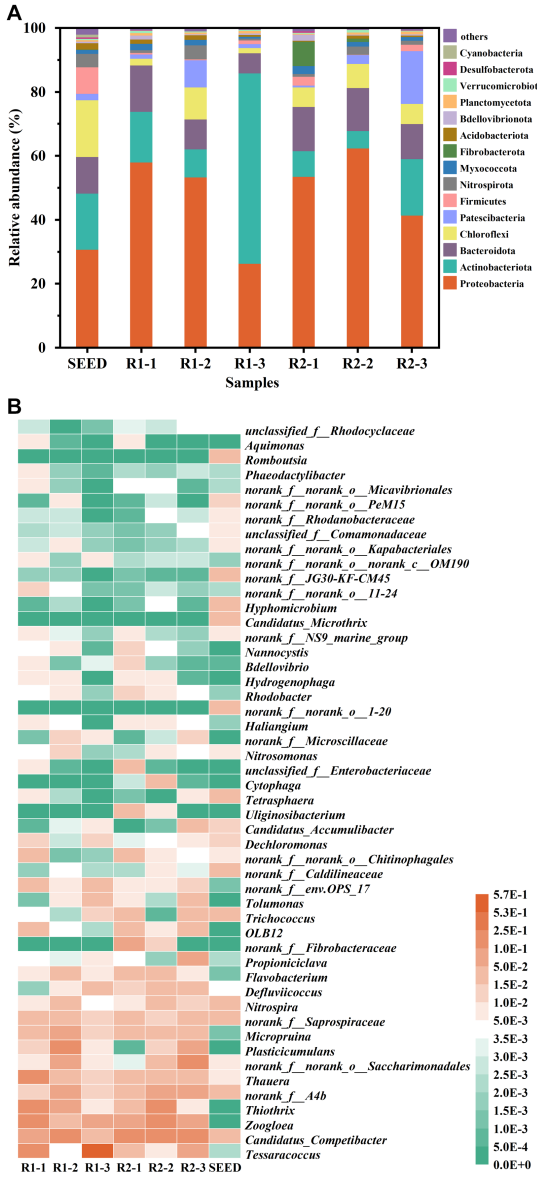

FIGURE 6
Relative abundance of the main phylum **(A)** and heat-map of the identified genus **(B)** of the seed sludge and AGS samples in R1and R2 at day 40, 70, and 150.

the higher concentration of NO_3^--N. Due to the sludge loss, the NO_2^--N oxidation rate in R2 was insufficient, which could not provide sufficient NO_3^--N for *Thauera*, resulting in its relatively low abundance (3.76%). *Thiothrix* is a typical filamentous bacterium (De Graaff et al., 2020), and *Zoogloea* has the ability to secrete a large amount of EPS (Xu et al., 2019). The enrichment of these two genera provided the basis for the rapid growth of AGS in R1, but the sludge expansion caused by the excessive proliferation of *Thiothrix* posed a risk to granule integrity. In R2, the relative abundance of *Zoogloea* was slightly lower than that of R1, which was inconsistent with its higher EPS content. This could be explained by the higher relative abundance of *Candidatus_Competibacter* in R2, which has been reported to be able to promote the secretion of PS-EPS, thus playing an important role in maintaining the stability of AGS (Song et al., 2022).

The microbial community structure of AGS at day 70 was drastically different from that of day 40. In R1, the relative abundances of *Thiothrix*, *Tessaracoccus*, and *Zoogloea* decreased to 6.26, 0.44, and 3.68%, while the relative abundances of *Candidatus_Competibacter*, *Plasticicumulans*, *norank_f__A4b*, *norank_f__norank_o__Saccharimonadales*, and *Micropruina* increased to 18.79, 10.87, 9.02, 7.61, and 6.52%, respectively. The decrease in relative abundance of *Zoogloea*, along with the increased relative abundances of *Plasticicumulans*, *norank_f__A4b*, and *norank_f__norank_o__Saccharimonadales*, which were known for their ability to hydrolyze EPS (Zhang et al., 2022; Jiang et al., 2023; Wang et al., 2023), collectively contributed to the reduction in EPS content during this stage. Interestingly, the relative abundance of *Thiothrix* increased to 19.25% in R2-2, however, no excessive filamentous bacteria were observed on the surface of granules in SEM images. This could be due to the fact that the hydrolysis of lignocellulose mainly occurred inside the granules, so filamentous bacteria tended to grow inward rather than outward expansion. The relative abundance of *Candidatus_Competibacter* and *Micropruina* in R2 showed a similar trend as R1, which increased to 17.57 and 3.67%, respectively. As the same with *Candidatus_Competibacter*, *Micropruina* also belongs to GAO (Shintani et al., 2000). As mentioned above, high temperature could inhibit the activity of PAOs, thereby providing GAOs a competitive advantage (Ab Halim et al., 2016), which was consistent with the low removal efficiency of PO_4^{3-}-P observed in both reactors at this stage.

It is noteworthy that *Tessaracoccus* was greatly enriched in R1-3, with a relative abundance of 57.15%. For a long time, *Tessaracoccus* has been regarded as a fermentative GAO (fGAO), but according to the study of Elahinik et al. (2022), it has been found that although *Tessaracoccus* lacks PHA synthase (phaC), it possesses some enzymes involved in poly-P metabolism, and the presence of polyphosphate kinase (ppk) suggests that *Tessaracoccus* might be capable of accumulating poly-P, but unable to utilize it for energy generation due to the absence of AMP phosphotransferase (pap). Taking into account the relatively low abundance of other PAOs (*Flavobacterium*, *Candidatus_Accumulibacter*) in R1, which were below 1%, and its lower activity in anaerobic phosphorus release and aerobic phosphorus accumulation, it can be inferred that *Tessaracoccus* is indeed involved in the phosphorus removal process, with a lower phosphorus accumulation rate compared to traditional PAOs. In R2, the combined relative abundance of *Flavobacterium* and *Candidatus_Accumulibacter* was 3.36%, which was 2.55 times higher than that in R1, resulting in a higher phosphorus conversion rate. Besides, the relative abundance of *Nitrosomonas* (AOB) and *Nitrospira* (NOB) in R2 was also 2.78 and 2.54 times higher, explaining its high ammonia oxidation and nitrite oxidation rates. It should be pointed out that the relative abundance of *norank_f__norank_o__Saccharimonadales* and *Plasticicumulans* in R2-3 increased to 15.22 and 6.13%, respectively, consistent with the decrease in EPS-PN content. Simultaneously, the relative abundance of *Thiothrix* decreased to <1%. Even so, the granules in R2 still maintained high mechanical strength, further confirming that lignocellulose could increase the structure stability of AGS.

4. Conclusion

This study investigated the influence of lignocellulose on the formation process and physicochemical characteristics of AGS. The results demonstrated that lignocellulose could increase the content of TB-PS in EPS. Additionally, it could act as skeletons during flocs aggregating, thus facilitating the formation of AGS with higher structural stability. Furthermore, lignocellulose could also regulate the microbial community structure of AGS, promote the enrichment of functional microorganisms such as DPAOs, AOB, and NOB, thus improving the conversion rates of pollutants. Therefore, proper control of the pretreatment process to ensure that more lignocellulose could enter the bioreactor will be an effective approach to enhance the practical application of AGS technology.

Data availability statement

The original contributions presented in the study are included in the article/Supplementary material, further inquiries can be directed to the corresponding author.

Author contributions

JX: Formal analysis, Funding acquisition, Methodology, Resources, Writing – review & editing, Conceptualization, Investigation. YG: Formal analysis, Investigation, Software, Visualization, Writing – original draft. XB: Formal analysis, Funding acquisition, Project administration, Supervision, Writing – review & editing. LL: Conceptualization, Project administration, Supervision, Writing – review & editing. WX: Investigation, Methodology, Visualization, Writing – review & editing. SL: Data curation, Methodology, Visualization, Writing – review & editing.

Funding

This research was supported financially by National Natural Science Foundation of China (No. 52200061) and Natural Science Foundation of Shandong Province (No. ZR2021QE274).

Conflict of interest

The authors declare that the research was conducted in the absence of any commercial or financial relationships that could be construed as a potential conflict of interest.

Publisher's note

Supplementary material

The Supplementary material for this article can be found online at: https://www.frontiersin.org/articles/10.3389/fmicb.2023.1254152/full#supplementary-material

References

Ab Halim, M. H., Nor Anuar, A., Abdul Jamal, N. S., Azmi, S. I., Ujang, Z., and Bob, M. M. (2016). Influence of high temperature on the performance of aerobic granular sludge in biological treatment of wastewater. *J. Environ. Manag.* 184, 271–280. doi: 10.1016/j.jenvman.2016.09.079

Adav, S. S., Lee, D.-J., Show, K.-Y., and Tay, J.-H. (2008). Aerobic granular sludge: Recent advances. *Biotechnol. Adv.* 26, 411–423. doi: 10.1016/j.biotechadv.2008.05.002

Adav, S. S., Lin, J. C.-T., Yang, Z., Whiteley, C. G., Lee, D.-J., Peng, X.-F., et al. (2010). Stereological assessment of extracellular polymeric substances, exo-enzymes, and specific bacterial strains in bioaggregates using fluorescence experiments. *Biotechnol. Adv.* 28, 255–280. doi: 10.1016/j.biotechadv.2009.08.006

Adler, A., and Holliger, C. (2020). Multistability and reversibility of aerobic granular sludge microbial communities upon changes from simple to complex synthetic wastewater and Back. *Front. Microbiol.* 11:574361. doi: 10.3389/fmicb.2020.574361

Amorim, C. L., Maia, A. S., Mesquita, R. B. R., Rangel, A. O. S. S., Van Loosdrecht, M. C. M., Tiritan, M. E., et al. (2014). Performance of aerobic granular sludge in a sequencing batch bioreactor exposed to ofloxacin, norfloxacin and ciprofloxacin. *Water Res.* 50, 101–113. doi: 10.1016/j.watres.2013.10.043

Andlar, M., Rezić, T., Marđetko, N., Kracher, D., Ludwig, R., and Šantek, B. (2018). Lignocellulose degradation: an overview of fungi and fungal enzymes involved in lignocellulose degradation. *Eng. Life Sci.* 18, 768–778. doi: 10.1002/elsc.201800039

Bao, R., Yu, S., Shi, W., Zhang, X., and Wang, Y. (2009). Aerobic granules formation and nutrients removal characteristics in sequencing batch airlift reactor (SBAR) at low temperature. *J. Hazard. Mater.* 168, 1334–1340. doi: 10.1016/j.jhazmat.2009.03.020

Benneouala, M., Bareha, Y., Mengelle, E., Bounouba, M., Sperandio, M., Bessiere, Y., et al. (2017). Hydrolysis of particulate settleable solids (PSS) in activated sludge is determined by the bacteria initially adsorbed in the sewage. *Water Res.* 125, 400–409. doi: 10.1016/j.watres.2017.08.058

Berlin, A., Maximenko, V., Gilkes, N., and Saddler, J. (2010). Optimization of enzyme complexes for lignocellulose hydrolysis. *Biotechnol. Bioeng.* 97, 287–296. doi: 10.1002/bit.21238

Campo, R., and Di Bella, G. (2019). Petrochemical slop wastewater treatment by means of aerobic granular sludge: effect of granulation process on bio-adsorption and hydrocarbons removal. *Chem. Eng. J.* 378:122083. doi: 10.1016/j.cej.2019.122083

Campo, R., Sguanci, S., Caffaz, S., Mazzoli, L., Ramazzotti, M., Lubello, C., et al. (2020). Efficient carbon, nitrogen and phosphorus removal from low C/N real domestic wastewater with aerobic granular sludge. *Bioresour. Technol.* 305:122961. doi: 10.1016/j.biortech.2020.122961

Cetin, E., Karakas, E., Dulekgurgen, E., Ovez, S., Kolukirik, M., and Yilmaz, G. (2018). Effects of high-concentration influent suspended solids on aerobic granulation in pilot-scale sequencing batch reactors treating real domestic wastewater. *Water Res.* 131, 74–89. doi: 10.1016/j.watres.2017.12.014

Chen, R., Nie, Y., Kato, H., Wu, J., Utashiro, T., Lu, J., et al. (2017). Methanogenic degradation of toilet-paper cellulose upon sewage treatment in an anaerobic membrane bioreactor at room temperature. *Bioresour. Technol.* 228, 69–76. doi: 10.1016/j.biortech.2016.12.089

Crutchik, D., Frison, N., Eusebi, A. L., and Fatone, F. (2018). Biorefinery of cellulosic primary sludge towards targeted short chain fatty acids, phosphorus and methane recovery. *Water Res.* 136, 112–119. doi: 10.1016/j.watres.2018.02.047

De Graaff, D. R., Van Loosdrecht, M. C. M., and Pronk, M. (2020). Stable granulation of seawater-adapted aerobic granular sludge with filamentous Thiothrix bacteria. *Water Res.* 175:115683. doi: 10.1016/j.watres.2020.115683

De Sousa Rollemberg, S. L., Mendes Barros, A. R., Milen Firmino, P. I., and Bezerra Dos Santos, A. (2018). Aerobic granular sludge: cultivation parameters and removal mechanisms. *Bioresour. Technol.* 270, 678–688. doi: 10.1016/j.biortech.2018.08.130

Eaton, A.Health Association, A.A., Clesceri, L.Federation, W.E., Association, Aph, Greenberg, A., Association, Aww (2005). Standard Methods for the Examination for Water and Wastewater. Washington, DC, New York: American Public Health Association.

Elahinik, A., Haarsma, M., Abbas, B., Pabst, M., Xevgenos, D., van Loosdrecht, M. C. M., et al. (2022). Glycerol conversion by aerobic granular sludge. *Water Res.* 227:119340. doi: 10.1016/j.watres.2022.119340

Franca, R. D. G., Pinheiro, H. M., Van Loosdrecht, M. C. M., and Lourenço, N. D. (2018). Stability of aerobic granules during long-term bioreactor operation. *Biotechnol. Adv.* 36, 228–246. doi: 10.1016/j.biotechadv.2017.11.005

Gerhardt, P., Wood, W. A., Krieg, N. R., and Murray, R. (1994). Methods for general and molecular bacteriology. Washington, DC, USA: American Society for Microbiology.

Han, X. (2022). Rapid formation of aerobic granular sludge by bioaugmentation technology: a review. *Chem. Eng. J.* 437:134971. doi: 10.1016/j.cej.2022.134971

Jiang, M., Ji, S., Wu, R., Yang, H., Li, Y.-Y., and Liu, J. (2023). Exploiting refractory organic matter for advanced nitrogen removal from mature landfill leachate via anammox in an expanded granular sludge bed reactor. *Bioresour. Technol.* 371:128594. doi: 10.1016/j.biortech.2023.128594

Kishida, N., Totsuka, R., and Tsuneda, S. (2012). Challenge for formation of aerobic granular sludge in a continuous-flow reactor. *J. Water Environ. Technol.* 10, 79–86. doi: 10.2965/jwet.2012.79

Kragelund, C., Levantesi, C., Borger, A., Thelen, K., Eikelboom, D., Tandoi, V., et al. (2007). Identity, abundance and ecophysiology of filamentous Chloroflexi species present in activated sludge treatment plants: ecophysiology of filamentous Chloroflexi species. *FEMS Microbiol. Ecol.* 59, 671–682. doi: 10.1111/j.1574-6941.2006.00251.x

Laguna, A., Ouattara, A., Gonzalez, R. O., Baron, O., Famá, G., Mamouni, R. E., et al. (1999). A simple and low cost technique for determining the granulometry of upflow anaerobic sludge blanket reactor sludge. *Water Sci. Technol.* 40, 1–8. doi: 10.2166/wst.1999.0371

Lashkarizadeh, M., Yuan, Q., and Oleszkiewicz, J. A. (2015). Influence of carbon source on nutrient removal performance and physical–chemical characteristics of aerobic granular sludge. *Environ. Technol.* 36, 2161–2167. doi: 10.1080/09593330.2015.1023364

Lemaire, R., Webb, R. I., and Yuan, Z. (2008). Micro-scale observations of the structure of aerobic microbial granules used for the treatment of nutrient-rich industrial wastewater. *ISME J.* 2, 528–541. doi: 10.1038/ismej.2008.12

Levine, A. D., Tchobanoglous, G., and Asano, T. (1991). Size distributions of particulate contaminants in wastewater and their impact on treatability. *Water Res.* 25, 911–922. doi: 10.1016/0043-1354(91)90138-G

Lourenço, N. D., Franca, R. D. G., Moreira, M. A., Gil, F. N., Viegas, C. A., and Pinheiro, H. M. (2015). Comparing aerobic granular sludge and flocculent sequencing batch reactor technologies for textile wastewater treatment. *Biochem. Eng. J.* 104, 57–63. doi: 10.1016/j.bej.2015.04.025

McSwain, B. S., Irvine, R. L., Hausner, M., and Wilderer, P. A. (2005). Composition and distribution of extracellular polymeric substances in aerobic flocs and granular sludge. *Appl. Environ. Microbiol.* 71, 1051–1057. doi: 10.1128/AEM.71.2.1051-1057.2005

Morgenroth, E., Kommedal, R., and Harremoës, P. (2002). Processes and modeling of hydrolysis of particulate organic matter in aerobic wastewater treatment – a review. *Water Sci. Technol.* 45, 25–40. doi: 10.2166/wst.2002.0091

Moy, Y. P., Tay, J. H., Toh, S. K., Liu, Y., and Tay, T. L. (2002). High organic loading influences the physical characteristics of aerobic sludge granules. *Lett. Appl. Microbiol.* 34, 407–412. doi: 10.1046/j.1472-765x.2002.01108.x

Nancharaiah, Y. V., and Kiran, K. R. G. (2018). Aerobic granular sludge technology: mechanisms of granulation and biotechnological applications. *Bioresour. Technol.* 247, 1128–1143. doi: 10.1016/j.biortech.2017.09.131

Rickert, D. A., and Hunter, J. V. (1967). Rapid fractionation and materials balance of solids fractions in wastewater and wastewater effluent. *J. Water Pollut. Control Fed.* 39, 1475–1486.

Ruiken, C. J., Breuer, G., Klaversma, E., Santiago, T., and van Loosdrecht, M. C. M. (2013). Sieving wastewater – cellulose recovery, economic and energy evaluation. *Water Res.* 47, 43–48. doi: 10.1016/j.watres.2012.08.023

Schwarzenbeck, N., Erley, R., and Wilderer, P. A. (2004). Aerobic granular sludge in an SBR-system treating wastewater rich in particulate matter. *Water Sci. Technol.* 49, 41–46. doi: 10.2166/wst.2004.0799

Shintani, T., Liu, W. T., Hanada, S., Kamagata, Y., Miyaoka, S., Suzuki, T., et al. (2000). Micropruina glycogenica gen. Nov., sp. nov., a new gram-positive glycogen-accumulating bacterium isolated from activated sludge. *Int. J. Syst. Evol. Microbiol.* 50, 201–207. doi: 10.1099/00207713-50-1-201

Song, X., Yu, D., Qiu, Y., Qiu, C., Xu, L., Zhao, J., et al. (2022). Unexpected phosphorous removal in a Candidatus_Competibacter and Defluviicoccus dominated reactor. *Bioresour. Technol.* 345:126540. doi: 10.1016/j.biortech.2021.126540

Szabó, E. (2017). Microbial population dynamics and ecosystem functions of anoxic/aerobic granular sludge in sequencing batch reactors operated at different organic loading rates. *Front. Microbiol.* 8:770. doi: 10.3389/fmicb.2017.00770

Tao, Y., Li, L., Ning, J., and Xu, W. (2023). Culturing partial-denitrification (PD) granules in continuous flow reactor with waste sludge as inoculum: performance, granular sludge characteristics and microbial community. *Environ. Technol.* 1–39, 1–14. doi: 10.1080/09593330.2023.2228993

Vashi, H., Iorhemen, O. T., and Tay, J. H. (2019). Extensive studies on the treatment of pulp mill wastewater using aerobic granular sludge (AGS) technology. *Chem. Eng. J.* 359, 1175–1194. doi: 10.1016/j.cej.2018.11.060

Vishniac, W., and Santer, M. (1957). The thiobacilli. *Bacteriol. Rev.* 21, 195–213. doi: 10.1128/br.21.3.195-213.1957

Wagner, J., Weissbrodt, D. G., Manguin, V., Ribeiro Da Costa, R. H., Morgenroth, E., and Derlon, N. (2015). Effect of particulate organic substrate on aerobic granulation and operating conditions of sequencing batch reactors. *Water Res.* 85, 158–166. doi: 10.1016/j.watres.2015.08.030

Wang, K., Ye, Q., Shen, Y., Wang, Y., Hong, Q., Zhang, C., et al. (2023). Biochar addition in membrane bioreactor enables membrane fouling alleviation and nitrogen removal improvement for low C/N municipal wastewater treatment. *Membranes* 13:194. doi: 10.3390/membranes13020194

Winkler, M. K. H., Bassin, J. P., Kleerebezem, R., Sorokin, D. Y., and Loosdrecht, M. C. M. V. (2012). Unravelling the reasons for disproportion in the ratio of AOB and NOB in aerobic granular sludge. *Appl. Microbiol. Biotechnol.* 94, 1657–1666. doi: 10.1007/s00253-012-4126-9

Xu, C., Liu, W., Sun, B., Zhang, S., Zhang, S., Yang, Y., et al. (2021). Multi-omics analysis reveals a dependent relationship between rumen Bacteria and diet of grass-and grain-fed yaks. *Front. Microbiol.* 12:642959. doi: 10.3389/fmicb.2021.642959

Xu, J., Pang, H., He, J., Wang, M., Nan, J., and Li, L. (2019). Enhanced aerobic sludge granulation by applying carbon fibers as nucleating skeletons. *Chem. Eng. J.* 373, 946–954. doi: 10.1016/j.cej.2019.05.126

Zhang, M., Tan, Y., Fan, Y., Gao, J., Liu, Y., Lv, X., et al. (2022). Nitrite accumulation, denitrification kinetic and microbial evolution in the partial denitrification process: the combined effects of carbon source and nitrate concentration. *Bioresour. Technol.* 361:127604. doi: 10.1016/j.biortech.2022.127604

frontiers | Frontiers in Microbiology

TYPE Review
PUBLISHED 04 October 2023
DOI 10.3389/fmicb.2023.1284369

OPEN ACCESS

EDITED BY
Huike Dong,
Institute of Tibetan Plateau Research (CAS), China

REVIEWED BY
Jingran Zhang,
Chinese Academy of Sciences (CAS), China
Liying Gong,
Southeast University, China

*CORRESPONDENCE
Xiuguo Lu
✉ 3326@ecjtu.edu.cn

RECEIVED 28 August 2023
ACCEPTED 20 September 2023
PUBLISHED 04 October 2023

CITATION
Huang S, Fu YL, Zhang HM, Wang CQ, Zou CL and Lu XG (2023) Research progress of novel bio-denitrification technology in deep wastewater treatment.
Front. Microbiol. 14:1284369.
doi: 10.3389/fmicb.2023.1284369

Research progress of novel bio-denitrification technology in deep wastewater treatment

Shan Huang, Yuling Fu, Huimin Zhang, Chuqiao Wang, Chenglong Zou and Xiuguo Lu*

School of Civil Engineering and Architecture, East China Jiao Tong University, Nanchang, China

Excessive nitrogen emissions are a major contributor to water pollution, posing a threat not only to the environment but also to human health. Therefore, achieving deep denitrification of wastewater is of significant importance. Traditional biological denitrification methods have some drawbacks, including long processing times, substantial land requirements, high energy consumption, and high investment and operational costs. In contrast, the novel bio-denitrification technology reduces the traditional processing time and lowers operational and maintenance costs while improving denitrification efficiency. This technology falls within the category of environmentally friendly, low-energy deep denitrification methods. This paper introduces several innovative bio-denitrification technologies and their combinations, conducts a comparative analysis of their denitrification efficiency across various wastewater types, and concludes by outlining the future prospects for the development of these novel bio-denitrification technologies.

KEYWORDS

novel bio-denitrification technology, deep wastewater denitrification, coupling process, denitrification performance, low-carbon

1. Introduction

With the ongoing advancements in industrialization and urbanization, excessive nitrogen emissions from industrial, domestic, and agricultural wastewater have resulted in environmental issues like eutrophication, unpleasant odors, and deterioration of water quality in surface bodies (Qu et al., 2019; Ceulemans et al., 2023; Xia and Yan, 2023). The primary denitrification methods encompass physicochemical and biological approaches. The physicochemical method mainly involves ion exchange, adsorption, chemical precipitation, and redox reactions, often requiring the addition of adsorbents, catalysts, and ion exchangers to achieve nitrogen removal. However, adsorption is sensitive to water quality variations, and adsorbents have a limited lifespan. Ion exchangers can lead to secondary pollution, while the use of catalysts increases treatment expenses (Soldatov et al., 2007; Tarpeh et al., 2017).

In contrast, the bio-denitrification process has gained popularity due to its cost-effectiveness, minimal by-product generation, dependable operation, and environmental compatibility (Zhang et al., 2016). Traditional bio-denitrification technology effectively treats nitrogen-containing wastewater through bio-nitrification (Eq. 1) and bio-denitrification (Eq. 2) processes. However, it necessitates aeration and the addition of organic carbon sources, which not only increase costs but can also contribute to secondary pollution, contradicting the low-carbon paradigm (Sanjrani et al., 2022). Consequently, the research and application of innovative bio-denitrification technologies hold significant importance for environmental preservation, ecological equilibrium, wastewater reclamation, energy conservation, and addressing emerging environmental challenges. This paper will introduce several novel bio-denitrification

technologies and their integration processes, assess their denitrification performance, and summarize their research advancements in the field of wastewater denitrification.

$$NH_4^+ + 2O_2 \rightarrow 2H^+ + H_2O + NO_3^- \quad (1)$$

$$2NO_3^- + 10H(\text{electron donor}) \rightarrow 2OH^- + 4H_2O + N_2 \quad (2)$$

2. Novel bio-denitrification process

2.1. Novel bio-denitrification technology

2.1.1. Short-cut nitrification denitrification

Voets et al. (1975) made a pivotal discovery regarding the accumulation of nitrite (NO_2^--N) during the nitrification process and introduced the concept of short-cut nitrification denitrification (SCND) technology. The fundamental principle involves the conversion of ammonia nitrogen (NH_4^+-N) into NO_2^--N through controlled reaction parameters (Eq. 1), followed by direct reduction of NO_2^--N to nitrogen (N_2) through denitrification (Eq. 2; Huang, 2021). This innovation results in significant savings, reducing aeration requirements by 25% and organic carbon source needs by 40% when compared to traditional bio-denitrification processes (Kornaros et al., 2010). The key to SCND technology lies in regulating the nitrification process to stop at the nitrite stage.

It has been demonstrated that the control of reaction temperature, pH, dissolved oxygen (DO) concentration, and sludge age can effectively modulate the growth conditions of ammonia-oxidizing bacteria (AOB) and nitrite-oxidizing bacteria (NOB), thereby facilitating NO_2^--N accumulation (Zhu et al., 2008). Currently, SCND technology has found practical applications in NH_4^+-N removal from landfill leachate (Zhang et al., 2020), sludge digestion liquid (Malamis et al., 2014), and biogas slurry (Chang et al., 2022; Chen et al., 2022), yielding significant results. In a study conducted by Chang et al. (2022) investigating the impact of the carbon-nitrogen ratio (C/N) on biogas slurry treatment within an activated sludge SCND system, it was observed that even with a reduced C/N ratio, NH_4^+-N and total nitrogen (TN) removal efficiencies could reach approximately 90%.

$$NH_4^+ + 1.5O_2 \rightarrow 2H^+ + NO_2^- + H_2O \quad (3)$$

$$2NO_2^- + 6H(\text{electron donor}) \rightarrow 2OH^- + 2H_2O + N_2 \quad (4)$$

2.1.2. Anaerobic ammonium oxidation

Anaerobic ammonium oxidation (ANAMMOX) technology involves the direct conversion of NH_4^+-N to N_2 under stringent anaerobic conditions, facilitated by anaerobic ammonia-oxidizing bacteria (AnAOB) utilizing NO_2^--N as the electron acceptor (Eq. 5; Kuenen, 2008). Therefore, ANAMMOX is well-suited for treating wastewater containing both NH_4^+-N and NO_2^--N. Notably, electron acceptor NO_2^--N can also be generated through short-cut nitrification (Eq. 3), making partial short-range nitrification an ideal precursor process for anaerobic ammonia oxidation (Wang J., 2021). The living conditions for AnAOB require strict anaerobic conditions, which contribute to energy savings by reducing aeration requirements. Moreover, the ANAMMOX process operates as an autotrophic process, eliminating the need for additional organic carbon sources, rendering it particularly suitable for denitrification in wastewater with low C/N ratios (Morales et al., 2015; Chini et al., 2019). Additionally, the stable pH levels maintained during ANAMMOX can preserve alkalinity, while AnAOB exhibits extended generation cycles and generates less sludge, substantially reducing the cost associated with excess sludge treatment and disposal (Jia et al., 2014; Ma et al., 2016).

$$NH_4^+ + 1.3NO_2^- + 0.13H^+ + 0.066HCO_3^- \rightarrow$$

$$1.02N_2 + 0.066CH_2O_{0.5}N_{0.15} + 2.03H_2O + 0.26NO_3^- \quad (5)$$

2.1.3. Simultaneous nitrification and denitrification

Simultaneous nitrification and denitrification (SND) technology involves the bio-denitrification process where nitrification and denitrification reactions take place simultaneously in both space and time. SND relies on the generation of an oxygen concentration gradient due to oxygen diffusion limitations, resulting in the formation of hypoxic microenvironments within the core of sludge flocs or within biofilms. These microenvironments support the coexistence of aerobic and hypoxic metabolic activities (Layer et al., 2020). This technology allows nitrification and denitrification reactions to occur in the same spatial domain, significantly reducing the required reactor volume (Third et al., 2005; Masoudi et al., 2018). Additionally, SND imposes minimal demands for aeration and organic carbon, resulting in a reduction of approximately 30% in sludge production compared to traditional bio-denitrification processes (Ma et al., 2017; Zhao et al., 2017). Furthermore, there is no need for sludge reflux, and the alkalinity consumed during the nitrification process can be replenished by the alkalinity generated during denitrification (Ling, 2020). This not only maintains reactor pH stability but also reduces costs and optimizes process operations.

The core of SND technology is the control of DO concentration, which can be categorized into aerobic, low oxygen, and ultra-low DO SND denitrification (Ling, 2020; Xiang, 2020). Temperature, pH, and the C/N ratio are also pivotal factors influencing SND technology (Ling, 2020). It's worth noting that autotrophic bacteria have a considerably slower growth and reproduction rate in comparison to heterotrophic bacteria. In long-term operation, heterotrophic denitrifying bacteria tend to become the dominant microbial community, reducing the significance of autotrophic nitrifying bacteria and subsequently affecting the denitrification effectiveness of SND (Jia et al., 2020).

2.1.4. Heterotrophic nitrification-aerobic denitrification

Robertson et al. (1985) achieved the successful isolation of a denitrifying Paracoccus bacterium, a heterotrophic microorganism with the unique ability to directly convert ammonia nitrogen in wastewater into gaseous nitrogen. These bacteria possess both

heterotrophic aerobic nitrification and heterotrophic aerobic denitrification functions, enabling them to utilize organic matter to convert NH_4^+-N, NO_2^--N, and nitrate nitrogen (NO_3^--N) into either organic nitrogen or gaseous nitrogen. In recent years, it has become evident that such functional microorganisms are widespread in nature, including species like *Paracoccus pantotrophus*, *Acinetobacter* sp., *Phytophthora* sp., *Diaphorobacter* sp., *Alcaligenes faecalis,* among others (Robertson et al., 1985; Xian et al., 2016; Jia et al., 2019). This denitrification method is known as heterotrophic nitrification aerobic denitrification (HN-AD; Robertson and Kuenen, 1990).

The HN-AD process, akin to SND, offers structural integration, reduced footprint, and simplified operational management. Moreover, heterotrophic microorganisms exhibit higher growth rates and denitrification capabilities (Yang Y. et al., 2017; Zhang H. H. et al., 2019; Zhang M. Y. et al., 2019), bestowing HN-AD technology with the advantages of rapid start-up, stable operation, and resilience to oxygen and organic substrates. However, the reaction process requires a higher organic carbon source and aeration rate compared to traditional biological denitrification. Therefore, it is most suitable for denitrification and decarbonization treatment of wastewater with a high C/N ratio, albeit with increase energy consumption and operational costs (Chen et al., 2014; Huang et al., 2021).

2.1.5. Granular sludge

Granular sludge is generally considered to be granular activated sludge that gradually forms a stable structure after condensing into flocs by free bacteria (Sarma et al., 2017). There are five theoretical mechanisms for its formation, including the filamentous bacteria hypothesis, selective pressure-driven hypothesis, extracellular polymer hypothesis, microbial self-aggregation hypothesis, and crystal nucleus hypothesis (Li, 2020). Depending on whether microorganisms require oxygen for growth, they can be divided into anaerobic granular sludge and aerobic granular sludge (AGS), with AGS being the more commonly used. Mature AGS typically exhibits an orange-yellow color, a smooth surface, and a spherical or ellipsoidal shape, with particle sizes ranging from 0.5 to 1.5 mm (Moy et al., 2002). The structure of AGS is dense and regular, with strong settling capabilities. Thanks to microorganisms' inherent self-solidification properties, AGS maintains its structural integrity even under dynamic conditions, forming agglomerated organisms without swelling or negatively affecting water quality (Mota et al., 2014). This characteristic enables AGS to efficiently remove high concentrations of toxic organic substances, nitrogen, and phosphorus (Kishida et al., 2009; He et al., 2020; Chen H. Y. et al., 2023).

In practical applications, the key to this technology lies in the domestication and cultivation of AGS. Factors significantly affecting AGS formation and performance include fluid shear force, COD load, DO, settling time, particle size, temperature, hydraulic retention time, sludge age, and the presence or absence of induced nuclei (Pishgar et al., 2020).

2.1.6. Other bio-denitrification technologies

In addition to the aforementioned technologies, novel bio-denitrification technologies also encompass sulfur autotrophic denitrification (Song et al., 2023), iron autotrophic denitrification (Zhao et al., 2022), hydrogen autotrophic denitrification (Dong et al., 2021), and other methods. While these autotrophic bio-denitrification technologies offer numerous advantages over heterotrophic bio-denitrification processes, such as conserving organic carbon sources, being suitable for treating low C/N ratio wastewater, and reducing sludge production, they do present some practical challenges in their application in wastewater treatment.

The research on sulfur autotrophic denitrification technology traces its origins back to the 1970s. Compared to other autotrophic denitrification methods, the reduced sulfides (S^0, S^{2-}, $Na_2S_2O_3$) used as electron donors are cost-effective and readily available, less sensitive to water quality variations, and easy to utilize. Moreover, due to the inclusion of S oxidation and N reduction in the sulfur autotrophic denitrification process, there is significant potential for waste resource utilization (Kosgey et al., 2022). However, the sulfur autotrophic denitrification reaction generates H^+, lowers the system's pH, and produces a substantial amount of environmentally polluting sulfate that must be controlled. High concentrations of sulfides can also impact microbial activity, hinder autotrophic denitrification efficiency, and especially affect the conversion of nitrate to nitrite (Beristain et al., 2006). Some studies have combined sulfur autotrophic denitrification with microbial fuel cell technology to achieve simultaneous organic matter removal and electricity generation. However, the deposition of elemental sulfur can lead to electrode poisoning or scaling, posing challenges to the further advancement of this technology (Lin et al., 2018; Wang and He, 2020).

Iron autotrophic denitrification technology is an autotrophic bio-denitrification method that employs Fe^0 or Fe^{2+} as electron donors (Zhao et al., 2022). Fe (II) is widely distributed in the environment and is cost-effective, but it presents challenges in maintaining system stability for continuous operation. Fe^0, on the other hand, offers superior electron-donating potential compared to Fe (II), leading to a significant reduction in the redox potential of denitrification sludge and improved system stability (Zhang Y. H. et al., 2014; Yu Y. et al., 2022). Currently, nano zero-valent iron is a key area of research in the field of iron autotrophic denitrification (Mofradnia et al., 2019). Various factors influence iron autotrophic denitrification, including temperature, pH, and the Fe/N ratio (Johnson et al., 2007; Oshiki et al., 2013; Yu Y. et al., 2022). pH regulation is particularly impactful, although it can increase the operational complexity of the iron autotrophic denitrification process. Moreover, the understanding of the denitrification process mechanism in this technology remains somewhat limited, especially regarding the relationship between its biological and chemical aspects (Yu Y. et al., 2022). Additionally, the microbial population and metabolic pathways in the iron autotrophic denitrification process are not yet fully understood, and further exploration is required to comprehend the reaction mechanism between iron ions and other compounds.

Hydrogen autotrophic denitrification involves the use of hydrogen bacteria to denitrify and remove nitrogen using H_2 as an electron donor (Dong et al., 2021). It boasts advantages such as high denitrification efficiency, rapid reaction rates, environmental cleanliness, and the ease of removing residual H_2 from water without requiring additional treatment. However, there are safety concerns associated with the flammability and explosiveness of H_2 when mixed with air, leading to transportation risks and elevated operation and maintenance costs. Additionally, the low solubility of H_2 in water, with only 1.6 mg H_2 dissolved per liter of water at 20°C, results in low utilization rates (30–50%). These factors have restricted the widespread adoption of this technology, and current research on

hydrogen autotrophic denitrification remains largely in the laboratory stage (Zhang Y. B. et al., 2014).

2.2. Novel bio-denitrification coupling technology

In recent years, most researchers have coupled new biological denitrification technologies to maximize their individual advantages and compensate for the limitations of independent use. This has resulted in the development of economically and environmentally friendly bio-denitrification technologies that hold great promise. Examples include partial short-cut nitrification ANAMMOX (PN-ANAMMOX; Qiu et al., 2021; Wang Z., 2021; Shang et al., 2023; Yuan et al., 2023), ANAMMOX-SND (Yu Y. et al., 2022), sulfur autotrophic-iron autotrophic denitrification (Yang et al., 2023), iron autotrophic-hydrogen autotrophic denitrification (Liang et al., 2022), and bioelectrochemical denitrification (Huang et al., 2020a; Prarunchaya et al., 2021). In this context, the focus will primarily be on the short-range nitrification anaerobic ammonia oxidation process and the bioelectrochemical system.

2.2.1. PN-ANAMMOX

PN-ANAMMOX is a novel coupled biological denitrification process discovered at a waste leachate treatment plant in the Mechernich region of Germany (Hippen et al., 1997). It combines the ANAMMOX process with the short-cut nitrification process, often uniting them within a single reactor (Lu et al., 2012; Wang Z., 2021). Short-cut nitrification entails the control of ammonia oxidation to the nitrite stage (Eq. 3), ensuring a continuous and stable supply of nitrite, the essential oxidation substrate for ANAMMOX. The ideal NO_2^--N to NH_4^+-N ratio is recognized as 1.3 (Eq. 3), though practical applications typically achieve a ratio of approximately 1, reflecting the challenge of controlling the short-cut nitrification process (Wang Z., 2021). In comparison to traditional bio-denitrification, short-cut nitrification inherently reduces aeration energy consumption, while AnAOB necessitates strict hypoxia. Consequently, this process can save nearly 60% of the energy demand for aeration compared to traditional bio-denitrification (Zaborowska et al., 2018). The estimated energy consumption for traditional bio-denitrification stands at approximately 2.4 $kW{\cdot}h{\cdot}kg^{-1}$, whereas the energy consumption of the PN-ANAMMOX process is approximately 1.0 $kW{\cdot}h{\cdot}kg^{-1}$ (Figueroa et al., 2012; Liang et al., 2016). Furthermore, both short-cut nitrification and ANAMMOX are autotrophic processes, eliminating the need for additional organic carbon sources, making them highly suitable for denitrifying wastewater with low C/N ratios. Additionally, PN-ANAMMOX significantly reduces sludge production by around 90% (Morales et al., 2015; Zaborowska et al., 2018; Chini et al., 2019).

However, it's important to note that the initiation and domestication of anaerobic ammonia-oxidizing bacteria are relatively time-consuming. AOB and NOB often coexist, and the removal of NOB from the system is one of the challenges of this process. Moreover, the denitrification efficiency of PN-ANAMMOX is generally influenced by process parameters such as DO concentration, COD concentration, heavy metals, temperature, pH value, and sludge age, contributing to the complexity of its operation (Lotti et al., 2012; Zuo et al., 2020).

2.2.2. Bioelectrochemical systems

Bioelectrochemical systems (BESs) have emerged in recent years as a technology that combines microbiology with electrochemistry to achieve wastewater treatment and energy recovery (Liu and Logan, 2004). BESs rely on electrically active microbial catalytic electrodes, where oxidation reactions occur at the anode and reduction reactions happen at the cathode (Chang et al., 2016; Huang, 2021). Due to its sustainability (Yang W. L. et al., 2017), strong pollutant removal capability (Cao M. J. et al., 2020), and low sludge production (Wang and He, 2020), it has become a new type of low-energy-consumption water treatment technology that has attracted significant attention (Nguyen and Babel, 2022). Currently, many studies have used BESs to enhance various bio-reaction processes, including the removal of pollutants like nitrogen (Cecconet et al., 2020), phosphorus (Elmaadawy et al., 2020), organic matter (Cao et al., 2021), and heavy metals (Cao L. B. et al., 2020) that are challenging to degrade. Some studies have also employed BESs to improve denitrification in low C/N ratio wastewater treatment. The enhancement mechanisms involve the positive effects of bioelectricity on microbial functional enzymes and genes, as well as the direct provision of electrons by bioelectricity to the denitrification process, achieving electro autotrophic denitrification (Huang et al., 2020a, 2022). In addition, for denitrification in wastewater containing high concentrations of hard-to-degrade organic matter, BESs can break down these complex compounds into simpler organic matter, providing an organic carbon source for denitrification (Huang et al., 2020b). However, it's important to note that BESs are primarily used for medium to low concentration nitrogen loads, and this technology is currently mainly under laboratory research, with the potential to become a mainstream nitrogen removal process in the future.

3. The denitrification performance

3.1. The denitrification performance of novel bio-denitrification technology

Section 2.1 introduces several emerging biological denitrification technologies while providing brief explanations of their application scope, advantages, disadvantages, and the factors influencing each technology. Among these aspects, the denitrification performance is a central concern for these innovative denitrification technologies. Table 1 presents the performance data related to nitrogen and carbon removal during the application of some of these novel biological denitrification technologies.

As shown in Table 1, these novel bio-denitrification technologies have been employed in various wastewater treatment processes, including membrane bioreactors (Chang et al., 2022; Chen et al., 2022) and biofilters (Song et al., 2023). Remarkably, these technologies are not limited to synthetic wastewater treatment (Francesca et al., 2021; Chang et al., 2022; Zhao et al., 2022; Jiang et al., 2023; Roumi and Debabrata, 2023; Sun et al., 2023) but have also demonstrated their effectiveness in treating practical wastewater sources such as landfill leachate (Zhang et al., 2020, 2023), biogas slurry (Chen et al., 2022), urban domestic sewage (Dong et al., 2021; Li Y. et al., 2023), secondary effluent from sewage treatment plants (Song et al., 2023), aquaculture

TABLE 1 The denitrification performance of a novel bio-denitrification technology.

Bio-denitrification technology	Denitrification system	Wastewater	Average nitrogen load	Influent C/N ratio	Average nitrogen and carbon removal efficiency			Ref
					COD	NH_4^+-N /NO_3^--N	TN	
SCND	Activated sludge	Landfill leachate	100 mg NH_4^+-N·L^{-1}	4.0–8.0	89%	99%	82%	Zhang et al. (2020)
	Membrane aerated biofilm reactor	Synthetic wastewater	62 mg NH_4^+-N·L^{-1}	4.0	97%	96%	72%	Chang et al. (2022)
	Moving-bed biofilm reactor	Synthetic wastewater	48 mg NH_4^+-N·L^{-1}	3.6	-	-	81–88%	Francesca et al. (2021)
	Fixed biofilm-activated sludge (IFAS)	Biogas slurry	400–800 mg NH_4^+-N·L^{-1}	11.7	-	94%	92%	Chen et al. (2022)
			600–800 mg NH_4^+-N·L^{-1}	6.2	-	91%	86%	
ANAMMOX	Activated sludge	Pharmaceutical wastewater	100 mg NH_4^+-N·L^{-1}	1.3	-	-	87%	Chen H. Y. et al. (2023)
	Expanded granular sludge bed	Synthetic inorganic wastewater	1,200 mg N·L^{-1}	1.1	-	-	95%	Jiang et al. (2023)
SND	Fixed bed folded plate bioreactor	Mariculture wastewater	120 mg NH_4^+-N·L^{-1}	4.0	-	99%	-	Guo et al. (2023)
	New air lift bioreactor	Urban sewage	40 mg NH_4^+-N·L^{-1}	3.8	-	-	>90%	Li Y. et al. (2023)
	Composite sequencing batch biofilm reactor	High salinity wastewater	40 mg NH_4^+-N·L^{-1}	10	96%	99%	91%	Li M. et al. (2023)
	Moving bed biological reactor	Synthetic wastewater	500 mg NH_4^+-N·L^{-1}	1.28	-	85–90%	91%	Roumi and Debabrata (2023)
HN-AD	Activated sludge	Chemical wastewater and pig farming wastewater	200–1,600 mg NH_4^+-N·L^{-1}	3, 5, 10, 15, 20, 25	-	>98%	-	Chen P. P. et al. (2023)
	Activated sludge	High salinity wastewater	94 mg NH_4^+-N·L^{-1}	5–15	-	98%	-	Huang et al. (2023)
AGS	Dehydrated sludge particles as inoculant	Artificially synthesized urban sewage	11 mg NH_4^+-N·L^{-1}	19	90%	95%	70%	Sun et al. (2023)
Other	Sulfur autotrophic denitrification filter	Secondary effluent from sewage treatment plant	12 mg NO_3^--N·L^{-1}	1.8	-	95%	-	Song et al. (2023)
	sulfur autotrophic denitrification filter	Landfill leachate	125 mg NO_3^--N·L^{-1}	0.1	-	-	90%	Zhang et al. (2023)
	Hydrogen autotrophic membrane bioreactor	Domestic wastewater	80 mg NO_3^--N·L^{-1}	2	-	88%	-	Dong et al. (2021)
	FeS_2 autotrophic denitrification filter	Synthetic wastewater	20 mg NO_3^--N·L^{-1}	0.5	-	90%	-	Zhao et al. (2022)

10.3389/fmicb.2023.1284369

TABLE 2 The denitrification performance of a novel bio-denitrification coupling technology.

Novel bio-denitrification coupling technology	Wastewater	Average nitrogen load	Influent C/N ratio	Average nitrogen and carbon removal efficiency			Ref
				COD	NH_4^+-N/ NO_3^--N	TN	
PN-ANAMMOX	Landfill leachate	1,454 mg NH_4^+-N·L^{-1}	3.0	-	93%	-	Wang Z. (2021)
PN-ANAMMOX	Rural domestic sewage	121 mg NH_4^+-N·L^{-1}	2.0	86%	-	90%	Yuan et al. (2023)
PN-ANAMMOX	Urban sewage	60 mg NH_4^+-N·L^{-1}	2.8	>76%	-	92%	Qiu et al. (2021)
PN-ANAMMOX	Domestic sewage	50 mg NH_4^+-N·L^{-1}	3.0	-	78%	-	Shang et al. (2023)
SND-ANAMMOX	Collagen sleeve wastewater	79–208 mg NH_4^+-N·L^{-1}	1.0–1.8	-	94%	80%	Yu Y. et al. (2022)
Hydrogen autotrophic denitrification in bioelectrochemical systems	Synthetic wastewater	20 mg NO_3^--N·L^{-1}	1.0	-	74%	54%	Prarunchaya et al. (2021)
SND in the multi-anode microbial fuel cells	Synthetic wastewater	64 mg NH_4^+-N·L^{-1}	3.5	94%	-	71%	Huang et al. (2020a)
Heterotrophic nitrification aerobic denitrification coupled AGS	Synthetic petroleum wastewater	65 mg NH_4^+-N·L^{-1}	1.5–12.3	-	92%	80%	Wang et al. (2022)
Enhanced iron and hydrogen autotrophic denitrification by biofilm coupled microelectrolysis of iron scrap	Synthetic wastewater	28 mg NH_4^+-N·L^{-1}	19	91%	93%	80%	Liang et al. (2022)
Sulfur autotrophic coupled iron autotrophic denitrification system	Synthetic wastewater	50 mg NO_3^--N·L^{-1}	0	-	-	90%	Yang et al. (2023)
Anaerobic nitrification coupled SND	Pharmaceutical wastewater	200 mg NH_4^+-N·L^{-1}	52.5	97%	96%	85%	Jia et al. (2023)

wastewater (Chen H. Y. et al., 2023; Guo et al., 2023), and chemical wastewater (Chen H. Y. et al., 2023; Chen P. P. et al., 2023). These novel bio-denitrification technologies exhibit versatility in handling a wide range of nitrogen concentrations, with initial nitrogen loads ranging from as high as 1,600 mgN·L^{-1} (Chen P. P. et al., 2023) to as low as 11 mgN·L^{-1} (Sun et al., 2023). Importantly, they consistently achieve robust denitrification effects, with denitrification efficiencies surpassing 70%, and in most cases, approaching 100%.

As shown in Table 1, autotrophic biological denitrification technology is primarily employed for the advanced treatment of low C/N ratio wastewater and has demonstrated significant advantages. Anaerobic ammonia oxidation technology, sulfur autotrophic, hydrogen autotrophic, and iron autotrophic biological denitrification technologies all exhibit treatment efficiencies exceeding 85% when applied to wastewater with a C/N ratio less than 3 (Dong et al., 2021; Zhao et al., 2022; Chen H. Y. et al., 2023; Jiang et al., 2023; Song et al., 2023; Zhang et al., 2023). Even in the study by Zhao et al. (2022), where iron autotrophic biological denitrification technology was employed to treat wastewater with an extremely low C/N ratio of 0.5, a denitrification efficiency of 90% was achieved. The widespread use of these autotrophic bio-denitrification technologies has the potential to effectively reduce chemical costs (related to organic carbon sources) and expenses associated with excess sludge treatment, aligning with the global low-carbon concept that has gained prominence in recent years.

3.2. The denitrification performance of novel bio-denitrification coupling process

Section 2.2 introduces several novel bio-denitrification coupling technologies, and Table 2 provides data on denitrification and carbon removal performance during the application of selected coupling denitrification technologies. As demonstrated in Table 2, the actual wastewater treated by these new biological denitrification coupling processes includes landfill leachate (Wang Z., 2021), domestic wastewater (Huang et al., 2020a; Prarunchaya et al., 2021; Qiu et al., 2021; Liang et al., 2022; Shang et al., 2023; Yang et al., 2023; Yuan et al., 2023), and chemical wastewater (Wang et al., 2022; Yu D. Y. et al., 2022; Jia et al., 2023), closely resembling the wastewater types addressed by the new biological denitrification technologies in Table 1. PN-ANAMMOX technology has emerged as the most prevalent coupling method in recent years, showcasing its versatility in handling a wide range of nitrogen loads and consistently achieving robust denitrification efficiency exceeding 90% (Qiu et al., 2021; Wang Z., 2021; Shang et al., 2023; Yuan et al., 2023).

The granular sludge technology primarily involves introducing granular sludge into the system, which, while shortening the reactor's startup time, does not exhibit high adaptability or resistance to sewage impact (Sun et al., 2023). Consequently, researchers have explored its combination with other

bio-denitrification technologies to cultivate specific granular sludge for wastewater treatment (Wang et al., 2022). However, the TN removal efficiency of this process has proven to be less than ideal. For instance, in a study by Sun et al. (2023), isolated AGS was applied to treat artificially synthesized urban wastewater, achieving a 95% removal efficiency for ammonia nitrogen, but only a 70% removal efficiency for TN. Similarly, Wang et al. (2022) utilized "heterotrophic nitrification aerobic denitrification" in conjunction with AGS to treat synthetic petroleum wastewater, attaining a 92% removal efficiency for ammonia nitrogen, while the TN removal efficiency reached only 80%. Therefore, whether used independently or in conjunction with other technologies, its TN removal efficiency falls short of that for ammonia nitrogen. Further investigation is needed to better understand the underlying reasons and explore potential enhancement measures.

Transportation safety risks associated with H_2 limit the application of hydrogen autotrophic denitrification (Zhang Y. H. et al., 2014). However, BES with external electric fields can produce hydrogen *in situ*, providing a local source of H_2 for hydrogen autotrophic denitrification (Prarunchaya et al., 2021). Nevertheless, the extra electricity needed for this coupled technology increases its operational costs, to some extent, restricting its large-scale practical application. Additionally, sulfur autotrophic denitrification faces challenges such as low pH values and secondary pollution due to sulfate by-products. The sulfur autotrophic coupled with iron autotrophic denitrification system effectively reduces sulfate by-products and exhibits robust denitrification performance (Yang et al., 2023).

4. Application prospect

4.1. Upgrading and renovation of urban sewage treatment plants

The novel bio-denitrification technology represents a promising sewage treatment approach with broad engineering applications. It effectively addresses the challenges associated with traditional denitrification processes, such as lengthy processing, substantial land requirements, high energy consumption, and significant financial investments (Zhang et al., 2022). In comparison to conventional biological denitrification methods, this innovative technology offers superior efficiency and adaptability. It can cater to the treatment requirements of various wastewater types and achieve efficient deep denitrification in low C/N ratio wastewater without the need for additional external carbon sources. Therefore, in light of current domestic and international policies aimed at improving effluent standards in urban sewage treatment plants, the novel bio-denitrification technology emerges as a favorable low-carbon choice.

4.2. Coupling with other technologies

The novel bio-denitrification technology not only compensates for the limitations of independent use through self-coupling but also pairs effectively with non-biological methods to provide reference parameters that are challenging to regulate in practical engineering. For instance, in treating highly concentrated toxic and hazardous wastewater, physical and chemical techniques such as adsorption, membrane separation, electrochemistry, and oxidation–reduction can be employed as pretreatment. Subsequently, they can be combined with biological denitrification technology for advanced treatment, thereby further expanding the practical application range and improving sewage treatment efficacy. The greater challenge for the future is to explore low-energy, cost-effective technologies while maximizing process coupling to overcome constraints in real-world wastewater scenarios and enable large-scale applications. This development direction aligns with the low-carbon concept and introduces innovative ideas for environmentally friendly denitrification.

4.3. The reduction of greenhouse gases emission

Chan-Pacheco et al. (2021) explored the substantial potential of combining new bio-denitrification technologies for the purification and reduction of denitrification gas pollutants, including N_2O, CH_4, and H_2S, which are presently significant greenhouse gases of global concern. This suggests that future research could delve into additional technology coupling approaches for greenhouse gas emission reduction, further contributing to the low-carbon concept.

4.4. Smart water management

In the practical application of novel bio-denitrification technologies, the cultivation and regulation of microbial communities are key factors for achieving efficient denitrification. However, challenges can arise, such as unstable environmental conditions or increased operating costs due to the need for adjustments in temperature, pH, and other parameters when cultivating these microorganisms. Therefore, it is worth considering the utilization of novel bio-denitrification technologies within the realm of smart water management, where the integration of automation, computer technology, and other advancements can standardize the domestication and cultivation of microorganisms. Simultaneously, this approach can help reduce the reliance on human resources and propel the advancement of new biological denitrification technology towards broader practical implementation.

5. Conclusion

This paper reviews the denitrification performance of novel bio-denitrification technologies and their combined applications, analyzes the recent research situation, and summarizes the future development direction and challenges of these technologies. Novel bio-denitrification technology is environmentally friendly and holds vast application prospects, aligning with the sustainable low-carbon development concept. With ongoing technological progress, novel bio-denitrification technologies are expected to expand their presence in various fields, contributing significantly to environmental protection and sustainable development.

Author contributions

SH: Funding acquisition, Investigation, Writing – original draft, Writing – review & editing. YLF: Investigation, Writing – original draft. HMZ: Writing – review & editing. CQW: Writing – review & editing. CLZ: Writing – review & editing. XGL: Writing – review & editing.

Funding

The author(s) declare financial support was received for the research, authorship, and/or publication of this article. This research was funded by the National Natural Science Foundation of China (42207159) and Jiangxi Provincial Natural Science Foundation (20232BAB214085).

Conflict of interest

The authors declare that the research was conducted in the absence of any commercial or financial relationships that could be construed as a potential conflict of interest.

Publisher's note

References

Beristain, C. R., Reyes, S. A., Pieter, R., Razo, F. E., and Jorge, G. (2006). Sulfide oxidation under chemolithoautotrophic denitrifying conditions. *Biotechnol. Bioeng.* 95, 1148–1157. doi: 10.1002/bit.21084

Cao, M. J., Feng, Y. J., Wang, N. Y., Li, Y. F., Li, N., Liu, J., et al. (2020). Electrochemical regulation on the metabolism of anode biofilms under persistent exogenous bacteria interference. *Electrochim. Acta* 340:135922. doi: 10.1016/j.electacta.2020.135922

Cao, L. B., Ma, Y. M., Deng, D. D., Jiang, H. C., Wang, J. X., and Liu, Y. (2020). Electricity production of microbial fuel cells by degrading cellulose coupling with Cr(VI) removal. *J. Hazard. Mater.* 391:122184. doi: 10.1016/j.jhazmat.2020.122184

Cao, X., Wang, H., Long, X. Z., Nishimura, O., and Li, X. N. (2021). Limitation of voltage reversal in the degradation of azo dye by a stacked double-anode microbial fuel cell and characterization of the microbial community structure. *Sci. Total Environ.* 754:142454. doi: 10.1016/j.scitotenv.2020.142454

Cecconet, D., Sabba, F., Devecseri, M., Callegari, A., and Capodaglio, A. G. (2020). In situ groundwater remediation with bioelectrochemical systems: a critical review and future perspectives. *Environ. Int.* 137:105550. doi: 10.1016/j.envint.2020.105550

Ceulemans, T., Verscheure, P., Shadouh, C., Van Acker, K., Devleesschauwer, B., Linard, C., et al. (2023). Environmental degradation and the increasing burden of allergic disease: the need to determine the impact of nitrogen pollution. *Front. Allergy* 4:1063982. doi: 10.3389/falgy.2023.1063982

Chang, M. D., Liang, B. R., Zhang, K., Wang, Y. Z., Jin, D. T., Zhang, Q. J., et al. (2022). Simultaneous shortcut nitrification and denitrification in a hybrid membrane aerated biofilms reactor (H-MBfR) for nitrogen removal from low COD/N wastewater. *Water Res.* 211:118027. doi: 10.1016/j.watres.2021.118027

Chang, C., Lu, X. B., Lei, Z. W., Wang, Z. L., and Zhao, C. (2016). 2-Mercaptopyridine as a new leveler for bottom-up filling of micro-vias in copper electroplating. *Electrochim. Acta* 208, 33–38. doi: 10.1016/j.electacta.2016.04.177

Chan-Pacheco, C. R., Valenzuela, E. I., Cervantes, F. J., and Quijano, G. (2021). Novel biotechnologies for nitrogen removal and their coupling with gas emissions abatement in wastewater treatment facilities. *Sci. Total Environ.* 797:149228. doi: 10.1016/j.scitotenv.2021.149228

Chen, H. Y., Li, X. K., Liu, G. G., Zhu, J., Ma, X. C., Piao, C. Y., et al. (2023). Decoding the carbon and nitrogen metabolism mechanism in anammox system treating pharmaceutical wastewater with varying COD/N ratios through metagenomic analysis. *Chem. Eng. J.* 457:141316. doi: 10.1016/j.cej.2023.141316

Chen, M. X., Wang, W. C., Feng, Y., Zhu, X. H., Zhou, H. Z., Tan, Z. L., et al. (2014). Impact resistance of different factors on ammonia removal by heterotrophic nitrification-aerobic denitrification bacterium *Aeromonas sp.* HN-02. *Bioresour. Technol.* 167, 456–461. doi: 10.1016/j.biortech.2014.06.001

Chen, Y. W., Wang, H., Gao, X. D., Li, X., Dong, S. Y., Zhou, H. Z., et al. (2022). COD/TN ratios shift the microbial community assembly of a pilot-scale shortcut nitrification-denitrification process for biogas slurry treatment. *Environ. Sci. Pollut. Res.* 29, 49335–49345. doi: 10.1007/s11356-022-19285-w

Chen, P. P., Zhai, T. R., Zhang, L. J., Zhao, T. T., Xing, Z. L., and Liu, H. (2023). Domestication and pilot-scale culture of mixed bacteria HY-1 capable of heterotrophic nitrification-aerobic denitrification. *Bioresour. Technol.* 384:129285. doi: 10.1016/j.biortech.2023.129285

Chini, A., Bolsan, A. C., Hollas, C. E., Antes, F. G., Fongaro, G., Treichel, H., et al. (2019). Evaluation of deammonification reactor performance and microrganisms community during treatment of digestate from swine sludge CSTR biodigester. *J. Environ. Manag.* 246, 19–26. doi: 10.1016/j.jenvman.2019.05.113

Dong, K., Feng, X. H., Wang, W. B., Chen, Y. C., Hu, W., Li, H. X., et al. (2021). Simultaneous partial nitrification and denitrification maintained in membrane bioreactor for nitrogen removal and hydrogen autotrophic denitrification for further treatment. *Membranes* 11:911. doi: 10.3390/membranes11120911

Elmaadawy, K., Liu, B. C., Hu, J. P., Hou, H. J., and Yang, J. K. (2020). Performance evaluation of microbial fuel cell for landfill leachate treatment: research updates and synergistic effects of hybrid systems. *J. Environ. Sci.* 96, 1–20. doi: 10.1016/j.jes.2020.05.005

Figueroa, M., Vázquez-Padín, J. R., Mosquera-Corral, A., Campos, J. L., and Méndez, R. (2012). Is the CANON reactor an alternative for nitrogen removal from pre-treated swine slurry? *Biochem. Eng. J.* 65, 23–29. doi: 10.1016/j.bej.2012.03.008

Francesca, I., Francesco, D. C., Francesco, G., Rudy, G., and Giovanni, E. (2021). Shortcut nitrification-denitrification and biological phosphorus removal in acetate-and ethanol-fed moving bed biofilm reactors under microaerobic/aerobic conditions. *Bioresour. Technol.* 330:124958. doi: 10.1016/j.biortech.2021.124958

Guo, P., Wang, Q., Ni, L. F., Xu, S. L., Zheng, D. Q., Wang, Y., et al. (2023). Improved simultaneous nitrification-denitrification in fixed-bed baffled bioreactors treating mariculture wastewater: performance and microbial community behaviors. *Bioresour. Technol.* 385:129468. doi: 10.1016/j.biortech.2023.129468

He, Q. L., Wang, H. T., Chen, L., Gao, S. X., Zhang, W., Song, J. Y., et al. (2020). Elevated salinity deteriorated enhanced biological phosphorus removal in an aerobic granular sludge sequencing batch reactor performing simultaneous nitrification, denitrification and phosphorus removal. *J. Hazard. Mater.* 390:121782. doi: 10.1016/j.jhazmat.2019.121782

Hippen, A., Rosenwinkel, K. H., Baumgarten, G., and Seyfried, C. F. (1997). Aerobic deammonification: a new experience in the treatment of waste waters. *Water Sci. Technol.* 35, 111–120. doi: 10.2166/wst.1997.0371

Huang, S. (2021). *Approach and mechanisms of enhanced cathode denitrification performance of low COD/N wastewater in the multi-anode microbial fuel cell*. Southeast University, Nan Jing, Jiangsu.

Huang, M., Cui, Y., Yang, H., Xu, M., Cui, Y., and Chen, Z. (2023). A halophilic aerobic-heterotrophic strain *Halomonas venusta* SND-01: nitrogen removal by ammonium assimilation and heterotrophic nitrification-aerobic denitrification. *Bioresour. Technol.* 374:128758. doi: 10.1016/j.biortech.2023.128758

Huang, S., Lu, Y., Li, X., Lu, Y. Z., Zhu, G., and Hassan, M. (2020b). Tertiary denitrification and organic matter variations of secondary effluent from wastewater treatment plant by the 3D-BER system. *Environ. Res.* 189:109937. doi: 10.1016/j.envres.2020.109937

Huang, F., Pan, L. Q., He, Z. Y., Zhang, M. Y., and Zhang, M. Z. (2021). Heterotrophic nitrification-aerobic denitrification characteristics and antibiotic resistance of two bacterial consortia from Marinomonas and Halomonas with effective nitrogen removal in mariculture wastewater. *J. Environ. Manag.* 279:111786. doi: 10.1016/j.jenvman.2020.111786

Huang, S., Zhang, J. R., Wang, C. Q., Zhu, G. C., and Hassan, M. (2022). Weak electric field effect of MFC biocathode on denitrification. *J. Environ. Chem. Eng.* 10:108596. doi: 10.1016/j.jece.2022.108596

Huang, S., Zhu, G., and Gu, X. (2020a). The relationship between energy production and simultaneous nitrification and denitrification via bioelectric derivation of microbial fuel cells at different anode numbers. *Environ. Res.* 184:109247. doi: 10.1016/j.envres.2020.109247

Jia, X. F., Fan, H. X., Liang, J. W., Dai, J. H., Sun, Y., and Mai, W. N. (2023). Performance analysis of anaerobic digestion coupled with simultaneous nitrification and

denitrification process for treating alcohol precipitation wastewater of Chinese patent medicine. *Water* 15:1939. doi: 10.3390/w15101939

Jia, F. X., Peng, Y. Z., and Yang, Q. (2014). Competition and synergism between anammox bacteria and other bacteria. *Acta Sci. Circumst.* 34, 1351–1361. doi: 10.13671/j.hjkxxb.2014.0206

Jia, Y. T., Zhou, M. M., Chen, Y. C., Hu, Y. Y., and Luo, J. (2020). Insight into short-cut of simultaneous nitrification and denitrification process in moving bed biofilm reactor: effects of carbon to nitrogen ratio. *Chem. Eng. J.* 400:125905. doi: 10.1016/j.cej.2020.125905

Jia, Y. T., Zhou, M. M., Chen, Y. C., Luo, J., and Hu, Y. Y. (2019). Carbon selection for nitrogen degradation pathway by *Stenotrophomonas maltophilia*: based on the balances of nitrogen, carbon and electron. *Bioresour. Technol.* 294:122114. doi: 10.1016/j.biortech.2019.122114

Jiang, M. T., Ji, S. H., Wu, R. X., Yang, H., Li, Y. Y., and Liu, J. Y. (2023). Exploiting refractory organic matter for advanced nitrogen removal from mature landfill leachate via anammox in an expanded granular sludge bed reactor. *Bioresour. Technol.* 371:128594. doi: 10.1016/j.biortech.2023.128594

Johnson, K. J., Ams, D. A., Wedel, A. N., Szymanowski, J. E. S., Weber, D. L., Schneegurt, M. A., et al. (2007). The impact of metabolic state on cd adsorption onto bacterial cells. *Geobiology* 5, 211–218. doi: 10.1111/j.1472-4669.2007.00111.x

Kishida, N., Tsuneda, S., Kim, J. H., and Sudo, R. (2009). Simultaneous nitrogen and phosphorus removal from high-strength industrial wastewater using aerobic granular sludge. *J. Environ. Eng.* 135, 153–158. doi: 10.1061/(ASCE)0733-9372(2009)135:3(153)

Kornaros, M., Dokianakis, S. N., and Lyberatos, G. (2010). Partial nitrification/denitrification can be attributed to the slow response of nitrite oxidizing bacteria to periodic anoxic disturbances. *Environ. Sci. Technol.* 44, 7245–7253. doi: 10.1021/es100564j

Kosgey, K., Zungu, P. V., Bux, F., and Kumari, S. (2022). Biological nitrogen removal from low carbon wastewater. *Front. Microbiol.* 13:968812. doi: 10.3389/fmicb.2022.968812

Kuenen, J. G. (2008). Anammox bacteria: from discovery to application. *Nat. Rev. Microbiol.* 6, 320–326. doi: 10.1038/nrmicro1857

Layer, M., Villodres, M. G., Hernandez, A., Reynaert, E., Morgenroth, E., and Derlon, N. (2020). Limited simultaneous nitrification-denitrification (SND) in aerobic granular sludge systems treating municipal wastewater: mechanisms and practical implications. *Water Res. X* 7:100048. doi: 10.1016/j.wroa.2020.100048

Li, S. (2020). *The research on efficiency and mechanism of aerobic granular sludge continuous flow process for nitrogen and phosphorus removal*. Harbin Institute of Technology, Harbin, Heilongjiang.

Li, M., Liu, R., Chen, J., Peng, Q., Liu, J., and She, Z. (2023). Effects of pH on simultaneous partial nitrification and denitrification performance. *Period. Ocean Univ. China* 53, 67–76. doi: 10.16441/j.cnki.hdxb.20220134

Li, Y., Liu, S. J., Lu, L. L., Wang, J. H., Huang, G. R., Chen, F. M., et al. (2023). Non-uniform dissolved oxygen distribution and high sludge concentration enhance simultaneous nitrification and denitrification in a novel air-lifting reactor for municipal wastewater treatment: a pilot-scale study. *Bioresour. Technol.* 384:129306. doi: 10.1016/j.biortech.2023.129306

Liang, Y. C., Daverey, A., Huang, Y. T., Sung, S. H., and Lin, J. G. (2016). Treatment of semiconductor wastewater using single-stage partial nitrification and anammox in a pilot-scale reactor. *J. Taiwan Inst. Chem. Eng.* 63, 236–242. doi: 10.1016/j.jtice.2016.02.036

Liang, Y. F., Pan, Z. R., Feng, H. B., Cheng, X. Y., Guo, T., Yan, A. Q., et al. (2022). Biofilm coupled micro-electrolysis of waste iron shavings enhanced iron and hydrogen autotrophic denitrification and phosphate accumulation for wastewater treatment. *J. Environ. Chem. Eng.* 10:108959. doi: 10.1016/j.jece.2022.108959

Lin, S., Mackey, H. R., Hao, T. W., Guo, G., Loosdrecht, M. C. M. V., and Chen, G. H. (2018). Biological sulfur oxidation in wastewater treatment: a review of emerging opportunities. *Water Res.* 143, 399–415. doi: 10.1016/j.watres.2018.06.051

Ling, F. (2020). Study on enhancement and kinetics of cathodic simultaneous nitrification and denitrification in microbial fuel cell system. *South. Univ. Nan Jing. Jiangsu* 186:109505. doi: 10.1016/j.envres.2020.109505

Liu, H., and Logan, B. E. (2004). Electricity generation using an air-cathode single chamber microbial fuel cell in the presence and absence of a proton exchange membrane. *Environ. Sci. Technol.* 38, 4040–4046. doi: 10.1021/es0499344

Lotti, T., Cordola, M., Kleerebezem, R., Caffaz, S., Lubello, C., and Loosdrechtet, M. C. M. (2012). Inhibition effect of swine wastewater heavy metals and antibiotics on anammox activity. *Water Sci. Technol.* 66, 1519–1526. doi: 10.2166/wst.2012.344

Lu, H. F., Zheng, P., Ji, Q. X., Zhang, H. T., Ji, J. Y., Wang, L., et al. (2012). The structure, density and settlability of anammox granular sludge in high-rate reactors. *Bioresour. Technol.* 123, 312–317. doi: 10.1016/j.biortech.2012.07.003

Ma, W. W., Han, Y. X., Ma, W. C., Han, H. J., Zhu, H., Xu, C. Y., et al. (2017). Enhanced nitrogen removal from coal gasification wastewater by simultaneous nitrification and denitrification (SND) in an oxygen-limited aeration sequencing batch biofilm reactor. *Bioresour. Technol.* 244, 84–91. doi: 10.1016/j.biortech.2017.07.083

Ma, B., Wang, S. Y., Cao, S. B., Miao, Y. Y., Jia, F. X., Du, R., et al. (2016). Biological nitrogen removal from sewage via anammox: recent advances. *Bioresour. Technol.* 200, 981–990. doi: 10.1016/j.biortech.2015.10.074

Malamis, S., Katsou, E., Fabio, S. D., Bolzonella, D., and Fatone, F. (2014). Biological nutrients removal from the supernatant originating from the anaerobic digestion of the organic fraction of municipal solid waste. *Crit. Rev. Biotechnol.* 34, 244–257. doi: 10.3109/07388551.2013.791246

Masoudi, S. M. A., Moghaddam, A. H., Sargolzaei, J., Darroudi, A., and Zeynali, V. (2018). Investigation and optimization of the SND-SBR system for organic matter and ammonium nitrogen removal using the central composite design. *Environ. Prog. Sustain. Energy* 37, 1638–1646. doi: 10.1002/ep.12847

Mofradnia, S. R., Ashouri, R., Tavakoli, Z., Shahmoradi, F., Rashedi, H., Yazdian, F., et al. (2019). Effect of zero-valent iron/starch nanoparticle on nitrate removal using MD simulation. *Int. J. Biol. Macromol. Struct. Funct. Interact.* 121, 727–733. doi: 10.1016/j.ijbiomac.2018.09.183

Morales, N., Río, Á. V. D., Vázquez-Padín, J. R., Méndez, R., Mosquera-Corral, A., and Campos, J. L. (2015). Integration of the Anammox process to the rejection water and main stream lines of WWTPs. *Chemosphere* 140, 99–105. doi: 10.1016/j.chemosphere.2015.03.058

Mota, C. R., Head, M. A., Williams, J. C., Eland, L., Cheng, J. J., and Reyes, F. L. D. L. (2014). Structural integrity affects nitrogen removal activity of granules in semi-continuous reactors. *Biodegradation* 25, 923–934. doi: 10.1007/s10532-014-9712-3

Moy, B., Tay, J., Toh, S., Liu, Y., and Tay, S. (2002). High organic loading influences the physical characteristics of aerobic sludge granules. *Lett. Appl. Microbiol.* 34, 407–412. doi: 10.1046/j.1472-765X.2002.01108.x

Nguyen, H. D., and Babel, S. (2022). Insights on microbial fuel cells for sustainable biological nitrogen removal from wastewater: a review. *Environ. Res.* 204:112095. doi: 10.1016/j.envres.2021.112095

Oshiki, M., Ishii, S., Yoshida, K., Fujii, N., Ishiguro, M., Satoh, H., et al. (2013). Nitrate-dependent ferrous iron oxidation by anaerobic ammonium oxidation (znammox) bacteria. *Appl. Environ. Microbiol.* 79, 4087–4093. doi: 10.1128/AEM.00743-13

Pishgar, R., Dominic, J. A., Tay, J. H., and Chu, A. (2020). Pilot-scale investigation on nutrient removal characteristics of mineral-rich aerobic granular sludge: identification of uncommon mechanisms. *Water Res.* 168:115151. doi: 10.1016/j.watres.2019.115151

Prarunchaya, P., Orapan, M., Palisa, M., Pakpoom, S., Nga, D. T., Auppatham, N., et al. (2021). Enhancement of nitrate removal under limited organic carbon with hydrogen-driven autotrophic denitrification in low-cost electrode bio-electrochemical reactors. *J. Chem. Technol. Biotechnol.* 96, 2520–2528. doi: 10.1002/jctb.6788

Qiu, S. J., Liu, J. J., Zhang, L., Zhang, Q., and Peng, Y. Z. (2021). Sludge fermentation liquid addition attained advanced nitrogen removal in low C/N ratio municipal wastewater through short-cut nitrification-denitrification and partial anammox. *Front. Environ. Sci. Eng.* 15, 107–116. doi: 10.1007/s11783-020-1318-x

Qu, J. H., Wang, H. C., Wang, K. J., Yu, G., Ke, B., Yu, H. Q., et al. (2019). Municipal wastewater treatment in China: development history and future perspectives. *Front. Environ. Sci. Eng.* 13, 3–9. doi: 10.1007/s11783-019-1172-x

Robertson, L. A., and Kuenen, J. G. (1990). Combined heterotrophic nitrification and aerobic denitrification in Thiosphaera pantotropha and other bacteria. *Antonie Van Leeuwenhoek* 57, 139–152. doi: 10.1007/BF00403948

Robertson, L. A., Kuenen, J. G., and Kleijntjens, R. (1985). Aerobic denitrification and heterotrophic nitrification by *Thiosphaera pantotropha*. *J. Microbiol. Serol.* 51:445. doi: 10.1007/BF02275068

Roumi, B., and Debabrata, M. (2023). Process optimization of a moving bed bioreactor undergoing simultaneous nitrification and denitrification for wastewater in the absence of organic carbon. *Environ. Technol.*, 1–15. doi: 10.1080/09593330.2023.2227388

Sanjrani, M. A., Nafees, A., Sakina, R., and Xue, G. (2022). A review on application of external carbon sources for denitrification for wastewater treatment. *Global NEST J.* 24, 105–118. doi: 10.30955/gnj.004248

Sarma, S. J., Tay, J. H., and Chu, A. (2017). Finding knowledge gaps in aerobic granulation technology. *Trends Biotechnol.* 35, 66–78. doi: 10.1016/j.tibtech.2016.07.003

Shang, T. T., Zhu, X. R., Gong, X. F., Guo, J. W., Li, X. Y., Zhang, Q., et al. (2023). Efficient nitrogen removal in a total floc sludge system from domestic wastewater with low C/N: high anammox nitrogen removal contribution driven by endogenous partial denitrification. *Bioresour. Technol.* 378:128995. doi: 10.1016/j.biortech.2023.128995

Soldatov, V. S., Sokolova, V. I., Medyak, G. V., Shunkevich, A. A., and Akulich, Z. I. (2007). Binary ion exchange equilibria in systems containing NO_3^-, Cl^- and SO_4^{2-} on fibrous anion exchangers with tetraalkylammomium groups. *React. Funct. Polym.* 67, 1530–1539. doi: 10.1016/j.reactfunctpolym.2007.07.018

Song, Q., Lin, F., Yu, G., Gao, M., and Zhang, Y. (2023). Pilot study on deep denitrification effect of sulfur autotrophic denitrification filter on secondary effluent. *Water Wastewater Eng.* 59, 21–25. doi: 10.13789/j.cnki.wwe1964.2022.04.26.0003

Sun, Z., Zhang, J. M., Wang, J., Zhu, H. X., Xiong, J. H., Nong, G. Y., et al. (2023). Direct start-up of aerobic granular sludge system with dewatered sludge granular particles as inoculant. *J. Environ. Manag.* 326:116540. doi: 10.1016/j.jenvman.2022.116540

Tarpeh, W. A., Udert, K. M., and Nelson, K. L. (2017). Comparing ion exchange adsorbents for nitrogen recovery from source-separated urine. *Environ. Sci. Technol.* 51, 2373–2381. doi: 10.1021/acs.est.6b05816

Third, K. A., Gibbs, B., Newland, M., and Cord-Ruwisch, R. (2005). Long-term aeration management for improved N-removal via SND in a sequencing batch reactor. *Water Res.* 39, 3523–3530. doi: 10.1016/j.watres.2005.06.014

Voets, J. P., Vanstaen, H., and Verstraete, W. (1975). Removal of nitrogen from highly nitrogenous wastewaters. *Water Pollut. Cont. Federation* 47, 394–398.

Wang, J. (2021). The performance and mechanism of completely autotrophic nitrogen removal process based on formic acid aided partial nitrification. South China University of Technology, Guangzhou, Guangdong.

Wang, Z. (2021). Process and mechanism based on anammox treating mature landfill leachate. Harbin Institute of Technology, Harbin, Heilongjiang.

Wang, Z. X., and He, Z. (2020). Demystifying terms for understanding bioelectrochemical systems towards sustainable wastewater treatment. *Curr. Opin. Electrochem.* 19, 14–19. doi: 10.1016/j.coelec.2019.09.001

Wang, J. J., Huang, B. C., Li, J., and Jin, R. C. (2020). Advances and challenges of sulfur-driven autotrophic denitrification (SDAD) for nitrogen removal. *Chin. Chem. Lett.* 31, 2567–2574. doi: 10.1016/j.cclet.2020.07.036

Wang, Q. H., Kong, J. W., Liang, J. H., EI-Din, M. G., Zhao, P., Xie, W. Y., et al. (2022). Nitrogen removal intensification of aerobic granular sludge through bioaugmentation with "heterotrophic nitrification-aerobic denitrification" consortium during petroleum wastewater treatment. *Bioresour. Technol.* 361:127719. doi: 10.1016/j.biortech.2022.127719

Xia, L. L., and Yan, X. Y. (2023). How to feed the world with less nitrogen pollution. *Nature* 613, 34–35. doi: 10.1038/d41586-022-04490-x

Xian, S. S., Chen, M. X., Xiong, R., and Tan, Z. L. (2016). Research advances of heterotrophic nitrification-aerobic denitrification under different factors. *Technol. Water Treat.* 42, 1–6. doi: 10.16796/j.cnki.1000-3770.2016.01.001

Xiang, Y. (2020). *Nitrogen removal capacity and pathways of the simultaneous nitrification and denitrification process under different oxygen conditions*. Chongqing University, Chongqing.

Yang, W. L., Kim, K. Y., Saikaly, P., and Logan, B. E. (2017). The impact of new cathode materials relative to baseline performance of microbial fuel cells all with the same architecture and solution chemistry. *Energy Environ. Sci.* 10, 1025–1033. doi: 10.1039/C7EE00910K

Yang, Y., Liu, Y. X., Yang, T., and Lv, Y. K. (2017). Characterization of a microbial consortium capable of heterotrophic nitrifying under wide C/N range and its potential application in phenolic and coking wastewater. *Biochem. Eng. J.* 120, 33–40. doi: 10.1016/j.bej.2016.12.008

Yang, B., Shun, W., Ainur, Z., Igor, V. S., PoHeng, L., and Zhan, X. M. (2023). High-rate iron sulfide and sulfur-coupled autotrophic denitrification system: nutrients removal performance and microbial characterization. *Water Res.* 231:119619. doi: 10.1016/j.watres.2023.119619

Yu, Y., Liu, N., Liao, Z., Zhao, J., and Zhang, Q. (2022). Research progress of iron-type denitrification removal technology. *China Environ. Sci.* 42, 83–91. doi: 10.19674/j.cnki.issn1000-6923.2022.0002

Yu, D. Y., Zhang, W. J., Wang, D. Q., and Jin, Y. (2022). Full-scale application of one-stage simultaneous nitrification and denitrification coupled with Anammox process for treating collagen casing wastewater. *Int. J. Environ. Res. Public Health* 19:5787. doi: 10.3390/ijerph19105787

Yuan, Y., Yongzhi, C., Xinbo, W., Hongzhong, D., Tianxu, Z., Jiao, M., et al. (2023). Enhanced nitrogen removal from rural domestic sewage via partial nitrification-anammox in integrated vertical subsurface flow constructed wetland. *Environ. Res.* 233:116338. doi: 10.1016/j.envres.2023.116338

Zaborowska, E., Majtacz, J., and Drewnowski, J. (2018). Improving the energy balance in wastewater treatment plants by optimization of aeration control and application of new technologies. Lublin University of Technology, Lublin, Poland, 2018, 317–328.

Zhang, D. W., Chen, L. W., Zhang, S. H., and Zhen, J. (2023). Denitrification performance and microbial community analysis of sulfur autotrophic denitrification filter for low-temperature treatment of landfill leachate. *J. Environ. Chem. Eng.* 11:109314. doi: 10.1016/j.jece.2023.109314

Zhang, Y. B., Feng, Y. H., Yu, Q. L., Xu, Z. B., and Xie, Q. (2014). Enhanced high-solids anaerobic digestion of waste activated sludge by the addition of scrap iron. *Bioresour. Technol.* 159, 297–304. doi: 10.1016/j.biortech.2014.02.114

Zhang, Z., Jiang, C., Zhang, W., Xiao, Z., Huang, X., Hua, T., et al. (2020). Short-term nitrification and de-nitrification test for landfill leachate. *J. Saf. Environ.* 20, 1083–1089. doi: 10.13637/j.issn.1009-6094.2019.0733

Zhang, X. X., Li, A., Szewzyk, U., and Ma, F. (2016). Improvement of biological nitrogen removal with nitrate-dependent Fe(II) oxidation bacterium *Aquabacterium parvum* B6 in an up-flow bioreactor for wastewater treatment. *Bioresour. Technol.* 219, 624–631. doi: 10.1016/j.biortech.2016.08.041

Zhang, Y. H., Ma, Z., Zhang, Z. B., and Sun, C. Z. (2014). Research progress in the influencing factors of autohydrogenotrophic biological denitrification for drinking water. *Indust. Water Treat.* 5, 1–14. doi: 10.12989/mwt.2014.5.1.001

Zhang, M. Y., Pan, L. Q., Huang, F., Gao, S., Su, C., Zhang, M. Z., et al. (2019). Metagenomic analysis of composition, function and cycling processes of microbial community in water, sediment and effluent of *Litopenaeus vannamei* farming environments under different culture modes. *Aquaculture* 506, 280–293. doi: 10.1016/j.aquaculture.2019.03.038

Zhang, Q., Xu, X. J., Zhang, R. C., Shao, B., Fan, K. L., Zhao, L., et al. (2022). The mixed/mixotrophic nitrogen removal for the effective and sustainable treatment of wastewater: from treatment process to microbial mechanism. *Water Res.* 226:119269. doi: 10.1016/j.watres.2022.119269

Zhang, H. H., Zhao, Z. F., Li, S. L., Chen, S. N., Huang, T. L., Li, N., et al. (2019). Nitrogen removal by mix-cultured aerobic denitrifying bacteria isolated by ultrasound: performance, co-occurrence pattern and wastewater treatment. *Chem. Eng. J.* 372, 26–36. doi: 10.1016/j.cej.2019.04.114

Zhao, J., Feng, L. J., Yang, G. F., Dai, J. C., and Mu, J. (2017). Development of simultaneous nitrification-denitrification (SND) in biofilm reactors with partially coupled a novel biodegradable carrier for nitrogen-rich water purification. *Bioresour. Technol.* 243, 800–809. doi: 10.1016/j.biortech.2017.06.127

Zhao, L. F., Xue, L. Y., Wang, L., Liu, C., and Li, Y. (2022). Simultaneous heterotrophic and FeS_2-based ferrous autotrophic denitrification process for low-C/N ratio wastewater treatment: nitrate removal performance and microbial community analysis. *Sci. Total Environ.* 829:154682. doi: 10.1016/j.scitotenv.2022.154682

Zhu, G., Peng, Y., and Guo, J. (2008). Biological nitrogen removal with nitrification and denitrification via nitrite pathway. *J. Harbin Inst. Tech.* 10, 1552–1557. doi: 10.1007/s00253-006-0534-z

Zuo, F. M., Sui, Q. W., Zheng, R., Ren, J. H., and Wei, Y. S. (2020). In situ startup of a full-scale combined partial nitritation and anammox process treating swine digestate by regulation of nitrite and dissolved oxygen. *Bioresour. Technol.* 315:123837. doi: 10.1016/j.biortech.2020.123837

frontiers | Frontiers in Microbiology

TYPE Original Research
PUBLISHED 05 October 2023
DOI 10.3389/fmicb.2023.1270658

OPEN ACCESS

EDITED BY
Yuanyuan Miao,
Qingdao University of Technology, China

REVIEWED BY
Garima Kaushik,
Central University of Rajasthan, India
Xiuhong Liu,
Beijing University of Technology, China
Yun Zhou,
Huazhong Agricultural University, China

*CORRESPONDENCE
Zhongyi An
✉ anzhongyi10000@163.com

RECEIVED 01 August 2023
ACCEPTED 12 September 2023
PUBLISHED 05 October 2023

CITATION
Zhang H, Shangguan M, Zhou C, Peng Z and An Z (2023) Construction of a mycelium sphere using a *Fusarium* strain isolate and *Chlorella* sp. for polyacrylamide biodegradation and inorganic carbon fixation.
Front. Microbiol. 14:1270658.
doi: 10.3389/fmicb.2023.1270658

Construction of a mycelium sphere using a *Fusarium* strain isolate and *Chlorella* sp. for polyacrylamide biodegradation and inorganic carbon fixation

Huichao Zhang[1], Mohan Shangguan[1], Chang Zhou[1], Zhaoyang Peng[2] and Zhongyi An[1]*

[1]School of Civil Engineering, Yantai University, Yantai, China, [2]The Architectural Design and Research Institute of HIT Co., Ltd., Harbin, China

In the context of global demand for carbon reduction, the formation of inorganic carbon (IC) in the wastewater from oil flooding becomes a potential threat. In this study, *Chlorella* sp. and *Fusarium* sp. were used to assemble a fungal-algal pellet to degrade polyacrylamide (PAM) and fix IC in synthetic oil-flooding wastewater. The results showed that the combination of *Chlorella* sp. and *Fusarium* sp. was more effective at degrading PAM and removing carbon than a monoculture. With PAM as the sole nitrogen source, the degradation of PAM by the consortium was enhanced up to 35.17 ± 0.86% and 21.63 ± 2.23% compared with the monocultures of fungi or microalgae, respectively. The degradation of the consortium was significantly enhanced by the addition of an external nitrogen source by up to 27.17 ± 2.27% and 22.86 ± 2.4% compared with the monoculture of fungi or microalgae, respectively. This may depend on the effect of synergy between the two species. For the removal of IC from the water, the removal efficiency of the consortium was higher than that of the microalgae by 38.5 ± 0.08%, which may be attributed to the ability of the fungi to aid in the adsorption of nutrients and its assimilation by the microalgae. Therefore, the *Fusarium*-*Chlorella* consortium can effectively degrade PAM, while simultaneously fixing carbon, which provides a feasible scheme for the treatment and carbon neutralization of the wastewater that contains PAM.

KEYWORDS

***Fusarium* sp., *Chlorella* sp., mycelial pellets, fungal-microalgal consortium, polyacrylamide removal**

1. Introduction

Polyacrylamide (PAM) is primarily used in the process of alkali/polymer/surfactant flooding, which results in a large amount of wastewater that contains a concentration of 300–800 mg/L PAM (Song et al., 2021). PAM can be hydrolyzed to form toxic acrylamide monomers, which have been shown to damage the nervous system of humans and animals (Albalawi et al., 2018). Furthermore, the carbon dioxide (CO_2) in the formation is dissolved into the flooding water to form dissolved inorganic carbon (DIC) with a CO_2 equivalent of 3 to 4 kg/m^3. The excessive emissions of CO_2 that cause the greenhouse effect have attracted global attention (Modak et al., 2018). Oversaturated CO_2 in the water poses the risk of escaping into

the atmosphere, thus, affecting the carbon cycle and disrupting the balance of carbon (Giménez-Gómez et al., 2023). Therefore, it is highly necessary to remove the PAM and DIC before the flooding wastewater is discharged.

The current research hotspots on the biodegradation of PAM primarily include two aspects. The first is the use of anaerobic, aerobic or anaerobic-aerobic combination bioreactors to treat PAM, such as sequencing batch reactor (SBR) systems, alkaline pre-fermentation for anaerobic digestion and anaerobic digestion under mesophilic conditions (Liu et al., 2021). Secondly, whether the bacterial strains are used individually or in combination to degrade PAM. In terms of its molecular structure, PAM is composed of main carbon chains and side chain amide groups. The mineralization of PAM requires the degradation of both the main carbon chain and side chain amide groups. Amidases can help microorganisms to degrade amide groups by catalyzing the hydrolysis of amide bonds to form ammonia and carboxylic acids, and these enzymes are produced by a variety of microorganisms, including bacteria, actinomycetes, fungi, and algae. Numerous studies have investigated the biodegradation of PAM by bacterial strains, such as *Bacillus* sp. (Nyyssölä and Ahlgren, 2019), *Acinetobacter* sp. (Zhang et al., 2021) and *Clostridium* sp. (Ma et al., 2010), but to our knowledge, the feasibility of the degradation of PAM by single algae species has not been reported. Similarly, previous studies have shown that the long carbon chains of PAM can be degraded by bacteria. Although there have been few studies on the degradation of long carbon chains of PAM by fungi, these microbes have a strong ability to degrade other complex carbon compounds, including crude oil and polycyclic aromatic hydrocarbons (PAHs) (Zain Ul Arifeen et al., 2022; Saravanan et al., 2023).

Currently, the pollutants in oil flooding wastewater are not limited to PAM but also include soluble inorganic carbon (IC). In previous studies, microalgae have been shown to have a superior ability to remove DIC. Both small and large algae can utilize carbonic anhydrase (CA) to metabolize IC (Vyrides et al., 2018; Thanigaivel et al., 2022). Furthermore, several microalgal species have been found to secrete amidases, including *Chlorella vulgaris, Scenedesmus obliquus, Chlamydomonas reinhardtii, Dunaliella salina,* and *Nannochloropsis oceanica* (Sheng et al., 2022). A fungal-algal particle system is an emerging microbial water treatment technology in which mycelial particles are used as special biological carriers to load algae and then used as microbial materials to treat water. Due to the high efficiency and safety of microbial technology, as well as the resistance to impact and stability of biological materials, it is gradually attracting the attention of researchers (Du et al., 2018; Ma et al., 2021; Li et al., 2023). Many researchers have also proven that fungal-algal pellets are highly efficient at treating organic wastewater (Zhou et al., 2018; Chen et al., 2020). However, few studies have investigated the removal of PAM-containing wastewater using fungi either alone or in a fungal-microalgal consortium.

In this study, *Fusarium* sp. was obtained by screening strains. Subsequently, *Fusarium* sp. and *Chlorella* sp. were co-cultured to form a *Fusarium-Chlorella* consortium. Based on the advantages of microalgae in wastewater treatment described above, this study investigated the differences in the efficiency of pollutant degradation among three different biological systems: single *Fusarium* sp. mycelial pellets, single *Chlorella* sp. and the *Fusarium-Chlorella* consortium in treating synthetic wastewater, as well as whether the addition of nitrogen sources for co-metabolism could enhance the ability of the three biological systems to degrade organic wastewater.

2. Materials and methods

2.1. Preparation of the microbial strains

2.1.1. Culturing of the microalgae

The microalgal species used in this study was *Chlorella sorokiniana* (FACHB-26), which was supplied by the Freshwater Algae Culture Collection at the Institute of Hydrobiology, Chinese Academy of Science (FACHB, Wuhan, China). Sterile Bold's Basal Medium (BBM) (Zhang et al., 2021) supplemented with PAM was used in this study. The species was radiantly acclimatized on a shaker (25 ± 2°C, light intensity of 3,000 l×, 12:12 h light: dark cycle). The initial concentration of PAM was set at 100 mg/L, and the concentration was gradually increased to 400 mg/L during a 20 days acclimatization period. This enabled the species to gradually adapt to the presence of PAM for further experiments.

2.1.2. Isolation and screening of the fungi

The samples used to isolate the filamentous fungi were collected from a revolving algal biofilm (RAB) reactor used to treat the wastewater that contained PAM (Zhang et al., 2021), which had been operating in the laboratory for 1 year. The algal biofilm was collected from the rotary belt of the RAB reactor by scraping, and it was then diluted to 10^{-5} using sterile water and coated on a solid medium with PAM as the sole source of nitrogen. Screened pure strains of fungi were picked for spore inoculation into liquid medium that contained PAM for shake flask domestication. The inoculum of fungal spores was 15%. The liquid medium was composed of 400 mg PAM, 1000 mg glucose, 100 mg $CaCl_2$, 500 mg $MgSO_4$, 500 mg KH_2PO_4, and 20 mL soil (unfertilized garden) suspension (per L) (Chang et al., 2020). The culture period (25 ± 2°C, 150 rpm) lasted for 7 days, and after the formation of complete mycelial pellets, the pellets were collected and transferred to new culture flasks for further acclimation and expansion.

2.1.3. Construction of the fungal-microalgal consortium

The optimal culture conditions for the most stable structure and the highest biomass in the shortest period were obtained after preliminary experiments. The consortium was constructed using the as-prepared synthetic wastewater in a flask culture system with 24 h light exposure (25 ± 2°C, 3,000 l×) and continual shaking at 150 rpm. The preliminary experiments revealed that the stability and biomass of the spheres formed by the inoculation of mycelia were higher than those formed by the inoculation of mycelial spheres that had already formed, and therefore, mycelia were inoculated into the microalgae to form the consortium used in this study. The fungal mycelia can potentially combine with the microalgae through rotation, entanglement, and adsorption to ultimately form a sphere, which resulted in a significant decrease in the microalgal biomass. Therefore, to ensure that the consortium can bind enough microalgal cells, the microalgae were first cultured to achieve a high OD value ($OD_{660} = 0.8$).

To establish whether the synergistic treatment effect of the microbial consortium on the wastewater that contained PAM was better than that of single fungal or microalgal systems, single system

treatment experiments were conducted to compare the degradation by the three systems under the same culture conditions.

2.2. Composition of the synthetic wastewater

The synthetic PAM wastewater used in this study was composed of 400 mg PAM (anionic, molecular weight 3×10^7), 1,000 mg $NaHCO_3$, 100 mg $CaCl_2$, 500 mg $MgSO_4$, 500 mg KH_2PO_4, and 20 mL soil suspension (per L). A control experiment was performed to explore whether the inclusion of a co-metabolic nitrogen source could improve the degradation of PAM in which 750 mg/L urea, 60 mg/L NH_4Cl or 300 mg/L yeast extract were added to the synthetic wastewater and compared to PAM as the sole nitrogen source.

2.3. Analytical methods

The concentration of PAM was determined using the starch cadmium iodide method (Zhao et al., 2019). A total organic carbon analyzer (TOC-VCPH, Shimadzu, Kyoto, Japan) was used to determine the concentrations of IC and TOC.

The removal efficiency (E, %) for the PAM, TOC and IC, which represents the percentage of pollutant mass removed from the influent, was calculated as follows:

$$E = \left[(C0 - C1) / C0 \right] \times 100\%$$

where C_0 and C_1 (mg/L) are the initial and end concentrations, respectively, in the solution.

Liquid samples of the PAM solution before and after sterilization and the HAPM solution after biodegradation were purified using methanol (Bao et al., 2010). The sample was added dropwise to a large excess of methanol, which caused the residual polymer in the sample to precipitate. The precipitated polymer was then filtered and washed twice with methanol before it was dried to a constant weight using a vacuum freeze dryer (SCIENTZ-18ND/A; Scientz Bio-Technology, Ningbo, China). After preparation, these samples were analyzed using Fourier transform infrared spectroscopy (FT-IR) (Thermo Nicolet, Thermo Fisher Scientific, Waltham, MA, United States).

Using a one-way analysis of variance (ANOVA), a statistical analysis was performed on the rates of degradation of PAM to determine significant differences ($p < 0.05$) among the three biological systems. The minimum significant difference between each pair of means was calculated.

The characterization was performed by analyzing the *18S rRNA* genes. The genomic DNA was extracted by collecting the cell precipitates from the original sample using a commercial DNA extraction kit (TGuide OSR-M502, TIANGEN Biotech, Beijing, China). The PCR was performed in a total volume of 50 μL that contained 25 μL polymerase premix (Takara Bio, Shiga, Japan), 1 μL DNA, 22 μL double-distilled H_2O, and 1 μL each of the forward and reverse primers. The PCR amplification was conducted as follows: 95°C for 5 min, followed by 35 cycles of 45 s at 95°C, 45 s at 56°C, and 60 s at 72°C. The 18S rRNA gene was amplified with Fung and NS1 primers (Fung: 5′-ATTCCCCGTTACCCGTTG-3′; NS1: 5′-GTAGTCATATGCTTGTCTC-3′). The samples were sequenced using an ABI PRISM 3100 Genetic Analyzer (Applied Biosciences, Waltham, MA, United States). The sequenced fragments were analyzed by the program Staden Package 2.0.0b to obtain a consensus sequence. The consensus sequence was searched in GenBank using BLASTn. The sequence data of the strains obtained were uploaded to GenBank under the accession number OR426650.

3. Results and discussion

3.1. Isolation, identification and performance of the fungal strain used to degrade PAM

3.1.1. Fungal isolation and identification

The pure strains were inoculated onto an inclined surface medium to detect the samples. After PCR amplification, the gene sequence that was isolated was identified as a species of *Fusarium* (Supplementary material). Fungi have mycelia, which use a process of winding and adsorption to form stable mycelial pellets in culture (Figure 1A). Compared with the use of single microbial strains to remove pollutants, the morphology and large specific surface area of the mycelial pellets enables greater contact and assimilation of the pollutants in wastewater (Li et al., 2023). More importantly, the formation of mycelial pellets is more conducive to the rapid separation of organisms and wastewater, which facilitates the reuse of microorganisms (Zhou et al., 2018). On this basis, the *Fusarium* mycelial pellet was used to package suspended algal cells, which consisted of the *Fusarium* mycelial pellet, and can effectively improve the ability to separate the algal cells and solution to achieve the goal of reusing them (Chen et al., 2020).

3.1.2. Effect of the fungal mycelial in the synthetic flooding wastewater to degrade PAM

During isolation of the fungal strain, fungal growth was achieved on the plate when PAM was used as the sole nitrogen source, indicating that the isolated strain could effectively utilize PAM for its growth. The degradation of PAM was significantly affected by the addition of different co-metabolic nitrogen sources within 10 days of the completion of culture cycle (Figure 1B). The rate of degradation of PAM was the highest in the experimental group with added urea, which reached 53.76 ± 2.97%, and corresponded to a reduction in the concentration of PAM by approximately 200 mg/L. The rate of degradation of PAM reached 49.88 ± 3.2% in the experimental group with the addition of NH_4Cl and 46.69 ± 0.57% with the addition of yeast extract, while only 26.74 ± 1.46% of the PAM was degraded when PAM was used as the sole nitrogen source.

A previous study showed that the process of PAM biodegradation begins with deamination by amidase catalysis (Nyyssölä and Ahlgren, 2019). As a polymeric compound, PAM cannot enter the intracellular portion of the *Fusarium* sp. cells through biofilms (Zhao et al., 2020). Therefore, when PAM is used as the sole source of nitrogen, *Fusarium* sp. cannot secrete many extracellular enzymes for a short time, thus, the efficiency of PAM degradation was the lowest. Furthermore, the addition of co-metabolic nitrogen sources could ensure the rapid growth of biomass, which results in the secretion of more extracellular amidase, thereby effectively improving the degradation of PAM. Therefore, the addition of a co-metabolic nitrogen source can promote the secretion of extracellular amidase, thereby improving the

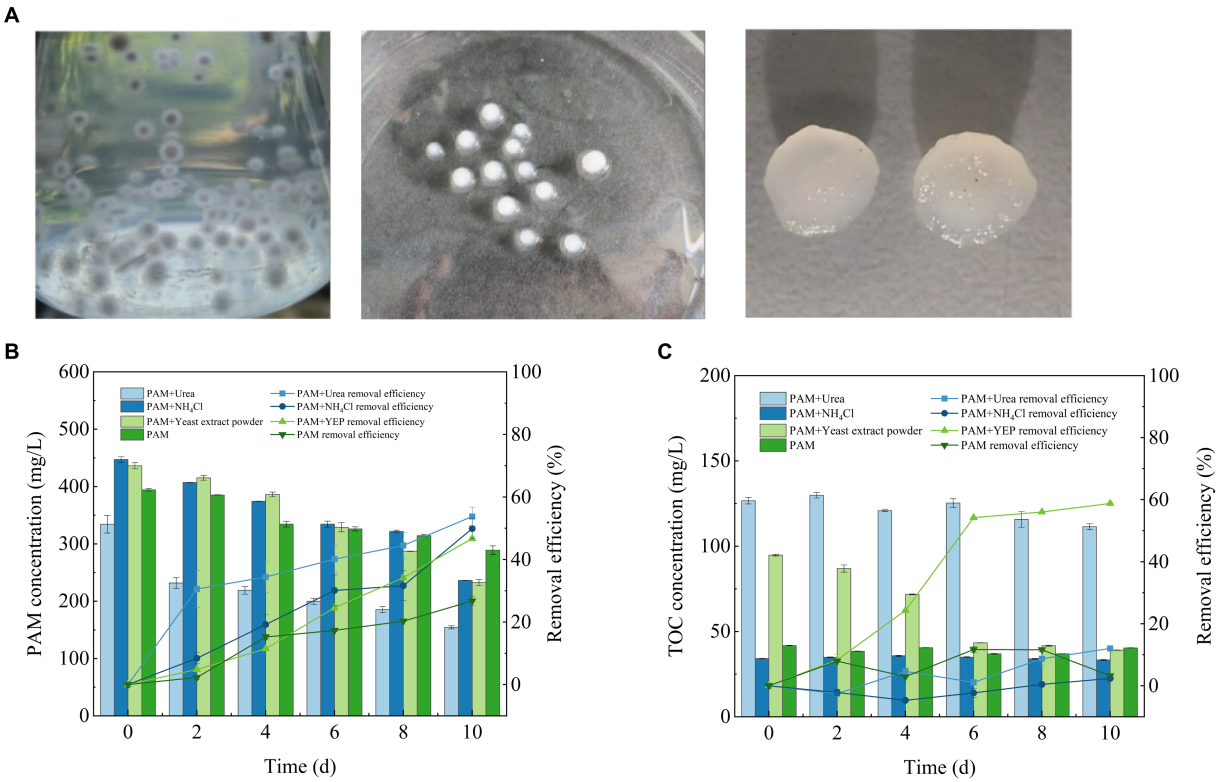

FIGURE 1
Fusarium mycelial pellet morphology **(A)** and its ability to remove PAM and TOC **(B)** PAM and **(C)** TOC. PAM, polyacrylamide; TOC, total organic carbon.

rate of degradation of PAM to some extent. The addition of urea promotes the secretion of extracellular amidase enzymes by *Fusarium* sp. and improves the rate of degradation of PAM, which is consistent with the findings of a previous study (Bao et al., 2010).

3.1.3. Ability of the mycelial pellets to remove TOC in the synthetic flooding wastewater

During the culture period, the efficiency of TOC removal from the synthetic wastewater by *Fusarium* sp. exhibited significant differences when different co-metabolic nitrogen sources were added (Figure 1C). The concentration of TOC was significantly reduced in the experimental groups supplemented with yeast extract, which reached removal efficiencies of 58.77 ± 0.35%. The TOC removal efficiency in the other three groups was only approximately 10%. Compared with the other three nitrogen sources, yeast extract contains not only nitrogen but also many trace elements and growth factors, such as nucleosides and amino acids among others. It is hypothesized that these growth factors and trace elements are more conducive to the growth of fungi, which facilitates the synergistic degradation of PAM.

3.2. Performance of *Chlorella* sp. at treating synthetic flooding wastewater

3.2.1. Growth curve of *Chlorella* sp. in the synthetic flooding wastewater

The change in algal biomass during the 6 days incubation period is shown in Figure 2A. Algal cultures exhibited significant growth when different co-metabolic nitrogen sources were added and reached a stable biomass until approximately 5 days before they started to decline.

3.2.2. Ability of *Chlorella* sp. to degrade PAM in the synthetic flooding wastewater

The degradation of PAM by *Chlorella* sp. was also affected by the addition of a co-metabolic nitrogen source (Figure 2B). The rate of degradation of PAM reached 58.07 ± 3.1% when supplemented with NH_4Cl, 48.11 ± 1.05% when supplemented with yeast extract, 38.2 ± 0.27% when supplemented with urea and 40.28 ± 2.83% when PAM was used as the sole nitrogen source. To remove the organic nitrogen, algae first degraded it into ammonia using various enzymes, which enables it to then be absorbed by the algal cells (Simsek et al., 2016). These results indicate that the algae *Chlorella* sp. had a stronger ability to utilize inorganic nitrogen sources than those of organic nitrogen, although the degradation of PAM was effectively promoted by the addition of an external nitrogen source, regardless of whether it was organic or inorganic.

3.2.3. Ability of *Chlorella* sp. to remove TOC and IC in the synthetic flooding wastewater

The ability of *Chlorella* sp. to remove TOC was significantly reduced during the 6 days culture cycle (Figure 2C). The rate of TOC removal reached 7.9 ± 1.28% when the system was supplemented with urea, −35.09 ± 2.72% when supplemented with NH_4Cl, 55.08 ± 0.14% when supplemented with yeast extract, and −24.5 ± 4.32% when PAM was used as the sole nitrogen source. This result shows that the

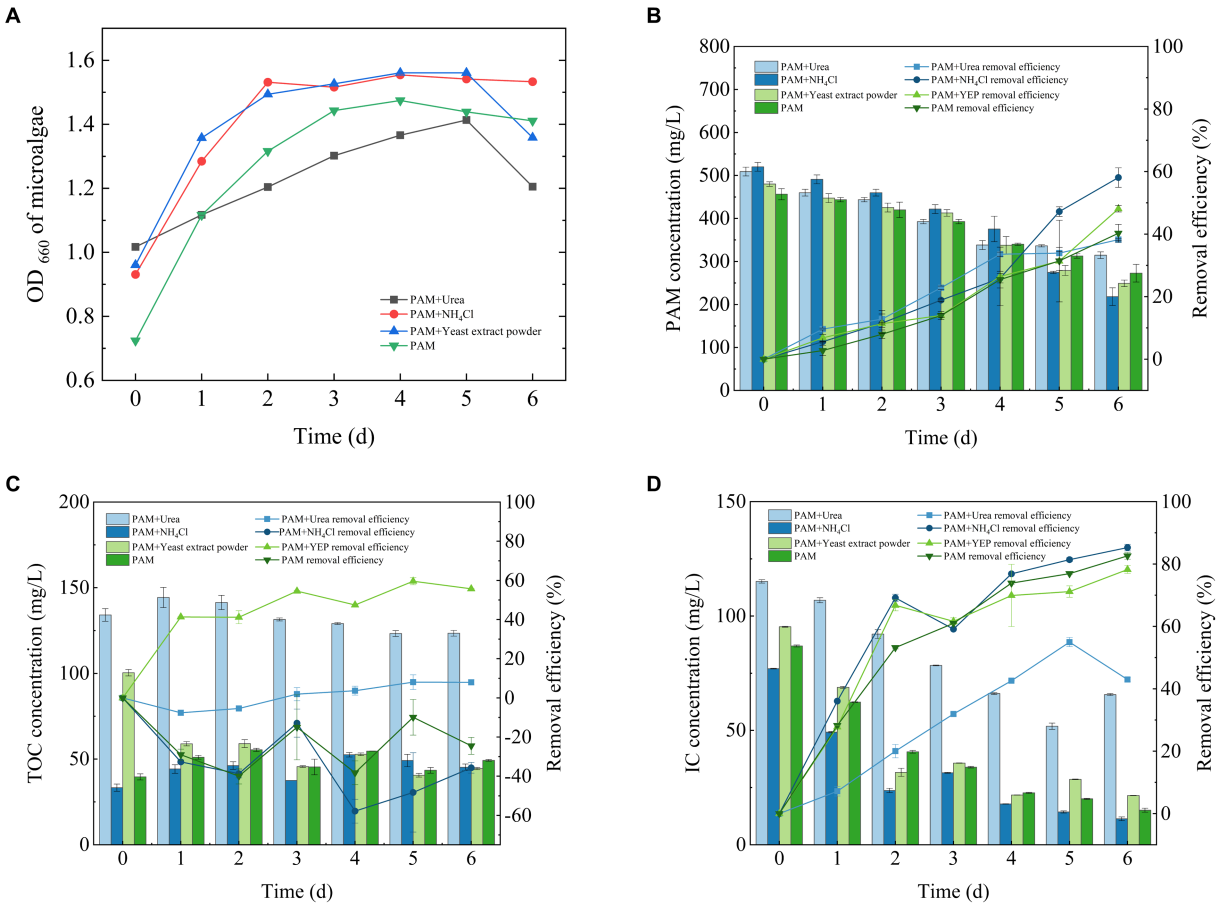

FIGURE 2
Growth curve of *Chlorella* sp. **(A)** and its ability to remove **(B)** PAM, **(C)** TOC and **(D)** IC. IC, inorganic carbon; PAM, polyacrylamide; TOC, total organic carbon.

microalgae were more effective at degrading TOC when adequate nutrients were available. However, as the experimental period extended, the organic matter generated by microalgal physiological activity accumulated, which led to a potential decrease in the efficiency of TOC removal and an increase in the levels of TOC.

During the culture period, *Chlorella* sp. was highly efficient at removing the IC from wastewater that contained PAM (Figure 2D). Approximately 90% of the IC was removed, which confirmed the suitability of the system for carbon sequestration. The efficiency of the IC removal was 42.97 ± 0.74% when the system was supplemented with urea, 85.28 ± 1.05% when supplemented with NH_4Cl, 79.14 ± 0.02% when supplemented with yeast extract and 82.62 ± 1.09% when PAM was used as the sole nitrogen source. This result also corresponds to a previous study that showed that microalgae are highly effective at fixing IC (Saravanan et al., 2022).

Chlorella can use both organic and IC sources (Nasir et al., 2015). A comparison of Figures 2C,D shows that when urea and yeast extract were used as co-metabolic nitrogen sources, the organic carbon in them could be utilized by *Chlorella*, thereby reducing the fixation of DIC in solution. Therefore, when urea and yeast extract were used as co-metabolic nitrogen sources, the TOC was removed when both nitrogen sources were used, but there was little removal of DIC. With ammonium chloride as a common metabolic nitrogen source and PAM as the only nitrogen source, there was little TOC in the system; *Chlorella* had to use DIC for growth, and during the process of growth, it secretes extracellular polymers, such as polysaccharides and proteins among others (Zhu et al., 2012). As a result, the two groups of TOC were negative, but the efficiency of the DIC fixed was positive.

3.3. Effectiveness of the *Fusarium-Chlorella* consortium at treating the synthetic flooding wastewater

3.3.1. Morphology of the fungal-microalgal consortium pellets

A previous study has described the mechanism of flocculation of the actinomycete *Streptomyces* sp. hsn06 on *Chlorella vulgaris* (Li et al., 2017) and demonstrated the potential ability of both microalgae and fungi to flocculate. Microalgae are mostly adsorbed onto the surface of mycelial pellets, while only a small number of microalgal cells exist within the internal structure of the fungal-microalgal consortium pellets (Figure 3A). This was consistent with the findings of previous research (Leng et al., 2021). The ratio of microalgae to fungi was 2:1. The final consortium sphere that was formed adsorbed a large number of microalgal cells with a dense and stable structure that exhibited

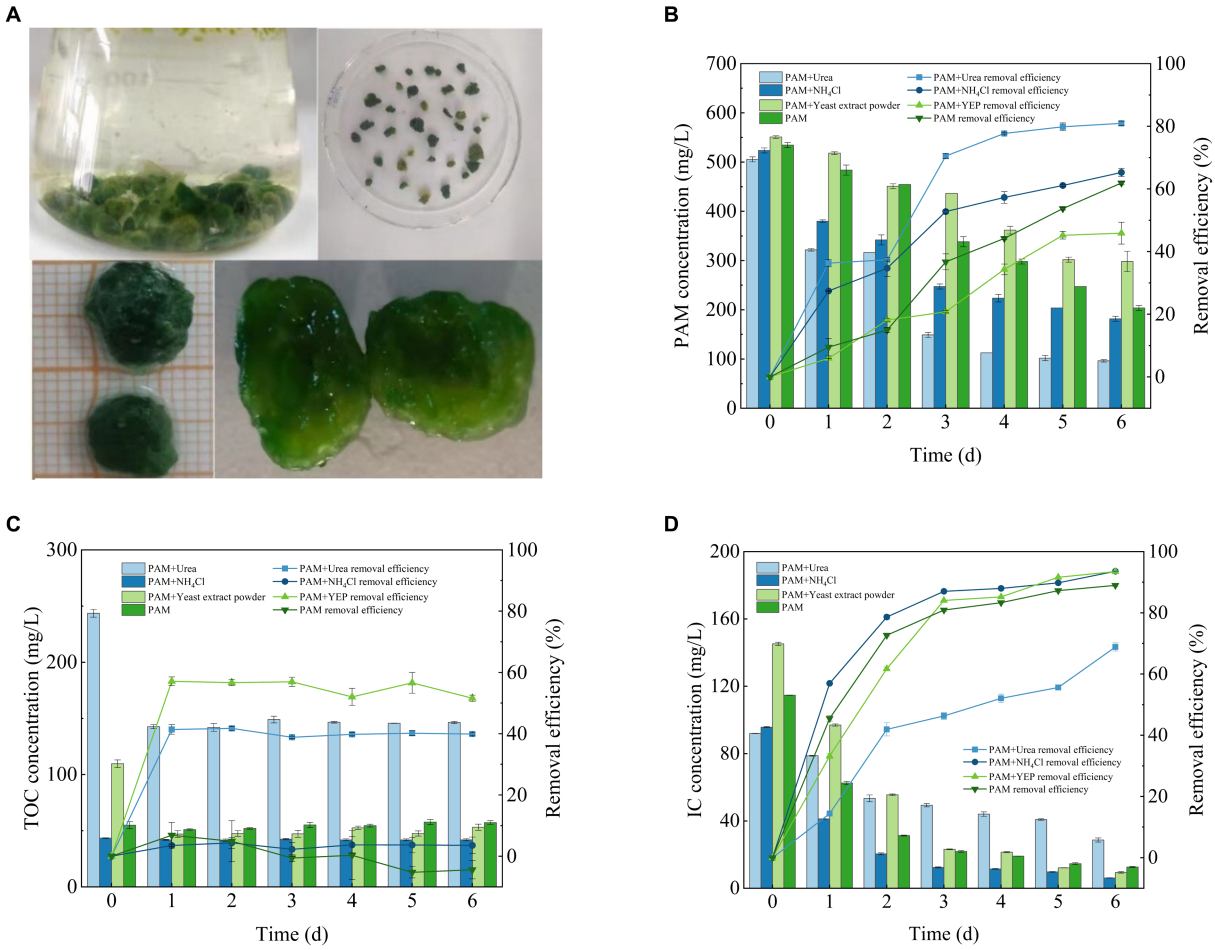

FIGURE 3
Fusarium-Chlorella consortium morphology **(A)** and its ability to remove **(B)** PAM, **(C)** TOC and **(D)** IC. IC, inorganic carbon; PAM, polyacrylamide; TOC, total organic carbon.

excellent settling performance (Figure 3A). This is advantageous for the subsequent harvesting of the algal biomass. The consortium was subjected to stability experiments in a gas column with an aeration rate of 135 L/min, and the consortium could remain stable without disintegrating for 48 h.

3.3.2. Ability of the *Fusarium-Chlorella* consortium to degrade PAM

The results described above showed that both algae and fungi could degrade PAM separately, and the performance of the *Fusarium-Chlorella* consortium at degrading PAM was higher than the performance of single systems (Figure 3B). The rate of degradation of PAM reached 80.93 ± 0.7% when the system was supplemented with urea, 65.27 ± 1.32% when supplemented with NH_4Cl, 45.88 ± 3.48% when supplemented with yeast extract and 61.91 ± 0.6% when PAM was used as the sole nitrogen source. Overall, the concentration of PAM decreased significantly, and the rate of degradation reached 80%, which indicated that the *Fusarium-Chlorella* consortium had a significant effect on the degradation of PAM. Previous studies have shown that fungal-microalgal consortia have been widely used in wastewater treatment (Muradov et al., 2015), and the results of this study confirmed that the microbial consortium was highly adaptable to wastewater that contained PAM, which made it suitable for use in conditions where PAM is the sole nitrogen source available for growth.

3.3.3. Ability of the *Fusarium-Chlorella* consortium to remove TOC and IC

The ability of the *Fusarium-Chlorella* consortium to remove TOC clearly differed when cultured with different co-metabolic nitrogen sources (Figure 3C). The rate of TOC removal reached 39.9 ± 0.41% when supplemented with urea, 3.56 ± 2.72% when supplemented with NH_4Cl, 51.58 ± 1.05% when supplemented with yeast extract and −4.4 ± 3.0% when PAM was used as the sole source of nitrogen. Therefore, the experimental groups supplemented with organic nitrogen sources provided another source of TOC in addition to PAM, which resulted in a significant decrease in the concentration of TOC. This may be due to the full utilization of additional sources of organic nitrogen. However, in the experimental groups where the inorganic nitrogen sources were supplemented or PAM was used as the sole nitrogen source, the concentration of TOC remained relatively stable with no significant changes observed. This may be attributed to the accumulation of some organic compounds that resulted from microbial metabolism during the cultivation period that were not utilized.

The degradation of IC by the *Fusarium-Chlorella* consortium over the 6 days culture period is shown in Figure 3D. The rate of IC removal reached 68.83 ± 1.32% in the group supplemented with urea, 93.58 ± 0.06% when supplemented with NH_4Cl, 93.48 ± 0.27% when supplemented with yeast extract and 88.97 ± 0.36% when PAM was used as the sole nitrogen source. Overall, the synergistic performance of the *Fusarium-Chlorella* consortium to treat IC was better than that of the single *Chlorella* sp. system with the ability to sequester carbon providing obvious advantages. These findings prove that the mechanisms of biodegradation by microalgae and fungi have synergistic effects, which results in their effective combination for wastewater treatment (Wang et al., 2022).

An analysis of the differences in the degradation efficiency of PAM among three different biological systems that did not include co-metabolic nitrogen sources was conducted. The results demonstrated a significant difference ($p = 0.003$) in the degradation capability among the three systems. This indicates that different biological systems exhibit significantly different abilities to degrade PAM, and the efficiency of the consortium to degrade PAM is significantly higher than that of a single system.

According to China's Petrochemical Pollutant Discharge Standard (GB31570-2015, China), the concentrations of PAM and IC in effluent are not clearly required, while the relevant stipulated parameter is the chemical oxygen demand (COD). In the GB31570-2015, the COD discharge standard in oil flooding wastewater requires less than 100 mg/L. The COD values of the simulated flooding wastewater treated by mycelia were usually between 150 mg/L and 200 mg/L, which cannot directly reach the standard. However, in practical applications, oil flooding wastewater is treated by combining a variety of treatment processes, such as anaerobic baffled treatment process and aerobic biofilm treatment process among others (Sang et al., 2015; Song et al., 2018, 2019). In practice, the mycelial pellet can be combined with various processes to successfully process the DIC.

3.4. Mechanisms for the removal of pollutants

3.4.1. Functional group analysis of PAM after biodegradation

To investigate the structural changes to PAM molecules after sterilization and biodegradation, the FT-IR spectra of different PAM samples were analyzed (Figure 4). The peaks observed at 1115, 1616, 1,666 and 3,200 cm^{-1} in the spectrum of PAM corresponded to the existence of C–N, N–H, C=O bonds and amide groups (Bao et al., 2010; Zhao et al., 2019).

A comparison of the FT-IR spectra for all three samples showed that the peaks that represented the C–N bonds, N–H bonds, C=O bonds and -NH_2 gradually disappeared, indicating that the side chains and amide groups of PAM were degraded. Furthermore, the peak that represented methylene at 1456 cm^{-1} also gradually disappeared, indicating that the carbon backbone of PAM was also degraded. Furthermore, upon comparing the spectra of the three samples between 3,100 cm^{-1} and 3,500 cm^{-1}, it was observed that the peaks had become wider. This indicated that the amide group had degraded into a carboxyl group (Bao et al., 2010). In comparison to the PAM degradation effects of high temperature sterilization and biodegradation, it was apparent that high temperature sterilization has some effect at degrading PAM, and the subsequent biodegradation fully degraded the PAM.

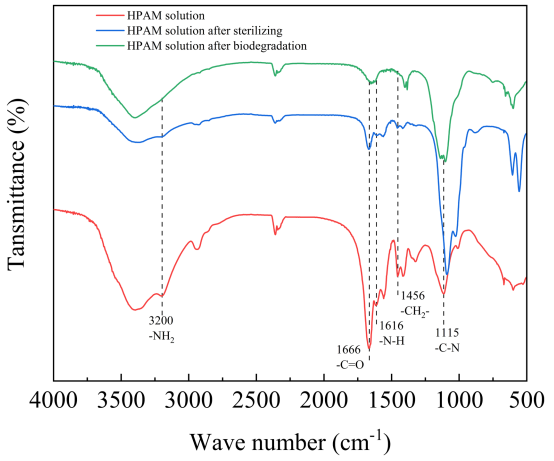

FIGURE 4
FT-IR analysis of PAM before and after biodegradation by the *Fusarium-Chlorella* consortium. FT-IR, Fourier transform infrared spectroscopy; PAM, polyacrylamide.

3.4.2. Possible mechanisms for the removal of PAM and IC

Based on the studies described above, three possible mechanisms for the removal of PAM, as well as that of the IC, by the biological systems were initially proposed.

When the experimental group without the use of additional nitrogen sources was used as an example, according to the metabolic pathway proposed in a previous study (Zhao et al., 2019) and the FT-IR results described above, the side chains of PAM were cleaved, which may be due to the role of extracellular amidases secreted by the microalgae and fungi to convert the amide group to carboxylate group; however, there was no carboxylate group that bound intramolecularly, which was slightly different from the findings of previous studies (Sang et al., 2015). Alternatively, it also proved that the microorganisms in this study could grow using PAM as the sole nitrogen source. In addition, the biomass still grew without the addition of an organic nitrogen source, and the FT-IR results showed that the main carbon chain of PAM was cleaved, which might be the result of the catalytic degradation of this carbon chain of PAM by a monooxygenase secreted by the microorganisms (Zhao et al., 2019). It also showed that PAM can be used as the sole source of carbon for microbial growth.

To remove the IC, we primarily rely on the biological fixation of IC by the microalgae in soluble carbonate compounds, such as $NaHCO_3$ (Molazadeh et al., 2019). Research has shown that microalgae primarily use CA to metabolize IC (Thanigaivel et al., 2022). In the Calvin cycle, microalgae absorb CO_2 and synthesize organic compounds to fix CO_2, and when the CO_2 dissolves, it converts the carbon into various forms of IC, thereby enabling the microalgae to remove the IC.

4. Conclusion

The assisted flocculation of the fungal spores can effectively immobilize the microalgal cells and achieve a stable consortium in a

short culture cycle. The removal effect of the *Fusarium-Chlorella* consortium for PAM and IC was much better than that of the two separate culture systems, and the efficiency of degradation of the pollutants could be significantly improved by the addition of an additional nitrogen source. The effluent of the degraded water was free of toxic byproducts, and the whole process was inexpensive and highly efficient, and it also provided ideas for the effective recovery of microalgae.

Data availability statement

The datasets presented in this study can be found in online repositories. The names of the repository/repositories and accession number(s) can be found below: GenBank, OR426650.

Author contributions

HZ: Funding acquisition, Writing – original draft. MS: Formal analysis, Investigation, Writing – original draft. CZ: —. ZP: —. ZA: Funding acquisition, Writing – review & editing.

Funding

The author(s) declare financial support was received for the research, authorship, and/or publication of this article. This study was supported by the National Natural Science Foundation of China (51704260), the Major Research and Development Projects of Shandong Province (2018GSF117045) and Project of Shandong Province Higher Educational Science and Technology Program (J17KB060).

Conflict of interest

ZP was employed by The Architectural Design and Research Institute of HIT Co., Ltd..

The remaining authors declare that the research was conducted in the absence of any commercial or financial relationships that could be construed as a potential conflict of interest.

Publisher's note

Supplementary material

The Supplementary material for this article can be found online at: https://www.frontiersin.org/articles/10.3389/fmicb.2023.1270658/full#supplementary-material

References

Albalawi, A., Alhasani, R. H. A., Biswas, L., Reilly, J., Akhtar, S., and Shu, X. (2018). Carnosic acid attenuates acrylamide-induced retinal toxicity in zebrafish embryos. *Exp. Eye Res.* 175, 103–114. doi: 10.1016/j.exer.2018.06.018

Bao, M., Chen, Q., Li, Y., and Jiang, G. (2010). Biodegradation of partially hydrolyzed polyacrylamide by bacteria isolated from production water after polymer flooding in an oil field. *J. Hazard. Mater.* 184, 105–110. doi: 10.1016/j.jhazmat.2010.08.011

Chang, C., Zhang, J., Liu, T., Song, K., Xie, J., Luo, S., et al. (2020). Rhizosphere fungal communities of wild and cultivated soybeans grown in three different soil suspensions. *Appl. Soil Ecol.* 153:103586. doi: 10.1016/j.apsoil.2020.103586

Chen, J., Ding, L., Liu, R., Xu, S., Li, L., Gao, L., et al. (2020). Hydrothermal carbonization of microalgae-fungal pellets: removal of nutrients from the aqueous phase fungi and microalgae cultivation. *ACS Sustain. Chem. Eng.* 8, 16823–16832. doi: 10.1021/acssuschemeng.0c05441

Du, Z. Y., Alvaro, J., Hyden, B., Zienkiewicz, K., Benning, N., Zienkiewicz, A., et al. (2018). Enhancing oil production and harvest by combining the marine alga *Nannochloropsis oceanica* and the oleaginous fungus *Mortierella elongata*. *Biotechnol. Biofuels* 11:174. doi: 10.1186/s13068-018-1172-2

Giménez-Gómez, P., Hättestrand, I., Sjöberg, S., Dupraz, C., Richardson, S., and Pamme, N. (2023). Distance-based paper analytical device for the determination of dissolved inorganic carbon concentration in freshwater. *Sens. Actuators B* 385:133694. doi: 10.1016/j.snb.2023.133694

Leng, L., Li, W., Chen, J., Leng, S., Chen, J., Wei, L., et al. (2021). Co-culture of fungi-microalgae consortium for wastewater treatment: a review. *Bioresour. Technol.* 330:125008. doi: 10.1016/j.biortech.2021.125008

Li, L., Liang, T., Qiu, S., Zhang, Y., Qu, J., Liu, T., et al. (2023). A rapid and simplified method for evaluating the performance of fungi-algae pellets: a hierarchical analysis model. *Sci. Total Environ.* 860:160442. doi: 10.1016/j.scitotenv.2022.160442

Li, Y., Xu, Y., Zheng, T., and Wang, H. (2017). Flocculation mechanism of the actinomycete Streptomyces sp. hsn06 on *Chlorella vulgaris*. *Bioresour. Technol.* 239, 137–143. doi: 10.1016/j.biortech.2017.05.028

Liu, X., Fu, Q., Liu, Z., Zeng, T., Du, M., He, D., et al. (2021). Alkaline pre-fermentation for anaerobic digestion of polyacrylamide flocculated sludge: simultaneously enhancing methane production and polyacrylamide degradation. *Chem. Eng. J.* 425:131407. doi: 10.1016/j.cej.2021.131407

Ma, L., Hu, T., Liu, Y., Liu, J., Wang, Y., Wang, P., et al. (2021). Combination of biochar and immobilized bacteria accelerates polyacrylamide biodegradation in soil by both bio-augmentation and bio-stimulation strategies. *J. Hazard. Mater.* 405:124086. doi: 10.1016/j.jhazmat.2020.124086

Ma, Y., Yu, H., Pan, W., Liu, C., Zhang, S., and Shen, Z. (2010). Identification of nitrile hydratase-producing *Rhodococcus ruber* TH and characterization of an amiE-negative mutant. *Bioresour. Technol.* 101, 285–291. doi: 10.1016/j.biortech.2009.07.057

Modak, N. M., Ghosh, D. K., Panda, S., and Sana, S. S. (2018). Managing green house gas emission cost and pricing policies in a two-echelon supply chain. *CIRP. J. Manuf. Sci. Technol.* 20, 1–11. doi: 10.1016/j.cirpj.2017.08.001

Molazadeh, M., Ahmadzadeh, H., Pourianfar, H. R., Lyon, S., and Rampelotto, P. H. (2019). The use of microalgae for coupling wastewater treatment with CO_2 biofixation. *Front. Bioeng. Biotechnol.* 7:42. doi: 10.3389/fbioe.2019.00042

Muradov, N., Taha, M., Miranda, A. F., Wrede, D., Kadali, K., Gujar, A., et al. (2015). Fungal-assisted algal flocculation: application in wastewater treatment and biofuel production. *Biotechnol. Biofuels* 8:24. doi: 10.1186/s13068-015-0210-6

Nasir, N. M., Bakar, N. S. A., Lananan, F., Abdul Hamid, S. H., Lam, S. S., and Jusoh, A. (2015). Treatment of African catfish, *Clarias gariepinus* wastewater utilizing phytoremediation of microalgae, *Chlorella* sp. with *Aspergillus niger* bio-harvesting. *Bioresour. Technol.* 190, 492–498. doi: 10.1016/j.biortech.2015.03.023

Nyyssölä, A., and Ahlgren, J. (2019). Microbial degradation of polyacrylamide and the deamination product polyacrylate. *Int. Bioteder. Biodegrad.* 139, 24–33. doi: 10.1016/j.ibiod.2019.02.005

Sang, G., Pi, Y., Bao, M., Li, Y., and Lu, J. (2015). Biodegradation for hydrolyzed polyacrylamide in the anaerobic baffled reactor combined aeration tank. *Ecol. Eng.* 84, 121–127. doi: 10.1016/j.ecoleng.2015.07.028

Saravanan, A., Deivayanai, V. C., Senthil Kumar, P., Rangasamy, G., and Varjani, S. (2022). CO_2 bio-mitigation using genetically modified algae and biofuel production towards a carbon net-zero society. *Bioresour. Technol.* 363:127982. doi: 10.1016/j.biortech.2022.127982

Saravanan, A., Karishma, S., Kumar, P. S., and Rangasamy, G. (2023). Biodegradation of oil-contaminated aqueous ecosystem using an immobilized fungi biomass and kinetic study. *Environ. Res.* 220:115252. doi: 10.1016/j.envres.2023.115252

Sheng, Y., Benmati, M., Guendouzi, S., Benmati, H., Yuan, Y., Song, J., et al. (2022). Latest eco-friendly approaches for pesticides decontamination using microorganisms and consortia microalgae: a comprehensive insights, challenges, and perspectives. *Chemosphere* 308:136183. doi: 10.1016/j.chemosphere.2022.136183

Simsek, H., Kasi, M., Ohm, J.-B., Murthy, S., and Khan, E. (2016). Impact of solids retention time on dissolved organic nitrogen and its biodegradability in treated wastewater. *Water Res.* 92, 44–51. doi: 10.1016/j.watres.2016.01.041

Song, T., Li, S., Ding, W., Li, H., Bao, M., and Li, Y. (2018). Biodegradation of hydrolyzed polyacrylamide by the combined expanded granular sludge bed reactor-aerobic biofilm reactor biosystem and key microorganisms involved in this bioprocess. *Bioresour. Technol.* 263, 153–162. doi: 10.1016/j.biortech.2018.04.121

Song, T., Li, S., Jin, J., Yin, Z., Lu, Y., Bao, M., et al. (2019). Enhanced hydrolyzed polyacrylamide removal from water by an aerobic biofilm reactor-ozone reactor-aerobic biofilm reactor hybrid treatment system: performance, key enzymes and functional microorganisms. *Bioresour. Technol.* 291:121811. doi: 10.1016/j.biortech.2019.121811

Song, T. W., Li, S. S., Yin, Z. C., Bao, M. T., Lu, J. R., and Li, Y. (2021). Hydrolyzed polyacrylamide-containing wastewater treatment using ozone reactor-up flow anaerobic sludge blanket reactor-aerobic biofilm reactor multistage treatment system. *Environ. Pollut.* 269:116111. doi: 10.1016/j.envpol.2020.116111

Thanigaivel, S., Vickram, S., Manikandan, S., Deena, S. R., Subbaiya, R., Karmegam, N., et al. (2022). Sustainability and carbon neutralization trends in microalgae bioenergy production from wastewater treatment: a review. *Bioresour. Technol.* 364:128057. doi: 10.1016/j.biortech.2022.128057

Vyrides, I., Andronikou, M., Kyprianou, A., Modic, A., Filippeti, A., Yiakoumis, C., et al. (2018). CO_2 conversion to CH_4 using zero valent iron (ZVI) and anaerobic granular sludge: optimum batch conditions and microbial pathways. *J. CO_2 Util.* 27, 415–422. doi: 10.1016/j.jcou.2018.08.023

Wang, S.-K., Yang, K.-X., Zhu, Y.-R., Zhu, X.-Y., Nie, D.-F., Jiao, N., et al. (2022). One-step co-cultivation and flocculation of microalgae with filamentous fungi to valorize starch wastewater into high-value biomass. *Bioresour. Technol.* 361:127625. doi: 10.1016/j.biortech.2022.127625

Zain Ul Arifeen, M., Ma, Y., Wu, T., Chu, C., Liu, X., Jiang, J., et al. (2022). Anaerobic biodegradation of polycyclic aromatic hydrocarbons (PAHs) by fungi isolated from anaerobic coal-associated sediments at 2.5 km below the seafloor. *Chemosphere* 303:135062. doi: 10.1016/j.chemosphere.2022.135062

Zhang, H., Li, X., An, Z., Liu, Z., Tang, C., and Zhao, X. (2021). Treatment of polyacrylamide-polluted wastewater using a revolving algae biofilm reactor: pollutant removal performance and microbial community characterization. *Bioresour. Technol.* 332:125132. doi: 10.1016/j.biortech.2021.125132

Zhao, L., Song, T., Han, D., Bao, M., and Lu, J. (2019). Hydrolyzed polyacrylamide biotransformation in an up-flow anaerobic sludge blanket reactor system: key enzymes, functional microorganisms, and biodegradation mechanisms. *Bioprocess Biosyst. Eng.* 42, 941–951. doi: 10.1007/s00449-019-02094-w

Zhao, L., Zhang, C., Lu, Z., Bao, M., and Lu, J. (2020). Key role of different levels of dissolved oxygen in hydrolyzed polyacrylamide bioconversion: focusing on metabolic products, key enzymes and functional microorganisms. *Bioresour. Technol.* 306:123089. doi: 10.1016/j.biortech.2020.123089

Zhou, K., Zhang, Y., and Jia, X. (2018). Co-cultivation of fungal-microalgal strains in biogas slurry and biogas purification under different initial CO_2 concentrations. *Sci. Rep.* 8:7786. doi: 10.1038/s41598-018-26141-w

Zhu, L., Qi, H., Lv, M., Kong, Y., Yu, Y., and Xu, X. (2012). Component analysis of extracellular polymeric substances (EPS) during aerobic sludge granulation using FTIR and 3D-EEM technologies. *Bioresour. Technol.* 124, 455–459. doi: 10.1016/j.biortech.2012.08.059

frontiers | Frontiers in Microbiology

TYPE Original Research
PUBLISHED 04 December 2023
DOI 10.3389/fmicb.2023.1307727

OPEN ACCESS

EDITED BY
Zhaoming Zheng,
Beijing University of Technology, China

REVIEWED BY
Yandong Yang,
Qingdao University of Technology, China
Huan Liu,
University of Technology Sydney, Australia
Xiaoxia Wang,
Qingdao University, China

*CORRESPONDENCE
Steven N. Liss
✉ steven.liss@torontomu.ca

RECEIVED 05 October 2023
ACCEPTED 16 November 2023
PUBLISHED 04 December 2023

CITATION
Aqeel H, Asefa B and Liss SN (2023) *Nitrospira* dominant pin-point flocs with granule-like settleability in stirred tank reactors with oxic/hypoxic/oxic zones.
Front. Microbiol. 14:1307727.
doi: 10.3389/fmicb.2023.1307727

Nitrospira dominant pin-point flocs with granule-like settleability in stirred tank reactors with oxic/hypoxic/oxic zones

Hussain Aqeel[1], Bruke Asefa[1] and Steven N. Liss[1,2,3]*

[1]Chemistry and Biology, Toronto Metropolitan University, Toronto, ON, Canada, [2]School of Environmental Studies, Queen's University, Kingston, ON, Canada, [3]Department of Microbiology, Stellenbosch University, Stellenbosch, Western Cape, South Africa

The characteristics of biomass and microbial community dynamics, in relation to autotrophic nitrification, were studied in two 20 L stirred tank reactors (STR) with oxic/hypoxic/oxic zones. The bioreactors were fed with synthetic wastewater with stepwise increasing ammonia concentrations (50–200 N mg/L) without organic substrate in the first phase (autotrophic phase) for 35 days (R1) and 15 days (R2), followed by a heterotrophic phase (with supplementation of organic substrate). The settling properties of the biomass, represented by pin-point flocs, gradually improved in both reactors during the autotrophic phase. The pin-point flocs of R1 exhibited granule-like settling properties. The SVI_{30} in RI gradually improved to 29 mL/g MLSS, and the corresponding SVI_{30}/ SVI_{10} gradually improved to 0.88 during the autotrophic phase. The settling properties of the biomass deteriorated in both bioreactors during the heterotrophic phase. The protein to polysaccharide ratio (PN:PS ratio) gradually increased in the extracted EPS (in both, loosely bound (LB) and tightly bound (TB) EPS) during the autotrophic phase, in both bioreactors. The TB:LB EPS ratio was higher when the pin-point flocs of R1 showed granule-like settling properties, followed by a decline in TB:LB EPS ratio during the heterotrophic phase. A combination of molecular approaches (droplet digital-PCR (dd-PCR) and 16S rRNA gene sequencing) revealed that *Nitrospira* were the predominant nitrifying bacteria in the pin-point flocs that show granular sludge-like settling properties during autotrophic phase in R1. Comammox *Nitrospira* was the dominant ammonia oxidizer in seed biomass and at low ammonia concentrations in both bioreactors. The relative abundance of canonical ammonia-oxidizing bacteria increased with an increase in influent-ammonia concentrations.

KEYWORDS

autotrophic nitrification, comammox *Nitrospira*, pin-point flocs, tightly bound/ loosely bound EPS, ammonia removal, microbial community dynamics

Introduction

Ammonia, produced as a by-product in various domestic and industrial sources, such as agricultural and commercial processes, when released into the environment can lead to effects on human and ecosystem health (Soler et al., 2021). The ineffective removal of ammonia in wastewater treatment can result in eutrophication, as a result of increasing populations, and subsequently reducing oxygen levels that harm aquatic ecosystems (Ronan et al., 2021).

Conventional biological ammonia removal is a two-step process, i.e., nitrification and denitrification. Nitrification is a bottleneck in ammonia removal processes because nitrifiers compete with the heterotrophs for space and nutrients in the outer layers of biofilms and flocs. Autotrophic nitrifiers are slow-growing and are more prone to washout (Aqeel et al., 2019; Ronan et al., 2021; Christiaens et al., 2022). It has been reported that the proportion of nitrifying bacteria in wastewater treatment systems is as low as 0.4%, which is below the detection limit of certain molecular techniques such as dot blot and DNA hybridization (Dionisi et al., 2002). The nitrifiers are sensitive to fluctuations in operation conditions such as pH, temperature, and influent concentrations (Dionisi et al., 2002; Aqeel and Liss, 2020). In contrast, denitrifying bacteria are relatively more abundant in wastewater treatment systems because most denitrifying bacteria can use dissolved oxygen as an electron acceptor in the absence of nitrates (Aqeel et al., 2021; Christiaens et al., 2022).

Microbial aggregation, an important process in biological treatment, is mediated by extracellular polymeric substance (EPS) that holds the cells together (Flemming et al., 2023). The role of EPS is complex in determining the structural characteristics of the suspended biomass. The quantity of EPS is considered critical where too little or too much can result in poor settling or bulking sludge (Huang et al., 2022). Protein and polysaccharides are the major components of the EPS. The polysaccharides are largely considered the polymers that hydrate the flocs that help in the diffusion of nutrients. However, too much polysaccharide content results in high water retention and poor separation of treated water from the biomass. The protein content of EPS helps in the cohesion of microbial cells to form large and compact flocs or granules. Too little protein content can contribute to the formation of small pin-point flocs that result in non-filamentous bulking and system failure (Basuvaraj et al., 2015; Flemming et al., 2023). Several studies show that the ratio of protein to polysaccharide or the balance between protein and polysaccharides is vital in the formation of compact microbial aggregates and the settling efficiency of the flocs and granules (Liao et al., 2001; Aqeel et al., 2016; Aqeel and Liss, 2022). However, granular sludge with good settling properties has been reported with relatively higher polysaccharide content compared to protein in the EPS (Aqeel et al., 2019). There are a growing number of studies that indicate the two-layered structure of the flocs and granules. The outer layer is made up of loosely bound EPS and the core is made up of tightly bound EPS (Basuvaraj et al., 2015; Aqeel et al., 2019; Huang et al., 2022). The loosely bound EPS is rich in polysaccharide and loosely bound cells; whereas the inner layer of flocs and granules with tightly bound EPS is rich in protein content that forms a cohesive and dense core (Basuvaraj et al., 2015). The loosely bound EPS (rather than tightly bound EPS) dictates the settling properties of a floc or a granule (Huang et al., 2022). The loosely bound EPS is readily lost during the washing steps in most EPS extraction protocols (Basuvaraj et al., 2015). Therefore, contradicting reports about the composition of EPS and settling properties of the suspended biomass are present in the literature.

There is a need to optimize operational conditions to support the growth and prevent the washout of nitrifying bacteria from wastewater treatment systems. Overall, this study investigated the impact of autotrophic conditions and stepwise increase in influent ammonia concentration on the biomass characteristics and microbial community dynamics under oxic/hypoxic/oxic zones in STRs. The microbial community dynamics were characterized using 16S rRNA gene sequencing and digital droplet-PCR (dd-PCR). The dynamics of nitrifying bacteria (ammonia-oxidizing bacteria, *Nitrospira, and* comammox *Nitrospira*) with change in feeding regime, and the impact of the organic substrate was explored. The paper describes unique features on both the physical–chemical features of the microbial structures and the dominant nitrifying bacteria in the system studied.

Materials and methods

Experimental setup

Bioreactors 1 (R1) and 2 (R2) were operated continuously for more than 50 days. The 20 L working volume bioreactor was designed to support an initial oxic zone followed by a hypoxic zone (mixed but not aerated), and a final oxic zone. The dissolved oxygen concentration in the oxic/hypoxic/oxic chambers was 5–6 mg/L, <1 mg/L, and 5–6 mg/L, respectively. The hypoxic chamber was designed to support the growth of denitrifying bacteria, where endogenous decay would be a source of an organic substrate. Air pumps connected with stone air diffusers were added into both oxic chambers for aeration and mixing of the biomass. An electric overhead stirrer mixer was added into the middle hypoxic chamber. Peristaltic pumps were used for continuous feeding and return activated sludge (RAS). Draining was controlled passively from the settling tank.

R1 and R2 were seeded with RAS collected from the Ashbridges Bay municipal wastewater treatment plant (Toronto, Ontario, Canada). The seed biomass was collected twice (about two months apart) for R1 and R2, respectively. The seed biomass was largely composed of pin-point flocs with poor settling properties. The initial sludge volume index (SVI) of activated sludge of seed biomass for both reactors was 160–170 mL/g MLSS. The hydraulic retention time (HRT) of 16 h was maintained in the reactors. The solid retention time (SRT) was maintained at 12 to 15 days in both bioreactors. However, SRT in R1 declined (5–6 days) during phase-one when biomass washout was observed in the bioreactor. The proportion of oxic/hypoxic/oxic chambers were 40, 30, and 30% of total bioreactor, respectively. Therefore, HRT in the oxic/hypoxic/oxic chambers was six hours and 24 min, four hours and 48 min, and four hours and 48 min, respectively.

The bioreactors were fed with synthetic wastewater with stepwise increasing concentration of ammonia (50–200 N mg/L) without organic substrate during the autotrophic phase for 35 days (R1) and 15 days (R2). The autotrophic phases were maintained to support the enrichment of autotrophic nitrifying. The length of phase-one was different in both reactors to study its effect on characteristics of biomass and microbial community during autotrophic phase and subsequent heterotrophic phase. The synthetic feed used has been described previously (Aqeel and Liss, 2020). The autotrophic feed (without organic substrate) was composed of increasing concentrations of ammonium sulfate (50–200 N mg/L), sodium bicarbonate (354.32 mg/L), magnesium sulfate heptahydrate (70.98 mg/L), calcium chloride dihydrate (29.34 mg/L), potassium dihydrogen phosphate (79.09 mg/L), iron (II) sulfate heptahydrate (4.98 mg/L), and the micronutrients.

EPS extraction

Biomass samples for EPS extraction were collected from the final oxic zone. Loosely bound (LB) and tightly bound (TB) EPS were

TABLE 1 Primer targets and sequences used for quantification microbial population by dd-PCR.

Primer pair	Target	Forward (5′-3′)	Reverse (5′-3′)	Reference
341f-518R	EUB	CCTACGGGAGGCAGCAG	ATTACCGCGGCTGCTGG	Agrawal et al. (2021)
AmoA1f-amoA2r	AOB	GGGGTTTCTACTGGTGGT	CCCCTCKGSAAAGCCTTCTTC	Agrawal et al. (2021)
Nitro1198f-Nitro1423r	*Nitrobacter*	CGGTTTTTTGAGATTTGCTAGGGGT	CTTCACCCCAGTCGCTGACC	Agrawal et al. (2021)
Nspra675f-Nspra-746r	*Nitrospira*	GCGGTGAAATGCGTAGAKATCG	TCAGCGTCAGRWAYGTTCCAGAG	Agrawal et al. (2021)
ComaA-244F- comaA-659R	Comammox clade A	TAYAAYTGGGTSAAYTA	ARATCATSGTGCTRTG	Pjevac et al. (2017)
ComaB-244F- comaB-659R0	Comammox clade B	TAYTTCTGGACRTIYTA	ARATCCARACDGTGTG	Pjevac et al. (2017)

extracted following a previous study (Basuvaraj et al., 2015). Briefly, biomass samples (35 mL) were collected from the bioreactors and centrifuged in a 50 mL falcon tube at 3000 g for 5 min. The supernatant was decanted, and the pellet was processed for LB and TB EPS extraction. The pellet was resuspended in the EPS extraction buffer (0.002 M Na_3PO_4, 0.004 mM NaH_2PO_4, 0.009 mM NaCl and 0.001 mM KCl) and vortexed for 1 min, followed by centrifugation at 4000 g for 10 min. The supernatant (LB EPS) was stored in a −80°C freezer. The pellet was resuspended in the EPS extraction buffer and pre-washed cation exchange resin (CER) (DowexR, Na + form, Sigma Aldrich). The resuspended pellet was vortexed for 60 min. Afterward, tubes were centrifuged at 9000 g for 10 min, and the supernatant (extracted TB EPS) was stored in a −80°C freezer (Basuvaraj et al., 2015). The protein and polysaccharide content in the extracted EPS was quantified as described previously by Aqeel et al. (2016). The EPS samples were stored in a −80°C freezer and all samples were processed together for protein and polysaccharide quantification to minimize the bias.

Microbial community composition

DNA extraction

Biomass samples were collected and stored in a −80°C freezer. Nucleic acid from all biomass samples was extracted using a QIAGEN QIAcube Connect (Qiagen, MD, USA) to automate the DNA extraction procedure. Approximately 100–150 mg of the wet pellet was used for DNA extraction. In the final step of the DNA extraction, 100 µL of nucleic acid-free water was used to elute the nucleic acid from the spin column. The DNA concentration was measured using a NanoPhotometer™ Pearl (Implen, Münchem, Germany). The DNA was then stored in a −80°C freezer until downstream analysis.

Digital droplet-PCR analysis

Quantification of total bacteria (EUB) and nitrifying bacteria (ammonia-oxidizing bacteria (AmoA), *Nitrobacter* (Nitro), *Nitrospira* (NSR), and comammox) was performed using digital droplet-PCR (dd-PCR). For the detection of comammox *Nitrospira*, two sets of primers (for clade A and B) were used: comaA-244F and coma-659 R and comaB-244F and comaB-659R (Pjevac et al., 2017). The primer sequences used to target EUB, AmoA, *Nitrobacter*, *Nitrospira* and Comammox are presented in Table 1. The primers were purchased from IDT (IDT, Coralville, Iowa, USA). The PCR conditions for each primer set were optimized by the thermal gradient cycles and template dilutions. The 10-fold dilutions of each sample were prepared in nuclease-free water. Based on the template concentration optimization results, three 10-fold serial dilutions were used as replicates for the dd-PCR analyses. The PCR plates were sealed using PX1™ PCR plate sealer (BioRad), and vortexed for one minute. The PCR plate was then centrifuged for 40 s in a mini plate centrifuge (VWR, Canada). The droplets were generated using an automated droplet generator (BioRad). The PCR reaction was performed in a thermal cycler (C1000 Touch™ Thermal cycler, BioRad). The droplets were read using QX200™ Droplet Reader (BioRad). The dd-PCR results were analyzed using QX manager (QX200™, BioRad).

16S rRNA gene sequencing

The genomic DNA samples were sent to the Genome Quebec Research and Testing Laboratory in Montréal, Québec for 16S rRNA gene sequencing (Illumina MiSeq). The DNA samples were amplified using PCR for amplicon preparations. The V3–V4 region of the 16S rRNA gene was amplified using primers 341F (CCTACGGGNG GCWGCAG) and 803R (CTACCRGGGT ATCTAATCC). A second PCR reaction was performed to incorporate sample-specific barcodes. The DNA concentration of all PCR reactions was measured using Picogreen so that the equimolar concentration of all samples could be used for sequencing. The amplicon library with an insert size of about 450 bases was sequenced with a paired-end 250 kit (Illumina MiSeq). The forward and reverse sequences from the Illumina paired-end sequences were merged using the DADA2 software. The markers, adapters, and errors in the sequences (including chimera sequences) were removed using the DADA2 pipeline (Callahan et al., 2016), 16S rRNA gene sequences were used to generate an operational taxonomic unit (OTU) table and a corresponding FASTA file. The sequences after the removal of chimeras and low-quality sequences, were analyzed using Microbiome Analyst. The assignment of the sequences was performed using SILVA taxonomy (Dhariwal et al., 2017; Chong et al., 2020) for alpha diversity analyses (based on observed species), and for relative abundance of bacteria. The 16S rRNA gene sequencing data have been submitted to the National Library of Medicine, National Center for Biotechnology Information. The sequence read archive (SRA) submission number is SUB13878507, and BioProject number is PRJNA1023363.

Results

Bioreactor performance and biomass characteristics

The bioreactors were seeded with RAS from the Ashbridges Bay municipal wastewater treatment plant (Toronto, Ontario, Canada). The

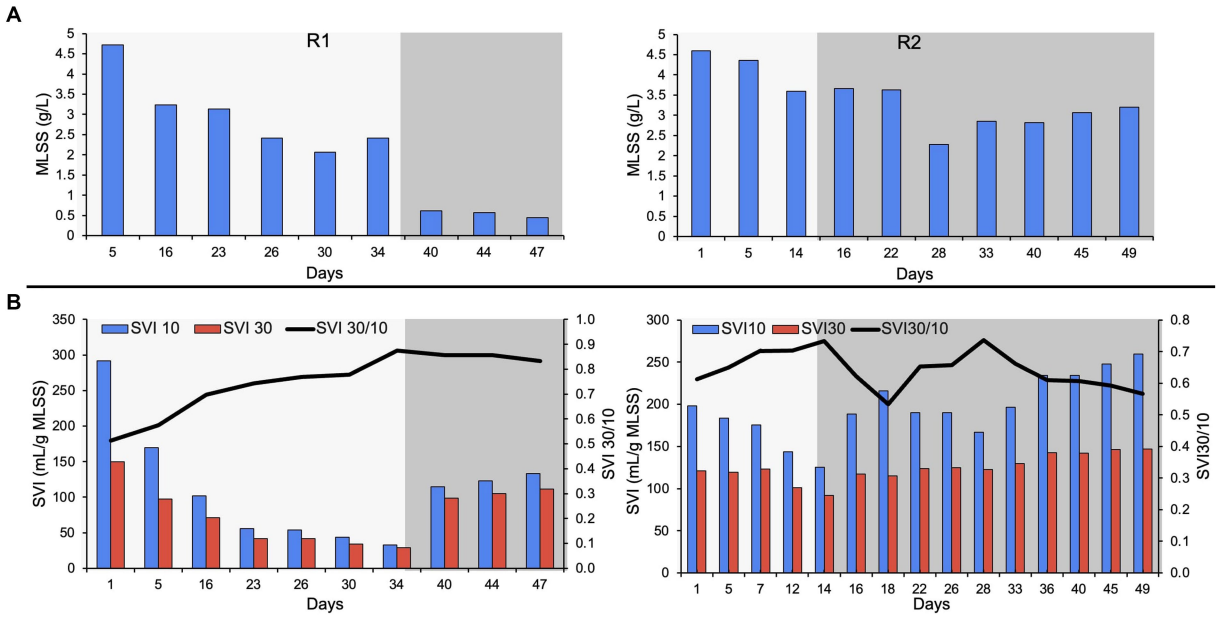

FIGURE 1
(A) MLSS in R1 and R2, **(B)** settleability of the biomass showing the SVI_{30}, SVI_{10} and SVI_{30}/ SVI_{10}. The lighter shade indicates phase one and the darker shade indicates phase two.

MLSS in R2 was relatively lower (4.4 g/L) compared to R1 (4.7 g/L), on day five of bioreactor startup (Figure 1). The biomass washout is expected during reactor startup due to a change in influent feed, from municipal wastewater to autotrophic synthetic feed. The ESS in both reactors was stabilized to below 100 mg/L after day 15 of bioreactor startup. The R2 was switched to phase-two on day 15 (the bioreactor with a short autotrophic phase). A transient increase in ESS was observed during the switch from phase-one to phase-two, in both reactors. The MLSS in R1 gradually declined to 2.07 g/L on day 30, during phase-one. The biomass loss due to the switch in feed (phase-two on day 35) resulted in very low MLSS (0.61 g/L) on day 40. The switch in feeding regime resulted in poorly settling and bulking sludge that resulted in biomass washout in R1. However, the bioreactor with a short autotrophic enrichment phase (R2) recovered after the switch in the feeding regime during phase-two. The MLSS in R2 was relatively higher (3.2 g/L) compared to R1 (0.45 g/L), at the end of the experiment (Figure 1).

Dense pin-point flocs 10–20 μm in size were observed during the autotrophic phase (phase-one) in both bioreactors (Supplementary Figure S1). During the autotrophic phase, the settling properties of the biomass gradually improved in both bioreactors with the formation of compact pin-point flocs. The SVI_{30} (ml/g MLSS), SVI_{10} (ml/g MLSS), and the ratio of SVI_{30} to SVI_{10} (SVI_{30}/ SVI_{10}) were used to characterize the settling properties of the flocs (Figure 1). SVI_{30} improved to 75 and 92 in R1 and R2 respectively, on day 15 of bioreactor operation. The SVI_{30}/ SVI_{10} of both bioreactors was 0.7 after 15 days of bioreactor operation during the autotrophic phase (Figure 1). In R1, the SVI_{30} improved to 29 mL/g MLSS, and the SVI_{30}/ SVI_{10} gradually improved to 0.88 on day 34 (Figure 1). However, after a relatively longer autotrophic phase, when the organic substrate was supplemented to R1 (during phase-two), the flocs were showing poor settling properties and biomass washout. The SVI_{30} declined from 29 to 111 mL/g MLSS and MLSS declined from 2.42 to 0.45 g/L, with the switch in synthetic feed composition. In R2, the SVI_{30} gradually increased to 147 mL/g MLSS, on day 49 of reactor operation. Whereas, in R2, the SVI_{30}/ SVI_{10} stabilized at 0.6 ± 0.1, and MLSS was maintained above 3 g/L (Figure 1). The settling properties of the biomass deteriorated in both reactors, after the supplementation of organic substrate (during phase-two).

Ammonia removal efficiency for R1 and R2 over the duration of approximately 50 days was 98.5 and 96.6%, respectively. The nitrification efficiency was 100% during the autotrophic phase, however, a drop in ammonia removal was observed during the heterotrophic phase (Figure 2). R1 and R2 maintained their nearly complete ammonia removal efficiency as higher concentrations of influent ammonia increased to 200 N mg/L (Figure 2). Nitrite concentrations in both reactors were also limited to nearly zero, as the average in each bioreactor was 0.15 mg/L and 1.27 mg/L, respectively. The nitrate accumulation was relatively higher in R1 to a maximum concentration of 132 N mg/L on day 49 of bioreactor startup. In R2 (the bioreactor operated with a shorter autotrophic phase) the nitrate accumulation was relatively lower (98 N mg/L) on day 49 (Figure 2).

Composition of extracellular matrix

In this study, loosely bound (LB) and tightly bound (TB) EPS were extracted separately from the biomass. The protein and polysaccharide content in each fraction of EPS was quantified. Overall, the polysaccharide concentration was relatively higher compared to the protein content, in LB EPS. It was reflected by a low protein to polysaccharide ratio (PN:PS ratio) in LB EPS extracted from pin-point flocs of R1 and R2 (Figure 3). The protein concentration was relatively higher (up to four-fold) in the TB EPS fractions compared to the respective LB EPS fractions (Figure 3).

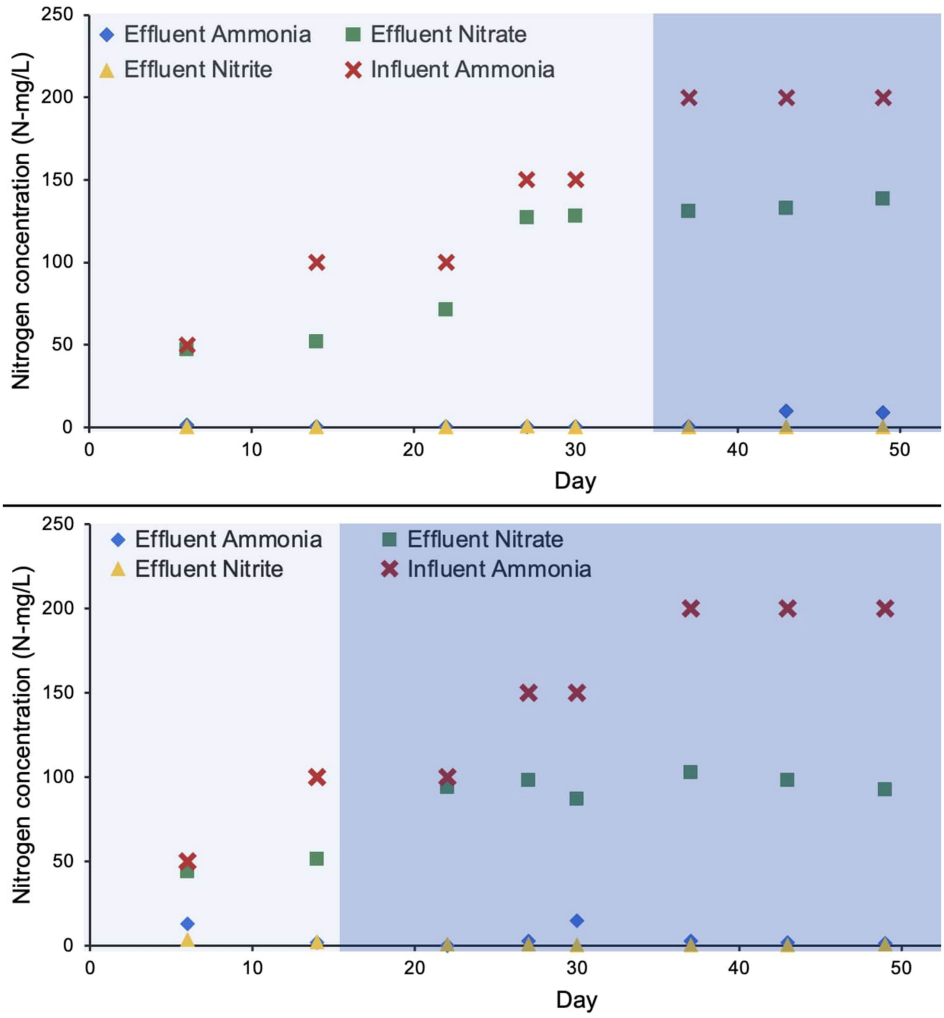

FIGURE 2
Concentration of nitrogen species during the bioreactor operation. The lighter shade indicates phase one and the darker shade indicates phase two.

In R1, protein and polysaccharide concentration in LB and TB EPS gradually increased during phase-one (Figure 3). The PN:PS ratio gradually decreased in both LB and TB EPS during phase-two, in R1. The PN:PS ratio in the TB EPS declined from 2.02 (during phase-one on day 25) to 0.95 (on day 46, during phase-two). In R2, a similar trend was observed during the autotrophic phase where an increase in PN:PS ratio was observed in both LB and TB EPS. However, in R2 (the bioreactor with a shorter phase-one) the PN:PS kept on gradually improving in TB EPS, during phase-two (Figure 3). In R1 the ratio of TB to LB EPS increased during the autotrophic phase followed by a decline in TB:LB ratio during the heterotrophic phase (Figure 3) when the organic substrate was supplemented with the synthetic feed. A similar trend was observed in R2, where TB:LB ratio gradually declined during phase-two (Figure 3).

Microbial community composition

16S rRNA gene sequencing

The 16S rRNA gene sequencing data (Illumina MiSeq PE 250) was analyzed using the Microbiome Analyst. Overall, the alpha diversity analyses (based on observed species) revealed that the microbial communities of R2 were relatively more diverse compared to R1 (Supplementary Figure S1). The relative abundance of bacteria related to families *Comamonadaceae* and *Rhodocyclaceae* gradually declined during the autotrophic enrichment phase in both bioreactors. The relative abundance of *Comamonadaceae* declined from 10.8 to 3.6% on day 34, followed by an increase in relative abundance to 14.5% on day 51 in R1 (Figure 4). In R2, the relative abundance of *Comamonadaceae* increased from 2.9% (on day 14 of bioreactor operation) to 13.3% (on day 49 of R2 operation). Similarly, the relative abundance of *Rhodocyclaceae* gradually declined from 9 to 1.5% on day 34, followed by an increase in relative abundance to 20% (on day 47 of R1 startup). In R2, the relative abundance of *Rhodocyclaceae* gradually declined from 10.5 to 3.7% during phase-one. During phase-two, the relative abundance of *Rhodocyclaceae* gradually increased to 26.4% (on day 56 of R2 startup). The relative abundance of bacteria related to the family *Nitrospiraceae* was higher during the autotrophic phase and then declined during the second phase when the organic substrate was supplemented into the synthetic feed. The relative abundance of *Nitrospiraceae* gradually increased from 0.1 to 15.4% (on day 34 of R1 operation) during phase-one (Figure 4). The relative abundance of *Nitrospiraceae* declined to 1.8% (on day 51 of R1 operation) during phase-two. In R2, the relative abundance of

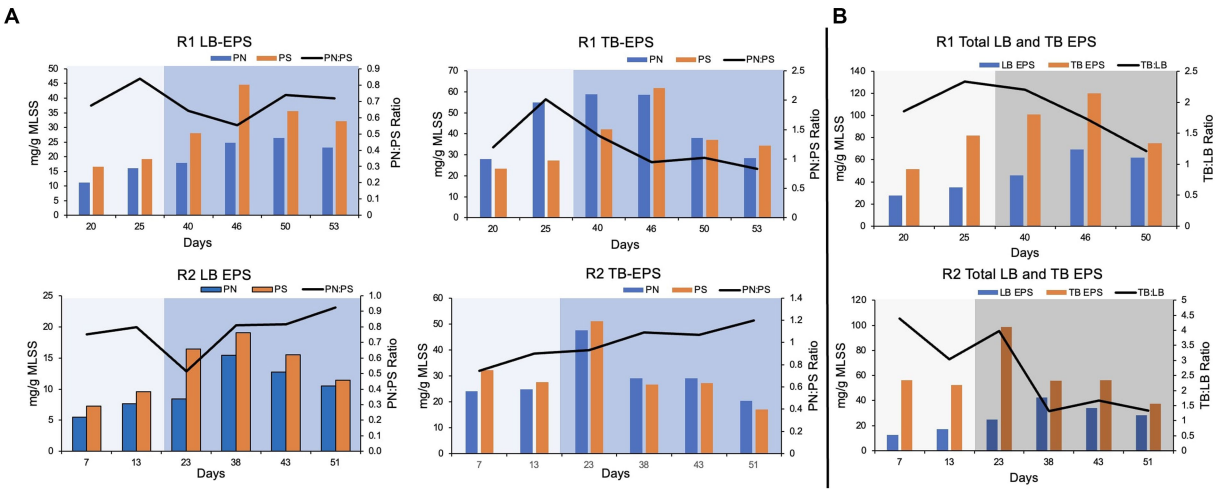

FIGURE 3
EPS composition. **(A)** Protein (PN) and polysaccharide (PS) content and PN:PS in the loosely (LB) and tightly bound (TB) extracted EPS. **(B)** TB and LB EPS and TB:LB ratio in the extracted EPS. The lighter shade indicates phase one and the darker shade indicates phase two.

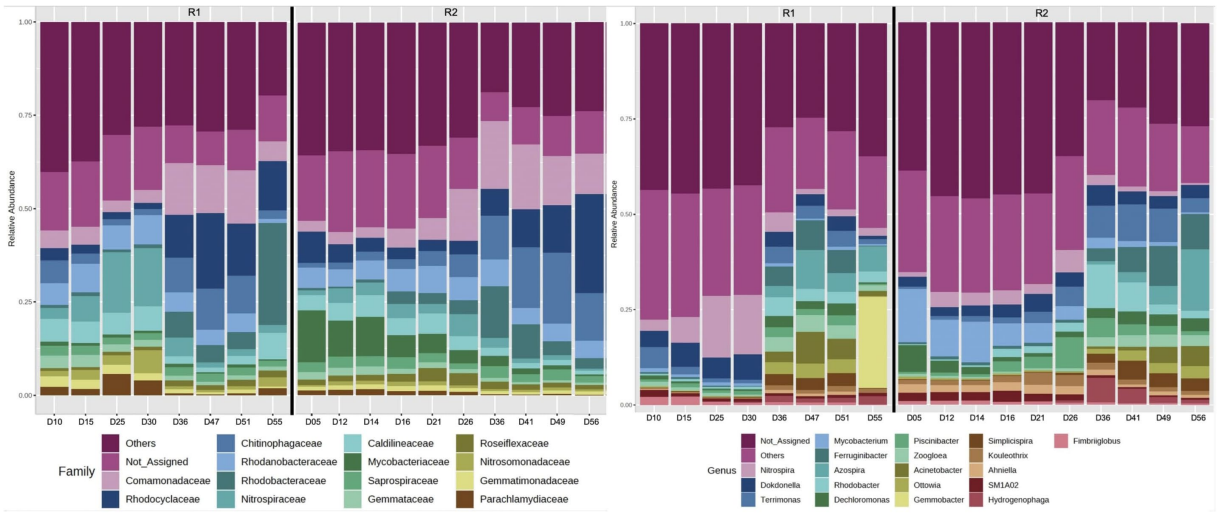

FIGURE 4
16S rRNA gene sequencing (Illumina MiSeq) showing the relative abundance of the most abundant families, and the relative abundance of the 20 most abundant genera. Phase one was up to day 35 in R1 and day 15 in R2.

Nitrospiraceae gradually increased from 0.6 to 3.4% on day 14 of bioreactor operation. During phase-two, the relative abundance of *Nitrospiraceae* gradually decreased to 0.5% (on day 56 of R2 startup).At the genus level, it was observed that the relative abundance of *Nitrospira*, *Dokdonella*, and *Candidatus Accumulibacter* was higher in both bioreactors during phase-one compared to phase-two of the feeding regime (Figure 4). The relative abundance of *Thauera*, *Zoogloea*, *Acinetobacter*, *Comamonas*, *Rhodobacter*, and *Dechloromonas* was relatively higher during phase-two (when the organic substrate was supplemented into the synthetic feed). At the species level, most of the low-count OTUs were filtered out, and only very few bacteria species were identified. As a result, analyses at the species level were not undertaken. However, the observation of a comammox species based on 16S rRNA gene sequencing warranted the quantification of comammox bacteria using dd-PCR.

Digital droplet-PCR

The dd-PCR was used to quantify total bacteria (EUB), *Nitrospira*, *Nitrobacter*, comammox, and ammonia-oxidizing bacteria (Figure 5). The primer sequences and targets used for quantification of bacteria are presented in Table 1. The dd-PCR has an upper limit of detection that can read up to 10^4 to 10^5 gene copies (depending on the amount of DNA templates used). Two or three successive serial dilutions were used for duplicate or triplicate dd-PCR experiments. It was helpful to detect the concentration of a bacteria that fluctuates with bioreactor operation. Additionally, the dd-PCR on two or three serial dilutions confirms the accuracy of the manual serial dilution of the samples. Total bacteria ranged from 10^7 to 10^8 gene copies/ ug of DNA extracted in both bioreactors. *Nitrobacter* was not detected (or amplified) in the DNA extracted from the flocs of both bioreactors. The enrichment of the *Nitrospira* was observed in both bioreactors during phase-one

when the synthetic feed lacked organic substrate. *Nitrospira* were the predominant nitrifying bacteria in both bioreactors and ranged from 10^4 to 10^6 gene copies/ ug of DNA extracted. The highest number of *Nitrospira* was observed when pin-point flocs showed granule-like settling properties (Figure 5). The abundance of comammox *Nitrospira* in the biomass samples was measured using dd-PCR when *Nitrospira Nitrosa* (a comammox *Nitrospira*) was observed in the 16S rRNA gene sequencing results. Overall, the abundance of comammox *Nitrospira* remained relatively constant in both bioreactors. The dd-PCR results show that the comammox *Nitrospira* were the predominant ammonia-oxidizing bacteria in the seed biomass collected from the municipal wastewater treatment plant and at low ammonia influent concentrations in the bioreactors. The abundance of ammonia-oxidizing bacteria increased from 10^2 to 10^5 with a stepwise increase in influent ammonia concentration (Figure 5).

Discussion

The characteristics of the biomass and microbial community dynamics were studied during autotrophic and heterotrophic phases in the STRs operated under oxic/hypoxic/oxic zones. The R1 was operated with a relatively prolonged autotrophic phase (phase-one), compared to R2. The organic substrate was supplemented in

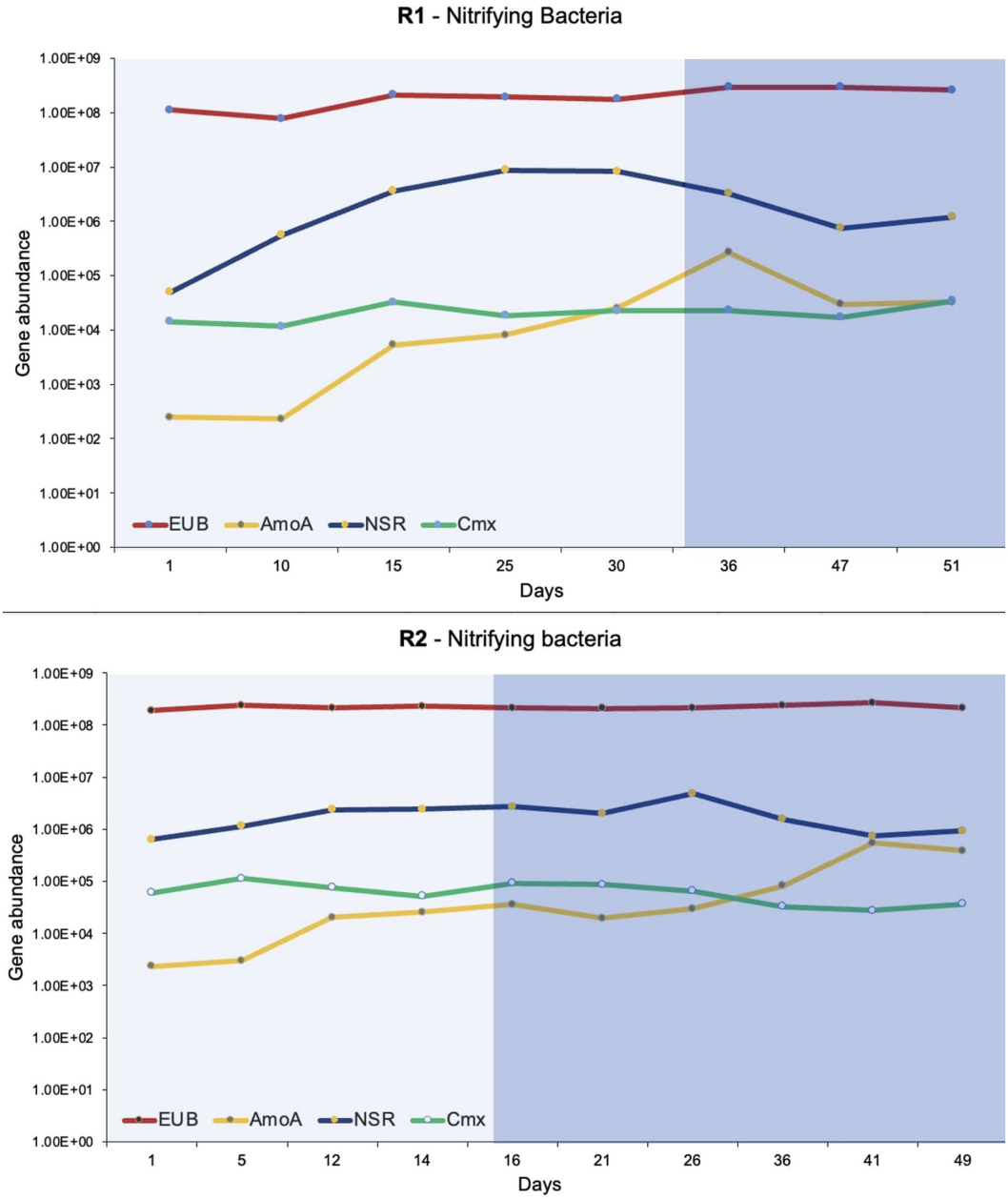

FIGURE 5
The dd-PCR results show the abundance of total bacteria (EUB), ammonia-oxidizing bacteria (AmoA), *Nitrospira* (NSR), and comammox (Cmx). The lighter shade indicates phase one and the darker shade indicates phase two.

phase-two to support the growth of heterotrophic denitrifying bacteria. Pin-point flocs with granular-sludge-like settling properties were formed in a 20 L stirred tank reactor (STR) operated with a relatively longer autotrophic phase (Supplementary Figure S1). The settling properties of the pin-point flocs improved gradually during the autotrophic enrichment phase. Whereas in the second phase with the supplementation of the organic substrate, the settling properties of biomass deteriorated in both bioreactors. The study shows that autotrophic bacteria improved the settling performance and heterotrophic bacteria deteriorated the settleability of the biomass.

Additionally, the operating conditions for this study were planned to understand the microbial community dynamics (of the nitrifying bacteria) with stepwise increasing influent ammonia concentrations. The stepwise increment in the influent ammonia concentration in synthetic feed (without organic substrate) has been used previously for the enrichment of autotrophic nitrifying bacteria (Aqeel and Liss, 2020). Microbial community dynamics of the k-strategist and r-strategist nitrifying bacteria were studied in the bioreactors operated with oxic/hypoxic/oxic zones. K-strategists are slow-growing bacteria (such as *Nitrospira*) with a high affinity for a substrate. R-strategists are fast-growing bacteria (such as *Nitrobacter*) with low affinity for a substrate (Yin et al., 2022). Filamentous bacteria are also k-strategist microbes because they are better adapted to limited resources due to their relatively higher surface area (Yin et al., 2022). To inhibit the growth of heterotrophic filamentous bacteria, the synthetic feed was made without an organic substrate. Furthermore, a hypoxic chamber was designed to support the growth of heterotrophic denitrifying bacteria that can use organic substrate from the endogenous decay, and oxidized nitrogen species as electron acceptors (Aqeel et al., 2019). Previous studies have shown that low DO concentrations inhibit filamentous growth (Adav et al., 2007; Aqeel et al., 2021). It was observed that in the present study, the filamentous bacteria that were present in the seed biomass were inhibited in both bioreactors, during the autotrophic phase.

Granule-like settling properties of pin-point flocs

The pin-point flocs are generally correlated to the poor settling of activated sludge. The seed biomass was predominantly composed of pin-point flocs that show poor settling properties (SVI of 160–170 mL/g MLSS). Enrichment of compact pin-point flocs and inhibition of filamentous bacteria was observed during the autotrophic phase that showed granule-like settling properties, in R1. The SVI_{30} and ratio of SVI_{30}/ SVI_{10} are used to show the quality and completeness of granular sludge. The SVI_{30} of granular sludge is usually less than 50 mL/g MLSS (Derlon et al., 2016; Sarma and Tay, 2018). In this study, the SVI_{30} improved to 29 mL/g MLSS during the autotrophic enrichment phase in R1 (Figure 1). The SVI_{30}/ SVI_{10} of close to 1 indicates the completeness of granular sludge (Schwarzenbeck et al., 2005; Aqeel and Liss, 2022). However, most granular sludge studies report ratios of SVI_{30}/ SVI_{10} between 0.7 to 0.9 (Derlon et al., 2016; Manavi et al., 2017; Aqeel et al., 2021). In this study, the $SVI_{30/10}$ of pin-point flocs improved to 0.88 on day 34 during the autotrophic enrichment phase (Figure 1).

The settling properties of R1 and R2 biomass were similar, during the autotrophic phase on day 15 (SVI_{30}/ SVI_{10} was 0.7 in both bioreactors). The R1 biomass showed granule-like settling properties on day 25. However, the autotrophic enrichment phase was relatively shorter in R2 (15 days). Therefore, the settling properties of the R2 biomass improved, but it was not like the settleability of a granular sludge. The settling properties of the biomass deteriorated during phase-two, in both bioreactors (Figure 1). The settling properties of R2 biomass did not improve like the settling properties of R1 biomass (during the autotrophic phase). However, the settling properties of R2 biomass did not deteriorate drastically, like R1 biomass, during the switch in the feeding regime.

The alpha diversity analyses of the microbial communities in R1 and R2 revealed that the microbial diversity was relatively lower in R1 which was operated with longer phase-one (Supplementary Figure S2). It was observed that the microbial selection/ enrichment during phase-one resulted in the enrichment of nitrifying bacteria (Figures 4, 5) and compact pin-point flocs that show granule-like settling properties (Figure 1). However, it resulted in the loss of the resilience of the bioreactor to changes in nutritional conditions. Therefore, during phase-two, sludge bulking was observed in R1 with an abundance of *Zoogloea* in the microbial community (Figure 4). The correlation between lack of microbial diversity during granule formation and subsequent granule instability has also been observed in granular sludge technology. Therefore, optimization of granule enrichment and the hybrid granulation (balance between flocs and granules) have been suggested for the stability of granular sludge (Aqeel et al., 2019). Similarly in this study, it was observed that where autotrophic conditions can propagate the enrichment of nitrifying bacteria and improve the settling properties of the biomass; optimization of conditions to find a balance is important for the stable operation of the biological nutrient removal bioreactors.

Extracellular matrix

The extracted loosely bound (LB) and tightly bound (TB) EPS content and composition are presented in Figure 3. The protein to polysaccharide ratio (PN:PS ratio) increased during the autotrophic phase in the TB and LB EPS extracted from pin-point flocs of both bioreactors. Basuvaraj et al. (2015) characterized the granular sludge and flocs, based on PN:PS ratio. The PN:PS ratio of the granular sludge was higher than 1.5 and the PN:PS ratio of the flocs was below one (Basuvaraj et al., 2015). In R1, the highest PN:PS ratio (>2) was observed on day 25 of bioreactor startup, when pin-point flocs were observed and exhibited granule-like settling properties. The PN:PS ratio in TB EPS extracted from R1, gradually decreased during phase-two which corresponds to the poor settling properties of the pin-point flocs (Figure 3). The PN:PS ratio in TB EPS extracted from R2 gradually increased with the bioreactor operation that corresponds to the stability in the settling properties of the R2 pin-point flocs during phase-two (Figure 1). The autotrophic enrichment phase resulted in the selection of compact flocs that show settling properties and EPS composition of a granular sludge, in R1. However, the PN:PS ratio and settling properties of the biomass during phase-two indicate that the R2 (that was operated with a shorter phase-one) better adapted to the change in feeding regime compared to the R1.

The TB and LB EPS fractions were extracted separately because the ratio of TB and LB EPS is an important indicator of the settling characteristics of the suspended biomass (Basuvaraj et al., 2015; Chen et al., 2019). The protein content in TB EPS was higher than the LB EPS, in both bioreactors. The PN:PS ratio was higher in TB EPS compared to

the LB EPS in both bioreactors (Figure 3). The results are consistent with previous studies that show protein content in the extracellular matrix is associated with the formation of cohesive and compact flocs (Liao et al., 2001; Basuvaraj et al., 2015; Aqeel et al., 2019). Therefore, TB EPS is more associated with the cohesiveness of flocs and LB EPS is associated with poor settleability of the flocs (Bezawada et al., 2013; Basuvaraj et al., 2015; Huang et al., 2022). Basuvaraj et al. (2015) differentiated the granular sludge and flocs based on the ratio of TB and LB EPS. It was reported that the TB:LB ratio is higher in the granular sludge compared to the flocs (Basuvaraj et al., 2015). In R1, the TB:LB ratio gradually increased during the autotrophic phase (Figure 3) with the observation of pin-point flocs that show granular-sludge-like settling properties (Figure 1). The TB:LB ratio of the pin-point flocs in R1 during phase-two gradually declined that correspond with poor settling properties.

The nitrifiers form small but very strong microcolonies, therefore most EPS extraction methods can not completely extract EPS (Huang et al., 2022). Nitrifying microcolonies remain largely intact under extreme physical and chemical treatments. *Nitrosomon*as and *Nitrospira* microcolonies are formed by physical entanglement of the extracellular polymers. Where *Nitrospira* microcolonies are relatively more cohesive than the *Nitrosomonas* microcolonies (Daims et al., 2001; Larsen et al., 2008). The nitrifying bacteria were enriched in this study, during the autotrophic phase in both bioreactors. Therefore, it is expected that the TB EPS was not completely extracted from the biomass. Although the TB:LB EPS ratio reported in this study is similar to a granular sludge; the actual TB EPS might have been higher in the biomass.

Compact pin-point flocs up to 20 μm in size were predominant during the autotrophic phase in R1 and R2. Previous studies have shown that nitrifying bacteria form dense microcolonies in the ranges from 9-25 μm (Larsen et al., 2008), similar to the pin-point flocs observed in this study. It is hypothesized that these pin-point flocs consist predominantly of nitrifying microcolonies. The autotrophic growth conditions presented in this study inhibited the growth of heterotrophic bacteria including filamentous bacteria which improved the overall settling properties of the biomass. Both molecular approaches (16S rRNA gene sequencing, and dd-PCR) show that nitrifying bacteria were predominant during the autotrophic phase. The relative abundance of *Nitrospira* was highest when the pin-point flocs of R1 showed granule-like settling properties. The abundance of nitrifying bacteria translated into 100% ammonia and nitrite removal efficiencies during the autotrophic, in R1 (Figure 2). However, the decline in ammonia removal efficiencies during phase-two, could be due to biomass washout in R1 (Figure 1).

Microbial community

16S rRNA gene sequencing revealed that the change in feeding regime resulted in a clear shift in microbial community from autotrophic nitrifying to heterotrophic denitrifying bacteria (Figure 4). For example, during phase-one autotrophic bacteria (*Nitrospira*) were predominant in the microbial community. Furthermore, the relative abundance of bacteria related to families *Rhodocyclaceae* and *Comamonadaceae* [known for denitrification (Pishgar et al., 2019)] gradually declined during the autotrophic phase in both bioreactors. During phase-two the heterotrophic bacteria were relatively more abundant. It was observed that at the family level the relative abundance of *Rhodocyclaceae* and *Comamonadaceae* increased, during phase-two in both bioreactors (Figure 4). Whereas the relative abundance of the dominant nitrifying bacteria (*Nitrospira*) declined during phase-two. At the genus level, it was observed that the aerobic denitrifier *Dokdonella* (Pishgar et al., 2019) was relatively a predominant denitrifier during phase-one in both bioreactors. During phase-two, *Acinetobacter*, *Simplicispira*, and *Dechloromonas* [denitrifiers (Pishgar et al., 2019)] were predominant in both bioreactors (Figure 4). *Dechloromonas* have also been found associated with denitrifying phosphorus accumulation organism (DPAO) (Weissbrodt et al., 2014). It is suggested that the oxic/hypoxic/oxic zones favored the growth of *Dechloromonas* in the bioreactors. The abundance of *Dechloromonas* has been observed previously in the laboratory-scale sequencing batch bioreactors operated with oxic/hypoxic/oxic conditions (Aqeel et al., 2021).

The abundance and microbial community dynamics of nitrifying bacteria were quantified using dd-PCR (Figure 5). It was observed that comammox *Nitrospira* was the dominant ammonia oxidizer in the seed biomass that was collected from a full-scale Ashbridges Bay wastewater treatment plant. Additionally, it was the dominant ammonia-oxidizer in both bioreactors at low ammonia influent concentrations (Figure 5). The comammox has relatively more affinity for dissolved oxygen and ammonia compared to the *Nitrosomonas* species. Therefore, comammox *Nitrospira* are capable to outcompete the ammonia-oxidizing bacteria under substrate-limiting conditions (Roots et al., 2019; Ren et al., 2020; Zhu et al., 2022). The comammox *Nitrospira* were largely identified in oligotrophic conditions such as drinking water treatment plants (Pinto et al., 2016; Maddela et al., 2022) or a biofilm growing 1,200 m below the surface of an oil exploration well (Daims et al., 2015; Roots et al., 2019). Therefore, it is considered that the canonical ammonia oxidizing bacteria may outcompete the comammox bacteria in nutrient-rich conditions in wastewater treatment plants (Roots et al., 2019). The hypothesis was verified by several initial studies that show comammox *Nitrospira* were absent or relatively low in abundance compared to ammonia-oxidizing bacteria in biological nutrient removal systems. Therefore, it was considered that comammox is irrelevant or less important in nitrogen cycling (Gonzalez-Martinez et al., 2016; Annavajhala et al., 2018). There is a growing number of evidence that shows an abundance of comammox *Nitrospira* in wastewater treatment systems, specifically at low dissolved oxygen concentrations (Roots et al., 2019).

Overall, the abundance of comammox *Nitrospira* remained constant during stepwise increments in influent ammonia concentration and during shifts in the feeding regime (phase-one and phase-two), in both bioreactors (Figure 5). The observation corresponds to the physiological and phylogenetic analyses that suggest comammox *Nitrospira* are resilient microorganisms that can withstand ammonia fluctuation and oxidative stress (Maddela et al., 2022).

The relative abundance of ammonia-oxidizing bacteria (compared to comammox *Nitrospira*) gradually increased with an increase in influent ammonia concentrations in both bioreactors (Figure 5). Many ammonia-oxidizing bacteria are r-strategists that are favored by increasing the concentration of the substrate (Yin et al., 2022). The results of the present study showed the dynamics of comammox *Nitrospira* and ammonia-oxidizing bacteria with increasing substrate concentrations. The insight will help to optimize the conditions to find a balance between the r and k strategist nitrifiers to treat high-strength ammonia wastewater and produce high-quality effluent.

The second step of nitrification is carried out by canonical nitrite-oxidizing bacteria (*Nitrospira* and *Nitrobacter*) and comammox bacteria. The two canonical nitrite-oxidizing bacteria compete for a common substrate where *Nitrobacter* is an r-strategist and *Nitrospira* is a k-strategist bacteria (Mehrani et al., 2023). The presence of *Nitrobacter* in a system is correlated to poor nitrification removal (Terada et al., 2010). The dd-PCR and 16SrRNA gene sequencing results show that *Nitrobacter* was absent (or below the detection limit) in both bioreactors. Both molecular approaches showed a gradual increase in *Nitrospira* abundance during phase-one (Figures 4, 5). The k-strategist nitrifying bacteria are known for polishing and producing high-quality effluent. In the present study up to 100% nitrification was observed during phase-one with the enrichment of *Nitrospira*.

In the present study, the stepwise incremental increase of ammonia concentration in the absence of organic substrate supported the enrichment of k-strategist bacteria, because there was minimal excess substrate for the growth of r-strategists. The abundance of k-strategists was correlated with the abundance of compact pin-point flocs and the absence of filamentous bacteria. The retention of pin-point flocs was observed to be correlated to the granule-like properties reflected in the EPS (TB/LB EPS ratio, and PN/PS ratio) and settling properties. Conversely, the introduction of an organic substrate (during the heterotrophic feeding regime) resulted in an abundance of r-strategist bacteria, and biomass washout in R1. The alpha diversity analyses show that the longer autotrophic enrichment phase in R1 resulted in the loss of microbial diversity that makes the biomass less resilient to the change in feeding regime. Optimization of the autotrophic and heterotrophic conditions to find a balance is desirable for the retention of nitrifying bacteria and the biological conversion of N_2 in wastewater treatment systems. In this study, the abundance of denitrifying bacteria was observed during phase-two which shows a potential for an efficient simultaneous nitrification and denitrification in a system. A stepwise incremental increase of the organic substrate during phase-two, to gradually enrich the heterotrophic denitrifying bacteria able to use nitrate as an electron acceptor in place of dissolved oxygen may provide a path for optimizing a two-step process of biological nutrient removal.

Conclusion

The paper describes unique features of both the physical–chemical characteristics of the microbial structures and the dynamics of dominant nitrifying bacteria in a system designed and operated to optimize autotrophic growth and to examine the influence of heterotrophic growth on nitrification. Comammox *Nitrospira* were the predominant ammonia-oxidizing bacteria in the seed in bioreactors and during treatment of relatively low influent ammonia concentrations. In response to increasing concentrations of ammonia, the relative abundance of AOB increased in relation to comammox *Nitrospira*. Optimizing for autotrophic conditions improved retention of the *Nitrospira* dominant pin-point flocs that exhibited granular sludge-like settling properties. The settling properties of biomass deteriorated in both bioreactors during the heterotrophic phase. Similarly, the PN:PS ratio in the EPS, and TB:LB EPS ratio gradually increased during the autotrophic phase, and declined during the heterotrophic phase. A relatively dominant autotrophic population enhances settling properties, whereas changing conditions that led to an increase in heterotrophic bacteria deteriorates the settling properties of the pin-point flocs.

Data availability statement

The datasets presented in this study are deposited in the NCBI database under accession number PRJNA1023363.

Author contributions

HA: Conceptualization, Data curation, Formal analysis, Investigation, Methodology, Project administration, Software, Validation, Visualization, Writing – original draft, Writing – review & editing. BA: Data curation, Methodology, Software, Writing – review & editing. SL: Conceptualization, Funding acquisition, Investigation, Resources, Supervision, Validation, Writing – review & editing.

Funding

The author(s) declare financial support was received for the research, authorship, and/or publication of this article. The work was funded by the Natural Sciences and Engineering Research Council of Canada (NSERC).

Acknowledgments

The authors acknowledge the Ashbridges Bay wastewater treatment plant, Toronto, Ontario, Canada for providing the biomass for the experiments; and Genome Quebec for 16S rRNA gene sequencing.

Conflict of interest

The authors declare that the research was conducted in the absence of any commercial or financial relationships that could be construed as a potential conflict of interest.

Publisher's note

Supplementary material

The Supplementary material for this article can be found online at: https://www.frontiersin.org/articles/10.3389/fmicb.2023.1307727/full#supplementary-material

References

Adav, S. S., Lee, D. J., and Lai, J. Y. (2007). Effects of aeration intensity on formation of phenol-fed aerobic granules and extracellular polymeric substances. *Appl. Microbiol. Biotechnol.* 77, 175–182. doi: 10.1007/s00253-007-1125-3

Agrawal, S., Weissbrodt, D. G., Annavajhala, M., Jensen, M. M., Arroyo, J. M., Wells, G., et al. (2021). Time to act–assessing variations in qPCR analyses in biological nitrogen removal with examples from partial nitritation/anammox systems. *Water Res.* 190:116604. doi: 10.1016/j.watres.2020.116604

Annavajhala, M. K., Kapoor, V., Santo-Domingo, J., and Chandran, K. (2018). Comammox functionality identified in diverse engineered biological wastewater treatment systems. *Environ. Sci. Technol. Lett.* 5, 110–116. doi: 10.1021/acs.estlett.7b00577

Aqeel, H., Basuvaraj, M., Hall, M., Neufeld, J. D., and Liss, S. N. (2016). Microbial dynamics and properties of aerobic granules developed in a laboratory-scale sequencing batch reactor with an intermediate filamentous bulking stage. *Appl. Microbiol. Biotechnol.* 100, 447–460. doi: 10.1007/s00253-015-6981-7

Aqeel, H., Basuvaraj, M., and Liss, S. N. (2021). Microbial population selection in integrated fixed-film sequencing batch reactors operated with different lengths of oxic and anoxic conditions. *Environ Sci: Water Res & Technol* 7, 913–926. doi: 10.1039/D0EW01022G

Aqeel, H., and Liss, S. N. (2020). Autotrophic fixed-film systems treating high strength Ammonia wastewater. *Front. Microbiol.* 11:551925. doi: 10.3389/fmicb.2020.551925

Aqeel, H., and Liss, S. N. (2022). Fate of sloughed biomass in integrated fixed-film systems. *PLoS One* 17:e0262603. doi: 10.1371/journal.pone.0262603

Aqeel, H., Weissbrodt, D. G., Cerruti, M., Wolfaardt, G. M., Wilén, B., and Liss, S. N. (2019). Drivers of bioaggregation from flocs to biofilms and granular sludge. *Environ Sci: Water Res & Technol* 5, 2072–2089. doi: 10.1039/C9EW00450E

Basuvaraj, M., Fein, J., and Liss, S. N. (2015). Protein and polysaccharide content of tightly and loosely bound extracellular polymeric substances and the development of a granular activated sludge floc. *Water Res.* 82, 104–117. doi: 10.1016/j.watres.2015.05.014

Bezawada, J., Hoang, N. V., More, T. T., Yan, S., Tyagi, N., Tyagi, R. D., et al. (2013). Production of extracellular polymeric substances (EPS) by Serratia sp.1 using wastewater sludge as raw material and flocculation activity of the EPS produced. *J. Environ. Manag.* 128, 83–91. doi: 10.1016/j.jenvman.2013.04.039

Callahan, B. J., McMurdie, P. J., Rosen, M. J., Han, A. W., Johnson, A. J. A., and Holmes, S. P. (2016). DADA2: high-resolution sample inference from Illumina amplicon data. *Nat. Methods* 13, 581–583. doi: 10.1038/nmeth.3869

Chen, X., Kong, F., Fu, Y., Si, C., and Fatehi, P. (2019). Improvements on activated sludge settling and flocculation using biomass-based fly ash as activator. *Sci. Rep.* 9:14590. doi: 10.1038/s41598-019-50879-6

Chong, J., Liu, P., Zhou, G., and Xia, J. (2020). Using MicrobiomeAnalyst for comprehensive statistical, functional, and meta-analysis of microbiome data. *Nat. Protoc.* 15, 799–821. doi: 10.1038/s41596-019-0264-1

Christiaens, A. S., Van Steenkiste, M., Rummens, K., and Smets, I. (2022). Amyloid adhesin production in activated sludge is enhanced in lab-scale sequencing batch reactors: feeding regime impacts microbial community and amyloid distribution. *Water Res X.* 17:100162. doi: 10.1016/j.wroa.2022.100162

Daims, H., Lebedeva, E. V., Pjevac, P., Han, P., Herbold, C., and Albertsen, M. (2015). Complete nitrification by Nitrospira bacteria. *Nature* 528, 504–509. doi: 10.1038/nature16461

Daims, H., Nielsen, J. L., Nielsen, P. H., Schleifer, K. H., and Wagner, M. (2001). In situ characterization of Nitrospira-like nitrite-oxidizing bacteria active in wastewater treatment plants. *Appl. Environ. Microbiol.* 67, 5273–5284. doi: 10.1128/AEM.67.11.5273-5284.2001

Derlon, N., Wagner, J., da Costa, R. H., and Morgenroth, E. (2016). Formation of aerobic granules for the treatment of real and low-strength municipal wastewater using a sequencing batch reactor operated at constant volume. *Water Res.* 105, 341–350. doi: 10.1016/j.watres.2016.09.007

Dhariwal, A., Chong, J., Habib, S., King, I. L., Agellon, L. B., and Xia, J. (2017). Microbiome analyst: a web-based tool for comprehensive statistical, visual and meta-analysis of microbiome data. *Nucleic Acids Res.* 45, W180–W188. doi: 10.1093/nar/gkx295

Dionisi, H. M., Layton, A. C., Harms, G., Gregory, I. R., Robinson, K. G., and Sayler, G. S. (2002). Quantification of *Nitrosomonas oligotropha*-like ammonia-oxidizing bacteria and Nitrospira spp. from full-scale wastewater treatment plants by competitive PCR. *Appl. Environ. Microbiol.* 68, 245–253. doi: 10.1128/AEM.68.1.245-253.2002

Flemming, H. C., van Hullebusch, E. D., Neu, T. R., Nielsen, P. H., Seviour, T., Stoodley, P., et al. (2023). The biofilm matrix: multitasking in a shared space. *Nat. Rev. Microbiol.* 21, 70–86. doi: 10.1038/s41579-022-00791-0

Gonzalez-Martinez, A., Rodriguez-Sanchez, A., Van Loosdrecht, M. C., Gonzalez-Lopez, J., and Vahala, R. (2016). Detection of comammox bacteria in full-scale wastewater treatment bioreactors using tag-454-pyrosequencing. *Environ. Sci. Pollut. Res.* 23, 25501–25511. doi: 10.1007/s11356-016-7914-4

Huang, L., Jin, Y., Zhou, D., Liu, L., Huang, S., Zhao, Y., et al. (2022). A review of the role of extracellular polymeric substances (EPS) in wastewater treatment systems. *Int. J. Environ. Res. Public Health* 19:12191. doi: 10.3390/ijerph191912191

Larsen, P., Nielsen, J. L., Svendsen, T. C., and Nielsen, P. H. (2008). Adhesion characteristics of nitrifying bacteria in activated sludge. *Water Res.* 42, 2814–2826. doi: 10.1016/j.watres.2008.02.015

Liao, B. Q., Allen, D. G., Droppo, I. G., Leppard, G. G., and Liss, S. N. (2001). Surface properties of sludge and their role in bioflocculation and settleability. *Water Res.* 35, 339–350. doi: 10.1016/S0043-1354(00)00277-3

Maddela, N. R., Gan, Z., Meng, Y., Fan, F., and Meng, F. (2022). Occurrence and roles of comammox bacteria in water and wastewater treatment systems: a critical review. *Engineering* 17, 196–206. doi: 10.1016/j.eng.2021.07.024

Manavi, N., Kazemi, A. S., and Bonakdarpour, B. (2017). The development of aerobic granules from conventional activated sludge under anaerobic-aerobic cycles and their adaptation for treatment of dyeing wastewater. *Chem. Eng. J.* 312, 375–384. doi: 10.1016/j.cej.2016.11.155

Mehrani, M. J., Kowal, P., Sobotka, D., Godzieba, M., Ciesielski, S., Guo, J., et al. (2023). The coexistence and competition of canonical and comammox nitrite oxidizing bacteria in a nitrifying activated sludge system–experimental observations and simulation studies. *Sci. Total Environ.* 864:161084. doi: 10.1016/j.scitotenv.2022.161084

Pinto, A. J., Marcus, D. N., Ijaz, U. Z., Bautista-de Lose Santos, Q. M., Dick, G. J., and Raskin, L. (2016). Metagenomic evidence for the presence of comammox Nitrospira-like bacteria in a drinking water system. *Msphere.* 1, 10–128. doi: 10.1128/msphere.00054-15

Pishgar, R., Dominic, J. A., Sheng, Z., and Tay, J. H. (2019). Denitrification performance and microbial versatility in response to different selection pressures. *Bioresour. Technol.* 281, 72–83. doi: 10.1016/j.biortech.2019.02.061

Pjevac, P., Schauberger, C., Poghosyan, L., Herbold, C. W., van Kessel, M. A., Daebeler, A., et al. (2017). AmoA-targeted polymerase chain reaction primers for the specific detection and quantification of comammox Nitrospira in the environment. *Front. Microbiol.* 8:1508. doi: 10.3389/fmicb.2017.01508

Ren, Y., Ngo, H. H., Guo, W., Wang, D., Peng, L., Ni, B. J., et al. (2020). New perspectives on microbial communities and biological nitrogen removal processes in wastewater treatment systems. *Bioresour. Technol.* 297:122491. doi: 10.1016/j.biortech.2019.122491

Ronan, E., Aqeel, H., Wolfaardt, G. M., and Liss, S. N. (2021). Recent advancements in the biological treatment of high strength ammonia wastewater. *World J Microbiol Biotechnol* 37:158. doi: 10.1007/s11274-021-03124-0

Roots, P., Wang, Y., Rosenthal, A. F., Griffin, J. S., Sabba, F., Petrovich, M., et al. (2019). Comammox Nitrospira are the dominant ammonia oxidizers in a mainstream low dissolved oxygen nitrification reactor. *Water Res.* 157, 396–405. doi: 10.1016/j.watres.2019.03.060

Sarma, S. J., and Tay, J. H. (2018). Aerobic granulation for future wastewater treatment technology: challenges ahead. *Environ Sci: Water Res & Technol* 4, 9–15. doi: 10.1039/C7EW00148G

Schwarzenbeck, N., Borges, J. M., and Wilderer, P. A. (2005). Treatment of dairy effluents in an aerobic granular sludge sequencing batch reactor. *Appl. Microbiol. Biotechnol.* 66, 711–718. doi: 10.1007/s00253-004-1748-6

Soler, P., Faria, M., Barata, C., García-Galea, E., Lorente, B., and Vinyoles, D. (2021). Improving water quality does not guarantee fish health: effects of ammonia pollution on the behaviour of wild-caught pre-exposed fish. *PLoS One* 16:e0243404. doi: 10.1371/journal.pone.0243404

Terada, A., Lackner, S., Kristensen, K., and Smets, B. F. (2010). Inoculum effects on community composition and nitritation performance of autotrophic nitrifying biofilm reactors with counter-diffusion geometry. *Environ Microbiol* 12, 2858–2872. doi: 10.1111/j.1462-2920.2010.02267.x

Weissbrodt, D. G., Shani, N., and Holliger, C. (2014). Linking bacterial population dynamics and nutrient removal in the granular sludge biofilm ecosystem engineered for wastewater treatment. *FEMS Microbiol. Ecol.* 88, 579–595. doi: 10.1111/1574-6941.12326

Yin, Q., Sun, Y., Li, B., Feng, Z., and Wu, G. (2022). The r/K selection theory and its application in biological wastewater treatment processes. *Sci. Total Environ.* 824:153836. doi: 10.1016/j.scitotenv.2022.153836

Zhu, G., Wang, X., Wang, S., Yu, L., Armanbek, G., Yu, J., et al. (2022). Towards a more labor-saving way in microbial ammonium oxidation: a review on complete ammonia oxidization (comammox). *Sci. Total Environ.* 829:154590. doi: 10.1016/j.scitotenv.2022.154590

Frontiers in Microbiology

Explores the habitable world and the potential of microbial life

The largest and most cited microbiology journal which advances our understanding of the role microbes play in addressing global challenges such as healthcare, food security, and climate change.

Discover the latest Research Topics

See more →

Frontiers

Avenue du Tribunal-Fédéral 34
1005 Lausanne, Switzerland
frontiersin.org

Contact us

+41 (0)21 510 17 00
frontiersin.org/about/contact